

Fall 2000

# Remote sensing of forest damage in the Czech Republic using hyperspectral methods

Petya K. Entcheva

*University of New Hampshire, Durham*

Follow this and additional works at: <https://scholars.unh.edu/dissertation>

---

## Recommended Citation

Entcheva, Petya K., "Remote sensing of forest damage in the Czech Republic using hyperspectral methods" (2000). *Doctoral Dissertations*. 2139.

<https://scholars.unh.edu/dissertation/2139>

This Dissertation is brought to you for free and open access by the Student Scholarship at University of New Hampshire Scholars' Repository. It has been accepted for inclusion in Doctoral Dissertations by an authorized administrator of University of New Hampshire Scholars' Repository. For more information, please contact [nicole.hentz@unh.edu](mailto:nicole.hentz@unh.edu).

## **INFORMATION TO USERS**

**This manuscript has been reproduced from the microfilm master. UMI films the text directly from the original or copy submitted. Thus, some thesis and dissertation copies are in typewriter face, while others may be from any type of computer printer.**

**The quality of this reproduction is dependent upon the quality of the copy submitted. Broken or indistinct print, colored or poor quality illustrations and photographs, print bleedthrough, substandard margins, and improper alignment can adversely affect reproduction.**

**In the unlikely event that the author did not send UMI a complete manuscript and there are missing pages, these will be noted. Also, if unauthorized copyright material had to be removed, a note will indicate the deletion.**

**Oversize materials (e.g., maps, drawings, charts) are reproduced by sectioning the original, beginning at the upper left-hand corner and continuing from left to right in equal sections with small overlaps.**

**Photographs included in the original manuscript have been reproduced xerographically in this copy. Higher quality 6" x 9" black and white photographic prints are available for any photographs or illustrations appearing in this copy for an additional charge. Contact UMI directly to order.**

**Bell & Howell Information and Learning  
300 North Zeeb Road, Ann Arbor, MI 48106-1346 USA  
800-521-0600**

**UMI<sup>®</sup>**



**REMOTE SENSING OF FOREST DAMAGE IN THE CZECH REPUBLIC  
USING HYPERSPECTRAL METHODS**

**BY**

**Petya K. Entcheva**

**B.S., Higher Institute of Forest Engineering, 1988**

**M.S., University of Massachusetts, 1994**

**DISSERTATION**

**Submitted to the University of New Hampshire  
in Partial Fulfillment of  
the Requirements for Degree of**

**Doctor in Philosophy**

**in**

**Natural Resources**

**September, 2000**



**UMI Number: 9983715**

**Copyright 2000 by  
Entcheva, Petya K.**

**All rights reserved.**

**UMI<sup>®</sup>**

---

**UMI Microform 9983715**

**Copyright 2000 by Bell & Howell Information and Learning Company.**

**All rights reserved. This microform edition is protected against  
unauthorized copying under Title 17, United States Code.**

---

**Bell & Howell Information and Learning Company  
300 North Zeeb Road  
P.O. Box 1346  
Ann Arbor, MI 48106-1346**

**ALL RIGHTS RESERVED**

**© 2000**

**Petya Entcheva**

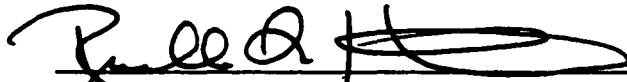
This dissertation has been examined and approved.



Dissertation Director, Barrett Rock, Director of Complex  
Systems Research Center, Professor of Natural Resources  
and Earth Oceans and Space



Mary Martin,  
Research Assistant Professor of Natural Resources



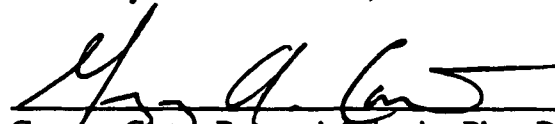
Russell Congalton, Professor of Remote Sensing and  
Geographic Information Systems



Thomas Lee, Associate Professor of Plant Biology  
(Ecology)



Matthew Kelly, Professor of Forest Resources;  
University of Massachusetts, Amherst



Gregory Carter, Research Scientist, Plant Physiological  
Ecology and Remote Sensing; NASA, Stennis Space  
Center



James Irons, Research Scientist, AST Earth Sciences  
Remote Sensing; NASA, Goddard Space Flight Center

June 1, 2000  
Date

## **ACNOWLEDGEMENTS**

I would like to thank my committee members for their support and advice during the course of this project: Dr. Barrett Rock, Dr. Mary Martin, Dr. Russell Congalton, Dr. Thomas Lee, Dr. Gregory Carter, Dr. James Irons and Dr. Matthew Kelty. My deepest gratitude and heartfelt thanks to Dr. Barrett Rock, my thesis advisor and principal investigator of this project, for his inspiration, encouragement and guidance in the completion of this work. Special thanks to my ex-officio committee members Dr. Kevin Smith and Dr. William Cibula, and to all of my advisors for the many fruitful discussions and for their generous help.

The collection and analysis of field data would not have been possible without the hard work of the team of Czech students and colleagues, especially Jitka Bilkova, Jana Albrechtova, Blanka Solkova, Ryan Huntley, Anja Woodington and Brandon Webb. I truly appreciate their good humor and patience to ensure the quality of the collected data.

I thank all of my friends and fellow graduate students for their good humor and support throughout the years. Many thanks to Karen Bushold, Faith Sheridan, Diana Wright and all of my friends from Complex Systems Research Center who helped me many times along the way.

In addition, I owe special thanks to the following people: Ing. Vladimir Henzlik from Lesproject for his guidance in the Krusne hory forests, for providing me with forestry maps and answering my many questions; to Dr. Martin Sima and Dr. Jindrih Rajl for assisting our field efforts; and to Dr. Gregory Carter and Dr. James Irons for the use of their imaging systems, which made this project possible.

**Finally to my family, for your understanding, love, support and encouragement over the years I can never thank you enough. I am deeply indebted to my husband, Michael Campbell. I thank you for the many hours contributed directly to this project, but most of all for your encouragement, sense of humor and love.**

**I would like to acknowledge the support of the NASA Terrestrial Ecosystems Program, NASA NA5-5192 grant, which funded this research.**

## TABLE OF CONTENTS

Acknowledgements . . . . .	iv
Abstract . . . . .	xx
<b>1 INTRODUCTION</b>	<b>1</b>
<b>2 BACKGROUND AND LITERATURE REVIEW</b>	<b>4</b>
2.1 Forest Decline in the Czech Republic . . . . .	4
2.2 Physiological Basis of Injury to Trees Caused by SO <sub>2</sub> Air Pollution and Acid Precipitation . . . . .	8
2.3 High Spectral Resolution and Narrow Band Remote Sensing for Forest Stress Detection . . . . .	13
<b>3 EVALUATION OF THE POTENTIAL OF NARROW BAND IMAGING FOR ASSESSMENT OF INITIAL CHANGES IN FOREST HEALTH</b>	<b>24</b>
3.1 Introduction . . . . .	24
3.2 Methods . . . . .	26
3.2.1 Evaluation of Narrow Band Imaging for Visualization of Initial Foliar Damage of Norway Spruce, 1995 . . . . .	27
3.2.3 Evaluation of Narrow Band Imaging for Spectral Characterization at Sample and Tree Crown Level . . . . .	30
3.3 Results and Discussion . . . . .	33
3.3.1 Damage Evaluation and Sample REIP Properties . . . . .	33
3.3.2 1995 Evaluation of NBIC Imagery for Initial Stress Detection . . . . .	34
3.3.3 Evaluation of the NBIC at the Foliar and Canopy Level, 1997 . . . . .	35
3.4 Conclusions . . . . .	38

<b>4</b>	<b>SPECTRAL AND BIOCHEMICAL PROPERTIES OF NORWAY SPRUCE FOLIAGE SAMPLES FROM A RANGE OF DAMAGE CONDITIONS</b>	<b>55</b>
4.1	Introduction . . . . .	51
4.2	Methods and Analysis . . . . .	58
4.2.1	Forest Stand Assessment Activities . . . . .	58
4.2.2	Sample Collections . . . . .	61
4.2.3	Pigment Analysis . . . . .	61
4.2.4	Spectral Reflectance Measurements of Fresh Foliage . . . . .	62
4.2.5	Determination of Foliar Chemical Constituents . . . . .	62
4.2.6	Spectral Analysis of Fresh Foliage . . . . .	65
4.2.7	Statistical Analyses . . . . .	68
4.3	Results and Discussion . . . . .	69
4.3.1	Evaluation of Forest Stand Parameters and Growth Characteristics in Relation to Damage Level . . . . .	69
4.3.2	Relationship Between Forest Damage Level and Foliar Pigments and Chemical Constituents . . . . .	72
4.3.3	Evaluation of Norway Spruce Spectral Reflectance Properties with Regard to Changes Occurring with Damage Level . . . . .	81
4.3.4	Evaluation of Spectral Indices with Regard to Separation of Damage Levels . . . . .	83
4.3.5	Relationship between Reflectance Indices and Canopy Pigments and Foliar Chemical Constituents . . . . .	89
4.4	Conclusions . . . . .	93
<b>5</b>	<b>SEPARATION OF INITIAL DAMAGE IN NORWAY SPRUCE CANOPIES ALONG A DAMAGE GRADIENT USING HYPERSPECTRAL ASAS DATA</b>	<b>144</b>
5.1	Introduction . . . . .	144

5.2	Methods . . . . .	147
5.2.1	Forest Health Evaluation and Stand Measurements . . . . .	148
5.2.2	Foliar Collections, Spectral Measurements and Laboratory Analyses . . . . .	149
5.2.3	ASAS Data Acquisition and Processing . . . . .	151
5.2.4	Site Identification on the ASAS Imagery and Extraction of Norway Spruce Canopy Spectra . . . . .	154
5.2.5	ASAS Spectral Analyses . . . . .	156
5.2.6	Relationship between Reflectance Indices Derived from Canopy Spectra (ASAS) and Foliar Spectra (GER2600) . . . . .	160
5.3	Results and Discussion . . . . .	161
5.3.1	Canopy Reflectance Properties . . . . .	161
5.3.2	Evaluation of Spectral Indices for Separation of Initial Damage Levels . . . . .	166
5.3.3	Evaluation of the Effect of the Decline on Forest Stand Parameters and Foliar Chemical Constituents . . . . .	169
5.3.4	Evaluation of the Relationships between Reflectance Indices and Forest Stand Parameters and Foliar Constituents . . . . .	172
5.3.5	Relationship between Reflectance Indices Derived from Canopy spectra (ASAS) and Foliar Spectra (GER2600) . . . . .	174
5.4	Conclusions . . . . .	175
<b>6</b>	<b>CONCLUSIONS</b>	<b>212</b>
	<b>REFERENCES</b>	<b>216</b>
	<b>APPENDIX</b>	<b>225</b>



## LIST OF TABLES

2.1	Criteria for field forest damage classification . . . . .	23
3.1	Forest damage evaluation criteria and damage level assignment . . . . .	40
3.2	Instruments and data acquisition parameters, Czech Republic 1995 . . . . .	40
3.3	Instruments and data acquisition parameters, Czech Republic 1997 . . . . .	41
3.4	Foliar and spectral reflectance data, Czech Republic 1997 . . . . .	42
3.5	Forest site characteristics, Czech Republic 1995 . . . . .	43
3.6	Red edge inflection point (REIP) of the samples selected for NBIC evaluation, Czech Republic 1995 . . . . .	44
3.7	Relationship between spectra for ground cover components . . . . .	44
3.8	Comparison among mean values of spectral bands and indices . . . . .	45
3.9	Comparison among mean values of spectral bands and indices . . . . .	46
3.10	Overall comparison among mean values for all spectral bands and for all spectral indices (ANOVA) . . . . .	47
4.1	Criteria for field forest damage classification . . . . .	96
4.2	Field data for the study areas in the Krusne hory, northwest Bohemia, Czech Republic acquired August 1998 . . . . .	97
4.3	Calibration and validation precision statistics . . . . .	98
4.4	2.5nm-Narrow Band Indices, Broad Band indices and 10nm-Band Ratios . . . . .	99

4.5	Derivative indices, Inverted Gaussian Model (IGM), Area parameters and Narrow Band Short Wave (SWIR) Indices . . . . .	100
4.6	Mean values for forest stand parameters, Czech Republic 1998 . . . . .	101
4.7	Analysis of variances for forest stand parameters and damage level . . . . .	101
4.8	Analysis of variances (ANOVA) conducted on foliar constituents . . . . .	102
4.9	Change (%) in foliar pigments and chemical constituents occurring with forest damage by needle age group . . . . .	103
4.10	Analysis of variances for foliar constituents and damage . . . . .	104
4.11	Narrow Band Indices (2.5nm) Analysis of variances (ANOVA), conducted on fresh foliage reflectance spectral indices . . . . .	105
4.12	Broad Band and 10nm-Band Indices Analysis of variances (ANOVA) conducted on fresh foliage reflectance spectral indices . . . . .	106
4.13	Derivative indices Analysis of variances (ANOVA) conducted on fresh foliage reflectance spectral indices . . . . .	107
4.14	IGM parameters Analysis of variances (ANOVA) conducted on fresh foliage reflectance spectral indices . . . . .	107
4.15	Area (AAL) parameters Analysis of variances (ANOVA) conducted on fresh foliage reflectance spectral indices . . . . .	108
4.16	Short Wave Infrared (SWIR) indices Analysis of variances (ANOVA) conducted on fresh foliage reflectance spectral indices . . . . .	108
4.17	Change (sensitivity in %) in reflectance Visible/Red Edge indices occurring with forest damage by needle age group . . . . .	109

4.18	<b>Change (sensitivity in %) in Broad Band Indices and 10nm-Band Ratios occurring with forest damage by needle age group . . . . .</b>	<b>110</b>
4.19	<b>Change (%) in derivative indices occurring with forest damage by needle age group . . . . .</b>	<b>111</b>
4.20	<b>Change (sensitivity %) in the Inverted Gaussian Model (IGM) parameters occurring with forest damage by needle age group . . . . .</b>	<b>111</b>
4.21	<b>Change (sensitivity %) in the Area Above the Line (AAL) parameters occurring with forest damage by needle age group . . . . .</b>	<b>112</b>
4.22	<b>Change (sensitivity %) in the Short Wave Infra-red (SWIR) indices occurring with forest damage by needle age group . . . . .</b>	<b>112</b>
4.23	<b>Analysis of variances for 2.5nm-Narrow Band Indices . . . . .</b>	<b>113</b>
4.24	<b>Analysis of variances for Broad Band Indices and 10nm-Band Ratios . . . . .</b>	<b>113</b>
4.25	<b>Analysis of variances for the Derivative indices . . . . .</b>	<b>114</b>
4.26	<b>Analysis of variances for the IGM parameters . . . . .</b>	<b>114</b>
4.27	<b>Analysis of variances for the AAL parameters . . . . .</b>	<b>114</b>
4.28	<b>Analysis of variances for the SWIR indices . . . . .</b>	<b>114</b>
4.29	<b>Narrow Band Indices (2.5nm) Correlation between indices and foliar pigments and chemical constituents . . . . .</b>	<b>115</b>
4.30	<b>Broad Band Indices and 10nm-Band Ratios Correlation between indices and foliar pigments and chemical constituents . . . . .</b>	<b>116</b>
4.31	<b>Derivative Indices correlation between indices and foliar pigments and chemical constituents . . . . .</b>	<b>117</b>

4.32	<b>Inverted Gaussian Model Parameters correlation between indices and foliar pigments and chemical constituents.</b>	117
4.33	<b>Area (AAL) Parameters Correlation between indices and foliar pigments and chemical constituents</b>	118
4.34	<b>Narrow-band Short Wave Infra-red (SWIR) indices Correlation between indices and foliar pigments and chemical constituents</b>	118
4.35	<b>Reflectance indices with highest potential for initial damage separation – Summary</b>	118
5.1	<b>Forest damage evaluation criteria and damage level assignment</b>	178
5.2	<b>Data for the study areas in northwest Bohemia, Czech Republic acquired August 1998</b>	179
5.3	<b>Airborne Solid-state Array Spectroradiometer (ASAS) flight parameters, Czech Republic 1998</b>	180
5.4	<b>Flight attributes for ASAS nadir data acquisition, Czech Republic 1998</b>	180
5.5	<b>Bands ratios and algorithms evaluated for stress detection.</b>	181
5.6.1	<b>ASAS indices tested for significant differences among damage levels (a)</b>	182
5.6.2	<b>ASAS indices tested for significant differences among damage levels (b)</b>	183
5.6.3	<b>ASAS indices tested for significant differences among damage levels (c)</b>	183
5.7.1	<b>Sensitivity of individual indices to damage level (a)</b>	184
5.7.2	<b>Sensitivity of individual indices to damage level (b)</b>	185
5.7.3	<b>Sensitivity of individual indices to damage level (c)</b>	185

<b>5.8</b>	<b>Canopy foliar pigments, chemical compounds and stand parameters tested for significant differences among damage levels (ANOVA)</b>	<b>. . . . 186</b>
<b>5.9</b>	<b>Correlation between stand parameters, foliar pigments and chemical constituents for the ASAS study areas</b>	<b>. . . . . 187</b>
<b>5.10.1</b>	<b>Correlation between ASAS indices and forest stand parameters (a)</b>	<b>. . . . 188</b>
<b>5.10.2</b>	<b>Correlation between ASAS indices and forest stand parameters (b)</b>	<b>. . . . 189</b>
<b>5.11</b>	<b>Correlation between ASAS indices and foliar constituents (a, b)</b>	<b>. . . . . 190</b>
<b>5.12</b>	<b>Relationship between indices computed using ASAS and GER2600</b>	<b>. . . . 191</b>

## LIST OF FIGURES

3.1	Narrow Band Imaging Camera System . . . . .	48
3.2	The radio tower used for NBICt acquisition . . . . .	49
3.3	View of a 30x30m plot outlined in the foot of the tower . . . . .	49
3.4	GER2600 Spectroradiometer . . . . .	50
3.5	NBIC images of spruce branch segments . . . . .	51
3.6	Relationship between VIRIS reflectance measurements and spectral values derived from the NBCS images and calibrated to reflectance . . . . .	51
3.7	Reflectance spectra from understory composition . . . . .	52
3.8	Reflectance data obtained from individual samples and tree crowns using the GER2600, NBICs (samples) and NBICt (tower) . . . . .	53
3.9	Overall comparison between bands and ratios . . . . .	54
4.1	Location of the study areas in the Krusne hory, Czech Republic . . . . .	119
4.2	Healthy and heavily damaged forests, Czech 1998 . . . . .	120
4.3	Determination of foliar chemical constituents . . . . .	121
4.4	Determination of foliar chemical constituents . . . . .	122
4.5	Area Index . . . . .	123
4.6	Forest stand parameters . . . . .	124
4.7	Forest yearly increment growth by damage class . . . . .	125
4.8.1	Pigments - Chlorophyll <i>a</i> . . . . .	126
4.8.2	Pigments - Chlorophyll <i>b</i> . . . . .	127

4.8.3	Pigments – Carotenoids . . . . .	128
4.8.4	Pigments - Chlorophyll ( <i>a+b</i> ) . . . . .	129
4.8.5	Pigments - ( <i>a+b</i> )/Carotenoids . . . . .	130
4.8.6	Pigments - Chlorophyll <i>a/b</i> . . . . .	131
4.8.7	Pigments - Dry weight/fresh weight . . . . .	132
4.9	Foliar Constituents – Nitrogen ratio levels . . . . .	133
4.10	Foliar Constituents – Relative constituents . . . . .	134
4.10.1	Foliar Constituents – Lignin . . . . .	135
4.10.2	Foliar Constituents – Cellulose . . . . .	136
4.10.3	Foliar Constituents – Polar . . . . .	137
4.10.4	Foliar Constituents – Non-polar . . . . .	138
4.11	Spectral reflectance of first-, second- and third-year Norway spruce needles by damage classes . . . . .	139
4.12	Spectral reflectance of DC0, DC1, DC2 and DC3 Norway spruce foliage by age groups . . . . .	140
4.13	Spectral reflectance difference of DC0, DC1, DC2 and DC3 Norway spruce foliage by age groups . . . . .	141
4.14	Spectral reflectance sensitivity of DC0, DC1, DC2 and DC3 Norway spruce foliage by age groups . . . . .	142
4.15	Overall Reflectance difference (averaged spectra across age groups) . . . . .	143
4.16	Reflectance Sensitivity (averaged spectra across age groups) . . . . .	143
5.1	Location of the study areas in the Krusne hory . . . . .	192
5.2	Extreme forest health conditions encountered during the present study. . . . .	193

5.3	High spectral resolution nadir data acquisition for the study sites . . . . .	194
5.4	Ground calibration of the ASAS data . . . . .	195
5.5	Evaluation of ASAS radiometric calibration . . . . .	196
5.6.1	Extraction of reflectance spectra for Norway spruce canopies from individual tree crowns (a-c, healthy DC0 and initial damage DC1). . . . .	197
5.6.2	Extraction of reflectance spectra from individual tree crowns (d, intermediate DC2 and severe DC3 damage) . . . . .	198
5.7.1	ASAS spectra extracted from individual tree crown (a, b) . . . . .	199
5.7.2	ASAS spectral extracted from tree crown (c, d) . . . . .	200
5.8	Reflectance of Norway spruce forest canopy . . . . .	201
5.9	Reflectance sensitivity of Norway spruce forest canopy. . . . .	202
5.10	Normalization of ASAS spectra . . . . .	203
5.11	First derivative transformation of ASAS reflectance spectra . . . . .	204
5.12.1	Optical indices computed using high spectral resolution ASAS data (a-l) . . . . .	205
5.12.2	Optical indices computed using high spectral resolution ASAS data (m-s) . . . . .	206
5.13	Landsat TM and Narrow-band ratios computed using high spectral resolution ASAS data . . . . .	207
5.14	Derivative indices computed using high spectral resolution ASAS data . . . . .	208
5.15	Inverted Gaussian Model (IGM) parameters computed using high spectral resolution ASAS data . . . . .	209
5.16	Comparison of indices for the same sites computed using canopy ASAS and foliar GER2600 reflectance data . . . . .	210



<b>5.16 Comparison of indices for the same sites computed using canopy ASAS and foliar GER2600 reflectance data . . . . .</b>	<b>211</b>
<b>A.1.1 Narrow Band Indices (2.5nm) – C1 . . . . .</b>	<b>226</b>
<b>A.1.2 Narrow Band Indices (2.5nm) – C2 . . . . .</b>	<b>227</b>
<b>A.1.3 Narrow Band Indices (2.5nm) – V1 . . . . .</b>	<b>228</b>
<b>A.1.4 Narrow Band Indices (2.5nm) – V2 . . . . .</b>	<b>229</b>
<b>A.1.1 Narrow Band Indices (2.5nm) – V3 . . . . .</b>	<b>230</b>
<b>A.1.6 Narrow Band Indices (2.5nm) – PRI1. . . . .</b>	<b>231</b>
<b>A.1.7 Narrow Band Indices (2.5nm) – PRI2 . . . . .</b>	<b>232</b>
<b>A.1.8 Narrow Band Indices (2.5nm) – PRI3 . . . . .</b>	<b>233</b>
<b>A.1.9 Narrow Band Indices (2.5nm) – RE1 . . . . .</b>	<b>234</b>
<b>A.1.10 Narrow Band Indices (2.5nm) – RE2 . . . . .</b>	<b>235</b>
<b>A.1.11 Narrow Band Indices (2.5nm) – RE3 . . . . .</b>	<b>236</b>
<b>A.1.12 Narrow Band Indices (2.5nm) – SR . . . . .</b>	<b>237</b>
<b>A.1.13 Narrow Band Indices (2.5nm) – SIPI. . . . .</b>	<b>238</b>
<b>A.1.14 Narrow Band Indices (2.5nm) – PRSI. . . . .</b>	<b>239</b>
<b>A.1.15 Narrow Band Indices (2.5nm) – RARS. . . . .</b>	<b>240</b>
<b>A.1.16 Narrow Band Indices (2.5nm) – GM1 . . . . .</b>	<b>241</b>
<b>A.1.17 Narrow Band Indices (2.5nm) – GM2 . . . . .</b>	<b>242</b>
<b>A.1.18 Narrow Band Indices (2.5nm) – Green . . . . .</b>	<b>243</b>
<b>A.1.19 Narrow Band Indices (2.5nm) –Lichtenthaler . . . . .</b>	<b>244</b>
<b>A.2.1 Broad Band Indices – TM3/TM1 . . . . .</b>	<b>245</b>
<b>A.2.2 Broad Band Indices – TM5/TM4 . . . . .</b>	<b>246</b>

<b>A.2.3 Broad Band Indices – NDVI</b>	<b>247</b>
<b>A.2.4 Broad Band Indices – TVI</b>	<b>248</b>
<b>A.2.5 Broad Band Indices – NDVI550</b>	<b>249</b>
<b>A.2.6 Broad Band Indices – NDVI675</b>	<b>250</b>
<b>A.2.7 Broad Band Indices – NDVI700</b>	<b>251</b>
<b>A.2.8 Narrow Band Ratios - R550/R700</b>	<b>252</b>
<b>A.2.9 Narrow Band Ratios - R840/R700</b>	<b>253</b>
<b>A.2.10 Narrow Band Ratios - R850/R550</b>	<b>254</b>
<b>A.3.1 Derivative Indices – REIPwave</b>	<b>255</b>
<b>A.3.2 Derivative Indices – REIPslope = Dmax.</b>	<b>256</b>
<b>A.3.3 Narrow Band Indices (2.5nm) – V4</b>	<b>257</b>
<b>A.3.4 Derivative Indices – Dmax/D714.</b>	<b>258</b>
<b>A.3.5 Derivative Indices – D717/D704</b>	<b>259</b>
<b>A.3.6 Derivative Indices – Dmax/D744</b>	<b>260</b>
<b>A.3.7 Derivative Indices - DRPI</b>	<b>261</b>
<b>A.3.8 Derivative Indices – DPR2.</b>	<b>262</b>
<b>A.3.9 Derivative Indices – DRPI2</b>	<b>263</b>
<b>A.3.10 Derivative Indices – DPR22</b>	<b>264</b>
<b>A.4.1 IGM Indices – Rs</b>	<b>265</b>
<b>A.4.2 IGM Indices – Ro</b>	<b>266</b>
<b>A.4.3 IGM Indices – <math>\lambda_o</math></b>	<b>267</b>
<b>A.4.4 IGM Indices – <math>\sigma</math></b>	<b>268</b>
<b>A.4.5 IGM Indices – <math>\lambda\pi</math>.</b>	<b>269</b>

<b>A.5.1</b>	<b>Area Indices - Slope.</b>	<b>270</b>
<b>A.5.2</b>	<b>Area Indices - Area</b>	<b>271</b>
<b>A.5.3</b>	<b>Area Indices – Intercept</b>	<b>272</b>
<b>A.5.4</b>	<b>Area Indices – Dept_Sum</b>	<b>273</b>
<b>A.6.1</b>	<b>SWIR Indices – SWIR1</b>	<b>274</b>
<b>A.6.2</b>	<b>SWIR Indices – SWIR12</b>	<b>275</b>
<b>A.6.3</b>	<b>SWIR Indices – SWIR2</b>	<b>276</b>
<b>A.6.4</b>	<b>SWIR Indices – SWIR22</b>	<b>277</b>

## **ABSTRACT**

### **REMOTE SENSING OF FOREST DAMAGE IN THE CZECH REPUBLIC USING HYPERSPECTRAL METHODS**

By

**Petya Entcheva**

University of New Hampshire, September 2000

The current study assesses the potential of hyperspectral data for monitoring the initial stages of damage in Norway spruce forests characterized by subtle changes in foliar chlorophyll and chemistry. Both field and airborne high spectral resolution reflectance measurements were obtained for selected study sites in the Krusne hory, Czech Republic.

High spectral resolution airborne canopy data and field foliar samples were acquired simultaneously in August 1998 for a total of 51 study sites within the Krusne hory. The sites were selected to represent a full range of damage conditions in even-aged Norway spruce (*Picea abies* (L.) Karst.) stands located between 820-920m elevation.

Based on dendrochronology, a decline in forest growth began in the late 1960s. All forests, regardless of damage class, were affected. An apparent recovery began during the mid-1980s.

Reflectance, foliar pigments, nitrogen and chemical constituents were determined for first-, second- and third-year needles. A strong correlation to damage was established for the foliar chemistry. A significant increase in polar compounds (such as tannins, sugars and starch) and a reduced needle lignification occurs with increasing damage.

**Foliar chemical constituents appear to be effective indicators of long-term environmental conditions. The strong relationship between damage level and polar compounds suggests high potential for use of these constituents as bio-indicators of stress.**

**Both field and airborne high spectral resolution data separate the initial forest damage classes. Based on field reflectance measurements for third-year needles, derivative indices from the red edge region were most strongly correlated to damage level, followed by indices ratioing damage-sensitive and damage-insensitive bands and a parameter describing the fit of an Inverted Gaussian curve. Red/red edge spectral data from the Airborne Solid State Array Spectrometer (ASAS) had the highest potential for separation of initial levels of damage, which corresponds with the region suggested as most sensitive to damage as seen in conducting the field reflectance measurements.**

**Both optical and derivative indices incorporating reflectance from the red edge region present the most potential as indicators of initial damage in both leaf and canopy spectra.**

## **Chapter 1**

### **INTRODUCTION**

Maintaining healthy and functional forest cover is of importance because forests are one of the major CO<sub>2</sub> sinks and O<sub>2</sub> sources, covering approximately 40% of the Earth's ice-free land surface (Waring and Running, 1998). A decline in forest health can result in abnormal reductions in forest ecosystem productivity and/or diversity, alter the ecosystem functioning processes and cause a significant effect on the terrestrial biogeochemical cycling. Forest monitoring is of critical importance for the early detection of forest decline or damage due to either natural (insect infestations) or anthropogenic (air pollution) factors. Initial damage detection is required for making timely management decisions.

Vegetation spectral properties are determined by pigment levels, internal structure, water content and biochemical constituents (Rock *et al.*, 1986 and 1988; Martin and Aber, 1997). Changes in amount of foliar chlorophyll, lignin, cellulose, nitrogen and the water content of the tissue are indicative of changes in tree health and produce diagnostic changes in the spectral signatures of vegetation (Rock *et al.*, 1986; Carter *et al.*, 1996). Chlorophyll and carotene concentration change and additional foliar compounds may build within the leaves in response to stress, in turn affecting the spectral properties of the vegetation foliage (Rock *et al.*, 1986; Martin, 1994; Martin and Aber, 1997). Foliar chemistry is considered to be a reflection of the growing conditions to which the trees were subjected at the time of needle formation and cell wall composition

is unlikely to change over time as growing conditions degrade or improve (McNulty *et al.*, 1991). Thus, monitoring of vegetation vigor based on remote sensing estimates of chlorophyll levels and foliar chemical constituents may allow detection of both the early stages of ecosystem decline, as well as long-term environmental conditions.

Remote sensing has proven useful in assessing changes in the extent, density and composition of vegetation (Waring and Running, 1998; Aber *et al.*, 1986). It provides an objective, economically-feasible opportunity for timely detection of changes in the forested cover, with large implications for validation of the existing physiological models of ecosystem function (Aber *et al.*, 1993). Previous research has developed the remote sensing capabilities for assessment of either very broad categories of forest damage on a regional scale, or a detailed estimation of forest health on a local scale (Rock *et al.*, 1993; Lambert *et al.*, 1995; Ardo *et al.*, 1997). High spectral resolution data have been used to measure canopy pigment levels and biochemistry. Hyperspectral systems that acquire data along the visible and near-infrared vegetation spectrum dominated by chlorophyll absorption may allow for monitoring of the early stages of damage in vegetation characterized by subtle reductions in chlorophyll concentrations (Rock *et al.*, 1988; Miller *et al.*, 1993).

High elevation spruce ecosystems are highly sensitive to environmental and climatic changes (NAPAP, 1990). The high elevation forests located in northern Bohemia along the borders of the Czech Republic and Germany grow in one of the most heavily polluted regions of the world (Materna, 1989; Klasterka, 1991; Klimont *et al.*, 1993). Within northwestern Bohemia, the Krušné hory mountains offer a unique opportunity to

**study the full gradient of forest decline conditions within a simple, homogeneous Norway spruce ecosystem located along a narrow elevational range.**

**The primary goal of this research is to assess the potential of airborne- and field-based high spectral resolution remote sensing and narrow band multispectral technology for separation of initial levels of forest damage. The objectives of the research are to:**

- 1. Assess the potential of multispectral narrow band video systems and field spectrometry for separation of damage levels;**
- 2. Document the extent of the changes in forest stand parameters, foliar pigments, chemistry and spectral signatures occurring with damage in Norway spruce foliage; and**
- 3. Evaluate the potential of airborne hyperspectral remote sensing for separation of the initial level of damage in the Norway spruce canopies from the Krusne hory, Czech Republic.**

**The format of this dissertation is structured such that the introduction and literature review chapters are followed by the research, separated into three independent chapters, addressing the objectives enumerated above.**



## **Chapter 2**

### **BACKGROUND AND LITERATURE REVIEW**

#### **2.1 Forest Decline in the Czech Republic**

##### **Forest decline**

Forest decline is defined as deterioration in forest health caused by a combination of stress factors leading to an abnormal reduction in growth in mature stands. Forest decline is not the result of normal maturation or senescence and cannot be attributed to a single predominant natural factor. Finally, forest decline is sufficiently severe and extensive so as to cause major concern and be detected by a routine forest monitoring and field investigations (NAPAP, 1990). Hyink and Zedaker (1987) characterize decline as a gradual loss of vigor involving reduced growth rate and increased susceptibility to secondary biotic and abiotic stress, which generally affects mature trees. Unless the stress factors are removed forest decline may lead to forest death.

##### **Spruce decline in the Czech Republic**

High elevation spruce forests in northern Bohemia, along the Krusne hory mountains that border the Czech Republic and Germany, inhabit one of the most heavily polluted regions of the world (Klimont *et al.*, 1993). This area of Central Europe has been exposed to severe levels of air pollution over the past 40 years. Sulfur dioxide (SO<sub>2</sub>) has been attributed as the primary factor responsible for the advanced forest decline in the Black

Triangle (Kubikova, 1991). The forests in the Krusne hory mountain range cover approximately 300,000 hectares. These forests have been planted and managed as monoculture plantations of Norway spruce (*Picea abies*) for at least the last 100 years (Henzlik, 1997). Due to the homogeneous forest type and the moderate changes in elevation throughout the region, as well as proximity to heavy pollution sources, the Krusne hory offers a unique opportunity to observe the full gradient of forest damage attributed to long-term exposure to extreme levels of air pollutants. The majority of the spruce forests in the Krusne hory have been classified as either damaged or heavily damaged (Rock *et al.*, 1994; Lambert *et al.*, 1995; Ardo *et al.*, 1997). Many areas have experienced nearly complete overstory mortality, resulting in full collapse of the ecosystem.

Evidence of abnormally reduced individual tree and forest stand growth plays a major role in the detection and evaluation of forest decline. Of key importance when evaluating forest decline is to consider the normal (i.e., expected) processes of tree growth in conjunction with the environmental and forest history factors affecting forest stand development.

Retention of multiple years of needles is an inherent characteristic of coniferous species. A new needle-age class (current-year needles) is being added each growing season, while the oldest needles are being shed as their physiological function is impaired. Depending on the growing conditions, Norway spruce can retain 15 or more years of needles (Delkov, 1984; field observations of the author). Under environmental stress, Lichtenthaler (1988) has reported a reduction of the number of needle-years retained with increasing levels of damage.

A variety of environmental factors affecting tree growth should be considered in forest decline assessments. Some of these parameters include: temperature, soil moisture, soil chemical and physical properties, soil microorganisms, precipitation, site topography (elevation, slope and aspect) and wind regime. The factors that have a significant impact on tree growth can be stratified into three major groups: site quality, stand density and stand age (Hyink and Zedaker, 1987). Site quality is a measure of the productive capacity of the environment. Within highly productive sites, young trees grow faster, reaching larger sizes in a shorter time with a more gradual natural rate of decline. Stand density is the measure of the number of tree stems per unit area. Stand density of shade-tolerant, even-aged species changes very little over time. In the case of mature spruce plantations, such as the forests in the Krusne hory, stand density can be considered a constant. Hyink and Zedaker (1987) define the difference between chronological and physiological age of a tree, stating that physiological age is of greater significance than chronological age with respect to tree growth. Physiological age can differ significantly within uneven-aged, uneven-spaced stands. Even-aged, regularly-spaced spruce plantations, as found in the Czech Republic, provide one of the rare examples where trees with the same chronological age may be at the same physiological age.

### **Field Evaluation of Forest Decline**

Site- and/or region-specific techniques are used to characterize and quantify forest canopy damage using ground-based observations. Typical forest decline evaluations involve assessing individual trees (i.e., crowns) within a larger forest stand. Standard variables recorded for each individual crown include: percent of crown defoliation, percent

of crown mortality, incidence and severity of chlorotic and/or necrotic foliage, and incidence of signs and/or symptoms of biotic pathogens (including insect damage; NAPAP, 1990).

Subjective estimates of within-crown defoliation and mortality are the primary variables used to categorize individual trees and the surrounding stand into damage classes. For example, forest decline assessments in the Krusne hory recognize five levels of Norway spruce foliar loss, with one class for healthy crowns and four categories defining progressively greater stages of defoliation (Lesproject, 1988; Henzlick, 1997; Ardo *et al.*, 1997). However, different countries have adopted unique defoliation class definitions. The German methods, developed for use with CIR photography in conjunction with forest field surveys, assign slightly defoliated crowns to the healthiest class (Hildebrandt and Gross, 1992). The current study adapted the German forest damage evaluation methods (Table 2.1).

The spectral response of forests classified from the ground as healthy (DC0) may be influenced by a combination of completely healthy stems and crowns displaying the earliest visual signs of damage. Similarly, the spectral properties of stands subjectively quantified as displaying initial damage (DC1) include individual healthy crowns, crowns with only slight defoliation (11%) and crowns with significant needle loss (25%). Here again, the spectral response of forests classified as DC1 is controlled by the combined reflectance properties of a continuous range of defoliation levels. Based on the absorption properties of chlorophyll, the spectral properties of foliage can provide an accurate indicator of plant growth conditions (Carter *et al.*, 1995). Current satellite-borne sensors, such as Landsat TM, may not detect the slight spectral shifts associated with a decline in forest health from DC0 to DC1 (Lambert, 1993, Lambert *et al.*, 1995; Rock *et*

al., 1994). The spatial and spectral limitations of multispectral satellite imagery can result in unreliable categorization of the spectrally mixed canopies associated with damaged stands. Lambert *et al.* (1995) accurately discriminated three levels of forest damage within the Krusne hory (healthy, moderate damage and heavy damage). Their approach employed a logit regression to classifying forest damage conditions with both Landsat TM imagery and ground-based forest inventory data.

Based on their assessment of TM damage discrimination capabilities, DC0 and DC1 were not separable, DC2 was discriminated with 83% accuracy and DC3 with 95% accuracy. Single bands (TM1, TM3, TM4 and TM7) were best for separation of damage classes, and band ratios did not improve the discrimination of damage classes.

Due to subtle alterations and visual similarities in crown foliar condition representative of the initial damage class (DC1), it is likely that visual field observations would score these trees and the surrounding stand as healthy. An imaging system capable of detecting these initial subtle changes in foliar condition could become a valuable tool for detection of early stages of forest stress. Detection and quantification of the initial stages of forest damage are essential to accurately monitor forest health and to implement effective corrective treatments. Therefore, improvements in remotely sensed data are needed to adequately assess the full range of forest decline categories, even in forest cover types such as the homogenous spruce stands of the Krusne hory.

## **2.2 Physiological Basis of Atmospheric Sulfur Dioxide and Acid Precipitation Injury to Trees**

Trees, by their nature, are stationary organisms unable to migrate to avoid the unfavorable fluctuations in their changing environment. Significant deviations from

optimal conditions that cause changes in plant responses at all functional levels result in plant stress (Larcher, 1995). Initially stress causes destabilization in structural and physiological functions. If the stress is short-lived and the tree is able to adjust, resistance to the stress agent increases and a new stable condition in physiological functions is attained. Plant physiological acclimation, or adaptation, is the ability of a plant to adjust to continuous stress conditions, and facilitates long-term survival (Alscher and Cumming, 1990). Prolonged stress conditions exceeding the adaptive limits can cause severe injuries, destruction of viable organs and tree death (Larcher, 1995).

### **Injury Caused by Sulfur Dioxide (SO<sub>2</sub>)**

Trees are exposed to air pollutants directly through the exchange of atmospheric gases or indirectly through the moisture absorbed from the soil. Atmospheric pollutants enter the plants through the open leaf stomata. After entering the plant tissue, air pollutants dissolve in the water resulting in direct damage to cellular structures (e.g., cell membranes; Schulze *et al.*, 1989). Such changes in foliar chemistry indirectly affect plant growth processes. Sulfur dioxide (SO<sub>2</sub>) represents an atmospheric pollutant that is toxic to plants, animals and humans (Lange *et al.*, 1989). The SO<sub>2</sub> molecules dissolve easily in water in the atmosphere and in soil surface moisture, forming acid precipitation. Comprehensive reviews of physiological effects of SO<sub>2</sub> are provided in Alscher and Cumming (1990), Smith (1990), Larcher (1995) and Lange *et al.* (1989).

The most prevalent atmospheric pollutant causing damage to plants is sulfur dioxide (SO<sub>2</sub>) (Krahl-Urban *et al.*, 1988). It is emitted to the atmosphere primarily during the burning of fossil fuels. Power generation, both industrial and domestic, provides the major portion of global sulfur dioxide emissions. When emitted via tall,

industrial smokestacks, SO<sub>2</sub> particles can be dispersed via long-range transport. Sulfur dioxide has a residence time in the atmosphere of up to three days. In the atmosphere, it reacts with moisture forming both sulfurous acid (H<sub>2</sub>SO<sub>3</sub>) and sulfuric acid (H<sub>2</sub>SO<sub>4</sub>). In some regions of Europe, especially in the Krusne hory, SO<sub>2</sub> is considered the decisive factor causing forest decline (Krahl-Urban *et al.*, 1988, Lange *et al.*, 1989).

SO<sub>2</sub> enters directly through the leaf stomata and is dissolved in the free space moisture within the leaf intercellular spaces. If the stomata are closed SO<sub>2</sub> cannot enter the leaf. However, if atmospheric concentrations are great enough, SO<sub>2</sub> can overcome stomatal resistance by causing loss of turgor in the epidermal cells surrounding the guard cells, leading to the opening of the stomata (Larcher, 1995). Inside the leaf, SO<sub>2</sub> dissolves in the intercellular space as SO<sub>3</sub>, and inside individual cells as SO<sub>4</sub> (Smith, 1990; Lee, 1995). Sulfur compounds exist naturally within plant cells. The protoplasm has a natural buffering detoxification mechanism against higher amounts. If too many sulfur groups enter the cell, they are converted to H<sub>2</sub>S and sent back to the atmosphere via gas exchange through the stomata (Larcher, 1995). If the cellular SO<sub>2</sub> exceeds the cell buffering capacity, the chloroplasts serve as an ion sink. All conifers, including spruce trees, use the C<sub>3</sub> pathway of photosynthesis. In C<sub>3</sub> plants SO<sub>2</sub> occupies the sites reserved for CO<sub>2</sub> fixation on *ribulose-1,5-bisphosphate carboxylases* (RUBISCO), leading to a reduction in the ability of the RUBISCO system to allocate CO<sub>2</sub>. This results in an inhibition of photosynthesis, often causing chlorophyll destruction and eventually cell death. As SO<sub>2</sub> exposure increases, more chlorophyll is lost and cell mortality continues. These pigment and cellular changes result in differences in foliar spectral properties, providing the basis for damage detection using remote sensing techniques

(Rock *et al.*, 1986). Conifers typically retain their needles for several years, with spruce holding functional needles for up to 15 years (Hosley, 1936). Therefore, spruce needles are among the most likely to be affected by chronic SO<sub>2</sub> exposure.

Smith (1990) describes the progression in foliar damage symptoms attributed to SO<sub>2</sub> exposure. Initial symptoms include the formation of faint, water-soaked necrotic spots on the needles. The necrotic spots are the result of the collapse of the mesophyll cells. The symptom is observed initially near the stomata. The necrotic areas dryout and become either a reddish-brown or yellowish (i.e., chlorotic) color. With advanced damage, the necrotic areas expand and the needle is eventually shed. Krahl-Urban *et al.* (1988) confirms that the most common symptoms of SO<sub>2</sub> pollution damage in conifers are chlorosis and needle loss.

### **Acid Precipitation**

Sulfur dioxide and nitrogen oxides can react with atmospheric oxygen and water vapor, producing acid rain. Pure rain is typically slightly acidic with a pH value ranging between 5 and 6. Average pH levels reported in the Krusne hory are around 4, with levels of 2 and 2.5 reported during winter fog episodes (Krahl-Urban *et al.*, 1988).

Sulfate and nitrate, in combination with other nutrients, are commonly used as agricultural fertilizers. Thus, in the soil they may have a beneficial effect on the plants. If the rate of sulfate and nitrate deposition exceeds the rate of uptake by the forest, soil acidification may occur (Schulze *et al.*, 1989).

Acid precipitation can cause cuticular erosion and other abnormalities leading to foliar leaching (Schulze *et al.*, 1989; Larcher, 1995). The cuticle, the outermost layer of spruce needles, is covered by cuticular waxes. Long-term exposure of spruce foliage to



acid precipitation has been shown to result in the leaching of calcium, magnesium and potassium (Smith, 1990). The especially damaging effect of acid precipitation in the form of fog has been noted. One hypothesis is that acid fog exposure causes cuticular wax aging and erosion leading to excessive foliar water loss. This effect could also increase the potential risk of foliar winter injuries.

Gruber (1994) and Larcher (1995) report that acid precipitation can cause direct damage to root apoplasts, leading to cell damage and disruption by affecting the distribution of growth hormones. Damage to the spruce taproot can cause the root architecture to shift from central to flat (Gruber, 1994). A flat root system is very unsuitable for the mountainous growth conditions in which spruce usually grows, causing the trees to become susceptible to wind damage and drought.

Acid rain deposits mobile anions (e.g.,  $\text{NO}_3^-$ ,  $\text{SO}_4^{2-}$ ) into the soil solution (Abrahamsen *et al.*, 1993). Since forest soils are typically nitrogen limited,  $\text{NO}_3^-$  deposition can initially have a beneficial affect. However, when sulfate and nitrogen inputs exceed the demand by the forest, these anions, along with basic cations (e.g.,  $\text{Ca}^+$ ,  $\text{K}^+$ ,  $\text{Mg}^+$ ), will be leached into the mineral soil leaving aluminum ions in the organic horizon (Smith, 1990; Abrahamsen, 1993). The nutrient cations are leached beyond the rooting zone and become unavailable, causing nutrient imbalances and plant growth decline (Mooney *et al.*, 1991). The normal capacity of the upper soil horizons to store leached cations can also be diminished. With an increase in soil pH, the cations can be displaced from the ion exchange sites on the clay particles by hydrogen ( $\text{H}^+$ ). In some highly acid soils with increased aluminum solubility, aluminum concentrations reach toxic levels.

Schulze *et al.* (1989) and Lange *et al.* (1989) report that acidification of the soil solution resulted in the reduction of root biomass in the upper, severely acidified mineral horizons, and caused an increase in root biomass in the organic layer. This change in root distribution with soil depth increased forest susceptibility to short-term surface drought.

Crown thinning is a commonly observed symptom associated with spruce forest damage attributed to acid precipitation. Defoliation has been documented as loss of older needles, missing current year needles and insufficient branching. Perhaps the most prominent symptom of advanced spruce decline is the "sub-top thinning." This is characterized by a complete lack of needles in the upper portion of the crown, while the lower functional part of the crown displays little or no needle loss (Gruber, 1994). Crown thinning has also been associated with needle desiccation that may be due to one or more of the following: (1) tree water deficiency (a systematic stress), (2) needle surface area damage associated with cuticular erosion, (3) blockage in the tree water transport system due to mechanical forces, and (4) needle abscission due to severe nutrient imbalance (Gruber, 1994).

In the Krusne hory (Erzgebirge Mountain), Lange (1989) reports higher levels of  $\text{NO}_2$  than  $\text{SO}_2$ . Because of the higher cellular capacity for reductive detoxification of  $\text{NO}_2$  than  $\text{SO}_2$ ,  $\text{NO}_2$  concentrations measured within leaves with open stomata were found to be low. Lange concludes that  $\text{SO}_2$ , although in lower concentrations in the atmosphere, presents the major threat to the spruce forests in this region.  $\text{SO}_2$  and  $\text{NO}_x$  have been reported to alter nutrient balances and reduce carbon transport to roots (Mooney *et al.*, 1991). This may result in more wood to be added to the upper bole and

less to the base, leading to a reduction in stem taper in most of the declining spruce forests throughout Central Europe.

Methods for diminishing the effects of SO<sub>2</sub>, NO<sub>2</sub> and acid rain include the spreading of powdered dolomite over the forest floor. Larcher (1995) reports that by applying dolomite, in conjunction with K and Mg fertilizers, chlorosis in coniferous forests can be treated successfully. This method has been applied in the Krusne hory to maintain a soil pH of 4.5, facilitating an improvement in overall forest growth.

### **2.3 Forest Stress Detection Using High Spectral Resolution Remote Sensing Systems**

During the past several decades, the field of ecological remote sensing has evolved significantly, including field and imaging spectrometers, multi-spectral and narrow-band systems.

#### **Field and Imaging Spectroradiometry**

Field spectroradiometry is a form of ground-based reflectance data collection for the determination of vegetation spectral response patterns (Lillesand and Kiefer, 1994). Spectroradiometers measure, as a function of wavelength, the energy reflected from an object. This can be done in the field or in a laboratory environment under controlled light conditions. The data are calibrated to reflectance using a spectral panel with known, stable reflectance properties. The current study uses two field spectroradiometers: (1) VIRIS (MARK IV), and (2) GER2600 (Geophysical Environmental Research Corp., New York, New York).

Imaging spectrometry acquires remotely sensed data over a large number of contiguous spectral bands such that a complete reflectance spectrum can be obtained for

the imaged region (Jensen, 1996). Airborne and satellite-borne scanners use an optomechanical system in which the detector elements scan the earth's surface perpendicular to the ground using a whisk- or push-broom motion. An optical system, including a prism, discrete detectors and filters, is used to record the incoming reflected and/or emitted radiation into multiple, narrow (i.e., < 25nm) spectral regions or bands.

The Airborne Solid-state Array Spectroradiometer (ASAS), used in the current study, is an airborne push-broom imaging radiometer, with a 512 x 62 pixel CCD area array. The instrument is maintained and operated by the Laboratory for Terrestrial Physics at the NASA Goddard Space Flight Center (NASA/GSFC, Russell *et al.*, 1997). ASAS produces an image strip 512 pixels wide for 62 spectral bands. The complete spectral range is from 410 to 1032nm with an approximately 10nm band-width (half max, full width). The optimal spectral performance of ASAS is in the 500-900nm region (Dabney *et al.*, 1999). Data are recorded as unsigned, 16-bit digital numbers and calibrated to radiometric units using laboratory-derived sensor gain coefficients (Kovalick *et al.*, 1994).

Critical steps in obtaining reliable hyperspectral imaging data for forest change detection includes both atmospheric and radiometric calibration. Some of the methods applied for atmospheric corrections include: scene average method, flat-field correction, single spectrum and empirical line algorithm. Atmospheric models such as 6S, LOWTRAN, MODTRAN and ATREM have also been used successfully to complete atmospheric and radiometric calibration (ACCP, 1994).

## **Forest Change Detection Using Hyperspectral Systems**

A reduction in the state of tree health often leads to changes in leaf cellular structure and chemical composition. During the initial stages of foliar damage cellular changes are frequently subtle as to be “pre-visual.” Plant vitality will irreversibly decline and dramatic visible changes (e.g., foliar loss, chlorosis, necrosis) will begin to occur as damage increases. Vegetation canopy spectral signatures are typically controlled by the biochemical properties of the foliage. Examples of these biochemical properties include: total chlorophyll concentration, relative concentrations of chlorophyll *a* and *b*, water content, lignin and cellulose concentrations, and foliar nutrient status (e.g., nitrogen concentration). Both foliar chlorophyll content and moisture content are considered to be accurate indicators of the state-of-health in a wide range of species (Horler *et al.*, 1983; Rock *et al.*, 1986, 1988, 1992; Vogelmann *et al.*, 1993). Significant loss of foliar biomass has been detected using various Landsat Thematic Mapper (TM) indices and band ratios, such as the Normalized Difference Vegetation Index (NDVI) and TM 5/4 (Lambert *et al.*, 1995; Rock *et al.*, 1993). However, subtle changes in vegetation health associated with vegetative biochemical properties cannot be detected using broadband spectral data.

A variety of techniques have been developed to investigate the relationships between spectral data and the physiological properties of vegetative canopies, including: multiple linear regression on the first and second derivative absorptance spectra, partial least squares on first derivative spectra and multivariate inversion techniques. The Accelerated Canopy Chemistry Program (ACCP, 1994) suggested that hyperspectral data allows detection of subtle differences in vegetation signatures, including the signatures of

individual leaves within complex canopies and quantitative estimates of chlorophyll concentrations (Miller *et al.*, 1990).

Within the last 20 years, near-infrared (NIR) spectroscopy has become a widely used tool for the quantitative assessment of chemical constituents for agricultural products (Williams and Norris, 1987; Wessman *et al.*, 1994; Bolster *et al.*, 1996). The NIR instruments are calibrated by making absorption measurements on a sample set for which the chemical analysis has been made. The NIR measurements of the calibration samples are then related, using regression procedures, to the values obtained by the laboratory analysis (Martin, 1994). Because of their importance in determining foliar decomposition rates, lignin and cellulose levels have been evaluated, while less attention has been paid to the remaining foliar compounds (ACCP, 1994).

Laboratory carbon constituent analysis allows for measurement of relative concentration of lignin, cellulose, polar and non-polar constituents (Newman *et al.*, 1994). *Non-polar* compounds include organic fats and waxes, largely allocated in the needle cuticles and governing foliar gas exchange and transport properties (Ferry and Ward, 1959). Increasingly, it has been shown that under the influence of air pollution the aging of cuticular waxes is accelerated and the levels of fats and oils increase, causing the occurrence of premature epistomatal structural wax agglomerates and the formation of scale-like wax structures covering the stomata and leading to leaf shedding when 80-90% of the stomata are closed (Shulze *et al.*, 1989). During the non-polar extraction step the organic solvent extracts as well most of the foliar pigments (e.g. chlorophyll). *Polar compounds* include phenols (tannins), simple sugars, starch and simple amino acids. Phenolic compounds have been documented to increase significantly with vegetation

damage (Boudet *et al.*, 1995; Soucupova *et al.*, 2000). The current study evaluates the relative changes in damage level of all four compounds.

A common method to enhance abrupt changes in the spectral curve of objects uses first derivative analyses. Wessman *et al.*, (1994), Martin (1994) and Martin and Aber (1997) used the first derivative of forest canopy reflectance spectra for calibration of hyperspectral data to *in situ* lignin and nitrogen concentrations. Demetriades-Shah *et al.* (1990) examined methods for generating derivatives of high spectral resolution data and the use of standard derivative band ratios with regard to the identification of vegetation chlorosis. Their results suggest that chlorosis can be detected using high spectral resolution derivatives while detection was not possible using ratio techniques.

Horler *et al.* (1983) used the first derivative of leaf reflectance spectra to locate the maximum in the 670-720nm region, known as the "red edge." A number of studies have shown that the wavelength position of the red edge inflection point (REIP) is highly correlated with the total amount of chlorophyll present in leaf material for a wide range of species (Kupiec and Curran, 1994; Horler *et al.*, 1983; Hoshizaki *et al.*, 1988; Miller *et al.*, 1990; Moss and Rock, 1991; Rock, *et al.*, 1986, 1988, 1992; Vogelmann *et al.*, 1993). The red edge inflection point is defined as the boundary between chlorophyll absorption in the red wavelengths and leaf scattering in the near-infrared (NIR) wavelengths. It is computed as the wavelength at which the first derivative of reflectance spectra has maximum value (Miller *et al.*, 1990; Rock *et al.*, 1986). REIP values in the 715-724nm range were identified as typical for healthy foliage, while values below 715nm were indicative of decreased chlorophyll concentrations.

Miller *et al.* (1990) stated that the approximation of the red edge position from simple derivative analysis depends on instrument spectral resolution because red edge normality shows an asymmetry in the first derivative curve. Miller *et al.* (1990) used an Inverted Gaussian Model (IGM) to extract red edge spectral information related to total chlorophyll content. This technique was independent of the variations of the first derivative curve. Miller *et al.* (1993) presents evidence that the relationship between total chlorophyll and red edge spectral parameters (e.g., Gaussian red edge reflectance minimum, Gaussian inflection point) provides a quantitative basis for predicting leaf chlorophyll content from Airborne Visible/Infrared Imaging Spectrometer (AVIRIS) data.

Chappelle *et al.* (1992) reports the R675/R700 ratio to be indicative of changes in chlorophyll *a* concentration and the R760/R500 to be indicative of changes in carotenoid concentration (for soybean leaves). The ratios of near-infrared reflectance (above 750nm) to reflectance at 700nm and 550nm were found to correlate well with chlorophyll *a* and total chlorophyll content of broadleaf species for several types of leaves (Gitelson and Merzlyak, 1994; Lichtenthaler, 1998). The commonly used normalized difference vegetation index (NDVI) was developed by contrasting the strong chlorophyll absorption in the red wavelengths with the high reflectance in the near-infrared wavelengths, and has been found insensitive to medium to high chlorophyll concentrations (Vogelmann *et al.*, 1993; Datt *et al.*, 1998). The RARS (R670/R700nm - ratio analysis of reflectance spectra; Chappelle *et al.*, 1992) has been suggested as useful for evaluation of the trends in pigment concentration between needle age classes and species for hemlock and red spruce (Rock *et al.*, 1994). A number of RARS modifications have been suggested by Datt (1998), as pigment specific. The modifications include RARSa (sensitive to



chlorophyll a concentration), RARSb (chlorophyll b specific) and RARSc (carotenoids). RARSa has been reported reliable in assessing relative differences in chlorophyll content with changes in spruce needle vitality and age (Rock *et al.*, 1994).

Stress indicator ratios, suggested by Carter (1994), include: 606/760nm, 695/420nm and 695/760nm. The 606/760 ratio produced values consistent with *in situ* spectroscopy values over the range of healthy, stressed and dead pines. This investigation suggests that, with proper calibration, hyperspectral band ratios are comparable with *in situ* spectrometer measurements.

Many of the algorithms reported in the literature have been developed using leaf reflectance measurements, and/or have been developed for assessment of changes in pigment concentration occurring with vegetation damage. With the current study, such algorithms are evaluated using spectra acquired at the foliar and forest stand level, and their potential for damage detection is assessed.

### **Narrow Band Imaging**

Narrow band imaging (NBI) acquires reflectance spectra within a small number of discrete regions. Compared to imaging spectrometry, NBI is a relatively young technology (Everitt *et al.*, 1990). It became available after the development of charged coupled device (CCD) detectors and analog video cameras. The NBI camera systems are less costly than hyperspectral systems due to the utilization of off-the-shelf components.

For monitoring studies, in order to detect and quantify a possible change, radiometric accuracy is critical. Methods for radiometric calibration (removal of atmospheric and haze effects) of video-imagery to *in situ* ground spectroscopy of black and white targets using standard regression analysis are proposed by Neale *et al.* (1995)

and Carter *et al.* (1996). The narrow band imaging camera (NBIC) system used in the current study was developed at Stennis Space Center (Carter and Miller, 1994). A detailed description of the NBIC system is provided by Carter *et al.* (1996).

Marsh *et al.* (1995) compares the application of video imagery and aerial photography for accuracy assessment of Landsat TM classified data. Aerospace video imaging systems have been used to detect or distinguish among many natural resource variables such as heavy grazing (Everitt *et al.*, 1990), mapping forest vegetation (Lowe *et al.*, 1995), wetland delineation, drought-stress and phytomass levels (Everitt *et al.*, 1990), fire, burned and clear-cut areas, soil salinity, plant communities and species (Wood *et al.*, 1995), gopher and ant mounds (Everitt *et al.*, 1990) and other applications reviewed in Everitt *et al.* (1990) and Pickup *et al.* (1995).

### **Forest Stress Detection Using Narrow Band Systems**

Cibula and Carter (1992) first visualized the "blue shift" of the red edge by photographing conifer seedlings through a 10 nm-bandpass interference filter centered at 700nm. Damaged vegetation often appears similar to healthy vegetation at wavelengths where absorption by accessory pigments is strong, such as in the red portion of the spectrum. Similarly, there is no significant difference between the spectral response of stressed and healthy vegetation within wavelengths where pigments do not absorb radiation, such as in the near-infrared. Ratios of stress-sensitive to stress-insensitive bands have been shown more effective in detection of early damage symptoms than single-band images (Carter and Miller, 1994; Carter *et al.*, 1996). This is due to the tendency of ratios to correct for wavelength-independent optical phenomena. The greatest change in reflectance associated with foliar damage for fully developed, green leaves was

reported to be in the narrow region from 690 to 700nm (Carter, 1993 and Carter *et al.*, 1996; Gitelson and Merzlyak, 1994). Due to relatively weak chlorophyll absorption near 700 nm, relatively low changes in chlorophyll concentration produce significant increases in leaf reflectance in this narrow region as compared to 680nm (Carter *et al.*, 1996). Therefore, as subtle changes in growth conditions result in initial chlorophyll loss, early shifts in leaf reflectance near 700nm can be observed. The increased reflectance in the 690 to 700nm spectral region has consistently been reported in response to a broad range of stress agents, including air pollutants, in a variety of species (Carter, 1993). This spectral shift corresponds to the "blue shift of the chlorophyll red edge," reported as highly correlated with reduced foliar chlorophyll content and plant stress (Gates *et al.*, 1965; Gates, 1980; Horler *et al.*, 1983; Rock *et al.*, 1986, 1988; Curran *et al.*, 1990; Buschmann and Nagel, 1993; Vogelmann *et al.*, 1993; Munden *e*

Damage Level (DC)	Defoliation <sup>1</sup> (%)	Ecosystem vitality status	
		Chlorosis absent	Chlorosis present
0	0 – 10	Healthy	Initial damage
1	11 – 25	Initial damage	Medium damage
2	26 – 60	Medium damage	Heavy damage
3	61 – 80	Heavy damage	Ecosystem collapse <sup>2</sup>
4	81 – 100	Ecosystem collapse <sup>2</sup>	Standing dead forest

<sup>1</sup> Characteristic of more than 70% of the trees within the stand

<sup>2</sup> At this stage more than 50% of the trees within the stand are dead

**Table 2.1 Criteria for field forest damage classification. Damage classification used by the current research in the Krusne hory, Czech Republic.**

## **Chapter 3**

### **EVALUATION OF THE POTENTIAL OF NARROW BAND IMAGING FOR ASSESSMENT OF INITIAL CHANGES IN FOREST HEALTH**

#### **3.1 Introduction**

Remotely sensed imagery has been used in many areas throughout North America and Europe to identify and monitor air pollution related to forest decline (Rock *et al.*, 1986; Vogelmann and Rock, 1988; Rock and Ardo, 1993; Lambert *et al.*, 1995). Given that air pollutants generally impact forest health over large (i.e., regional) areas, satellite-borne digital imagery sensors, with wide area coverage, have been the primary source of remotely sensed data. However, multispectral satellite imagery is limited by coarse spectral and spatial resolutions (Rock and Ardo, 1993; Lambert *et al.*, 1995). Within the Krusne hory, Lambert (1993) has demonstrated the use of Landsat TM satellite imagery to accurately delineate three discrete damage classes, including healthy, damaged and dead forests. Therefore, remote sensing techniques capable of separating the initial levels of damage are needed.

Monitoring vegetation vigor based on estimates of chlorophyll concentrations may allow for pre-visual damage detection in the earliest stages of ecosystem stress. Depending on the severity of stress and the accompanying chlorosis, this reflectance response can be detected prior to damage symptoms apparent to the unaided eye (Cibula and Carter, 1992, Carter *et al.*, 1996). Reflectance sensitivity near 550nm has been

reported as less reliable for stress detection as compared to reflectance near 700nm (Cibula and Carter, 1992; Carter, 1994; Carter *et al.*, 1996). Reflectance measurements near 700nm, as well as ratios using 700nm and near-infrared reflectance, may provide an optimal basis for the remote sensing of incipient chlorosis and plant stress (Carter *et al.*, 1996). Among several ratios tested, 695/760nm was the most consistent indicator of plant stress (Carter, 1994; Carter and Miller, 1994). Reflectance values in the near infrared (NIR), short wave infrared (SWIR) and the SWIR/NIR ratio, have been shown highly correlated to foliar moisture content (Hunt *et al.*, 1989). Both chlorophyll content and foliar moisture content are considered to be accurate indicators of state-of-health in a wide range of species (Hoshizaki *et al.* 1988; Rock *et al.*, 1988, 1994). These studies indicate that while TM data (e.g. ratios) may be correlated with indicators of forest health, imaging spectrometer data with many narrow bands within specific wavelength regions (e.g., 700 – 750nm) will be more useful in detecting the earliest signs and symptoms of forest decline. The remote sensing studies assessing differences in vegetation health based on chlorophyll estimates use high spectral resolution data. Further research is needed to assess the potential of other remote sensing techniques to provide useful spectral data (comparable to hyperspectral) for canopy health assessments implemented at both the foliar level and at the forest canopy scale.

An emerging market in the remote sensing industry is the use of inexpensive airborne multispectral and hyperspectral sensors for both applied imaging (i.e., aerial mapping) and basic research. The spectral resolution of an airborne sensor is based on the type of detection devices employed. The least expensive systems use standard optical lenses and CCD technology. Most standard CCD's have a limited spectral range, covering

approximately 400 to 1100nm with optimal performance in the middle of this range (Buil, 1991). However, the optical lenses are easily fitted with interchangeable band pass interference filters. The interference filters can be purchased with either wide or narrow band passes. Narrow band multispectral airborne sensors offer an alternative to the spectrally and spatially coarse satellite-borne sensors for detecting and discriminating discrete levels of forest damage (Carter *et al.*, 1994). The drawbacks to these sensors include both the limited area of coverage as compared to multispectral satellite images, and the limited full spectral range as compared to true imaging spectrometers.

The goal of this research was the preliminary evaluation of the potential of narrow band imaging technology for Norway spruce damage detection. Specific objectives were to:

1. assess the abilities of a narrow band imaging camera system to visually display changes in Norway spruce reflectance associated with the initial stages of foliar damage, and
2. evaluate the capabilities of a narrow band imaging video camera system at both the foliar and canopy levels by comparing acquired video spectra to spectroradiometer reflectance measurements.

### **3.2 Methods**

A field study was conducted during August 1995 to assess the capabilities of a narrow band imaging camera (NBIC) system to detect spectral changes in Norway spruce reflectance associated with the initial stages of air pollution related to foliar damage. Specific methods were developed to visually compare adjacent foliar samples classified as healthy and initially damaged. A second field experiment was conducted in August 1997 to evaluate the capabilities of an NBIC at both the foliar and canopy levels. Methods were developed to compare spectroradiometer reflectance measurements with NBIC reflectance

measurements. The NBIC reflectance measurements were extracted from images acquired from foliar samples and from *in situ* tree crowns.

### **3.2.1 Evaluation of Narrow Band Imaging for Visualization of Initial Foliar Damage of Norway Spruce, 1995**

#### **Site and Representative Tree Selection and Sample Collection**

A series of potential sample sites were identified within the Krusne hory using 1991 Landsat TM imagery, 1994 1:25000 color infrared (CIR) aerial photography and 1:5000 Czech forestry maps. Sites were located within homogenous Norway spruce (*Picea abies*) forests between 900-1000 meters above mean sea level. Only spruce stands covering a minimum of 5 hectares were selected. Forest health was assessed using methods established by Hildebrandt and Gross (1992). Table 3.1 gives detailed definitions for each of the five damage classes. A total of seven spruce stands were eventually selected and sampled. Each stand was characterized by installing a 30x30m fixed-area sample site. An 11.3m radius circular plot was established at the center of the square sample site. Differentially-corrected GPS coordinates were acquired at the center of each site. A variety of forest inventory variables were collected with the circular plot, including: diameter-at-breast-height (dbh), stem height, stand density and basal area factor. Four 1x1m squares were randomly located within each plot. Spruce regeneration density and age were measured within each square. The percentage understory vegetation cover was also measured with the random squares. Three representative overstory spruce trees were selected and permanently marked with aluminum tags.



### **1995 Spectroradiometer Measurements**

One branch from each of the three representative stems was selected for spectral scanning. Pole pruners were used to collect branches from the upper portion of the crowns. The branch samples were immediately sealed in plastic bags with wet paper towels, placed in coolers of ice and taken to the laboratory for scanning. One-, two- and three-year old branch segments (branchlets) were separated and arranged in non-reflective (i.e. black coated) trays. Reflectance spectra were recorded using a GER Mark IV Visible Infrared Intelligent Spectrometer (VIRIS, Geophysical Environmental Research Corp., New York, New York). The instrument covers the 300 to 3000nm spectral region. The instrument measures passive reflectance over 350 bands with band width at full-max half-width of 2nm resulting in 4nm spectral resolution (Vogelmann *et al.*, 1986). The VIRIS was nadir-oriented at a height of 50cm above the branchlets. The samples were illuminated under a constant hemispherical, tungsten light source oriented at a 45° angle of incidence. Three VIRIS measurements (each measurement being an average of six consecutive scans) were acquired for each sample, with the sample rotated between measurements to limit the effects of random scattering. The three spectral reflectance measurements from each sample were averaged at each wavelength.

REIP values were computed for all foliar samples. Healthy (DC0) and initial damage (DC1) samples had REIP values in the range 716-724nm. Foliar samples from DC2 and DC3 crowns had REIP values less than 716nm.

Based on the damage evaluation and the REIP spectral analyses, two sets of samples were selected from Site 6 for NBIC imaging. One set was from a healthy crown (DC0) and one set was from a crown displaying initial damage symptoms (DC1). Each set contained

first-, second- and third-year branchlets. Therefore, a total of six foliar samples were used for the side-by-side NBIC visualization of healthy versus initially damaged foliage.

### **1995 Narrow Band Camera Image Acquisition**

The first-, second- and third-year branchlets from Site 6 were arranged by year in a non-reflective (black coated) dish and illuminated with the same hemispherical, tungsten light source. The NBIC system consisted of a black and white CCD camera (570 horizontal x 485 vertical elements, Model WV-BL202, Panasonic, Secaucus, NJ, USA) connected to a video cassette recorder (Model AG-2400, Panasonic, Secaucus, NJ) and a 9 cm black and white monitor (Model M300, Auto Vision Systems, Miami, FL, USA). Specifications of the system and the experimental setup are provided in Table 3.2. The system was powered by a 12v battery. Images were acquired through a 50 mm telephoto lens and a filter wheel with 10nm band pass interference filters centered at 670nm, 700nm and 720nm (Andover Corporation, Salem, NH, USA). NBIC frames were acquired with the field-of-view including the dish and a spectralon calibration panel. A total of 18 camera images were acquired (Figure 3.1).

Commercial software was used to capture and digitize the video frames. The digitized images were then processed using FIGMENT (Miller, 1993) and ERDAS Imagine (ERDAS, Inc., 1996). The image digital numbers were converted to reflectance using methods described by Carter *et al.* (1996). Five samples (or clusters) of 400 to 500 pixels were extracted from within each calibrated image. For each individual band, the average of the five clusters represented the spectral mean.

### **3.2.2 Evaluation of Narrow Band Imaging for Spectral Characterization at Sample and Tree Crown Level**

#### **Study Area, Narrow-band Camera Image Acquisition and Foliar Sampling**

On 20 August 1997, NBIC frames were acquired over a 30x30m sample plot near Horni Blatna in the Krusne hory. The sample plot was established at the southern base of a 60m tall radio tower (Figure 3.2). A description of the NBIC system and specifications of the acquisition from the tower are provided in Table 3.3. The system was mounted at the top of the tower with the lens pointed at approximately 10-20 degrees from vertical. From this height, the instantaneous field of view (IFOV) of the camera system at full zoom was roughly 3x3m, with a nominal spatial resolution of approximately 2cm at the center of the oblique frame. The images were not geometrically corrected for distortions in spatial resolution resulting from the very low oblique viewing angle (Figure 3.3). A four-panel spectralon reflectance standard (model SRT-MS-050, Labsphere, Inc., North Sutton, NH) was placed within the sample plot. The four gray levels on the spectralon reference include: 99%, 50%, 25% and 12% reflectance.

The vegetation within the sample plot (Figure 3.3) included: a broadleaf grass (*Calimagrastis vilosa*), raspberry (*Rubus spp.*) and a broadleaf perennial (*Senecio senecio*). Camera images were acquired over each of these background vegetation types. *Rubus spp.* and *Senecio senecio* were in bloom during the acquisition. Foliar samples of the herbaceous vegetation were collected immediately after imaging, including flower heads. Five samples were collected from each understory cover type. The samples were secured in airtight plastic bags and placed on frozen blue ice for short-term storage.

The camera lens was then directed at individual Norway spruce (*Picea abies*) crowns within and surrounding the sample plot. The zoom capability of the camera system

made it possible to capture multispectral video covering specific segments of individual branches within the selected spruce crowns. Images were acquired within three representative crowns, with the lens focused on three separate sunlit (i.e. bright) branches. Images of the reflectance standard were collected regularly throughout the acquisition phase to provide reflectance calibration spectra. Pole pruners were used to remove the imaged branches for laboratory spectral analyses. As with the understory, the removed branches were sealed in plastic bags and stored on ice. The Norway spruce canopy surrounding the tower was classified as DC1 (initial damage).

#### **Narrow Band Camera and GER2600 Spectra Acquisition - Individual Samples**

Laboratory spectra of the understory vegetation and the spruce branches were collected within 12 hours of sampling. Spectra were acquired for each sample using both a GER2600 spectroradiometer (Figure 3.4) and the NBIC. Table 3.3 provides the components and specifications for both instruments. The Norway spruce samples were separated into first, second and third year age classes. Subsamples of herbaceous vegetation and individual spruce branchlets were placed in a non-reflective (black) dish. The dish was illuminated with a hemispherical, tungsten light source. GER2600 spectral measurements were replicated three times, with the sample rotated between each measurement. Periodic measurements of a spectralon standard were collected for reflectance calibration. Post-processing of the GER2600 spectra included averaging at each wavelength of the replicate measurements for a sample and reflectance calibration.

NBIC frames of the herbaceous vegetation and the spruce branchlets were acquired using the same methods as with the GER2600. However, the spectralon panel was included

in the IFOV of the narrow band camera to allow for reflectance calibration. The NBIC filter wheel was fitted with 443nm, 550nm, 675nm, 698nm and 720nm band interference filters.

The camera images from both the tower (NBICt) and the laboratory (NBICs) were digitized using standard commercial software. Each image was inspected for overall visual quality and frames with excessive numbers of saturated pixels were discarded. The digital numbers from the best images were then converted to reflectance using methods described by Carter *et al.* (1996). Spectral signatures were extracted from the herbaceous and branchlet frames by averaging five samples (or clusters) of 400 to 500 pixels each. These “signatures” were then averaged to produce mean spectra for each of the groundcover species and the spruce branchlets. Table 3.4 presents a summary for the spectral data acquired from the 1997 Norway spruce samples.

Ratioing individual bands, seven spectral indices were computed from each data type suggested by previous studies as being sensitive to vegetative stress (Hunt, *et al.*, 1987; Rock, *et al.*, 1988, 1994; Carter, 1994; Chappelle *et al.*, 1992; Gitelson and Merzlyak, 1994; Zarco-Tejada *et al.*, 1999). It is somewhat controversial as to which band combination may be more sensitive to damage. Chappelle *et al.* (1992) suggests 720/675 to be more sensitive to damage, while Carter *et al.* (1996) suggests 720/698. To assess the potential of the different data types, comparisons were made between individual bands and ratios.

The relationships between the GER2600 spectra, the NBICs reflectance values and the NBICt reflectance values were evaluated using pairwise analysis of variance (ANOVA) procedures (SYSTAT:7.0, 1997). The analyses tested for significant differences between the means for individual bands and band ratios (Zar, 1996).

### **3.3 Results and Discussion**

The results presented below are divided into two sections. The first section evaluates the NBIC spectra and the VIRIS spectra acquired during the 1995 sampling campaign. The second section presents results from the 1997 study, comparing GER2600 and NBIC spectra acquired from foliar samples and individual tree crowns.

#### **3.3.1 Damage Evaluation and Sample REIP Properties**

During 1995, seven study sites were sampled representing the full range of decline (Table 3.5). All trees were more than 40 years old. One site supported a healthy stand (DC0), three sites displayed initial damage symptoms (DC1), a single site showed signs of medium damage (DC2), while only one site had severe overstory damage (DC3). A final sample site had experienced full ecosystem collapse (DC4) and supported only dead standing and fallen stems. Canopy closure decreased and percentage of ground cover increased as damage level increased.

Preliminary evaluation of the VIRIS spectra red edge properties established that REIP values from all sites varied between 705nm and 724nm (Entcheva *et al.*, 1996). Table 3.6 summarizes the red edge properties of the spectra acquired by the NBI camera system from two branch samples collected at Site 6. One crown was scored as DC0 and the other as DC1. Visually the two trees displayed slight differences in foliar retention and neither displayed chlorosis. Spectra from the DC0 tree had generally higher REIP values than samples from the DC1 crown (Table 3.6).

### **3.3.2 1995 Evaluation of NBIC Imagery for Initial Stress Detection**

Figure 3.5 provides three NBIC frames depicting a side-by-side comparison of the healthy and initially damaged foliage from Site 6. The branch segments are paired with the healthy sample on the left and the sample from a crown displaying initial damage on the right. At 670nm both the healthy and damaged branch segments maintain a low reflectance due to strong absorption by chlorophyll. At 700nm, the damaged foliage appears to have slightly higher overall reflectance as compared to the healthy foliage. At 720nm, both groups of branch segments are equally bright. Therefore, the 700nm filter appears to provide the greatest potential for initial visual stress discrimination.

When comparing samples from different age groups, the first-year needles appeared brighter for both healthy and damaged foliage at 700nm. The second-year needles appeared very similar across all three wavelengths. The third-year foliage depicted the largest visual contrasts. At both 700 and 720nm, the damaged foliage appeared brighter than the healthy needles. Therefore, third-year needles may provide the highest potential for separation of healthy and initially damaged foliage.

Figure 3.6 shows the relationship between VIRIS and NBIC reflectance measurements. The VIRIS data points represent the mean of the three scans for each of six samples. The VIRIS single bands centered at 670nm, 700nm, and 720nm were used for the comparison and plotting of the 18 data points. ANOVA results revealed a highly significant relationship between the VIRIS and the NBIC data ( $r^2 = 0.83$ ,  $p < 0.01$ ). However, Figure 3.6 shows that the overall NBIC reflectance values are slightly lower than the VIRIS reflectance measurements.

### 3.3.3 Evaluation of the NBIC at the Foliar and Canopy Level, 1997

The following results present analyses of the similarities and differences between the three data sources for both ground cover vegetation and Norway spruce spectra. The three unique sources are: (1) GER2600 spectra for individual samples, (2) NBICs spectra acquired from laboratory imagery of individual samples, and (3) NBICt spectra acquired from tower images of ground cover components and individual branches representative for the tree crown and health condition.

#### Comparison of spectra for representative ground cover components

Figures 3.7a, 3.7b and 3.7c depict the spectral curves for the groundcover vegetation sampled within the 30x30 m plot at the base of the tower. In general, the reflectance data acquired from the tower (NBICt) is higher than the data acquired from individual samples at all bands. The NBICt reflectance values for *C. vilosa* are highly correlated with the reflectance data collected by both the NBICs and the GER2600 (Table 3.7). However, the NBICt spectra for *Rubus spp.* is two- to three-times brighter than either of the laboratory acquired reflectance values (Figure 3.7b). Table 3.7 shows low correlations between the tower spectra and the laboratory spectra for *Rubus spp.* Similarly, the NBICt reflectance values for *S. senecio* are significantly brighter than the laboratory measurements (Figure 3.7c). *C. vilosa* presented a homogenous groundcover, while *Rubus spp.* and *S. senecio* were both flowering, producing a mixed spectral response.

These results suggest that both NBICs and NBICt measurements collected from the more homogenous component compared better, and that the spectral variations within cover type may present difficulties for obtaining reliable narrow band spectra.



### **Comparison for Norway Spruce Samples**

Figure 3.8 compares Norway spruce spectra acquired in the laboratory with the GER2600, the NBICs and the NBCSt. As with the groundcover, the spectral data from the NBICs have higher reflectance values as compared to the GER2600 at all bands. The differences are likely due to both the unique spectral and optical properties of the instruments. The NBICs data were calibrated to reflectance based on the manufacturer's specifications of the gray scale spectralon panel. GER2600 data were calibrated using a white spectralon panel. No direct cross-calibration between instruments was performed. This is likely contributing to the reflectance differences.

The variation within data was band-specific for both instruments, with larger variation seen for the NBICs at bands 550nm and 720nm (Table 3.8a). Comparing means from individual bands between the GER2600 and NBICs found high correlations at bands 675nm, 698nm and 443nm (Table 3.9a). The reflectance at bands 675nm and 698nm had the least variation within data (Table 3.8a) for both GER2600 and NBIC. It appears that the variation within data is smaller at the bands strongly associated with chlorophyll absorption.

The results for the band ratios are presented in Table 3.8b. The NBICs spectral indices had comparatively larger variations, with greatest deviations for 720/675, 720/550 and 550/675. When comparing the ratio means for the GER2600 and the NBICs, it appears that results are similar. For the 720/698 and 720/675 indices, it appears that 720/698 provides results more closely comparable to the GER2600 results, suggesting a higher potential of the ratio for across-instruments comparisons. Comparing GER2600 data with the NBICs, the ratios 720/698, 720/675, 720/550 and (675-550)/720 were not

statistically different (Table 3.9b). These findings illustrate the potential of narrow band ratios from samples to provide similar results to those obtained with the spectroradiometer.

### **Comparison Between data obtained at tree foliar and canopy level**

The NBICt reflectance values are much higher than the GER2600 and the NBICs spectra at all wavelengths (Figure 3.8). However, the general trend of the data acquired at the tree canopy level is similar to the spectral response obtained at sample level. NBICt data for individual bands were found statistically different and strongly correlated with the data from samples for both NBICs and GER2600 (Table 3.9a). This indicates the potential of the NBICt approach for across scale comparisons. The band correlations between the NBICt and the GER2600 were generally higher as compared to the band correlations between NBICt and NBICs (Table 3.9a). This difference could be due in part to the larger variation seen within the NBICs data (Table 3.8a). The differences in the calibration procedures for the NBICs and the NBICt may also explain the lower correlations. The NBICt spectra were calibrated to reflectance using the gray scale panel made at SSC by Carter (Carter *et al.*, 1996). Therefore, a direct NBICt to GER2600 data calibration was obtained by measuring the spectral properties of the gray scale panel with the GER2600. A direct calibration was not performed for the NBICs and NBICt spectra.

There was no statistically significant difference for the ratio 720/675 between the GER2600 and NBICt (Table 3.9b). All other indices were significantly different. The high correlation between indices from the two data sets implies that the narrow band system can provide spectra similar to that of the spectroradiometer.

When comparing data between NBICs and NBICt, no statistically significant differences were found for band ratios (Table 3.9b) with the exception of 443/698, which was significantly different but strongly correlated.

These results demonstrate the potential of the narrow band system to provide data comparable to field spectrometer results at the sample and at the tree canopy level.

#### **Overall comparison between bands and ratios**

Comparison of the slope of the relationship among bands with the relationship among indices (Figure 3.9a, 3.9b and 3.9c; Table 3.10) revealed that the indices have a slope closer to 1 in all cases, while the slope of the individual bands is steeper. These results indicate a higher potential of the indices for data comparisons across scales and instruments.

### **3.4 CONCLUSIONS**

The narrow band imaging camera system allowed for visualization of the vegetation spectral changes in red edge parameters occurring between healthy foliage and initially damaged foliage.

The narrow band camera provided data comparable to the field spectrometer measurements within spectral bands associated with chlorophyll absorption. Band ratios computed from the narrow band camera spectra correlated better with the spectrometer data as compared to the individual spectral bands at both the foliar and the tree canopy level. These results demonstrate the high potential of spectral indices for across-instruments and across-scales comparisons, suggesting a high capability of the NBIC for forest stress detection and monitoring.

**Further research should evaluate the capability of narrow band imaging for stress detection by comparing spectral data over multiple damage classes and multiple sites. The application of vegetation indices and the red edge properties for Norway spruce stands should be emphasized.**

Damage Class	Code	Percent Defoliation (%)	Forest Health Status	
			without chlorosis	with chlorosis
Healthy	0	0 – 10	Healthy	Initial damage
Initial	1	11 – 25	Initial damage	Medium damage
Medium	2	25 – 60	Medium damage	Heavy damage
Severe	3	60 – 99	Heavy damage	Forest ecosystem collapse - Dead
Dead	4	100	Forest ecosystem collapse - Dead	Standing dead forest

**Table 3.1: Forest damage evaluation criteria and damage level assignment**

Specification	Sources of spectral data, August 1995		
	VIRIS <sup>1</sup> (dual beam)		NBIC
Spectral bandwidth (at full width half-max)	2nm 4nm	300-1000nm 1000-3000nm	10nm (+-5nm of band center)
Spectral region used/ Bands/filters used	300-1000nm		670nm, 700nm, 720nm
Spatial resolution	2x4cm; nadir		15x15cm FOV; pixel size ~2mm; nadir
Light source	300W tungsten hemispherical lamp; 45° angle of incidence with sample		
Calibration source	Spectralon <sup>3</sup> white	Spectralon <sup>4</sup> - 4 shades of gray from white to black	
Distance from sample/ Tower height	45cm		45cm

<sup>1</sup> Visible Infra-Red Intelligent Spectroradiometer (VIRIS, MARK IV; Geophysical Environmental Research Corp., New York, New York)

<sup>2</sup> Narrow Band Imaging Camera (NBIC; Imager Sony XC-77 video camera, RS-170 analog output)

<sup>3</sup> Spectralon reflectance reference SRT-99-050 (Labsphere, Inc., North Sutton, NH)

<sup>4</sup> Spectralon reflectance reference model SRT-MS-050, comprised of 4 gray levels: 99%, 50%, 25% and 12% reflectance (Labsphere, Inc., North Sutton, NH)

**Table 3.2: Instruments and data acquisition parameters, Czech 1995**

Specification	Sources of spectral data, August 1997			
	GER2600 <sup>1</sup> (single beam)		NBICs <sup>2</sup>	NBICt <sup>2</sup>
Spectral bandwidth (at half-max full width)	2.5nm 11.5nm	300-1050nm 1050-2500nm	10nm	10nm
Spectral region used/ Bands filters used	300-1050nm		443nm, 550nm, 675nm, 698nm, 720nm	
Spatial resolution	3°FOV – 6x5cm diameters; nadir		15x15cm FOV; 2mm; nadir	Skewed, ~2cm, 10-20° off nadir
Light source	Tungsten hemispherical lamp, 45° angle of incidence		Solar, imaging within 1hr of solar noon	
Calibration source	Spectralon <sup>3</sup> white		Spectralon <sup>4</sup> - 4 shades of gray from white to black	Grey scale <sup>5</sup> , 5 cards, shades of gray from white to black
Distance from sample/ Tower height	50cm		60m	

<sup>1</sup> GER2600 (Geophysical Environmental Research Corp., New York, New York)

<sup>2</sup> Narrow Band Imaging Camera (NBICs-samples/ NBICt-tower; NBIC developed at SSC, specifications in Carter et al., 1996; Components: Sony XC-77 video camera, 50mm telephoto lens, Narrow band filters, BW monitor, VHS video cassette recorder, 12V battery, VHS video tape)

<sup>3</sup> Spectralon reflectance reference SRT-99-050 (Labsphere, Inc., North Sutton, NH).

<sup>4</sup> Spectralon reflectance reference SRT-MS-050, comprised of 4 gray levels: 99%, 50%, 25% and 12% reflectance (Labsphere, Inc., North Sutton, NH)

<sup>5</sup> Grey scale was composed of 5 cards ranging from white to black, card reflectance in the 670-760nm range was 88%, 28.9%, 9.8%, 4.5% and 2.5%; Scale prepared and calibrated to reflectance at SSC, MI (Carter et al., 1996)

**Table 3.3: Instruments and data acquisition parameters, Czech republic 1997**

Sample unit	Instrument and data acquisition level (sample vs. branch/crown)					
	GER2600 - branch samples		NBICs - branch samples		NBICt - tower, individual branches	
	# samples	# scans	# samples	# spectra	# samples	# spectra
Tree crowns	3		3		3	3 images
Branches per tree	1		1	3 images	1	9, 9, 9 spectra/branch
Ages of needles sampled	1 2 3	3 3 3	3 3 3	9 9 9	- - -	not possible to separate age classes
Total acquired	9	27	9	27	3	27

**Table 3.4: Foliar and spectral reflectance data acquired in August 1997.** The data was acquired for the comparison between foliar to branch/crown level between the GER2600 spectrometer and NBICs

Site Number	Elevation (meters above msl)	Damage Class		Stand Age (years)	Canopy Height (m)		Canopy Closure (%)	Ground Cover (%)
		Photo	Field		Mean	St.Dev.		
1	950	0	0	75	15.8	1.52	93	8
2	980	1	1	70	16.1	2.41	59	32
3	975	3	2/3	110	18.4	3.76	70	85
4	1150	4	4	120	13.4	3.45	35	100
5	950	-	3	85	12.9	1.27	55	75
6	935	0	0/1	40	15.3	2.5	90	0
7	920	2	1	70	19.4	2.13	83	70

**Table 3.5: Forest site characteristics, Czech Republic 1995**



Tree damage level Field evaluation	Year	REIP	Std. Error	Std. Dev.
0	1	720.5833	0.91	1.57
0	2	721.1067	1.05	1.81
0	3	721.1067	1.38	2.4
1	1	716.92	1.62	3.43
1	2	721.63	1.27	3.14
1	3	718.4867	1.81	3.27

**Table 3.6: Red edge inflection point (REIP) of the samples selected for NBIC evaluation, Czech 1995**

Species	GER2600 vs. NBICs		GER2600 vs. NBICt		NBC Samples vs. NBICt	
	r	p(<=)	r	p(<=)	r	p(<=)
<i>Calimagrostis vilosa</i>	0.93	0.02	0.89	0.01	0.97	0.01
<i>Rubus spp.</i>	0.95	0.01	0.64	0.23	0.59	0.29
<i>Scenecio scenecio</i>	0.81	0.18	0.72	0.04	0.43	0.42

**Table 3.7: Relationship between spectra for ground cover components (ANOVA)**

a.

Spectral Bands	GER2600			NBIC Samples			NBIC Tower		
	Mean (%)	St. Dev.	St. Err.	Mean (%)	St. Dev.	St. Err.	Mean (%)	St. Dev.	St. Err.
443	2.2	0.66	0.22	6.6	10.7	0.20	18.2	2.28	.072
550	4.9	1.41	0.47	16.9	9.37	1.74	31.2	4.45	1.41
675	2.5	0.74	0.25	7.5	1.11	0.21	10.1	1.77	0.56
698	5.4	1.54	0.51	11.2	1.87	0.35	15.19	1.35	0.43
720	13.2	4.08	1.36	32.1	11.92	2.21	47.2	5.30	1.68

b.

Spectral Indices	GER2600			NBIC Samples			NBIC Tower		
	Mean	St. Dev.	St. Err.	Mean	St. Dev.	St. Err.	Mean	St. Dev.	St. Err.
720/698	2.4	0.12	0.04	2.8	0.71	0.13	3.1	0.39	0.12
720/675	5.3	0.55	0.18	4.4	1.80	0.33	4.8	0.91	0.29
720/550	2.7	0.12	0.04	2.3	1.24	0.23	1.5	0.18	0.06
(675-550)/720	-0.2	0.02	0.01	-0.3	0.18	0.03	-0.5	0.05	0.02
550/675	2.0	0.16	0.05	2.2	0.98	0.18	3.1	0.38	0.12
443/698	0.4	0.03	0.01	0.6	0.18	0.03	1.2	0.05	0.02
698/675	2.2	0.15	0.05	1.5	0.36	0.07	1.5	0.16	0.05

**Table 3.8: Comparison among mean values of spectral bands (a) and spectral indices (b)**

a.

Spectral Bands ( nm )	GER2600 vs. NBICs		GER2600 vs. NBICt		NBICs vs. NBICt	
	r	p-value	r	p-value	r	p-value
443	0.89	< 0.001	0.98	< 0.001	0.96	< 0.001
550	0.56	0.001	0.97	< 0.001	0.60	< 0.001
675	0.90	< 0.001	0.94	< 0.001	0.66	< 0.001
698	0.82	< 0.001	0.96	< 0.001	0.71	< 0.001
720	0.61	< 0.001	0.97	< 0.001	0.54	< 0.001

b.

Spectral Indices	GER2600 vs. NBICs		GER2600 vs. NBICt		NBICs vs. NBICt	
	r	p-value	r	p-value	r	p-value
720/698	0.22	0.181	0.77	< 0.001	0.23	0.143
720/675	0.23	0.155	0.31	0.193	0.11	0.491
720/550	0.16	0.333	0.97	< 0.001	0.29	0.071
(675-550)/720	0.24	0.138	0.96	< 0.001	0.43	0.005
550/675	0.10	0.542	0.89	< 0.001	0.44	0.005
443/698	0.49	0.002	0.99	< 0.001	0.85	< 0.001
698/675	0.64	< 0.001	0.90	< 0.001	0.02	0.956

**Table 3.9. Comparison among mean values of spectral bands (a) and spectral indices (b) (ANOVA)**

	Sample Size (n)	GER2600 vs. NBICs		GER2600 vs. NBICt		NBICs vs. NBICt	
		r	p-value	r	p-value	r	p-value
Bands	5	0.93	0.005	0.88	0.046	0.95	0.011
Indices	7	0.97	< 0.001	0.87	0.010	0.94	0.001

**Table 3.10. Overall comparison among mean values for all spectral bands and for all spectral indices (ANOVA)**

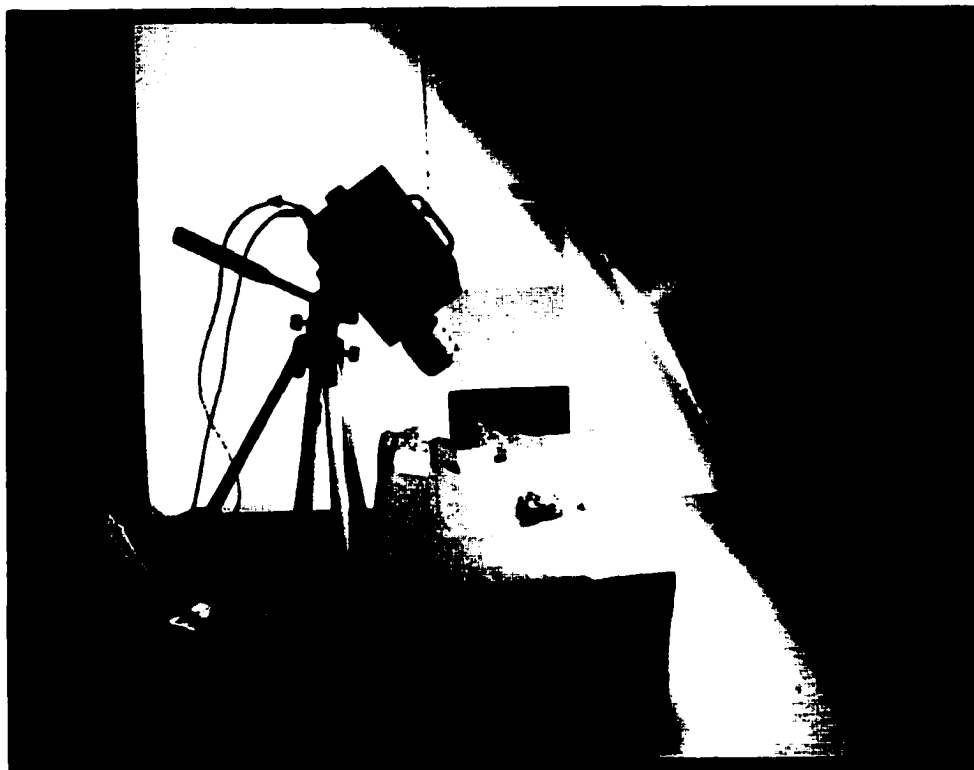


**Figure 3.1: Narrow Band Imaging Camera System (NBIC; NASA SSC, Mississippi).**

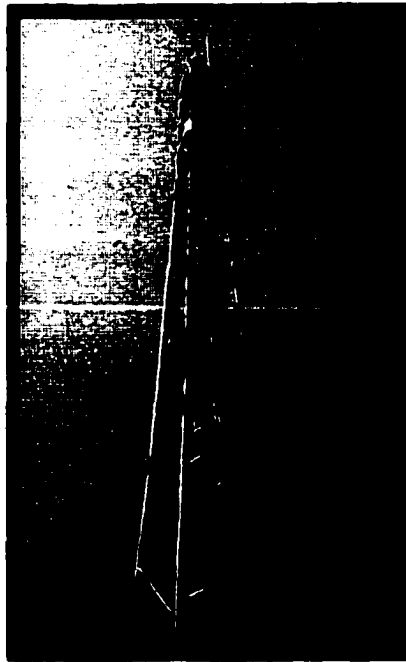


**Figure 3.2: The radio tower used for NBICt acquisition. 60m radio tower located in the area of Horni Blatna, Czech Republic, 1997.**



**Figure 3.3: View of a 30x30m plot outlined in the foot of the tower. The tree canopies sampled are not within the plot.**

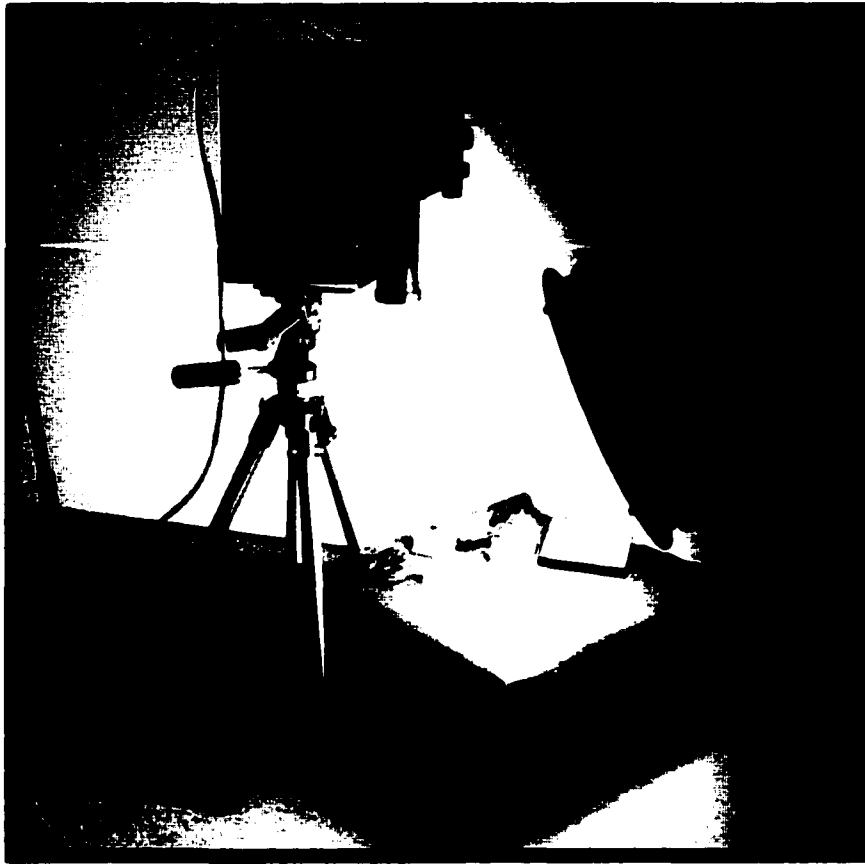


**Figure 3.4: GER2600 Spectroradiometer. Samples of first second and third year of needles were placed vertically in the field of view of the instrument for spectral scanning. For conversion of the spectra to reflectance periodically was scanned a white spectralon panel**

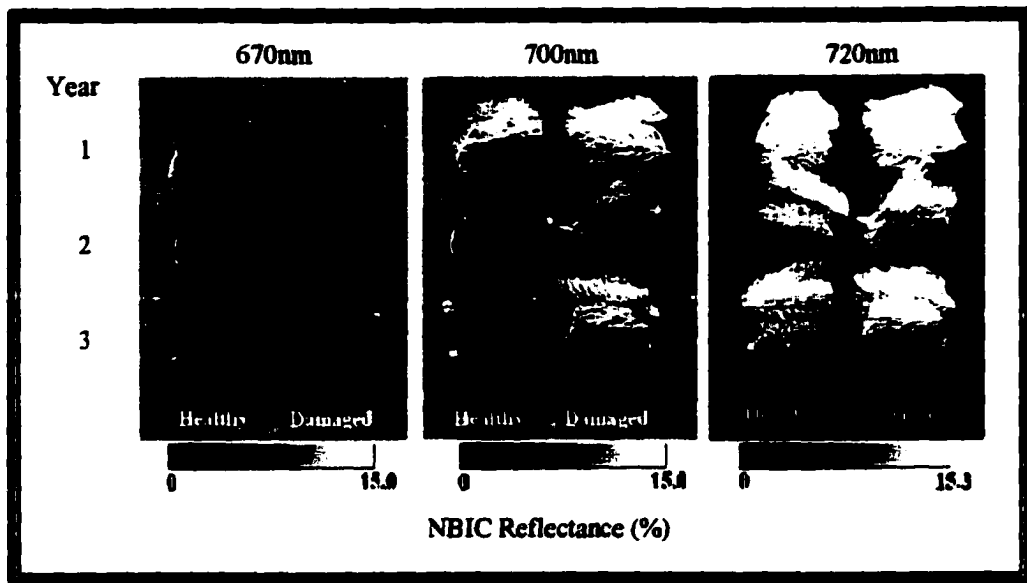


**Figure 3.5:** NBIC images of spruce branch segments from healthy (on left) tree and tree with initial symptoms of decline (15% foliar loss) on right. Reflectance spectra from the samples were obtained by measurements with the VIRIS. The branch segments on the images were sampled to obtain NBIC estimates of spectral reflectance.

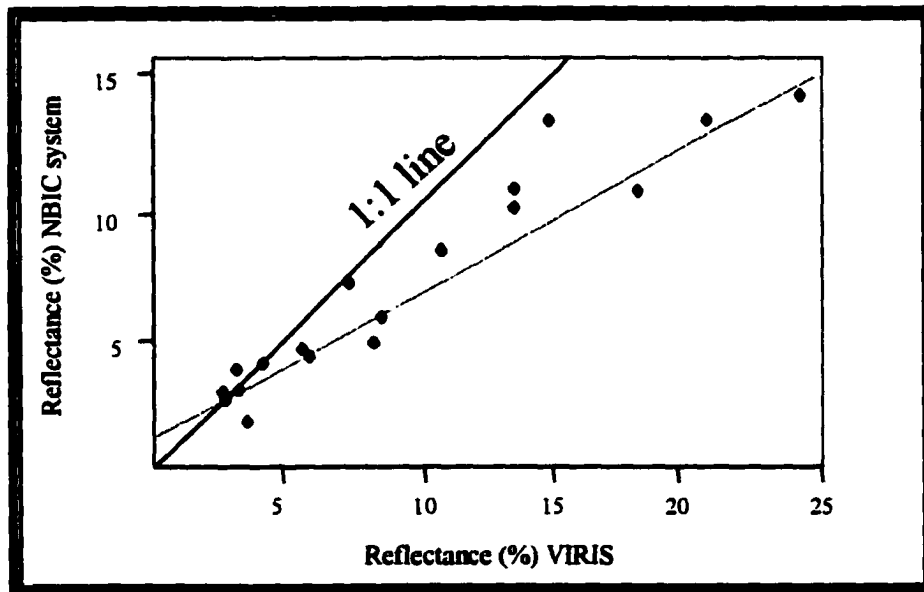


**Figure 3.6:** Relationship between VIRIS reflectance measurements and spectral values derived from the NBIC system and calibrated to reflectance. Analysis of the variances (ANOVA) comparing the estimates shows statistically significant difference between the means, and strong correlation between VIRIS and NBIC estimates.



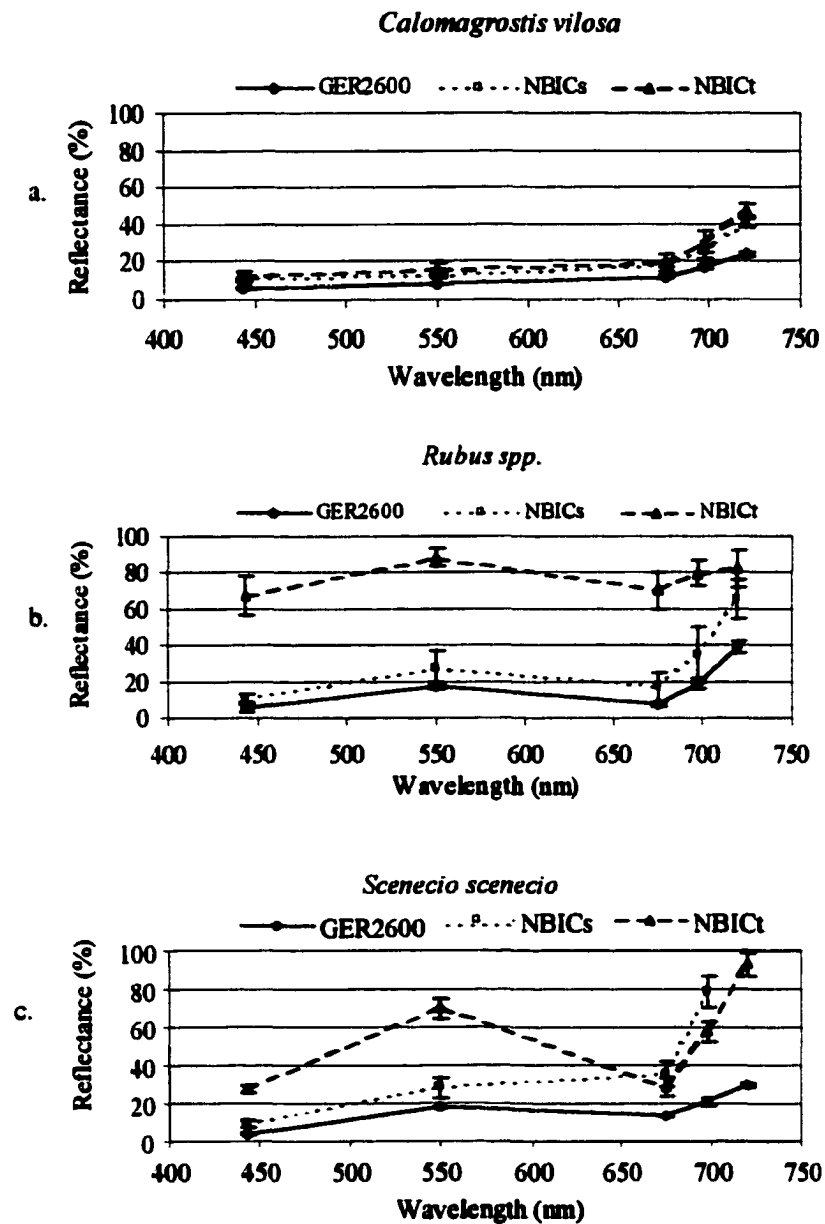


**Figure 3.7: Reflectance spectra from understorey composition. Plotted are means and standard deviations. The spectra homogenous cover of *Calomagrostis vilosa* (a) compared closer than the data from *Rubus spp.*(b) and *Scenecio sp.* (c), where there were present flowers and dry twigs.**

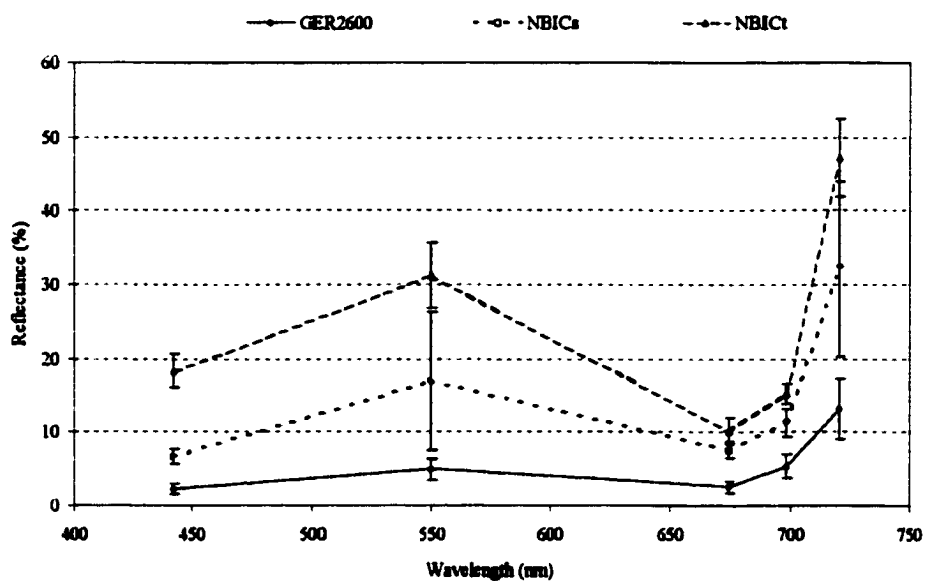


**Figure 3.8: Reflectance data obtained from individual samples and tree crowns using the GER2600, NBICs (samples) and NBICt (tower). Plotted are means and standard deviations.**

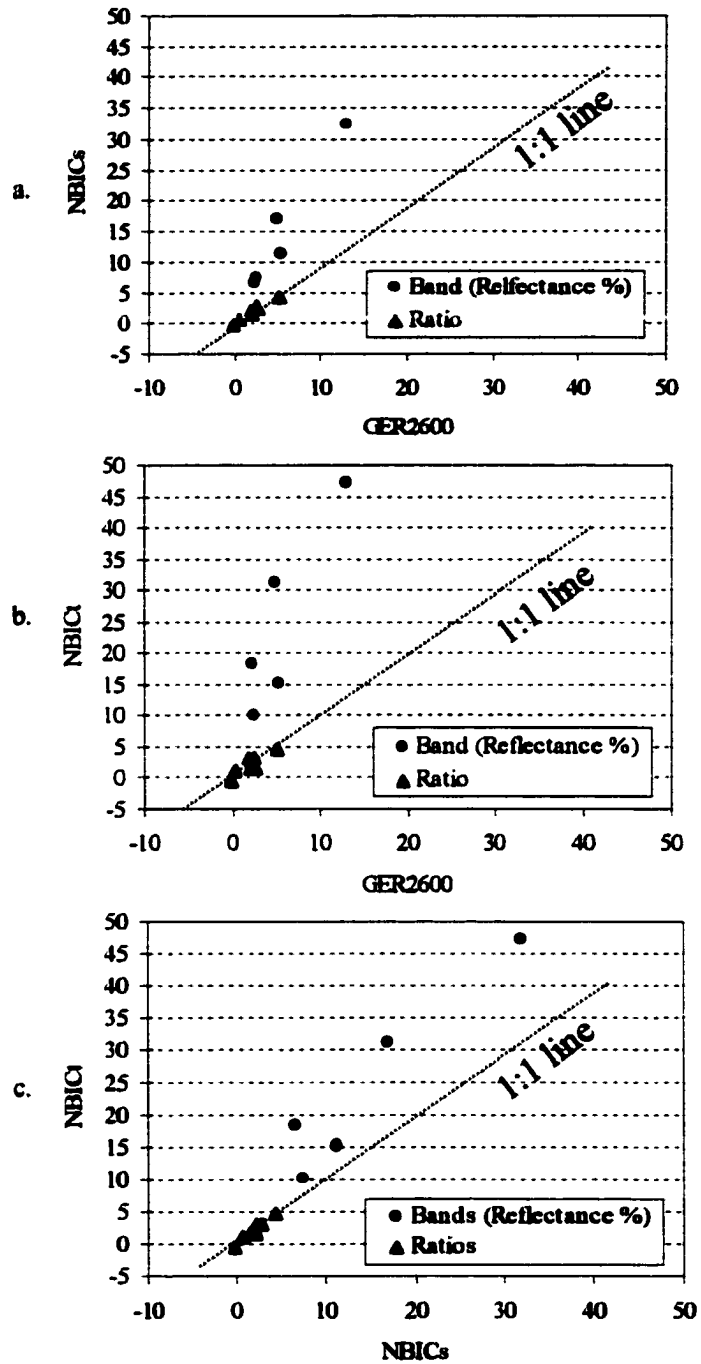


**Figure 3.9: Overall comparison between all bands and ratios.**  
 (a) GER2600 vs. NBICs, (b) GER2600 vs. NBICt, and (c) NBICs vs. NBICt.

## Chapter 4

### **SPECTRAL AND BIOCHEMICAL PROPERTIES OF NORWAY SPRUCE FOLIAGE SAMPLES FROM A RANGE OF DAMAGE CONDITIONS**

#### **4.1 Introduction**

The high elevation forests located in northern Bohemia along the borders of the Czech Republic, Germany and Poland grow in one of the most heavily polluted regions of the world (Materna, 1989; Klasterska, 1991; Klimont *et al.*, 1993). Within northwestern Bohemia, the Krusne hory mountains offer a unique opportunity to study the full gradient of forest decline conditions within a simple, homogeneous Norway spruce ecosystem located along a single mountain plateau (Figure 4.1). Exposure to severe levels of air pollution (mainly SO<sub>2</sub>) over the past 40 years is the major factor responsible for the forest damage (Materna, 1989; Kubikova, 1991; Kubelka *et al.*, 1993). Norway spruce (*Picea abies* (L.) Karst.) is the dominant tree species in these mountains, and extensive clear cutting of damaged and dying trees has resulted in a sharp decline in the area covered by forest (Materna, 1989; Rock *et al.*, 1994).

Foresters recognize a total of five levels of forest decline in Norway spruce stands based on ground assessment and/or aerial photo interpretation of percent foliar loss (Table 4.1). Chlorosis, when present, is noted in ground-based assessment, and is used to assign a higher damage class (DC) to a given tree than the DC determined by foliar loss alone. Landsat Thematic Mapper (Landsat<sup>TM</sup>)-based assessment of forest damage conditions is unable to separate the initial stages of forest damage (DC1) in the Krusne

hory (Lambert *et al.*, 1995). Current field-evaluation methods of assigning damage classes to individual trees or forest stands based on visual assessment of foliar loss vary by country and largely depend on the qualification of the forester performing the evaluation. Therefore, they are limited as a tool for obtaining ground validation data on a large scale for evaluating the accuracy of satellite-based damage assessments (NAPAP, 1990). Remote sensing in narrow spectral bands could provide the accurate and efficient means required for monitoring forest health conditions (Rock *et al.*, 1986; Vogelmann and Rock, 1988; Miller *et al.*, 1990; Zarco-Tejada *et al.*; 1999).

Vegetation spectral properties are determined by foliar pigment levels, cellular structure, water content and biochemical components (Rock *et al.*, 1986, 1988; Martin and Aber, 1997). As unfavorable growth conditions (such as air pollution damage) cause tree physiological stress and foliar chlorophyll content decline, needle reflection typically begins to decrease in red and blue-green (Waring *et al.*, 1998; Rock *et al.*, 1986; Vogelmann *et al.*, 1986; Carter *et al.*, 1996). Consequently, the foliar reflectance of the incident radiation in the visible spectrum increases, providing an optical indicator of stress. Leaf spectral properties in the visible and visible/near-infrared portion of the spectrum (450-720nm) are governed mostly by pigment concentration, with the strong absorption feature in the red at approximately 680nm associated with chlorophyll concentration (chlorophyll *a* and *b*). The relative change in reflectance due to stress in the 450-720nm region is reported to be maximal at 535-640nm and 685-700nm, suggesting a high potential for damage detection using these spectral regions (Carter, 1994). Thus, monitoring of vegetation vigor based on remote sensing estimates of pigment levels may allow damage detection in the early stages of ecosystem stress before extensive foliar loss occurs.

**Chlorophyll and carotene concentration change and additional pigments (e.g. tannins) may build within the leaves in response to stress affecting the spectral properties of the vegetation foliage (Rock *et al.*, 1986; Vogelmann and Rock, 1988; Moss *et al.*, 1998). Foliar chemistry is considered to be a reflection of the growing conditions to which the trees were subjected at the time of needle formation, as cell wall composition is unlikely to change over time as growing conditions degrade or improve (McNulty *et al.*, 1991). Thus, monitoring of vegetation vigor based on estimates of chlorophyll levels may allow damage detection in the early stages of ecosystem stress, while using spectral estimates of foliar chemical constituents may be more indicative of long-term vegetation health.**

**For coniferous species such as Norway spruce, foliage age is an inherent factor influencing the analyses. A needle-age dependency of chlorophyll concentration has been previously reported (for Norway spruce in decline) with the current-year of needles having lower concentrations than the older needles (Lichtenthaler, 1988). Fumigation appeared to accelerate the differences in needle chlorophyll content appearing with age. Therefore, when conducting damage assessment analysis at the foliar level it is important to consider the normal differences occurring with needle age.**

**Remote sensing methods for documenting and monitoring forest conditions at the foliar and stand level are needed, since the visual assessment methods are subjective, very labor intensive, costly and time consuming. Evaluation of the remote sensing methods for characterizing foliar and stand conditions based on amount of foliar constituents, especially separation of subtle changes in initial damage level, could**

provide the needed base for establishing more accurate forest health evaluation procedures.

The major goals of the study were:

1. characterization of spectral and foliar properties associated with Norway spruce forest health conditions, and
2. evaluation of remote sensing techniques for separation of forest damage.

Specific objectives include:

- to characterize significant changes in foliar constituents and spectral signatures which may occur with increase in damage level for first-, second- and third-year Norway spruce needles;
- to determine the spectral regions most sensitive to initial symptoms of forest damage;
- to identify the spectral indices most useful in separating the range of decline conditions present in the Krusne hory, and
- to assess the relationship between spectral indices and foliar constituents.

## **4.2 Methods and Analytical Procedures**

### **4.2.1 Forest Ground Assessment Activities**

#### **Forest health evaluation**

Forest condition was assessed during July and August of 1998 using methodology for evaluating individual trees crowns (Table 4.1) established for use with CIR photography and forest field survey (Hildebrandt and Gross, 1992). As in terrestrial forest health inventories, five damage levels can be distinguished using this methodology. Level

0 indicates “healthy” (no visible damage symptoms) level 4 indicated “dead” (Figure 4.2). Determination of damage class (DC) includes evaluation of: (1) crown thinning characteristics and foliar loss: healthy 0-10%, initial damage 11-25%, intermediate level 26-60%, heavy damage 61-90%; (2) crown type (for spruce: brush, comb or plate), form and shape; (3) presence/absence of chlorosis (yellowing of the needles due to chlorophyll loss; and (4) foliar retention of individual branches. Since the focus of the current research is on the separation of the initial stages of forest decline, damage level 4 stands (nearly dead) were excluded from the study.

### **Site and Tree Selection**

Using 1996 Landsat TM imagery, 1997 color infrared (CIR) aerial photography (1:25 000) and forestry maps (1:5000), homogenous Norway spruce (*Picea abies*) forests were selected that were larger than 5ha, had similar site characteristics and were located within the elevation gradient 900-1000m above sea level.

During forest health evaluation, both stand and tree damage conditions were determined and the forests were classified into four categories (Table 4.1). For evaluation and foliar collections within the research areas, 53 intensive (30x30m) research sites were selected randomly within the Krusne hory mountains. The sites were assigned to damage class as follows: 15 DC0, 12 DC1, DC2 and DC3 (2 sites were not sampled). The center of each site was permanently marked, located on a topographic map and georeferenced using a GPS unit. In each of the sites, stand structure and tree damage class were characterized. Table 4.2 represents the full list of field measurements performed. Within a 11.3m radius circular plot located at the center of the study site, forest stand parameters such as stand density, biomass, basal area (BA), tree diameter at breast height (DBH), tree



height and canopy closure were measured. Five overstory trees representative of the stand damage level and forest growth parameters were selected and marked permanently with aluminum tags. These five trees were used further for foliar sample selection and tree increment cores collection.

#### **Collection and analysis of tree increment cores**

To evaluate forest growth trends across the damage gradient in the Krusne Hory, radial tree increment cores were taken at breast-height from the five representative trees from each of the intensive study sites. Multiple cores were taken from some trees due to rot or other wood defects. The total number of usable increment cores collected in 1998 was 246 (57 from DC0, 61 from DC1, 69 from DC2, and 60 from DC3). In the field, cores were labeled, placed in plastic straws and refrigerated at 6-7 C°. Upon return to the University of New Hampshire, the cores were supported on corrugated cardboard until air-dried and glued into grooved wooden blocks. Care was taken to orient the transverse surface of each core parallel to the surface of the wooden mount. Mounted cores were sanded using 150 grit and 220 grit sandpaper. Ring widths were measured to the nearest 0.01mm using a movable stage equipped with a digital output device. Ring width series were crossdated and checked for consistency and outliers using Cofecha software. Increment cores containing outlier ring width series were remeasured.

To evaluate growth trends, ring width series were first separated into age and damage classes and then bootstrap averages and 95% confidence intervals were calculated (Cook, 1992). The bootstrap confidence intervals are robust over a wide range of statistical estimation problems (Monsteller and Tukey, 1977). Regional climate data

covering the period from 1963 to 1995 and regression procedures were used for assessing the effects of precipitation and temperature on tree growth.

#### **4.2.2 Sample Collections**

Foliar sampling was conducted at all 53 intensive study sites between August 15 and 28. At each plot, foliar samples for laboratory analysis of chemical constituents and spectral characterization were collected from five representative trees. Branch samples were collected from the middle third portion of the active tree crown. Because needle retention is related to state-of-health, collection of needle material focused on 1st, 2nd and 3rd year needles. Two separate sets of foliar samples from the same branch were collected – one set for spectral analysis and another set for determining foliar pigment levels.

#### **4.2.3 Pigment analysis**

For chlorophyll assessment (chlorophyll a, chlorophyll b, total chlorophyll and carotenoids) needles were collected (by tree and age classes) and placed in 80% v/v acetone distilled water at the time of the collection. The vials were kept frozen for 12-24 hours. During that time the samples were taken to the laboratory for pigment extraction. For the analyses, the facilities of the Dept. of Plant Physiology at Charles University, Prague were used. For pigment extraction, a 5-day procedure ensuring 97% efficiency of pigment extraction was applied (Šolcová, 1999). For computations of the concentrations of chlorophyll *a* and *b* and total carotenoids, equations suggested by Wellburn (1994) were used. In this paper we present our statistical analysis and evaluation of the results for the pigment data.

#### **4.2.4 Spectral reflectance measurements of fresh foliage**

The set of samples collected for spectral analysis were immediately sealed in plastic bags with wet paper towels, placed on ice in coolers and taken to the field laboratory within two to four hours of collection. One, two and three year old branch segments were identified, separated and arranged in trays. Spectral reflectance data for the samples were recorded using a GER2600 Visible Infrared Spectrometer set up in a controlled environment, using a constant tungsten light source (Rock *et al.*, 1994). To limit the effects of scattering due to needle arrangement, three measurements were taken from each sample, rotating the sample 90° after each scan. The 3 spectral reflectance measurements from each sample were averaged at each wavelength.

#### **4.2.5 Analysis of air dry foliage for determination of foliar chemical constituents**

Bolster *et al.* (1996) have developed equations for determining foliar constituents in healthy Norway spruce foliage. The process includes two steps: (1) NIR spectral measurements and chemical analysis, and (2) development of calibration equations for predicting foliar chemical constituent levels. Since our sites represent an extreme gradient in forest damage conditions, the development of new equations was required to account for the possibly larger range in foliar chemical constituents.

##### **NIR spectral measurements and chemical analysis**

To determine chemical constituent levels (e.g. lignin, cellulose, nitrogen), after the fresh samples were scanned with the GER2600 spectrometer they were transferred by age class of needles into labeled paper bags, air-dried and transported to the University of New Hampshire (UNH). At UNH the samples were ground in a Wiley mill to 1mm

particles and homogenized. Prior to analysis the samples were dried in a forced-air convection oven at 70°C for 15 hours and cooled to room temperature in desiccators. Immediately after that, the samples were scanned on a NIR\_Systems 6500 monochromator (NIR\_Systems Inc., Silver Spring, MD) following the procedure described in Bolster *et al.* (1996). The spectrometer scans at wavelengths from 400 to 2498nm at 2nm intervals with a bandwidth of 10nm. Because absorbance is directly proportional to the concentration of absorbing chemical constituents of a sample, a transformation of reflectance data (R) to apparent absorbance (A) ( $A = \log(1/R)$ ; Williams and Norris, 1987) is done automatically within the software prior to storing the spectral values. The software used for both data collection and analysis is ISI Version 3 (Infrasoft International Software; Silver Spring, MD).

A set of samples representing the full range of damage conditions were selected for lignin and cellulose estimation from the processed and scanned samples for chemical analysis. A total of 42 samples from first- and third-year foliage (year 1998 and 1996) were selected. Prior to the analyses, the samples were oven dried at 70°C for 24 hours and kept in desiccators. Carbon constituent analyses were performed using a series of extractions following the methods described in details by Newman *et al.* (1994). Data for non-polar, polar, lignin and cellulose compounds were obtained. Organic non-polar components such as fats, waxes and other organic soluble materials were removed by boiling two grams of sample material in dichloromethane for five hours. With this process a large amount of the pigments present in the tissue were also extracted. Polar compounds such as phenols, simple sugars, starch and simple amino acids were extracted by boiling a sub-sample of 1.5g of tissue from the non-polar analysis for three hours. Acid soluble compounds (cellulose) were extracted by digesting a 0.5g subsample from

the post-polar tissue into 7.5ml 72% sulfuric acid for 1 hour in a 30°C water bath, then diluting the samples 28:1 with de-ionized water and boiling (4 hours). At the end of the process the samples were filtered. The residual material was considered lignin. The mass lost during digestion was considered cellulose (Newman *et al.*, 1994). Using this method, foliar constituents are determined as relative percentages of the initial sample weight and the total of foliar lignin, cellulose, polar and non-polar constituents amount up to 100%.

For laboratory measurement of nitrogen levels, 45 samples covering the extent of damage were processed at the Analytical Laboratory; Department of Plant, Soil and Environmental sciences; University of Maine; Orono, Maine.

#### **Analysis of NIR absorbance spectra for estimation of foliar chemistry**

First and second derivatives of absorbance were calculated, and 3-, 4-, 6- and 8-step smoothing were applied to the data as “pre-treatment” to eliminate spectral offset variations. This eliminated linear spectral trends and reduced the interference among spectral components with regard to wavelength (William and Norris, 1987).

During a calibration process, the relationship between the NIR absorption data and the set samples with known/determined chemical composition was established. Following the NIR procedures, the relationship between absorbance values ( $\log(1/R)$ ) and the reference data is an approximation product of regression analysis (Williams and Norris, 1987).

One calibration equation was developed for estimating nitrogen and another for estimating lignin, cellulose, polar and non-polar constituents. In this study, two methods for developing calibration equations for prediction of lignin, cellulose, nitrogen, polar and non-polar components were tested: (1) stepwise multiple linear regression (SMLR), and (2) partial least-squares regression (MPLS) (Williams and Norris, 1987). The MPLS

procedure proved to be optimal and was used for developing both calibration equations. The prediction ability of the method was measured in terms of standard error of calibration (SEC) and standard error of prediction (SEP). The combination of pre-treatment and regression method producing lowest SEC and SEP was selected for the analysis.

Precision calibration and validation statistics for the developed equations are provided in Table 4.3. Figures 4.3 (a), (b) and (c) present regression statistics, and Figures 4.4 (a) and (b) the estimates for foliar constituents derived using: (1) the ACCP (1994) equation, and (2) the Czech98 equations developed with this study. The coefficient of determination ( $r^2$ ) and the standard error of prediction (SEP) allow for a comparison of the performance of the cellulose, lignin and nitrogen equations. Because the Czech98 calibration equations exhibited a constantly higher performance (higher  $r^2$  and lower SEP) they were used to estimate foliar chemical constituent levels for the dry foliage dataset.

Figures 4.3 (c) and (d) present regression and precision statistics for polar and non-polar constituents. The coefficient of determination for non-polar (e.g. waxes) constituents is relatively low – the lowest for the Czech98 analysis, indicating lower performance of the calibration equation and potentially lower precision of the estimates for this constituent.

#### **4.2.6 Spectral analysis of fresh foliage using GER2600 data**

Reflectance differences were computed by subtracting the mean reflectance at each wavelength of healthy from damaged samples. To determine the relative change or sensitivity of needle reflectance to the damage, the reflectance differences of DC1, DC2 and DC3 were divided by the reflectance of the DC0 level (Carter, 1993). Reflectance

differences and sensitivity for averaged across age groups spectra (to tree level) were also computed. The relationship between the decline conditions and foliar reflectance properties at tree level was evaluated by statistical comparisons of the damaged needles to the healthy (DC0). The significance level (significant  $p \leq 0.05$ ; highly significant  $p \leq 0.01$ ) of the reflectance differences at each wavelength was determined by ANOVA and the Tukey-Kramer pairwise mean comparisons test (SYSTAT 7.0; SPSS Inc., 1997). Reflectance sensitivity was considered to be significant at the wavelengths where the corresponding difference was significant (Carter, 1993).

Previous investigations have identified a wide range of indices as indicators of vegetation physiological properties. We have evaluated the potential of spectral indices used by other investigators to assess damage for Norway spruce stands. Based on our spectral analysis, a few new spectral ratios were also developed. A list of the formulas used for computation of the indices is presented in Tables 4.4 and 4.5. The spectral indices are presented in the following 6 groups based on their bandwidth, the spectral regions they cover and the data treatment involved for their computation: (1) 2.5nm-Narrow Band Indices, (2) Broad Band Indices and 10nm-Band indices, (3) Derivative Indices, (4) Inverted Gaussian Model (IGM) parameters, (5) Area parameters, and (6) Narrow Band Short Wave (SWIR) Indices. The computation of some of the more complex indices is described below.

The 2.5nm-Narrow band Indices use visible and NIR bands of the spectrum and are products of direct (simple) computation. The group of the Broad Band Indices include widely used indices, such as Landsat<sup>TM</sup> 5/4, 3/1, NDVI (Normalized difference vegetation index) and modified versions of Landsat<sup>TM</sup> indices suggested as effective indicators of vegetation parameters. Also included in the Broad Band Indices group are a

number of indices, ratioing 10nm broad bands. These indices were developed to assess the potential for stress detection of multispectral systems.

The red edge inflection position (REIP), defined as the boundary between chlorophyll absorption in the red wavelengths and leaf scattering in the near-infrared (NIR) wavelengths, was computed as the wavelength at which the first derivative has maximum value (Horler *et al.*, 1983; Rock *et al.*, 1986).

Miller *et al.*, (1990) demonstrated that the approximation of the red edge position from simple derivative analysis depends on instrument spectral resolution and suggested the use of the inverted Gaussian model (IGM) for obtaining red edge parameters. Using IGM with the current study the following parameters were generated:  $\lambda_0$  (wavelength at which the minimum reflectance in the chlorophyll absorption feature occurs),  $R_0$  (amount of reflectance at  $\lambda_0$ ),  $R_s$  (maximum amount of reflectance in the 720-800nm region),  $\lambda_\pi$  (the wavelength at which the maximum of the first derivative of reflectance occurs,  $\lambda_\pi = \text{REIP}$ ) and  $\sigma$  ( $\sigma = \lambda_\pi - \lambda_0$ ). An inverted Gaussian curve was fitted to the data using the equation:

$$R(\lambda) = R_s - ((R_s - R_0) \exp(-(\lambda_0 - \lambda)^2 / 2\sigma^2)).$$

For representation of the red edge, IGM requires initial estimation of the parameters of the model, which is done by careful analysis of the spectra (Miller *et al.*, 1990). In the current study the starting IGM parameters were  $\sigma = 40\text{nm}$ ,  $R_0 = 5\%$ ,  $\lambda_0 = 675\text{nm}$ ,  $R_s = 40$ .

Computed from the indices suggested in the literature as sensitive to stress are the following:  $D_{\text{max}}/D_{704}$  and  $D_{714}/D_{704}$  (D- value product of the first derivative of reflectance computation,  $D_{\text{max}}$  is the maximum value of the first derivative in the red edge region,  $D_{\text{max}} = R_{\text{slope}}$ ). To express the differences in the shape of the first



derivative curve among damage levels, we developed the derivative indices:  $D_{max}/D_{714}$  and  $D_{max}/D_{744}$ .

Based on our spectral analyses, two groups of indices were developed. The first group characterizes the spectral change appearing with damage in the red edge region by computing the area between the vegetation curve and the line connecting the green peak and the NIR maximum (AAL; Figure 4.5). The computation produces the parameters: area, and slope, intercept and dept-sum, as intermediate steps in calculating the area index. The second group expresses the spectral differences appearing with damage in the Short Wave Infrared (SWIR) 1365-1460nm and 1890-1950nm regions.

The relationship between canopy pigments, foliar chemical constituents and the spectral reflectance indices was assessed using the average to tree level foliar pigments, chemical constituents and reflectance measurements.

Many of the algorithms reported in the literature have been developed for assessment of pigment levels. The sensitivity of such algorithms to changes in pigment concentration occurring with vegetation damage needs to be evaluated (Datt *et al.* 1998).

#### **4.2.7 Statistical Analyses**

Analysis of variances was conducted to test the differences among damage levels for the forestry stand and individual tree measurements, foliar pigment and chemical constituent measurements, and spectral reflectance indices (ANOVA; SYSTAT 7.0; SPSS Inc., 1997). Damage class (DC) and/or first-, second- and third-year category foliage (Year), as well as the interaction term (Year x DC), were evaluated as main effects. The significance of the differences was determined using the Tukey-Kramer test (Zar, 1996). The overall correlation of the indices to damage was evaluated by

conducting one way ANOVA and specifying damage level as a class variable (Zar, 1996).

### **4.3 Results and Discussion**

#### **4.3.1 Evaluation of Forest Stand Parameters and Growth Characteristics in Relation to Damage Level**

##### **Forest stand parameters**

To determine the extent to which some of the stand parameters, such as stand density, basal area (BA), diameter at breast height (DBH), tree height, canopy closure and elevation were related to damage, ANOVA was conducted. Table 4.6 presents the stand data. The probabilities of obtaining greater values of the F statistic ( $p > F$ ) and the coefficients of multiple determination ( $r$ ) are presented in Table 4.7. Figure 4.6 depicts the differences between LS means by damage level. Standard errors are used to display the significance of the difference between means determined using ANOVA.

Damage level was significantly correlated ( $r=0.67$ ,  $p=0.001$ ) with the average tree height (Figure 4.6a), which decreased with damage level with statistically significant differences between healthy and both DC1 and DC2 (no significant difference between DC1 and DC2), and severely damaged (DC3). Stand age (Figure 4.6b) was significantly higher for the healthy stands, while there was no significant difference between DC1, DC2 and DC3. A relatively high correlation was established between damage and canopy closure ( $r=0.61$ ,  $p=0.104$ ), observing a decrease in canopy closure with damage (Figure 4.6c.). A strong relationship was established between damage and elevation ( $r=0.62$ ,  $p=0.005$ ), with a trend of heavier damage present in the lower elevations (Figure 4.6d). Forest damage was strongly correlated to tree DBH ( $r=0.69$ ,  $p=0.012$ ), with a statistically

significant difference between healthy and DC2 and DC3 (Figure 4.6e). Stand density (Figure 4.6f) and total basal area (Figure 4.6g) had a low relationship to damage. Stand density was significantly higher at DC3 as compared to DC0 and DC2, but was not significantly different from DC1.

The trend in increased damage with decreased stand age may be due to the more damaged forests dying or being harvested earlier. Since canopy closure is one of the main characteristics evaluated during the field assessment of forest health, the strong correlation to damage was anticipated. The lack of statistically significant differences for canopy closure between healthy and the DC1 demonstrates the low relative importance of this parameter for field separation of initial damage, and the need of spectral remote sensing tools for separation of the subtle differences in forest health.

A trend of heavier forest damage occurring at the higher elevations in the Krusne hory has been reported in broad elevational ranges (601-800m and 801-1000m) by previous investigations (Rock *et al.*, 1994; Ardo *et al.*, 1997; Lambert *et al.*, 1995). The study sites for the current research were selected within approximately 100m elevational gradient (850-950m). Within this limited elevation range, observing a trend of heavier damage at the lower elevations (opposite to the previously reported) is of surprise. The trend may be due to the closer proximity of the heavily damaged sites to the emission sources from the valley, and the fact that polluted air mass movements more frequently occur at the topographic low points.

## **Relationships between tree yearly increment growth and forest damage level using a dendrochronology approach**

The average age of the trees across damage classes was 54 years. In general, the trees from the healthy sites were older, with some individual trees up to 100 years old. During the period 1920-1965, the trees from all damage classes grew at an approximately steady rate (Figure 4.7). An apparent decline in forest growth began in 1965-67 for the heavily and intermediately damaged trees (DC3 and DC2), while the healthier forest (DC0 and DC1) decline began in the late 1960s or early 1970s. All spruce forests in the area of Krusne hory were affected (including DC0). In the period 1970 - 1984, tree growth was significantly impaired. An apparent recovery began during the mid-1980s. The trend of yearly tree increment growth increase was observed for all damage classes (including DC3). It is questionable if the decrease in growth rate since 1990-95 is due to a regular pattern in the climate cycling, or if in the past few years the forests have entered a new decline condition.

The effect of temperature on tree growth was found not to be significant for both healthy and decline sites ( $p > 0.05$ ,  $r^2 = 0.01$ ). Multiple regression analysis suggests that precipitation was significantly related ( $p < 0.05$ ,  $r^2 = 0.73$ ) to the growth rate of the healthy trees (DM0), while no significant relationship was established ( $p > 0.05$ ,  $r^2 = 0.06$ ) between precipitation and the growth of the damaged trees (DM1, DM2 and DM3). This result suggests a strong relationship between tree growth and precipitation for the healthy trees (DM0). For the damaged trees (DC1, DC2 and DC3) there is a de-coupling of growth rate and the limiting ecological factor for the region – precipitation.

The trend of increase in the yearly tree increment growth beginning in 1980-85 suggests that with the current study we are possibly addressing tree physiology in a stage of forest recovery, or the long-term effect of the decline after the main stress factors have been released.

The recovery in forest growth since 1985 is likely due to corrective measures employed by the Czech government and industry. These corrective measures include the spreading of crushed dolomite (calcium/magnesium carbonate, beginning in 1984) by helicopter over damaged forest stands in the Krusne hory, and a reduction of SO<sub>2</sub> emissions from power-generating plants (beginning 1990) (Kubelka, et al., 1993).

#### **4.3.2 Relationship between forest damage level and foliar pigments and chemical constituents**

##### **Foliar pigments**

The current results are based on our analysis of the pigment data obtained from fresh foliar samples by our Czech colleagues (Solcova, 1999).

Chlorophyll *a*, *b*, total chlorophyll (*a+b*) and carotenoid levels increased significantly (on a gram per gram dry weight,  $p < 0.01$ ) with increase in age of the foliage (Figures 4.8.1, 4.8.2, 4.8.3 and 4.8.4). This finding (current-year needles having lower concentrations than older needles) complies with the trend reported for Norway spruce in decline by Lichtenthaler (1988). While Wellburn (1994) observed no direct SO<sub>2</sub> effects on chlorophyll content and/or composition of the chloroplast pigments, fumigation appeared to accelerate the differences in needle chlorophyll content appearing with age. Schulze *et al.* (1989) reports an increase in total chlorophyll with needle age for healthy trees, while damaged trees showed no difference, or a slight decrease in chlorophyll

levels. Schulze *et al.* (1989) compared only two damage levels – healthy and heavily damaged, presenting a limitation for the comparison to our findings. The pigment analysis demonstrated an increase in chlorophyll level with needle age, and a decrease within needle age group with increased levels of damage (Figures 4.8.1, 4.8.2, 4.8.3 and 4.8.4).

With the analyses of variances, the combined effect of foliage age and damage was established not to be significant for all pigments and the pigment ratios (Table 4.8).

The pigment ratio of total chlorophyll to carotenoids ((a+b)/Car; Figure 4.8.5) was able to separate DC0/DC1 from DC2/DC3, but was not able to separate the initial damage (DC1) from healthy (DC0).

For the chlorophyll *a/b* ratio, the effect of damage differed with foliage age (Figure 4.8.6). With damage level the ratio increased, and for first-year foliage there were statistically significant differences between healthy and all damage levels. Second-year needles exhibited a significant increase only between heavy damage and all other levels, while for third year needles there was a slight increase from DC0 to DC1, and a decrease from DC1 to DC2 and DC3, with significant differences between DC1 and DC3 (Figure 8.6a). It is of interest to note the change in the trend with age occurring with an increase in damage levels (Figure 8.6b). For DC0 and DC1, there is a slight increase in the ratio with increase in needle age, while for DC2 and DC3 there is a decrease in the ratio with age. There was a statistically significant difference between first- and second-year foliage as a group and third-year needles. The change in the age pattern occurring with damage level illustrates a potential of the chlorophyll *a/b* ratio as a bio-indicator of damage.

With increasing damage level, pigment levels and pigment ratio values decreased, but there were no statistically significant differences in pigment level ( $p > 0.05$ ; ANOVA and Tukey-Kramer test) between healthy trees (DC0) and initially damaged (DC1), and between moderately and severely damaged. For all pigments, highly significant differences ( $p < 0.01$ ) occurred between DC0-DC1 and DC2-DC3. The significant difference for chlorophyll *a*, *b* and total chlorophyll between the DC0-DC1 and the DC2-DC3 was most pronounced for the third-year needle age class (Figures 4.8.1a, 4.8.2a, 4.8.3a). Foliar pigment levels measured were within the "normal" range for Norway spruce needles as reported for decline conditions (Lichtenthaler, 1988).

The change in each pigment level occurring with damage was evaluated by calculating the difference between a particular damage level and healthy, as a percentage of healthy (Table 4.9). The largest changes between healthy and DC1 for foliar pigments occurred for carotene for all needle-age groups, chlorophyll *b* for first- and second-year needle age class and total chlorophyll (*a+b*) for the first age group. This indicated a potential for these pigments as bioindicators of forest health status in the Norway spruce forests in the Krusne hory. However, these pigments are not useful in separating the initial levels of stress (between DC0 and DC1). Although there are apparent trends and statistically significant differences for pigment levels occurring with damage class, the overall correlation of the pigment levels to damage class was relatively low, with a low confidence of the analysis (Table 4.10).

The system for forest damage evaluation used in the current study includes a number of factors, of which only presence or absence of chlorosis is directly related to pigment concentration. In the absence of chlorosis, other canopy characteristics such as

canopy closure, crown shape and needle retention could result in high (DC2, DC3) damage level. This provides an explanation for the low correlation between foliar pigment levels and forest damage class.

The dry weight to fresh weight ratio increased significantly with the increase in age of the needles, and did not change significantly with the increase of the damage level (Figure 4.8.7). This result indicates a low potential for this parameter as an indicator of damage in the Krusne hory.

#### **Foliar nitrogen and nitrogen to total chlorophyll ratio**

The results for foliar nitrogen and total chlorophyll to nitrogen levels are presented in Figure 4.9.

Foliar nitrogen (Figure 4.9a) levels for healthy foliage did not differ statistically between age groups, while for the damaged needles (DC1, DC2, DC3), nitrogen level increased significantly from first- to second-year needles, and decreased significantly from second to third year. There was no significant difference between first- and third-year needles from the same damage level (ANOVA, significant combined effect of year and damage). Our findings suggest re-allocation of nitrogen from third-year needles to first-year needles, while for second-year needles nitrogen levels remain stable across damage levels.

The results for the nitrogen/total chlorophyll ratio display no significant interaction between the effects of age and damage ( $(a+b)/N$  in Fig. 4.9b), and a significant increase in values with heavy damage and age (Fig. 4.9c and 4.9d). The ratio of total chlorophyll to nitrogen level significantly differ from healthy (DC0), with an increase in stress level (DC1 and DC2) and with an advance of the stress conditions to severe damage (DC3) (Fig. 4.9d). There were no significant differences between DC1



and DC2. The relative change in the ratio as a percentage of healthy is also relatively high (Table 4.9), suggesting that the total chlorophyll to nitrogen ratio provides a sensitive bio-indicator of initial stress for Norway spruce. Previously, it has been reported that with an increase in vegetation stress level, an imbalance of nitrogen to pigment levels may occur (Schulze *et al.*, 1989).

Nitrogen availability, believed to be a key factor of plant productivity, is reported to influence photosynthetic pigment content by nitrogen deficiency causing a decrease in  $\alpha$ -carotene (suggested as most sensitive pigment to nitrogen deficiency; Schulze *et al.* 1989). Schulze (1989) reports that with increasing N supply for Norway spruce, the supply of Mg becomes limited, leading to growth decline.

In the current study, a general decrease in total carotene level was noted with damage and a trend of a decrease in the carotene to nitrogen ratio (Table 4.9). While the sensitivity of the ratio to damage was relatively high, the relationship of this ratio to damage was not statistically significant ( $p>0.05$ ,  $r=0.49$ ; Table 4.10). This result indicates a low potential of the carotenoid/N ratio as an indicator of early damage in the Norway spruce foliage from the Krusne hory.

#### **Changes with damage level in foliar lignin and cellulose, polar and non-polar compounds**

When interpreting the results for the foliar chemical constituents, it is important to consider that based on the laboratory analysis, lignin, cellulose, polar and non-polar constituents add up to a total of 100%. Therefore an increase in one or a few of the constituents leads to a relative decrease in the remaining compounds (Figure 4.10).

Lignin levels differed significantly with damage level, with significant decrease from DC0 to DC1 and a more significant drop in amount for DC2 and DC3 as a group. No significant difference was seen between mean levels from the moderately (DC2) to severely (DC3) damaged forests (Figure 4.10.1b). Total lignin levels did not differ significantly with foliar age (Table 4.8), and the trends expressed with damage level did not differ by needle age group (Figure 4.10.1c).

An increase in cell wall lignification has been considered a common plant response to pathogen attacks and wounding (Oven and Torelli, 1994). However, our results suggest that in forests growing under a long-term exposure to air pollution stress, where the effect of the decline has been continuous and persisting for a large portion of the trees' life, lower tissue lignification occurs in foliage under higher stress levels, resulting in a higher susceptibility to mechanical and insect damage. The overall variation in lignin content across all damage levels was approximately 2% from the total. Confirming our results, trends in increasing lignin levels with decreasing nitrogen deposition (across a nitrogen deposition gradient, with largest differences in lignin concentrations of approximately 9%) have been reported earlier for red spruce by McNulty *et al.* (1991). The lack of difference in lignin content with age group demonstrates that the needles were fully-grown and lignification was completed at the time of the foliar collection. The fully mature condition is an important consideration in interpreting foliar pigment and chemistry levels across the age classes.

Cellulose levels differed significantly with needle age and damage (Figure 4.10.2), with overall lower cellulose concentrations present in older needles at the more damaged sites (Figure 4.10.2b). A high correlation of cellulose to damage ( $r=0.67$ ,

$p < 0.01$ ; Table 4.8), and a significant combined effect of age and damage was observed (Table 4.8; Figure 4.10.2a). Differences between damage levels were exaggerated with needle age. Since cellulose levels do not change after the needle growth is completed, the relatively lower levels of cellulose in second- and third-year needles could be explained by 2 hypotheses. First, it is possible that growing conditions three years ago in the area were more limiting as compared to the present (1998), and due to that, lower amounts of cellulose were formed in the older foliage. A second possible explanation relates to the presence of relatively larger amounts of other compounds, such as non-polar and polar compounds (Figure 4.10.3 and Figure 4.10.4) in these age classes, thus resulting in a relative reduction in cellulose in the older needles. A consideration of the increase in water-soluble phenolic compounds (most likely tannins) with damage level supports the later hypothesis.

Polar compounds (i.e. tannins, sugars and starch) increased significantly with age and damage level (Figure 4.10.3b and 4.10.3c), with a relatively large increase from first-year needles to second, and relatively similar amounts for second- and third-year needles (Figure 4.10.3c). For first-year needles, there was a larger amount of polar compounds in needles from higher damage level (Figure 4.10.3a). Polar compound levels increased significantly from first- to second-year needles for all damage levels, while a relative maximum level of nearly 35% of total foliar constituents was reached for third-year needles from the most damaged trees DC3. There is a significant increase in polar constituents from second- to third-year needles for DC0 and DC1, while there is no significant difference between DC2 and DC3.

Non-polar compounds (i.e. waxes, oils and soluble in organic solvent pigments, such as chlorophyll) increased in value with age and damage level (Figure 4.10.4) and did significantly differ statistically. ANOVA indicated a significant combined effect of age and damage (Table 4.8). The age differences between needles were exaggerated with an increase in damage level. For DC0, DC1 and DC2 trees, there is a significant difference between first- and second-year foliage, and no significant difference between second- and third-year, while for severely damaged trees (DC3) there are significant differences among all needle age categories (Figure 4.10.4a).

Evaluating the relative change in the chemical compounds occurring with damage, non-polar and polar constituents appear to have the highest sensitivity to damage conditions for all age groups (Table 4.9). Evaluating the overall correlation of the constituents to damage level, considerable correlation is found for the polar constituent (Table 4.10;  $r=0.80$ ,  $p=0.009$ ), suggesting the greatest potential of this foliar compound as a bio-indicator of early damage levels to Norway spruce. The overall change with age and damage in the amount of non-polar constituents (approximately 1%) is considerably smaller than the change in the amount of polar constituent (approximately 7%). Our findings demonstrate that the dominant change in foliar chemistry is an increase in the amount of polar constituents with an increase in needle age and damage level, resulting in a decrease/imbalance with damage in the relative amounts of the remaining foliar lignin and cellulose constituents.

A strong correlation was established between polar compounds and cellulose ( $r=0.80$ ,  $p<0.01$ ), non-polar compounds and lignin ( $r=-0.87$ ,  $p<0.01$ ), and a relatively lower correlation between non-polar and cellulose ( $r=-0.69$ ,  $p<0.01$ ) and cellulose and

**lignin ( $r=0.65$ ,  $p=0.02$ ). The low correlations established between non-polar and polar and polar and lignin demonstrates their relatively low interdependence. The strong correlation between polar constituents and cellulose, since foliar cellulose levels are stable once established, demonstrates the significant role of the polar compounds in altering the foliar chemical balance.**

**A significant increase in polar and non-polar constituents with an increase in damage corresponds with the findings in previous studies, reporting an increase due to vegetation stress for similar chemical compounds (Rock *et al.*, 1986; Baudet *et al.*, 1995; Schulze *et al.*, 1989; Moss *et al.*, 1998; Vogelmann and Rock, 1988; Slocupova *et al.*, 2000). Schulze *et al.* (1989) reports an increase in cuticular waxes with damage for Norway spruce. Rock *et al.* (1986) and Moss *et al.* (1998) report increased tannin levels with cellular changes in the mesophyll cells due to ozone air pollution damage in red spruce in New England. Booker *et al.* (1996) describes an increase in phenolic compounds due to elevated ozone exposure in pines, while our Czech colleagues indicate increasing levels of tannins in Norway spruce needles with damage (Soukupova *et al.*, 2000). Our finding (of an increase in polar compounds with an increase in damage level coincident with decreasing lignin and cellulose levels) demonstrates a trend for Norway spruce foliage that has been suggested by previous research, and indicates that the increase in phenolic compounds with damage is likely a typical response to damage for coniferous.**

### **4.3.3 Evaluation of Norway spruce spectral reflectance properties with regard to changes occurring with damage level**

First-, second- and third-year needle reflectance properties exhibit changes with age and damage class. In general, reflectance decreased with an increase in age throughout the measured spectral range for all damage classes (Figure 4.11 and 4.12). As needles aged the variation in the spectra also increased (Figure 4.11). The variation in reflectance also increased with an increase in damage level. As a result, the greatest changes in reflectance were observed in the third-year foliage damage DC3 (Figure 4.11d). The NIR (800-1350nm) reflectance is the highest for the first-year needles, regardless of damage class, decreasing for the second- and third-year needles (Figure 4.12).

In the NIR region, reflectance for first-year needles increased with an increase in damage, while in contrast, reflectance for the third-year needles decreased with an increase in damage level (Figure 4.13a and 4.13c). For second-year needles, the NIR changes were insignificant (Figure 4.13b). The results for third-year foliage are in general agreement with previous reports (Rock *et al.*, 1988; 1992) documenting a decrease in reflectance in the NIR with increase in foliar damage. Reflectance in this region is a function of the cellular structure of the foliage (Gates, 1980; Rock *et al.*, 1986).

In the red/NIR spectral region (650-720nm), reflectance increased with increase in damage in all age categories (Figure 4.14). The increase in reflectance in the red region is explained by a stress-induced decrease in leaf chlorophyll content. This is supported by the trend of reduction in total chlorophyll content seen in DC2 and DC3 needles when compared with the higher levels in DC0 and DC1 (Figures 4.8.1-4.8.5).

For all ages and damage levels, the largest differences in sensitivity peaks occurred in the 680-740nm region (maxima at 695nm; Figure 4.14). Relatively smaller but significant differences in sensitivity peaks occurred at 1400-1550nm (maxima at 1475nm) and 1900-2050nm (maxima at around 2000nm), suggesting a potential for damage detection of using these Short Wave Infrared (SWIR) spectral regions.

Reflectance differences and sensitivity, averaged across age groups to tree level, are presented in Figures 4.15 and 4.16. Spectral regions of highly statistically significant differences are shown on Figure 4.16: to DC1 with red arrows (top, continuous line), and to both DC2 and DC3 with blue arrow (lower, interrupted line). The absolute reflectance minimum in the chlorophyll well was located at 667nm, with significant differences in reflectance at this wavelength among all damage classes. Needle reflectance averaged across age groups to tree level spectra increased with increasing damage level. For DC2 and DC3, reflectance increased throughout broad spectral regions: for DC2 – 440-1235nm, 1340-1745nm and 1855-2250nm; and for DC3 - 530-737nm, 885-2250nm (Figure 4.15 and Figure 4.16). In contrast, the initial damage (DC1) reflectance increased in more narrow bands: 495-520nm, 670-740nm, 1395-1565nm and 1894-2175nm. For DC1, significant differences spectra occurred in the 677-705nm region with a maximum at 695nm, 1400-1515nm with a maximum at 1454nm, and 1905-2125nm with a maximum at 2000nm (Figure 4.16).

These results indicate the 675-705nm region as optimal for early stress (DC1) detection, and illustrate the higher potential for separation of the initial damage level for high spectral resolution and narrow band instruments, as compared to broad band systems. The high sensitivity to damage of reflectance spectra in the region 675-705nm

with a maximum at around 705nm, confirms for Norway spruce the region of maximum sensitivity demonstrated earlier for loblolly pine by Carter (1993).

#### **4.3.4 Evaluation of Spectral Indices with Regard to Separation of Damage Levels**

The current study evaluated the spectral indices presented in Tables 4.4 and 4.5 with regard to separation of damage levels in Norway spruce. The general trends observed within the data with damage and age are presented. The results for individual indices are organized in six groups, based on their spectral properties and the analysis involved. The six groups include: (1) 2.5nm-Narrow Band Indices: visible and NIR band ratios suggested in the literature as sensitive to changes in pigment levels or vegetation; (2) Broad Band Indices: widely used Landsat<sup>TM</sup> and 10nm-Band Ratios; (3) Derivative indices; (4) Inverted Gaussian Model parameters; (5) Area Above the vegetation curve/Line (AAL) estimates; and (6) Short Wave Infrared (SWIR) band ratios. Figures for each index are cited in Tables 4.4 and 4.5 and included in the Appendix. The trends in the data occurring with damage and the statistical significance of the differences between means (ANOVA) are displayed by plotting LS Means and standard errors. The significance of both effects (age and damage) by index type are presented in ANOVA tables (Tables 4.11 to 4.16). The sensitivity (% relative change for DC0) by age classes is presented in Tables 4.17 to 4.22. The overall relationship of each index to damage, regardless of needle age, is presented in Tables 4.23 to 4.28. The sensitivity of a particular index to individual damage level, and the overall coefficients of determination of the indices to damage, were used as indicators for evaluating the detection potential of the algorithms. The results for the indices performing best for separation of initial damage levels are summarized and compiled into the final Table 4.35.



There were statistically significant differences for healthy and damaged vegetation, or among damage levels for all evaluated indices with the exception of DPR1, DPR2, DPR21 and DPR22 (ANOVA, significant  $p < 0.05$ , Highly significant  $p < 0.001$ ; Tables 4.11 to 4.16).

Evaluating the trends in the indices by age groups, a consistent pattern of the changes with damage and statistically significant differences were noted only for the third-year needle age group (with the exemption of RE1). The results for second- and third-year needles did not present a constant trend with damage. These results suggest that sampling and spectral analysis of third-year needles provides the most potential for damage separation.

The only exception was the RE1 index, which exhibits highly significant differences for first-year needles between DC0/DC1 and DC2 and DC3. RE1 averages the reflectance in the region 675-705nm, where the absorbance due to chlorophyll is the strongest. There were lower levels of chlorophyll in younger needles, with the least amount in first-year needles (Figure 4.8.4). The results suggest that the RE1 index is able to separate damage levels when relatively lower amounts of chlorophyll are present, while most other indices are capable of damage separation in the presence of higher chlorophyll levels.

To identify the indices with the best potential for separation of initial damage level (DC1), only the results for the indices having the highest correlation, sensitivity to the decline and statistically significant differences among means per damage level are discussed further.

## **2.5nm-Narrow Band Indices**

Among the 2.5nm-Narrow Band Indices (group 1), PRI1 had the highest correlation ( $r=0.69$ ,  $p=0.05$ ) and sensitivity to decline for third-year needles, followed by PRI3 ( $r=0.65$ ,  $p=0.03$ ). Both indices separated healthy from DC1/DC2, and both groups from DC3. PRI1 decreases with damage when PRI3 increases in value with damage class. A common factor for both indices is the use of a band at 570nm, related to chlorophyll and carotene levels (Chappelle *et al.*, 1992), and less sensitive to pigment change bands. For third-year needles, GM2 had a relatively high sensitivity and correlation ( $r=0.64$ ,  $p<0.001$ ), decreasing with damage. It ratios a band in the NIR plateau (at 750nm, with relatively low sensitivity to damage), with a band located at 700nm (in the region of highest sensitivity to DC1) (Figure 4.16).

The RARS and SR ratio, suggested as strongly correlated to chlorophyll levels (Chappelle *et al.*, 1992) had relatively high sensitivity to damage, but a low correlation to the damage classes. They were able to separate DC3 from DC0 and DC2 from DC0 and DC3, RARS increasing and SR decreasing with damage, but were not able to separate the early damage from healthy and DC1 from DC2.

These results demonstrate that when using 2.5nm narrow spectral bands from the visible/NIR region, simple band ratios can separate initial damage level (DC1) from healthy (DC0). The ratio of a sensitive to pigment change band to non-sensitive band (e.g. the indices PRI1, PRI3 and GM2) provided optimal results for stress detection with narrow band indices as it has been reported previously by Carter (1994).

### **Broad Band Indices**

The Landsat TM NDVI, TVI, TM5/4, TM3/1 indices had relatively low correlation and sensitivity to damage level. These indices were able to separate DC2 and DC3 from DC0/DC1 for all age groups with lower values of the indices for higher damage levels. Only TM3/1 for third-year needles was able to separate the means from all damage levels. These results suggest a limited potential for separation of initial levels of damage for broad band systems. This finding corresponds with previous research conducted on damage discrimination in the Norway spruce forests of Krusne hory (Lambert *et al.*, 1995). Using LandsatTM, Lambert *et al.* (1995) were able to separate tree damage categories – healthy, moderate and heavy damage, but not the initial damage level (DC1) from healthy (DC0).

The modified LandsatTM indices using one narrow band at regions related to chlorophyll absorbency (550nm, 675nm and 700nm) had only a slightly higher correlation to damage than the original indices and were able to separate only DC3 from the remaining damage classes.

The 10nm-Band ratios showed a higher correlation to damage level (R550/R700,  $r=0.60$ ) than the LandsatTM indices and the modified LandsatTM, and for third-year needles, comparatively higher sensitivity. The results suggest higher potential for discrimination for the narrow band indices as compared to the broad band LandsatTM, although both are not able to separate healthy (DC0) from initial damage level (DC1).

### **Derivative indices**

Among the derivative indices evaluated, V4 (D715/D704,  $r=0.68$ ) and Dmax/D704 ( $r=0.63$ ) exhibited the highest relationship and sensitivity to the decline for

third-year needles. They were able to separate DC0 from DC1/DC2 (not separating DC1 and DC2), and from DC3. Both indices decreased in value with an increase in damage level.

Band ratios of derivative spectra have been suggested as strongly related to chlorophyll *a* or total chlorophyll concentrations, and their potential as bioindicators of damage has been hypothesized (Zarco-Tejada *et al.*, 1999). Our results demonstrate that derivative ratios are strongly indicative of vegetation damage and capable of separation of healthy forest from the initial damage levels.

REIPslope also had a high correlation ( $r=0.66$ ,  $p=0.06$ ) and sensitivity to damage, decreasing with increase in damage. This index was able to separate all damage levels for third-year needles. REIPwave also decreased with increase in damage. It had a relatively low sensitivity to damage, and a correlation of  $r=0.58$  ( $p>0.05$ ). REIPwave was able to separate DC3 from the remaining damage levels for all needle ages. For the third age group REIPwave was not able to separate DC0 and DC1, but statistically was able to separate DC2 and DC3 from DC0/DC1. A comparison of the REIPslope and REIPwave performance indicates REIPslope as having larger potential as indicator of initial damage.

Previous research demonstrates the high relationship of the REIPwave parameters to total chlorophyll level (Rock *et al.*, 1986, Vogelmann and Rock, 1991). With the current study, no significant differences were established for total chlorophyll levels between DC0 and DC1. The results for REIPwave not separating DC0 and DC1 comply with the trend observed in the chlorophyll concentration with damage, indicating the potential of this ratio as an indicator of pigment level.

### **Inverted Gaussian Model (IGM) parameters**

The Inverted Gaussian Model (IGM) parameters had a relatively low correlation to damage level.  $R_s$  and  $R_o$  exhibited had high sensitivity levels to damage.  $R_o$  had the higher sensitivity to damage (Table 4.20). Only for third-year needles were both  $R_s$  and  $R_o$  able to separate all damage levels.

For this study, the IGM parameters were computed using uniform (the same for all spectra) initial values as suggested by Miller *et al.* (1990). Bonham-Carter (1988) suggests more precise calibration of the model to be performed by varying the initializing parameters to achieve a minimum in average fitting.

### **Area parameters**

The AAL parameters had a relatively low overall correlation to damage, and only for third-year needles had a relatively high sensitivity to damage. For third-year needles, all parameters were able to separate among all damage levels, with Area having slightly higher sensitivity values. Area, Slope and Depth\_sum increased with damage when the Intercept parameter decreased.

### **Narrow Band Short Wave Indices (SWIR)**

The SWIR indices showed a low correlation and sensitivity to damage. Using third-year needles, they were able to separate DC3 and DC2 from DC0/DC1. Among these indices, SWIR22 provided the greatest separation (sensitivity of  $-17.45$  to DC2, and  $-46.9$  to DC3) when decreasing, with an increase in damage level. The SWIR indices use bands from the regions 1400-1515nm and 1905-2125nm exhibiting relative sensitivity peaks to damage (Figure 4.16). While our results demonstrate a potential of these indices for separation of advanced levels of damage, these indices would not be useful for separation of initial levels of decline.

### **Overall comparison among the indices most sensitive to stress**

Comparing the sensitivity and correlation of the indices from the six different groups, the overall highest potential for separation of initial damage levels was established for PRI1, followed by PRI3, REIPslope, GM2, Dmax/D704 and RE1. PRI1 and V4 were equally highly related to damage.

From the Broad Band Ratios group, R550/R700 performed best, but it was also not able to separate DC0 from DC1.

Common factors for all of the indices separating healthy from initial damage are the use of 2.5nm spectral resolution and ratioing highly sensitive to damage bands with relatively insensitive bands. Only PRI1 does not use bands from the red edge region of the spectrum.

#### **4.3.5 Relationship between reflectance indices and canopy pigments and foliar chemical constituents**

To evaluate the direct correlation of the calculated indices to foliar pigments and chemical constituents, a correlation analysis was conducted. The results are presented by grouping the indices into: 2.5nm-Narrow Band Ratios, Broad Band Indices, Derivative Indices, IGM parameters, Area parameters and SWIR indices (Tables 4.29 to 4.34).

##### **Relationship between indices and pigment levels**

Among the 2.5nm-Narrow Band Indices V2, V3, GM1, SR, PRI2 and GM2 had the higher correlation coefficients to pigments (to chlorophyll b), although all were lower than  $r=0.60$ . The level of correlation established between foliar pigments and the spectral indices was lower than the correlation established between foliar chemical constituents and indices (Table 4.29).

This finding was unexpected since the indices use mostly red edge bands strongly related to chlorophyll levels. A possible explanation for the low pigments-to-indices relationship provides the use of one set of samples for measuring pigment levels and a second set of samples from the same branch for spectral measurements and estimation of foliar chemical components. Although for the correlation analysis the data was averaged to stand level, the large amount of variability within branches and within stands make the direct comparison difficult. It is also likely that the relationships between foliar pigments could be better expressed by power, exponential or polynomial equations. Similar equations have been suggested for use in developing predictive equations for the estimation of pigment levels (Blackburn, 1998). The development of predictive equations for estimation of pigment levels based on fresh foliar GER2600 spectra is beyond the scope of the current investigation.

#### **Relationship between indices and chemical compounds**

To establish the link between foliar bio-indicators and the indices sensitive to damage, the relationships between reflectance indices and foliar pigments and structural chemical constituents were evaluated. Tables 4.29 to 4.34. depict the relationships between all indices and foliar compounds. A summary of the findings for the indices performing best with regard to separation of initial damage levels is presented in Table 4.35.

Correlation analysis revealed a low relationship between nitrogen level and all spectral indices (Tables 4.29-4.34). This result suggests that reflectance indices are not useful for assessment of forest nitrogen levels, while the NIR methods are able to produce accurate nitrogen estimates using absorbance data.

When evaluating the relationship between the spectral indices and foliar lignin, cellulose, polar and non-polar constituents, it is important to consider that they are estimated as relative concentrations from the leaf tissue (totaling up to 100%), and variations in one or a few of the constituents cause a change in the others. Therefore they are strongly inter-related, with a strong correlation established by this study between cellulose and polar ( $r=-0.80$ ), lignin and non-polar ( $r=-0.86$ ) and lignin and cellulose ( $r=0.65$ ).

A strong relationship was established for most of the indices to cellulose levels (Tables 4.29-4.34). Among the 2.5nm-Narrow Band Ratios, the best relationships to cellulose were PRI1 ( $r=0.62$ ), PRI2 ( $r=-0.63$ ), SR ( $r=0.60$ ) and GM2 ( $r=0.61$ ). PRI1 and PRI2 also showed a high correlation to polar constituents with correlation coefficients of  $r=-0.60$  and  $r=0.62$ , respectively.

The LandsatTM and 10nm-Band indices had low correlation coefficients to all chemical constituents, with the highest correlation from this group established to cellulose for the narrow band R840/R700 ( $r=0.58$ ) and R840/R550 ( $r=0.54$ ), and to non-polar constituents (Tables 4.30).

Among all indices, the derivative indices V4 (D715/D705) and D717/D704 had the highest correlation coefficients to both foliar pigments and foliar chemical constituents. The V4 index performed better than D717/D701, having  $r=0.74$  and  $r=0.71$  to cellulose, and  $r=0.64$  and  $r=0.62$  to chlorophyll *b*, respectively. Both indices had comparatively higher coefficients to polar and non-polar compounds, and also to total chlorophyll (*a+b*) and chlorophyll ratios (Table 4.31).

Derivative analysis are suggested as less sensitive to the effects of variable irradiance and background scatter on the spectra (Lucas et al., 2000). Our results show



that these indices have a high potential for separating damage levels and relate best to the foliar chemistry. Therefore, these indices (V4 and D717/D705) show the highest potential as bio-indicators of initial levels of forest damage.

The correlation of the IGM parameters (AAL and SWIR indices) to both pigment levels and foliar chemical constituents was comparatively low.

The IGM parameters have been shown by previous studies to be highly correlated to pigment levels and stress (Miller et al., 1990). Our results suggest that more accurate calibration when varying the initial parameters for optimization of the model is needed. In this study, fixed initial parameters for  $R_s$ ,  $R_o$ ,  $\sigma$  and  $\lambda_o$  were used as suggested by Miller *et al.* (1990), when in contrast, Bonham-Carter (1988) recommends that all four parameters be varied for achieving a minimum in the average fitting error.

The ALL and SWIR indices were developed based on our spectral analysis. The ALL parameters use the bands from approximately 550nm to 750nm, including bands reported in previous research as strongly related to a number of pigments and to foliar scattering. Therefore, the ALL are not specific to a particular pigment or chemical compound, but are specific to damage level. The AAL low direct correlation to foliar compounds was anticipated. The SWIR indices ratio bands have been reported in previous studies to be associated with nitrogen (SWIR2 and SWIR22) and lignin (SWIR1 and SWIR12). Therefore, the high correlation of the indices to these compounds was expected.

Among IGM, ALL and SWIR indices Area,  $R_o$  and SWIR22 had high sensitivity and presented the potential for separation of all damage levels for third-year needles.

#### **4.4 Conclusions**

The current study established that all forests in the Krusne hory mountains were affected by the growth decline beginning around 1965-67, with tree growth being most impaired in the period 1970-84. Forest growth recovery began around 1980-85 and was apparent for all forest damage classes until 1990-95. Therefore, the current research addresses foliar physiological and spectral properties in a state of forest recovery. At the present, it is possible that the forests are entering decline conditions again. Further research is needed to establish if the present growth decline may be an effect of the normal climate cycling.

Pigment levels were relatively stable across the damage gradient. Norway spruce foliage pigment levels increased significantly with increase in foliage age, while within age groups a trend in decreasing pigment levels was established with increasing damage level. Within age groups, pigment levels decreased with damage, with no significant difference in foliage between healthy and DC1. This finding corresponds with the apparent recovery in forest growth observed since the late 1980s' in the Krusne hory, and suggests that pigment levels appear to be less reflective of the long-term effects of the pollution decline, and more indicative of the short-term changes in the environment.

Nitrogen level did not differ with age for healthy needles, but for damaged foliage the second needle age group had a significantly higher nitrogen level than first-year and third-year needles.

This study established a strong correlation to damage for the foliar structural chemical constituents. The more damaged needles exhibited a significant increase in foliar polar compounds and a lower needle lignification. Non-polar and polar constituents had the highest sensitivity, with polar the highest correlation to damage level. Foliar

structural chemical compounds (e.g. polar and lignin) appear to be effective indicators of the long-term environmental conditions. The strong relationship revealed between damage level and polar compounds suggests a high potential for use of these constituents (most likely tannins) as bio-indicators of stress.

A general foliar spectral trend was established in decreasing reflectance with increasing foliage age, corresponding well with the increase in needle pigment levels and the relative increase in polar and non-polar constituents. In the NIR region, an apparent trend of increasing reflectance with increasing damage level was established for third-year foliage, which corresponds with the trend indicative of vegetation damage as suggested by Rock (1986). In contrast, there was a slight increase in reflectance for first- and second-year foliage in the NIR, indicating the use of these age groups of needles for stress detection as being problematic.

This study demonstrated that indices using reflectance data from third-year needles are the most sensitive to damage effects.

In the red edge region, an apparent trend of increasing reflectance with increasing damage level was revealed for the third-year needles. This trend is suggested as a typical indicator of vegetation damage (Rock *et al.*, 1986). The largest sensitivity peaks for all age groups occurred in the 690-705nm portion of the red edge region, indicating the highest potential for stress detection of bands and band ratios from this region, as suggested by Carter (1994).

Relatively smaller peaks in spectral sensitivity to damage were established in the regions 1395-1565nm and 1695-2175nm, indicating a smaller potential for damage separation of bands and indices from these regions. Band ratios from the 1395-1565nm

region were able to separate only DC3 from DC0, DC1 and DC2 as one group, while indices from the 1695-2175nm region performed better and were able to separate DC2 and DC3 from healthy and DC1, but did not separate DC0 from DC1.

The derivative indices from the red edge region (V4 and Dmax/D704) were most strongly correlated to damage, followed by the 2.5nm-Narrow Band indices using green band at 530nm (PRI1, PRI2), or red edge bands at 700nm (RE1 and GM2).

The correlation established between foliar pigments and indices was lower than the correlation established between foliar chemical constituents and indices. Only the narrow band red edge indices exhibited the high correlation.

The strongest relationship was revealed for cellulose and polar (e.g. tannins, sugars, starch). Since foliar cellulose levels are stable, polar compounds appear to be the compounds most responsive to damage, and present the physiological basis for the use of the indices as bio-indicators.

This study indicates the highest potential of the derivative spectral indices and narrow band ratios from the red edge as spectral indicators of forest stress.

This study indicates a high potential of derivative spectral indices and band ratios from the red edge region, and of cellulose and polar chemical compounds as indicators of forest stress. Further investigations of similar datasets from different geographical locations and a variety of tree species are needed to validate the potential and determine the accuracy of the foliar spectral indices and chemical constituents for the discrimination of forest damage levels.

Damage Level (DC)	Defoliation <sup>1</sup> (%)	Ecosystem vitality status	
		Chlorosis absent	Chlorosis present
0	0 – 10	Healthy	Initial damage
1	11 – 25	Initial damage	Medium damage
2	26 – 60	Medium damage	Heavy damage
3	61 – 80	Heavy damage	Ecosystem collapse <sup>2</sup>
4	81 – 100	Ecosystem collapse <sup>2</sup>	Standing dead forest

<sup>1</sup> Characteristic of more than 70% of the trees within the stand

<sup>2</sup> At this stage more than 50% of the trees within the stand are dead

**Table 4.1: Criteria for field forest damage classification**

Data	Acquisition	Sites/Samples
<b>Study sites</b>	<b>30x30m sites into 90x90m areas,</b>	<b>53 sites</b>
<b>Forest damage class evaluation</b>	<b>12-14 sites per damage class healthy(DC0), initial(C1), intermediate(DC2), and heavy damage(DC3)</b>	<b>(intensive sites) 15 DC0, 12 DC1, 14 DC2, 12 DC3</b>
<b>Site elevation and map location</b>	<b>Survey maps, CIR photos</b>	<b>53 sites</b>
<b>Site GPS position</b>	<b>Field visit, Trimble differential GPS</b>	<b>53 sites</b>
<b>Tree diameter at breast height</b>	<b>Tree diameter at 1.30m height, DBH tape</b>	<b>51 sites</b>
<b>Forest canopy closure</b>	<b>1/10 acre plot, forest densiometer</b>	<b>51 sites</b>
<b>Stand density</b>	<b>1/10 acre plot, prism</b>	<b>51 sites</b>
<b>Stand height</b>	<b>Height of the forest canopy, clinometer</b>	<b>51 sites</b>
<b>Individual trees damage class</b>	<b>DC0, DC1, DC2 and DC3</b>	<b>53 sites, 265 trees</b>
<b>Tree height</b>	<b>Height of the 5 representative trees, clinometer</b>	<b>255 trees</b>
<b>Tree age and growth rate</b>	<b>Cores from 5 trees per stand</b>	<b>246 cores</b>
<b>Spruce foliar samples collection</b>	<b>I<sup>st</sup>, II<sup>nd</sup> and III<sup>rd</sup> year of needles, 5 trees/site</b>	<b>51 sites, 765 samples</b>
<b>Photography for site characterization</b>	<b>35 mm camera</b>	<b>51 sites</b>
<b>Fresh foliage reflectance spectra</b>	<b>Spectra from 5 representative trees per site, GER2600<sup>1</sup></b>	<b>765 samples</b>
<b>Foliar chlorophyll and carotenoids levels</b>	<b>Laboratory extraction and analyses, Solcova (1999)</b>	<b>765 samples</b>
<b>Air-dried, 1mm ground, foliage absorbance spectra</b>	<b>Spectra from 5 representative trees per site, NIR<sup>2</sup></b>	<b>765 samples</b>
<b>Spruce foliage chemical constituents</b>	<b>Laboratory foliar chemical analysis (Newman <i>et al.</i>, 1994)</b>	<b>42 samples</b>
<b>Lignin, cellulose and nitrogen levels</b>	<b>NIR spectroscopy (Bolster <i>et al.</i>, 1996)</b>	<b>765 samples</b>

<sup>1</sup> Field spectrometer GER2600

<sup>2</sup> NIR laboratory spectrometer

**Table 4.2: Field data for the study areas in the Krusne hory, northwest Bohemia, Czech Republic, August 1998**

	Foliar Constituents	Mean	St. Deviation	SEP	Terms	SEC	R2	SECV
1	Cellulose (%)	38.64	2.49	0.85	5	0.89	0.87	1.46
2	Lignin (%)	25.61	2.48	0.86	5	1.06	0.82	1.67
3	Polar (%)	31.85	3.60	0.83	5	0.78	0.95	1.31
4	Polar + Non-polar (%)	35.76	3.95	0.34	5	0.80	0.96	1.39
5	Non-polar (%)	3.91	Calculated as a difference between 4 and 3					
6	Nitrogen (%)	1.44	0.106	0.037	5	0.03	0.90	0.06

**Table 4.3: Calibration and validation precision statistics (R2 - goodness of fit, SEP - standard error of prediction, Terms - number of factors used in the statistical analysis, SECV – standard error of cross validation).**

Indices	Algorithm	Figure
	<b>1. 2.5nm-Narrow Band Ratios</b>	
C1	$R^{695}/R760$	A.1.1
C2	$R695/R420$	A.1.2
V1	$R740/R720$	A.1.3
V2	$(R734-R747)/(R715+R726)$	A.1.4
V3	$(R734-R747)/(R715+R720)$	A.1.5
PRI1	$(R530-R570)/(R530+R570)$	A.1.6
PRI2	$(R550-R530)/(R550+R530)$	A.1.7
PRI3	$(R570-R540)/(R570+R540)$	A.1.8
RE1	Average R(675...705)	A.1.9
RE2	Average R(714...725)	A.1.10
RE3	Average R(730...745)	A.1.11
SR	$R775/R675$	A.1.12
SIPI	$(R800-R450)/(R800-R650)$	A.1.13
PSRI	$(R680-R500)/750$	A.1.14
RARS	$R800/R670$	A.1.15
GM1	$R750/R550$	A.1.16
GM2	$R750/R700$	A.1.17
Green	$R554/R675$	A.1.18
Lichtenthaler	$R440/R690$	A.1.19
	<b>2. Broad Band Indices</b>	
TM3/TM1	$(\text{Average } R(620..690))/(\text{Average } R(450..520))$	A.2.1
TM5/TM4	$(\text{Average } R(1550..1750))/(\text{Average } R(760..900))$	A.2.2
NDVI	$(TM4-TM3)/(TM4+TM3)$	A.2.3
TVI	$\text{SQRT} ((NDVI+0.5)*100)$	A.2.4
NDVI550	$(TM4-R550)/(TM4+R550)$	A.2.5
NDVI675	$(TM4-R675)/(TM4+R675)$	A.2.6
NDVI700	$(TM4-R700)/(TM4+R700)$	A.2.7
	<b>10nm-Band Ratios</b>	
R550/R700	$R550/R700$	A.2.8
R850/R700	$R850/R700$	A.2.9
R850/R550	$R850/R550$	A.2.10

<sup>1</sup> R – spectral reflectance (%)

**Table 4.4: 2.5nm-Narrow Band Indices, Broad Band indices and 10nm-Band Ratios**



Indices	Algorithm	Figure
	<b>3. Derivative Indices</b>	
REIPwave	Position of D' maximum in the 670-730nm region	A.3.1
REIPslop=Dmax	D maximum in the 670-730nm region	A.3.2
V4=D715/D705	D715/D705	A.3.3
DMAX/D714	Dmax/D714	A.3.4
DMAX/D704	Dmax/D703.10	A.3.5
DMAX/D744	Dmax/D744.5	A.3.6
DPR1	$D_{\lambda_0}/D_{(\lambda_0+12)}$	A.3.7
DPR2	$D_{\lambda_0}/D_{(\lambda_0+22)}$	A.3.8
DPR21	$D_{\lambda_0}/D_{703}$	A.3.9
DPR21	$D_{\lambda_0}/D_{720}$	A.3.10
	<b>4. Inverted Gaussian Model (IGM) Parameters</b>	
R <sub>s</sub>	R maximum in the 670-850nm region, IGF <sup>4</sup>	A.4.1
R <sub>o</sub>	R minimum in the 670-850nm region, IGF	A.4.2
$\lambda_0$	Wavelength position of R <sub>o</sub> , IGF	A.4.3
$\sigma$	$(\lambda_0 - \lambda_{\pi})$ , IGF	A.4.4
$\lambda_{\pi}$	Wavelength position of Dmax, IGF	A.4.5
	<b>5. Area</b>	
Slope	Slope of the line connecting the green and the NIR peak	A.5.1
Area	Area between the vegetation curve and the line in "Slope"	A.5.2
Intercept	Product of the Area calculation	A.5.3
Dept_sum	Product of the Area calculation	A.5.4
	<b>6. Narrow Band Short Wave (SWIR) Indices</b>	
SWIR1	R1365/R1455	A.6.1
SWIR12	$(R1365 - R1456)/(R1365 + R1456)$	A.6.2
SWIR2	R1890/R1950	A.6.3
SWIR22	$(R1890 - R1951)/(R1890 + R1951)$	A.6.4

<sup>4</sup> D - derivative value, product of first derivative transformation of reflectance

**Table 4.5: Derivative indices, Inverted Gaussian Model (IGM), Area parameters and Narrow Band Short Wave (SWIR) Indices**

Stand parameters	Damage Level			
	0	1	2	3
Tree Height (m)	21.75	19.10	19.61	15.87
DBH (cm)	37.13	34.67	32.81	25.16
Age (years)	62.69	50.00	52.70	48.37
Elevation (m asl)	879.82	908.59	871.28	827.35
Canopy Closure (%)	76.14	75.91	67.48	58.90
Stand Density (trees/ha)	617.50	666.53	594.26	731.91
Total Basal Area (m <sup>2</sup> /ha)	28.22	29.98	25.62	28.57

**Table 4.6: Mean values for forest stand parameters, Krusne hory, Czech republic 1998 (n=51).**

Stand Variable	n (sites)	F-ratio	p	r
Tree height	51	6.46	0.001	<u>0.67</u>
DBH	51	4.07	0.012	<u>0.69</u>
Age	51	1.99	0.128	0.39
Elevation	51	4.81	0.005	<u>0.62</u>
Canopy Closure	51	1.95	0.135	0.61
Total Basal Area (BA)	51	0.61	0.611	0.20
Stand Density	51	0.30	0.826	0.16
Tree Damage Class	51	59.28	0.000	0.98

**Table 4.7: Analysis of variances for forest stand parameters and damage level**

Effects	Chlorophyll a			Chlorophyll b			Chlorophyll (a+b)			Carotenoids		
	df	F-ratio	P	df	F-ratio	P	df	F-ratio	P	df	F-ratio	P
Year	2	74.83	0.000	2	72.20	0.000	2	75.70	0	2	92.94	0
Damage Class	3	5.92	0.001	3	6.11	0.000	3	6.10	0.001	3	2.09	0.0998
Year*Damage Class	6	0.75	0.607	6	0.80	0.572	6	0.71	0.645	6	0.86	0.5249
Error	728			728			728			728		

Effects	Chlorophyll a/b			Carotenoids/Nitrogen			(a+b)/Car			N/(a+b)			Dw/Fw		
	df	F-ratio	P	df	F-ratio	P	df	F-ratio	P	df	F-ratio	P	df	F-ratio	P
Year	2	9.95	0.000	2	63.51	0	2	7.68	0.001	2	78.67	0.000	2	35.25758	0
Damage Class	3	7.90	0.000	3	6.40	0	3	7.50	0.000	3	8.39	0.000	3	1.797409	0.146
Year*Damage Class	6	6.84	0.000	6	1.17	0.32	6	1.49	0.177	6	1.15	0.334	6	1.861941	0.085
Error	728			728			728			728			728		

Effects	Nitrogen			Lignin			Cellulose			Non-polar Constituents			Polar Constituents		
	df	F-ratio	P	df	F-ratio	P	df	F-ratio	P	df	F-ratio	P	df	F-ratio	P
Year	2	12.68	0.000	2	4.04	0.018	2	145.73	0.000	2	37.70	0.000	2	46.00	0.000
Damage Class	3	1.85	0.136	3	89.01	0.000	3	68.74	0.000	3	11.49	0.000	3	128.85	0.000
Year*Damage Class	6	4.74	0.030	6	0.418	0.867	6	7.58	0.006	6	89.13	0.000	6	0.67	0.415
Error	764			764			764			764			764		

**Table 4.8: Analysis of variances (ANOVA) conducted on foliar constituents. Needle damage class and age (year) are the main effects.**

Pigments and Foliar Constituents	Year 1				Year2				Year3			
	DC0	DC1	DC2	DC3	DC0	DC1	DC2	DC3	DC0	DC1	DC2	DC3
Chlorophyll <i>a</i>	0	-2.19	-6.51	-15.35	0	-0.57	-6.97	-9.44	0	1.35	-13.45	-11.55
Chlorophyll <i>b</i>	0	-3.56	-10.54	-21.17	0	-0.91	-7.98	-12.87	0	0.37	-13.40	-6.50
Carotenoids	0	-3.71	-4.22	-9.12	0	1.03	-3.12	-1.42	0	1.87	-11.24	-4.57
( <i>a+b</i> )	0	-2.55	-7.57	-16.88	0	-0.66	-7.23	-10.32	0	1.10	-13.44	-10.24
<i>a/b</i>	0	1.47	4.48	6.91	0	0.61	1.10	3.96	0	1.47	0.16	-0.97
Nitrogen (N)	0	0.56	-1.55	-1.09	0	2.37	2.92	5.37	0	1.12	1.57	1.07
Lignin	0	-0.16	-9.76	-13.91	0	-0.27	-10.61	-14.93	0	-0.22	-9.24	-12.91
Cellulose	0	-2.60	-6.09	-11.15	0	-2.78	-6.72	-11.04	0	-2.40	-4.76	-9.78
Polar	0	3.56	14.02	19.93	0	3.95	14.30	18.40	0	2.86	9.37	12.71
Non-polar	0	5.52	37.17	85.29	0	2.40	33.38	79.13	0	3.58	33.08	78.54
N/( <i>a+b</i> )	0	-3.45	-11.10	-17.58	0	-4.95	-13.72	-19.78	0	-4.61	-19.50	-9.14
Carotenoids/N	0	-6.03	-9.07	-10.93	0	-3.07	-9.77	-11.69	0	-4.06	-17.68	-3.81
Dw/Fw	0	-1.48	-1.82	-0.69	0	4.90	3.96	6.55	0	-0.79	3.10	7.31

**Table 4.9: Change (%) in foliar pigments and chemical constituents occurring with forest damage by needle age group :**

Dependent Variable	F-ratio	p	r
Chlorophyll a	1.353	0.269	0.428
Chlorophyll b	1.372	0.263	0.453
Carotenoids	0.682	0.567	0.273
Total Chl. (a+b)	1.367	0.265	0.436
a/b	1.261	0.299	0.563
Dw/Fw	1.316	0.281	0.456
Nitrogen (N)	0.365	0.779	0.183
N/(a+b)	3.848	0.016	<u>0.652</u>
Carotenoids/N	2.135	0.111	0.488
Lignin	1.949	0.134	0.521
Cellulose	5.935	0.002	<u>0.671</u>
Polar	4.272	0.009	<u>0.802</u>
Non-Polar	2.566	0.065	0.422

**Table 4.10: Analysis of variances for foliar constituents and damage**

Effects	C1			C2			V1=R740/R720			V2			V3		
	df	F-ratio	P	df	F-ratio	P	df	F-ratio	P	df	F-ratio	P	df	F-ratio	P
Year	2	18.25	0.000	2	5.15	0.006	2	120.19	0.000	2	16.00	0.000	2	15.94	0.000
Damage Class	3	14.16	0.000	3	6.40	0.000	3	0.44	0.726	3	5.86	0.001	3	5.62	0.001
Year*Damage Class	6	3.48	0.000	6	4.22	0.000	6	1.52	0.014	6	4.78	0.000	6	3.32	0.000
Error	729			729			729			729			729		
Effects	PRI1			PRI2			PRI3			RE1			RE2		
Year	2	19.28	0.000	2	167.40	0.000	2	76.23	0.000	2	609.75	0	2	1346.57	0
Damage Class	3	14.11	0.000	3	1.84	0.139	3	14.94	0.000	3	1.94	0.121	3	4.81	0.003
Year*Damage Class	6	2.67	0.000	6	2.95	0.000	6	2.83	0.000	6	2.55	0	6	3.09	0
Error	729			729			729			729			729		
Effects	RE3			SR			SIPI			PSRI			RARS		
Year	2	1392.7	0	2	22.59	0	2	68.09	0	2	62.79	0.000	2	27.05	0.000
Damage Class	3	11.13	0	3	8.63	0	3	14.58	0	3	3.37	0.018	3	12.85	0.000
Year*Damage Class	6	3.86	0	6	3.32	0	6	3.29	0	6	3.97	0.000	6	3.40	0.000
Error	729			680			680			729			729		
Effects	GM1			GM2			Green			Lichtenthaler					
Year	2	23.01	0	2	28.00	0	2	431.04	0.000	2	0.81	0.444	2	0.81	0.444
Damage Class	3	9.08	0	3	9.39	0	3	2.38	0.069	3	5.15	0.002	3	5.15	0.002
Year*Damage Class	6	3.32	0	6	3.31	0	6	3.50	0.000	6	3.99	0.000	6	3.99	0.000
Error	729			729			729			729			729		

Table 4.11: Narrow Band Indices (2.5nm): Analysis of variances (ANOVA), conducted on fresh foliage reflectance spectral indices

Effect	TM3/1			TMS/4			NDVI			TVI		
	df	F-ratio	P	df	F-ratio	P	df	F-ratio	P	df	F-ratio	P
Year	2	0.25	0.779	2	289.11	0.000	2	37.06	0.000	2	31.31	0.000
Damage Class	3	7.73	0.000	3	12.76	0.000	3	25.82	0.000	3	24.64	0.000
Year*Damage Class	6	9.04	0.000	6	6.07	0.000	6	3.50	0.002	6	1.26	0.263
Error	729			729			729			729		
Effect	NDVI550			NDVI675			NDVI700					
	df	F-ratio	P	df	F-ratio	P	df	F-ratio	P			
Year	2	21.12	0.000	2	51.71	0.000	2	17.67	0.000			
Damage Class	3	10.94	0.000	3	13.47	0.000	3	13.16	0.000			
Year*Damage Class	6	3.17	0.000	6	3.41	0.000	6	3.39	0.000			
Error	729			729			729					
Effect	R550/R700			R850/R700			R850/R550					
	df	F-ratio	P	df	F-ratio	P	df	F-ratio	P			
Year	2	111.45	0.000	2	20.34	0.000	2	24.61	0.000			
Damage Class	3	1.95	0.120	3	8.68	0.000	3	7.91	0.000			
Year*Damage Class	6	3.32	0.000	6	3.34	0.000	6	3.38	0.000			
Error	729			729			729					

**Table 4.12: Broad Band and 10nm-Band Indices: Analysis of variances (ANOVA) conducted on fresh foliage reflectance spectral indices**

Effect	REIP wave			REIP slope			V4			Dmax/D704			Dmax/D714		
	df	F-ratio	P	df	F-ratio	P	df	F-ratio	P	df	F-ratio	P	df	F-ratio	P
Year	2	4.57	0.011	2	718.26	0.00	2	23.13	0.000	2	21.87	0	2	2.55	0.078
Damage Class	3	18.70	0.000	3	20.56	0.00	3	32.27	0.000	3	18.96	0	3	3.48	0.016
Year*Damage Class	6	0.57	0.752	6	15.39	0.00	6	2.89	0.009	6	1.98	0.0656	6	0.65	0.686
Error	729			729			729			726			726		
Effect	Dmax/D744			DPR1			DPR2			DPR21			DPR22		
	df	F-ratio	P	df	F-ratio	P	df	F-ratio	P	df	F-ratio	P	df	F-ratio	P
Year	2	5.95	0.003	2	0.29	0.745	2	0.62	0.538	2	0.79	0.455	2	0.83	0.435
Damage Class	3	1.24	0.293	3	0.52	0.669	3	0.51	0.673	3	0.53	0.664	3	0.55	0.649
Year*Damage Class	6	1.66	0.128	6	0.98	0.435	6	1.05	0.393	6	1.07	0.377	6	1.05	0.394
Error	726			729			729			729			729		

**Table 4.13: Derivative indices: Analysis of variances (ANOVA) conducted on fresh foliage reflectance spectral indices**

Effect	Rs			Ro			$\lambda_0$			$\sigma$			$\lambda\pi$		
	df	F-ratio	P	df	F-ratio	P	df	F-ratio	P	df	F-ratio	P	df	F-ratio	P
Year	2	1070.31	0.000	2	11.18	0.000	2	5.37	0.005	2	2.246	0.107	2	13.71	0.000
Damage Class	3	12.67	0.000	3	16.03	0.000	3	5.44	0.001	3	4.350	0.005	3	12.27	0.000
Year*Damage Class	6	15.32	0.000	6	2.81	0.010	6	3.53	0.002	6	3.680	0.001	6	0.62	0.718
Error	725			725			725			725			725		

**Table 4.14: IGM parameters: Analysis of variances (ANOVA) conducted on fresh foliage reflectance spectral indices**



Effect	AREAS			Slope			Intercept			Depth_sum		
	df	F-ratio	P	df	F-ratio	P	df	F-ratio	P	df	F-ratio	P
Year	2	959.77	0	2	938.52	0	2	787.73	0	2	960.638	0
Damage Class	3	14.788	0	3	13.92	0	3	14.42	0	3	14.79	0
Year*Damage Class	49	3.646	0	49	4.09	0	49	4.111	0	49	3.646	0
Error	680			680			680			680		

**Table 4.15. Area (AAL) parameters: Analysis of variances (ANOVA) conducted on fresh foliage reflectance spectral indices**

Effect	SWIR1			SWIR12			SWIR2			SWIR22		
	df	F-ratio	P	df	F-ratio	P	df	F-ratio	P	df	F-ratio	P
Year	2	123.11	0.000	2	170.88	0.00	2	96.57	0.000	2	108.08	0.000
Damage Class	3	13.97	0.000	3	13.39	0.00	3	6.09	0.000	3	5.21	0.001
Year*Damage Class	6	5.49	0.000	6	6.90	0.00	6	6.74	0.000	6	7.14	0.000
Error	729			729			729			729		

**Table 4.16. Short Wave Infrared (SWIR) indices: Analysis of variances (ANOVA) conducted on fresh foliage reflectance spectral indices**

Optical Indices	Year 1				Year2				Year3			
	DC0	DC1	DC2	DC3	DC0	DC1	DC2	DC3	DC0	DC1	DC2	DC3
C1	0	-1.15	4.72	13.61	0	2.56	10.84	22.86	0	4.52	8.09	39.08
C2	0	-0.47	2.99	6.70	0	3.40	4.72	11.01	0	4.56	7.28	20.36
V1	0	0.42	0.30	-3.44	0	-0.69	-0.57	-4.26	0	1.73	9.83	15.54
V2	0	1.90	2.60	-8.52	0	-1.61	-0.89	-11.40	0	-5.09	-13.25	-28.13
V3	0	1.97	2.56	-9.05	0	-1.76	-1.05	-12.13	0	-5.29	-14.16	-29.77
PRI1	0	-0.54	-3.92	-53.05	0	-10.21	-12.46	-54.29	0	-18.81	-40.38	-85.68
PRI2	0	1.24	7.40	15.19	0	0.46	3.96	7.07	0	2.20	6.65	3.13
PRI3	0	0.20	1.41	-18.55	0	-5.16	-4.90	-24.81	0	-9.06	-18.95	-44.08
RE1	0	0.26	10.47	19.01	0	1.10	7.70	11.63	0	0.71	3.56	5.05
RE2	0	0.85	11.59	11.77	0	-0.54	6.72	2.00	0	-2.96	-3.02	-11.95
RE3	0	1.32	11.82	8.45	0	-1.22	6.00	-1.92	0	-4.85	-6.88	-19.44
SR	0	0.29	1.65	-6.45	0	-1.91	-0.46	-9.45	0	-3.84	-8.08	-21.07
SIPI	0	0.24	1.29	-1.34	0	-0.47	0.12	-3.36	0	-0.82	-1.96	-7.76
PSRI	0	-27.15	-19.28	13.78	0	-2.14	-0.69	18.22	0	-3.39	40.10	68.26
RARS	0	-2.38	-9.07	28.41	0	3.48	0.22	36.85	0	4.97	15.41	63.52
GM1	0	0.31	1.82	-5.95	0	-1.75	-0.05	-8.91	0	-3.61	-7.60	-20.34
GM2	0	0.93	1.19	-7.70	0	-2.28	-1.33	-10.59	0	-4.07	-10.74	-23.97
Green	0	2.22	6.91	6.83	0	-0.93	0.03	-4.10	0	1.00	-4.90	-11.47
Lichtenthaler	0	0.42	-1.31	-7.70	0	-1.28	-1.60	-6.84	0	-3.15	-8.38	-13.48

**Table 4.17: Change (sensitivity in %) in reflectance Visible/Red Edge indices occurring with forest damage by needle age group**

Indices	Year 1				Year2				Year3			
	DC0	DC1	DC2	DC3	DC0	DC1	DC2	DC3	DC0	DC1	DC2	DC3
TM3/TM1	0	-2.15	-2.94	6.80	0	1.27	3.37	10.63	0	1.27	3.37	10.63
TM5/TM4	0	-1.65	-5.86	7.52	0	4.10	8.94	30.38	0	4.10	8.94	30.38
NDVI	0	0.34	1.35	-2.74	0	-0.63	0.00	-4.53	0	-1.17	-2.72	-9.53
TVI	0	0.11	0.42	-0.99	0	-0.20	0.00	-1.53	0	-0.37	-0.86	-3.12
NDVI550	0	0.22	1.06	-2.59	0	-0.64	0.19	-3.56	0	-2.03	-2.83	-8.87
NDVI675	0	0.44	1.60	-2.56	0	-0.57	0.08	-4.70	0	-0.88	-2.81	-9.99
NDVI700	0	0.58	1.02	-5.40	0	-1.10	-0.41	-6.44	0	-2.64	-5.33	-14.37
TM1	0	1.92	7.58	9.30	0	-0.48	0.95	2.66	0	-0.48	0.95	2.66
TM2	0	0.56	8.40	14.80	0	0.91	0.38	1.50	0	0.91	0.38	1.50
TM3	0	-0.66	3.60	18.03	0	1.29	4.12	15.07	0	1.29	4.12	15.07
TM4	0	1.77	12.76	8.55	0	-5.35	-7.47	-20.34	0	-5.35	-7.47	-20.34
TM5	0	0.13	6.47	9.98	0	-1.08	0.39	-0.63	0	-1.08	0.39	-0.63
R550/R700	0	0.71	-0.51	-2.76	0	-0.66	-1.42	-2.90	0	-0.38	-3.65	-5.34
R840/R550	0	0.53	2.45	-5.05	0	-1.62	0.50	-8.00	0	-3.52	-7.02	-19.27
R840/R700	0	1.18	2.03	-6.69	0	-2.21	-0.72	-9.71	0	-3.98	-10.25	-23.08

**Table 4.18: Change (sensitivity in %) in Broad Band Indices and 10nm-Band Ratios occurring with forest damage by needle age group**

Derivative Indices	Year 1				Year2				Year3			
	DC0	DC1	DC2	DC3	DC0	DC1	DC2	DC3	DC0	DC1	DC2	DC3
REIP wave	0	0.11	-0.07	-0.46	0	-0.05	-0.04	-0.39	0	-0.13	-0.26	-0.57
REIP slope	0	1.31	10.78	3.04	0	-2.09	3.97	-8.19	0	-6.93	-12.41	-29.68
V4	0	0.06	-1.39	-4.50	0	-0.80	-1.62	-4.39	0	-2.17	-5.02	-9.38
DmaxD704	0	0.08	-2.41	-5.60	0	-1.62	-3.67	-6.23	0	-2.23	-8.54	-12.60
DmaxD714	0	0.52	0.01	4.25	0	-0.32	-1.57	11.11	0	-0.46	-3.50	2.22
DmaxD744	0	-2.77	-4.75	-1.54	0	2.66	-1.35	3.12	0	3.06	5.76	8.40
DPR1	0	-7.69	-0.87	-35.95	0	-80.43	-86.39	-85.95	0	37.75	119.24	247.30
DPR2	0	-10.57	0.12	-45.24	0	-77.32	-84.10	-84.41	0	-0.72	111.00	231.17
DPR21	0	-11.52	-0.46	-46.37	0	-76.03	-83.65	-83.72	0	-10.10	99.75	212.00
DPR22	0	-13.18	-0.26	-49.56	0	-74.42	-83.45	-83.96	0	-13.04	89.18	180.26

**Table 4.19: Change (%) in derivative indices occurring with forest damage by needle age group**

IGM Parameters	Year 1				Year2				Year3			
	DC0	DC1	DC2	DC3	DC0	DC1	DC2	DC3	DC0	DC1	DC2	DC3
Rs	0	2.57	12.10	8.13	0	-0.32	6.59	1.13	0	-3.26	-5.54	-15.60
Ro	0	1.01	4.93	8.92	0	6.98	14.70	20.82	0	8.19	25.70	41.24
$\lambda_0$	0	-0.06	-0.18	-2.00	0	-0.08	-0.18	-0.13	0	-0.13	-0.28	-0.32
$\sigma$	0	-0.25	-0.53	32.52	0	-0.39	-0.76	0.22	0	-0.65	-0.79	0.87
$\lambda\pi$	0	-0.07	-0.20	-0.30	0	-0.10	-0.21	-0.11	0	-0.15	-0.31	-0.26

**Table 4.20: Change (sensitivity %) in the Inverted Gaussian Model (IGM) parameters occurring with forest damage by needle age group**

AAL Parameters	Year 1				Year2				Year3			
	DC0	DC1	DC2	DC3	DC0	DC1	DC2	DC3	DC0	DC1	DC2	DC3
Area	0	2.37	13.34	6.09	0	-2.33	5.02	-7.55	0	-6.42	-10.58	-28.28
Slope	0	1.95	12.81	6.84	0	-1.85	5.92	-5.31	0	-6.36	-8.95	-24.99
Intercept	0	2.03	13.13	6.06	0	-2.03	6.00	-6.48	0	-7.01	-9.75	-27.25
Dept_Sum	0	2.33	13.33	6.02	0	-2.30	5.02	-7.52	0	-6.41	-10.54	-28.25

**Table 4.21: Change (sensitivity %) in the Area Above the Line (AAL) parameters occurring with forest damage by needle age group**

Indices	Year 1				Year2				Year3			
	DC0	DC1	DC2	DC3	DC0	DC1	DC2	DC3	DC0	DC1	DC2	DC3
SWIR1	0	-0.63	-4.96	1.26	0	1.06	-3.42	3.79	0	1.25	4.11	14.36
SWIR12	0	0.62	4.72	0.05	0	-1.10	3.60	-2.77	0	-1.35	-4.11	-13.66
SWIR2	0	0.39	-1.51	-0.08	0	0.16	-1.40	0.05	0	0.22	2.13	6.05
SWIR22	0	-2.46	9.31	1.87	0	-1.60	10.91	1.01	0	-1.91	-17.45	-46.94

**Table 4.22: Change (sensitivity %) in the Short Wave Infrared (SWIR) indices occurring with forest damage by needle age group**

Index	F-ratio	p	r	n (sites)
C1	1.35	0.269	0.50	49
C2	2.26	0.094	0.53	49
V1	1.35	0.271	0.58	49
V2	3.35	0.027	0.53	49
V3	3.39	0.026	0.54	49
PRI1	4.90	0.005	<u>0.69</u>	49
PRI2	4.58	0.007	0.57	49
PRI3	3.16	0.034	<u>0.66</u>	49
RE1	1.00	0.401	<u>0.65</u>	49
RE2	0.22	0.880	0.45	49
RE3	1.32	0.281	0.36	49
SR	3.52	0.022	0.54	49
SIPI	1.77	0.166	0.47	49
PSRI	2.01	0.126	0.45	49
RARS	1.22	0.313	0.44	49
GM1	6.03	0.002	0.56	49
GM2	9.27	0.000	0.64	49
Green	0.50	0.687	0.21	49
Lichtenthaler	5.44	0.003	0.52	49

**Table 4.23: Analysis of variances for 2.5nm-Narrow Band Indices**

Index	F-ratio	p	r	n (sites)
TM1	0.56	0.646	0.31	49
TM2	0.68	0.567	0.38	49
TM3	1.17	0.333	0.47	49
TM4	2.31	0.089	0.41	49
TM5	1.26	0.300	0.38	49
NDVI	1.77	0.167	0.48	49
TVI	1.68	0.185	0.47	49
TM31	2.24	0.096	0.48	49
TM54	1.63	0.195	0.57	49
NDVI550	3.48	0.023	0.51	49
NDVI675	1.48	0.234	0.46	49
NDVI700	2.98	0.041	0.57	49
R550/R700	1.14	0.342	<u>0.61</u>	49
R840/R550	3.23	0.031	0.49	49
R840/R700	3.18	0.033	0.57	49

**Table 4.24: Analysis of variances for Broad Band Indices and 10nm-Band Ratios**

Index	F-ratio	p	r	n (sites)
REIP wave	3.13	0.035	<u>0.58</u>	49
REIP slope	2.67	0.059	<u>0.66</u>	49
V4	4.61	0.007	<u>0.69</u>	49
Dmax/D704	3.33	0.028	<u>0.63</u>	49
Dmax/D714	0.30	0.828	0.17	49
Dmax/D744	0.66	0.584	0.21	49
DPR1	1.09	0.363	0.28	49
DPR2	0.99	0.408	0.26	49
DPR21	0.95	0.425	0.26	49
DPR22	0.98	0.411	0.26	49

**Table 4.25: Analysis of variances for the Derivative indices**

Index	F-ratio	p	r	n (sites)
Rs	1.43	0.248	0.42	49
Ro	2.26	0.094	0.49	49
$\lambda_0$	1.50	0.227	0.42	49
$\sigma$	0.85	0.475	0.37	49
$\lambda\pi$	3.18	0.033	0.43	49

**Table 4.26: Analysis of variances for the IGM parameters**

Index	F-ratio	p	r	n (sites)
Area	2.13	0.109	0.36	49
Slope	2.40	0.081	0.40	49
Intercept	2.65	0.060	0.40	49
Depth_sum	2.13	0.110	0.36	49

**Table 4.27: Analysis of variances for the AAL parameters**

Index	F-ratio	p	r	n (sites)
SWIR1	1.02	0.393	0.27	49
SWIR12	0.78	0.509	0.24	49
SWIR2	0.22	0.880	0.12	49
SWIR22	0.18	0.911	0.11	49

**Table 4.28: Analysis of variances for the SWIR indices**

Indices	<i>a</i>	<i>b</i>	Carotene	( <i>a+b</i> )	<i>a/b</i>	N	Lignin	Cellulose	Polar	Non-polar	N/( <i>a+b</i> )	Car./N	Dw/Fw
C1	-0.25	-0.29	-0.19	-0.26	0.31	-0.06	-0.33	-0.39	0.37	0.41	-0.30	-0.22	0.27
C2	-0.35	-0.39	-0.27	-0.36	0.30	-0.07	-0.36	-0.45	0.41	0.45	-0.42	-0.33	0.24
V740_720	0.00	0.00	0.02	0.00	0.12	0.29	-0.41	-0.16	0.33	-0.07	-0.19	-0.16	0.04
V2	-0.47	-0.53	-0.33	-0.49	0.47	-0.24	-0.36	-0.56	0.48	0.48	-0.44	-0.27	0.38
V3	-0.47	-0.54	-0.33	-0.49	0.48	-0.24	-0.37	-0.57	0.49	0.48	-0.45	-0.27	0.38
PR11	0.36	0.40	0.25	0.38	-0.40	0.03	0.50	<u>0.62</u>	<u>-0.60</u>	-0.51	0.44	0.30	-0.48
PR12	-0.47	-0.52	-0.35	-0.49	0.47	-0.22	-0.46	<u>-0.63</u>	<u>0.62</u>	0.31	-0.50	-0.34	0.49
PR13	-0.28	-0.30	-0.18	-0.29	0.33	0.03	-0.45	-0.52	0.51	0.47	-0.36	-0.24	0.41
RE1	-0.31	-0.38	-0.23	-0.33	0.48	0.02	-0.46	-0.43	0.47	0.42	-0.36	-0.24	0.17
RE2	-0.11	-0.17	-0.09	-0.12	0.33	0.13	-0.29	-0.12	0.22	0.11	-0.15	-0.11	-0.07
RE3	0.11	0.07	0.06	0.10	0.12	0.23	-0.12	0.14	-0.01	-0.11	0.06	0.02	-0.24
SR	0.47	0.52	0.32	0.49	-0.46	0.22	0.33	<u>0.60</u>	-0.48	-0.55	0.47	0.28	-0.44
SIP1	0.16	0.20	0.11	0.17	-0.25	-0.01	0.23	0.31	-0.27	-0.36	0.19	0.12	-0.25
PSR1	-0.01	-0.05	-0.04	-0.02	0.15	0.07	-0.27	-0.03	0.14	0.15	0.02	0.00	-0.11
RARS	-0.12	-0.15	-0.09	-0.13	0.19	0.03	-0.26	-0.26	0.26	0.32	-0.17	-0.12	0.19
GM1	0.47	0.51	0.31	0.48	-0.44	0.22	0.32	0.58	-0.46	-0.54	0.45	0.27	-0.43
GM2	0.46	0.51	0.31	0.47	-0.49	0.19	0.45	<u>0.61</u>	-0.55	-0.57	0.45	0.27	-0.40
GREEN	-0.31	-0.30	-0.22	-0.31	0.10	-0.33	-0.01	-0.27	0.17	0.03	-0.29	-0.20	0.26
Lichtenthaler	0.29	0.33	0.20	0.30	-0.33	0.11	0.47	0.40	-0.43	-0.45	0.29	0.19	-0.19

**Table 4.29: Narrow Band Indices (2.5nm): Correlation between indices and foliar pigments, and indices and chemical constituents**



Indices	a	b	Carotene	(a+b)	a/b	N	Lignin	Cellulose	Polar	Non-polar	N/(a+b)	Car./N	Dw/Fw
TM1	-0.07	-0.12	-0.07	-0.08	0.23	0.03	-0.07	-0.01	0.02	0.17	-0.08	-0.06	-0.14
TM2	-0.19	-0.25	-0.12	-0.21	0.39	0.13	-0.11	-0.26	0.17	0.41	-0.23	-0.13	0.08
TM3	-0.09	-0.13	-0.05	-0.10	0.27	0.22	-0.18	-0.22	0.19	0.38	-0.16	-0.10	0.11
TM4	0.30	0.30	0.19	0.31	-0.14	0.21	0.19	0.44	-0.35	-0.28	0.32	0.20	-0.38
TM5	0.33	0.31	0.29	0.33	0.02	0.53	-0.01	0.15	-0.11	0.12	0.22	0.18	-0.22
NDVI	0.18	0.21	0.13	0.19	-0.24	-0.01	0.27	0.32	-0.30	-0.37	0.21	0.15	-0.23
TVI	0.17	0.20	0.13	0.18	-0.23	-0.01	0.27	0.31	-0.29	-0.36	0.21	0.15	-0.22
TM31	-0.07	-0.09	-0.02	-0.08	0.16	0.22	-0.19	-0.26	0.22	0.33	-0.14	-0.08	0.21
TM54	-0.02	-0.04	0.04	-0.02	0.21	0.27	-0.31	-0.30	0.30	0.38	-0.14	-0.07	0.16
NDVI550	0.44	0.48	0.31	0.45	-0.39	0.21	0.26	0.52	-0.40	-0.50	0.43	0.28	-0.39
NDVI675	0.13	0.17	0.10	0.14	-0.21	-0.04	0.26	0.27	-0.26	-0.34	0.17	0.12	-0.18
NDVI700	0.37	0.42	0.27	0.39	-0.39	0.14	0.38	0.51	-0.46	-0.49	0.38	0.26	-0.35
R550_700	0.12	0.15	0.08	0.13	-0.26	-0.04	0.48	0.28	-0.40	-0.27	0.15	0.10	-0.11
R840_550	0.46	0.51	0.32	0.48	-0.42	0.25	0.26	0.54	-0.41	-0.50	0.43	0.26	-0.40
R840_700	0.45	0.51	0.31	0.47	-0.47	0.21	0.40	0.58	-0.50	-0.53	0.43	0.26	-0.38

**Table 4.30: Broad Band Indices and 10nm-Band Ratios: Correlation between indices and foliar pigments, and indices and chemical constituents**

Indices	<i>a</i>	<i>b</i>	Carotene	( <i>a+b</i> )	<i>a/b</i>	N	Lignin	Cellulose	Polar	Non-polar	N/( <i>a+b</i> )	Car./N	Dw/Fw
REIP wave	0.28	0.32	0.19	0.29	-0.32	0.02	0.34	0.47	-0.44	-0.35	0.36	0.24	-0.32
REIP slope	0.38	0.43	0.28	0.40	-0.47	0.13	0.56	<u>0.60</u>	<u>-0.63</u>	-0.44	0.45	0.31	-0.46
V4	0.58	<u>0.64</u>	0.40	<u>0.60</u>	-0.58	0.24	0.56	<u>0.74</u>	<u>-0.69</u>	<u>-0.61</u>	<u>0.60</u>	0.38	-0.54
Dmax/D704	0.55	0.62	0.40	0.57	-0.59	0.21	0.49	0.71	-0.64	-0.54	0.57	0.37	-0.49
Dmax/D744	-0.34	-0.38	-0.30	-0.36	0.24	-0.09	-0.11	-0.23	0.16	0.21	-0.31	-0.26	0.05
Dmax/D714	0.12	0.11	0.05	0.12	-0.05	-0.02	-0.08	0.12	-0.06	0.17	0.12	0.05	-0.09
DPR1	-0.20	-0.21	-0.18	-0.20	0.23	-0.33	-0.07	-0.23	0.14	0.31	-0.12	-0.09	0.18
DPR2	-0.21	-0.21	-0.19	-0.21	0.22	-0.32	-0.10	-0.22	0.15	0.31	-0.13	-0.10	0.17
DPR21	-0.21	-0.21	-0.19	-0.21	0.21	-0.31	-0.11	-0.22	0.15	0.30	-0.13	-0.10	0.17
DPR22	-0.20	-0.20	-0.18	-0.20	0.20	-0.30	-0.10	-0.21	0.14	0.30	-0.12	-0.10	0.16

**Table 4.31: Derivative Indices:** Correlation between indices and foliar pigments, and indices and chemical constituents.

Indices	<i>a</i>	<i>b</i>	Carotene	( <i>a+b</i> )	<i>a/b</i>	N	Lignin	Cellulose	Polar	Non-polar	N/( <i>a+b</i> )	Car./N	Dw/Fw
Rs	0.20	0.18	0.11	0.20	0.05	0.34	-0.15	0.19	-0.02	-0.12	0.10	0.02	-0.29
Ro	-0.36	-0.41	-0.28	-0.38	0.35	-0.35	-0.37	-0.27	0.33	0.30	-0.28	-0.18	0.02
λo	0.23	0.26	0.21	0.24	-0.18	0.24	0.33	0.29	-0.33	-0.25	0.23	0.19	-0.15
σ	0.02	0.00	0.01	0.01	0.09	0.13	-0.19	-0.16	0.18	0.24	-0.06	-0.06	0.16
λπ	0.31	0.33	0.27	0.32	-0.15	0.45	0.23	0.20	-0.24	-0.07	0.24	0.18	-0.04

**Table 4.32: Inverted Gaussian Model Parameters:** Correlation between indices and foliar pigments, and indices and chemical constituents.

Indices	a	b	Carotene	(a+b)	a/b	N	Lignin	Cellulose	Polar	Non-polar	N/(a+b)	Car./N	Dw/Fw
Area	0.24	0.23	0.17	0.24	-0.05	0.28	0.03	0.29	-0.17	-0.26	0.18	0.11	-0.31
Slope	0.27	0.26	0.19	0.27	-0.04	0.34	-0.03	0.29	-0.13	-0.25	0.20	0.11	-0.31
Intercept	-0.30	-0.30	-0.21	-0.30	0.08	-0.35	0.01	-0.32	0.16	0.28	-0.23	-0.13	0.33
Depth_sum	0.24	0.23	0.17	0.24	-0.05	0.28	0.03	0.29	-0.17	-0.26	0.18	0.11	-0.31

**Table 4.33: Area (AAL) Parameters: Correlation between indices and foliar pigments, and indices and chemical constituents.**

Indices	a	b	Carotene	(a+b)	a/b	N	Lignin	Cellulose	Polar	Non-polar	N/(a+b)	Car./N	Dw/Fw
SWIR1	0.06	0.04	0.03	0.05	0.03	0.11	-0.04	-0.04	0.01	0.22	0.03	0.00	-0.03
SWIR12	-0.09	-0.07	-0.05	-0.09	0.01	-0.12	-0.03	-0.02	0.06	-0.19	-0.07	-0.03	0.08
SWIR2	-0.26	-0.25	-0.27	-0.26	-0.12	-0.19	-0.20	-0.13	0.16	0.12	-0.26	-0.28	0.03
SWIR22	0.26	0.25	0.27	0.26	0.13	0.20	0.19	0.11	-0.15	-0.11	0.26	0.28	-0.02

**Table 4.34: Narrow-band Short Wave Infrared (SWIR) indices: Correlation between indices and foliar pigments, and indices and chemical constituents.**

Indices	Correlation to DC		Sensitivity to damage for Year 3 needles			Correlation to Pigment Levels				Correlation to Foliar Constituents			
	p	r	Year3 DC1	Year3 DC2	Year3 DC3	a	b	(a+b)	N/(a+b)	Lignin	Cellulose	Polar	Non-polar
PR11	0.005	<u>0.69</u>	-18.81	-40.38	-85.68	0.36	0.40	0.38	0.44	0.50	<u>0.62</u>	<u>-0.60</u>	-0.51
PR13	0.034	<u>0.66</u>	-9.06	-18.95	-44.08	-0.28	-0.30	-0.29	-0.36	-0.45	-0.52	0.51	0.47
REIPslope	0.059	<u>0.66</u>	-6.93	-12.41	-29.68	0.38	0.43	0.40	0.45	0.56	0.56	<u>0.60</u>	<u>-0.63</u>
GM2	0.000	<u>0.64</u>	-4.07	-10.74	-23.97	0.38	0.43	0.47	0.45	0.45	<u>0.61</u>	-0.55	-0.57
Dmax/D704	0.028	<u>0.63</u>	-2.23	-8.54	-12.60	0.55	<u>0.62</u>	0.57	0.57	0.49	0.71	-0.64	-0.54
V4	0.007	<u>0.69</u>	-2.17	-5.02	-9.38	0.58	<u>0.64</u>	<u>0.60</u>	<u>0.60</u>	0.56	<u>0.74</u>	<u>-0.69</u>	<u>-0.61</u>
RE1	0.401	<u>0.65</u>	0.71	3.56	5.05	-0.31	-0.38	-0.33	-0.36	-0.46	-0.43	0.47	0.42
R550/R700	0.342	<u>0.61</u>	-0.38	-3.65	-5.34	0.12	0.15	0.13	0.15	0.48	0.28	-0.40	-0.27

**Table 4.35: Reflectance indices with highest potential for damage separation – Summary: Correlation between the indices and damage level, foliar pigments, and indices and chemical constituents. The indices performing best for damage separation are sorted by their sensitivity to initial damage (DC1). The R550/R700 performed best from the Broad Band Ratios, but is not able to separate DC0 and DC1.**

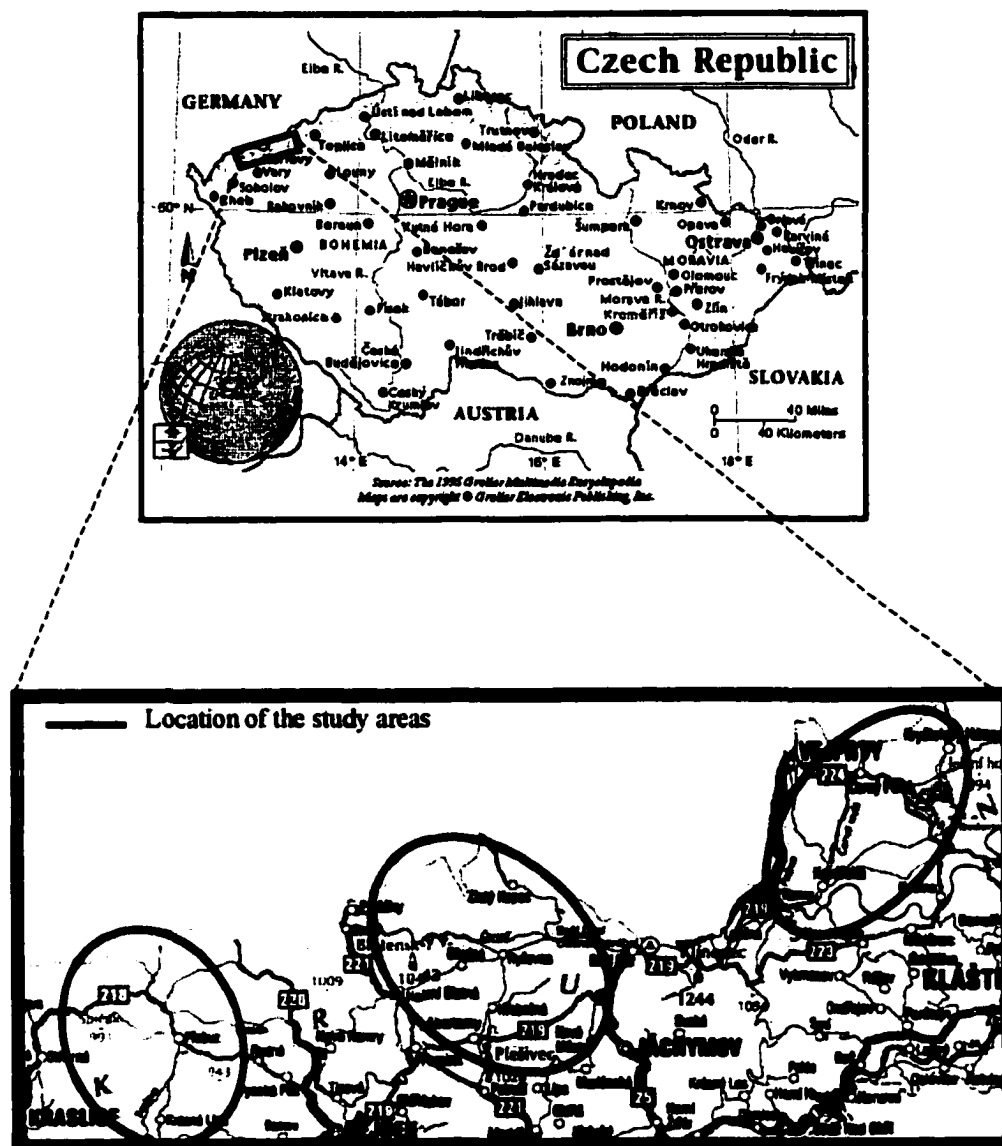


**Figure 4.1:** Location of the study areas in the Krusne hory, Czech Republic. The study area represents the full range of forest health conditions (DC0-DC3) due to SO<sub>2</sub> pollution.

**Healthy (DC0) Forest,  
Czech Republic**



**Heavily Damaged (DC3) Forest,  
Czech Republic**

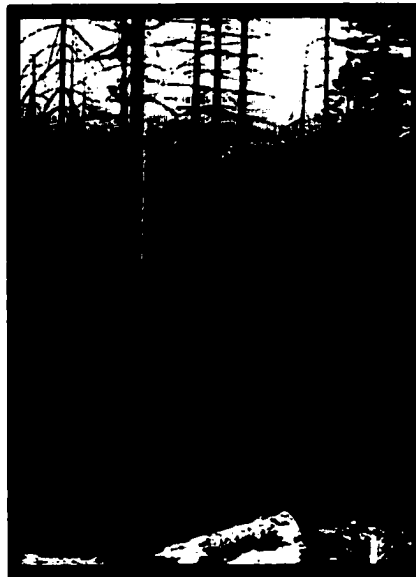


**Figure 4.2: Healthy and heavily damaged forests, Czech 1998.**

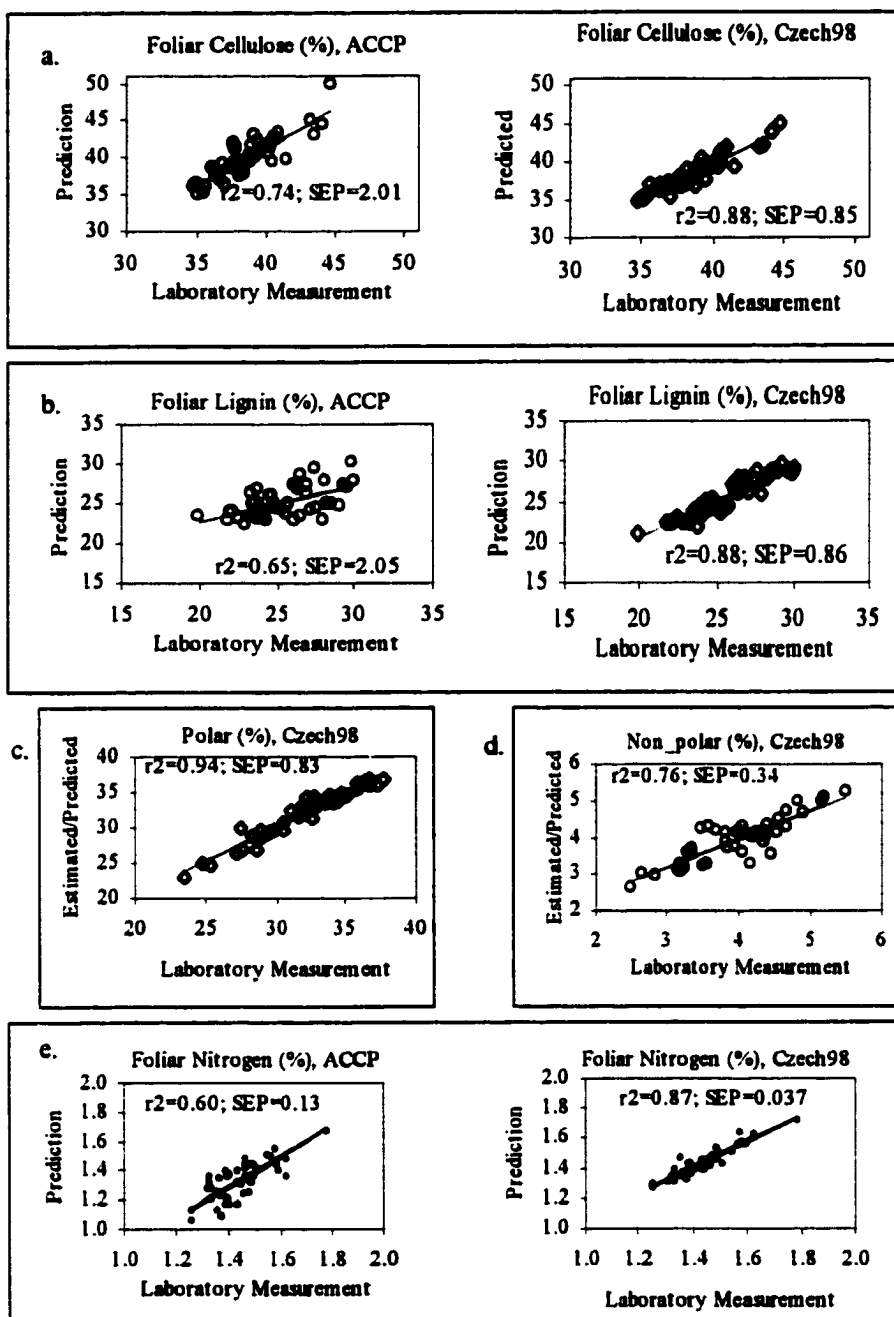


**Figure 4.3: Determination of foliar chemical constituents. Regression statistics: (a)cellulose, (b)lignin levels, (c) foliar polar constituents, (d) non-polar constituents, and (e) foliar nitrogen level.**

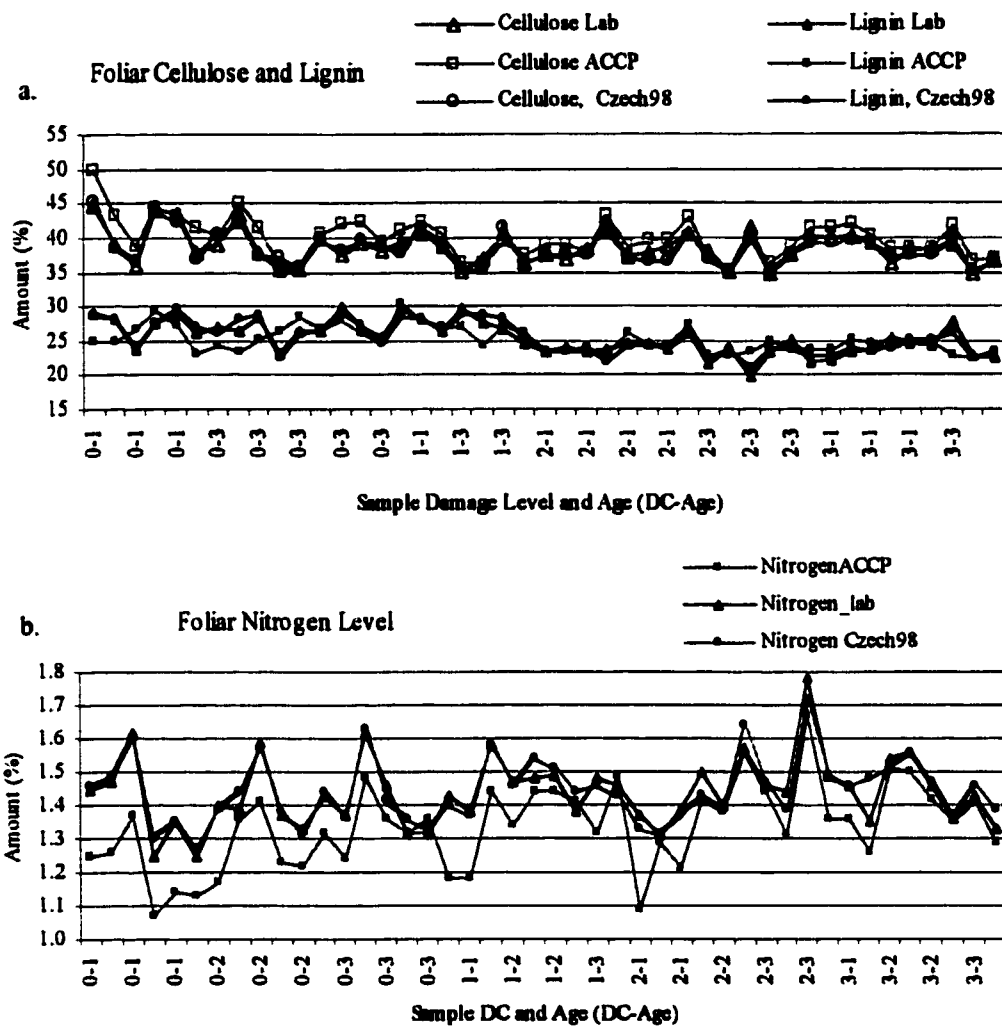


**Figure 4.4: Determination of foliar chemical constituents. Validation plots by sample: (a) foliar cellulose and lignin levels, (b) foliar nitrogen level.**

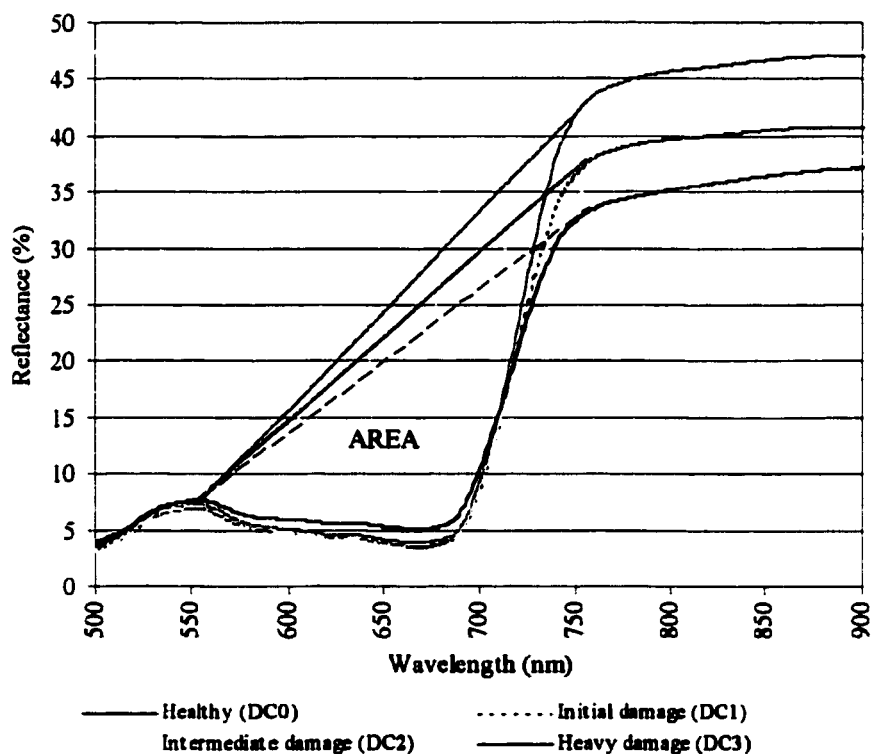


**Figure 4.5: Area Index.** The area between the vegetation curve and a line connecting the green peak and the shoulder of the NIR plateau at around 750nm (Area index) decreases with increase in damage level. The slope and the intercept of the line connecting the green peak and the shoulder of the NIR plateau also change with damage. Plotted are representative spectra for each damage level.



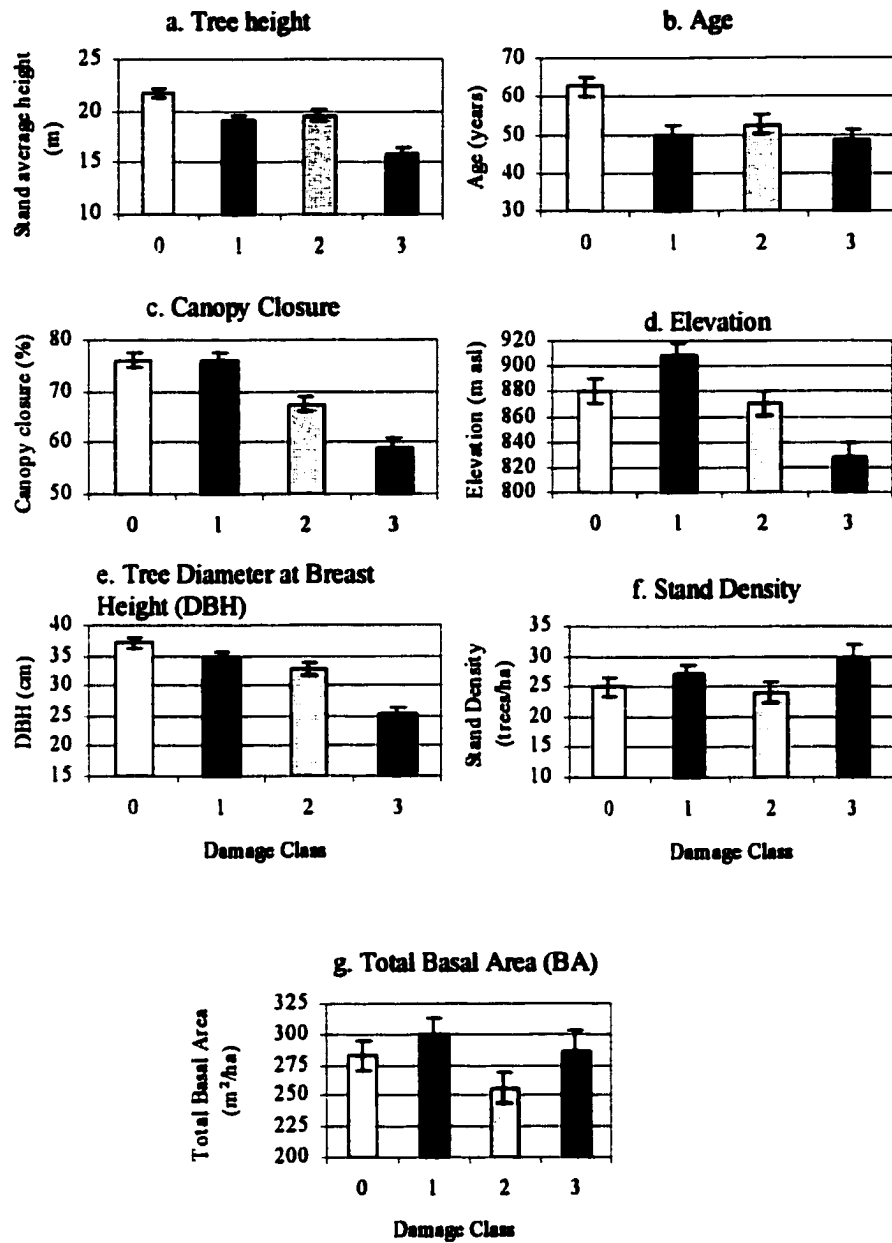


**Figure 4.6: Forest stand parameters.**

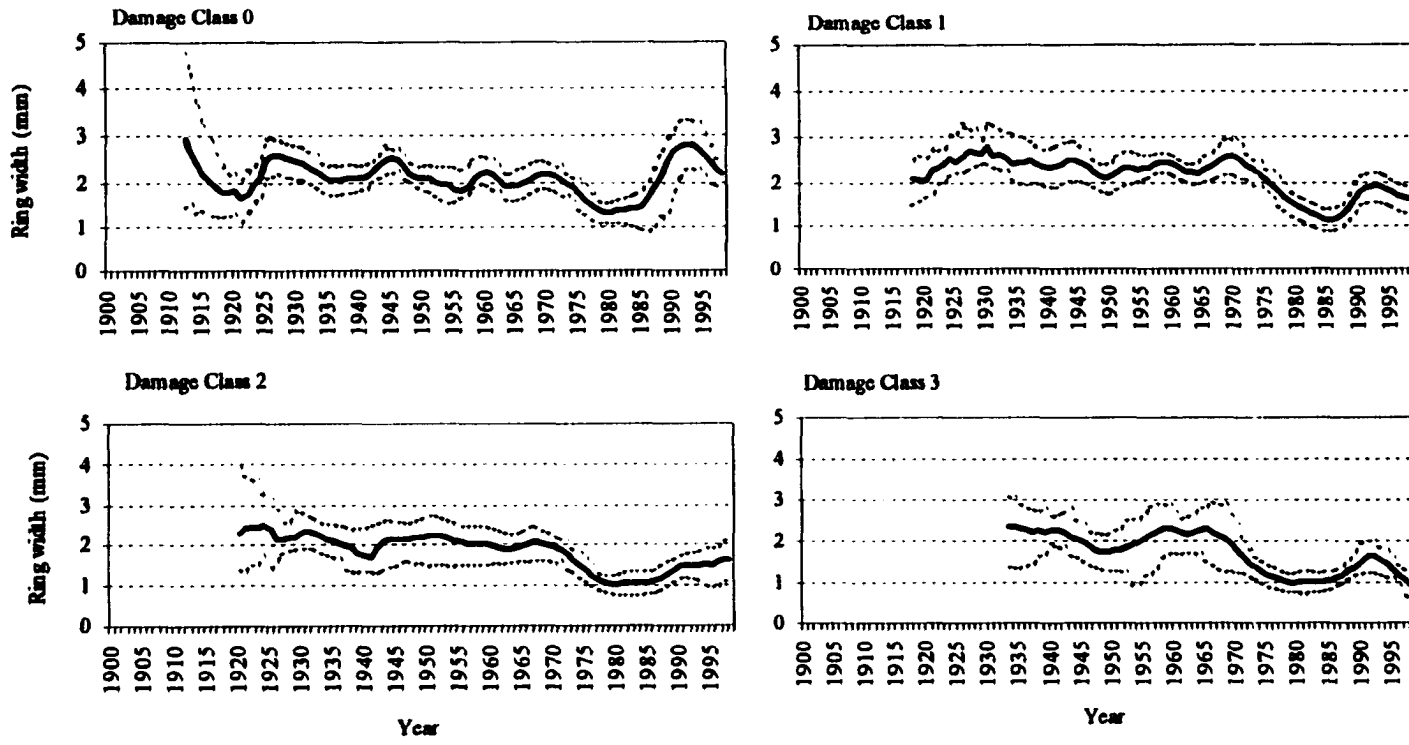


**Figure 4.7: Forest yearly increment growth by damage class.** Plotted are population means and 95% confidence intervals, based on dendrochronology assessment and bootstrapping statistical procedure.

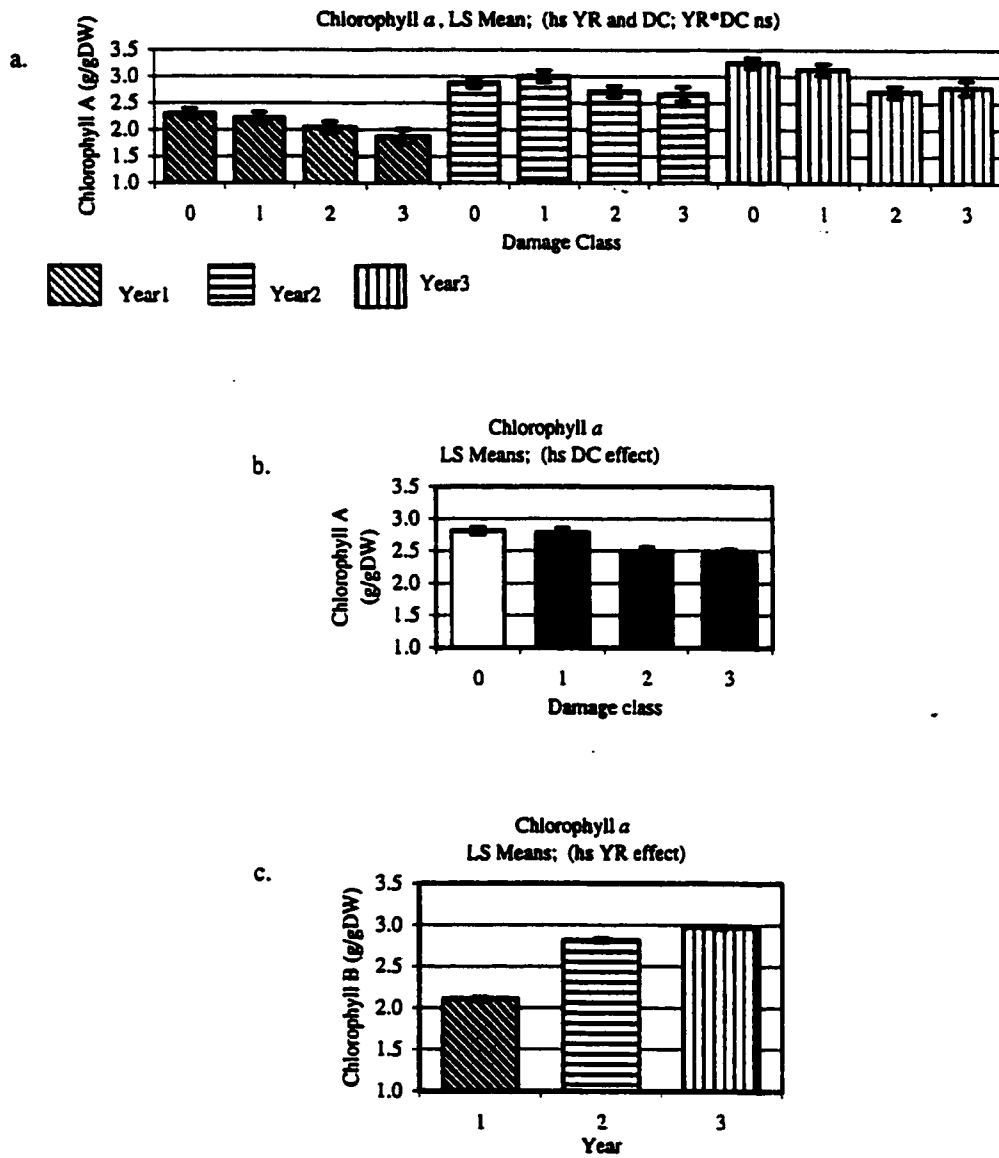


**Figure 4.8.1: Pigments. Chlorophyll *a* :** Least square (LS) means and standard errors are plotted. The effects of (a) damage and age together, (b) damage and (c) age are evaluated.

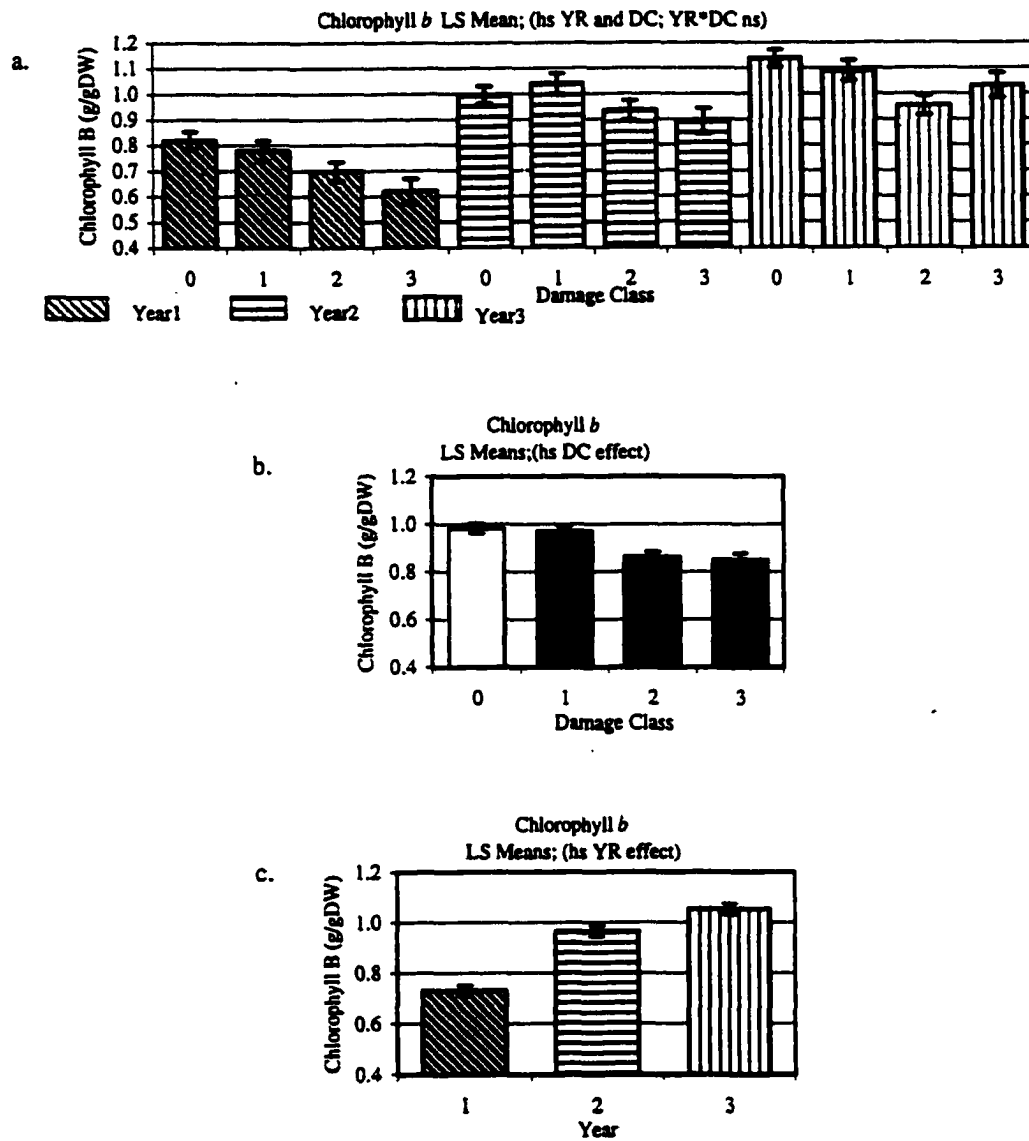


**Figure 4.8.2: Pigments. Chlorophyll *b* :** Least square (LS) means and standard errors are plotted. The effects of (a) damage and age together, (b) damage and (c) age are evaluated.

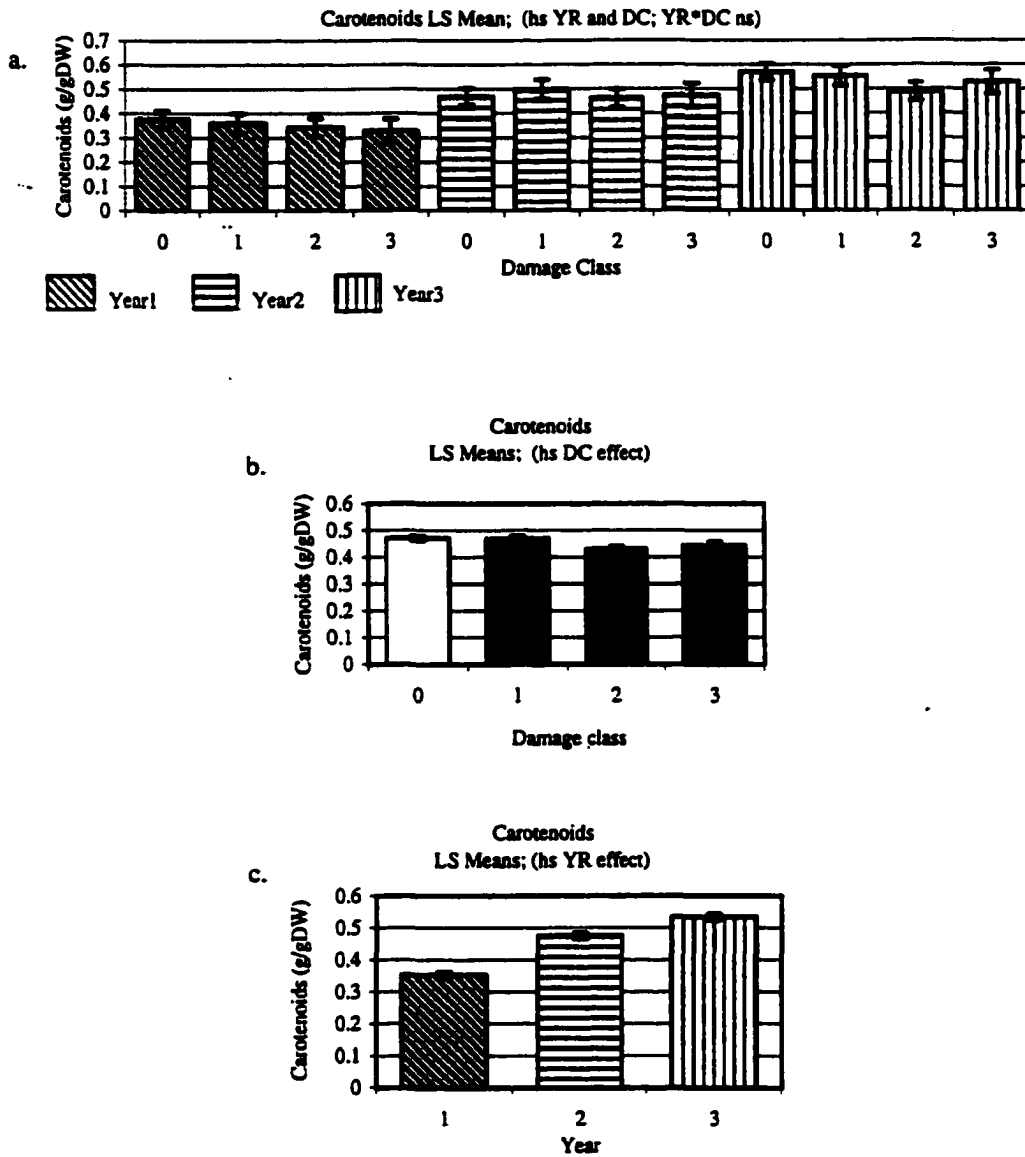


**Figure 4.8.3: Pigments. Carotenoids: Least square (LS) means and standard errors are plotted. The effects of (a) damage and age together, (b) damage and (c) age are evaluated.**

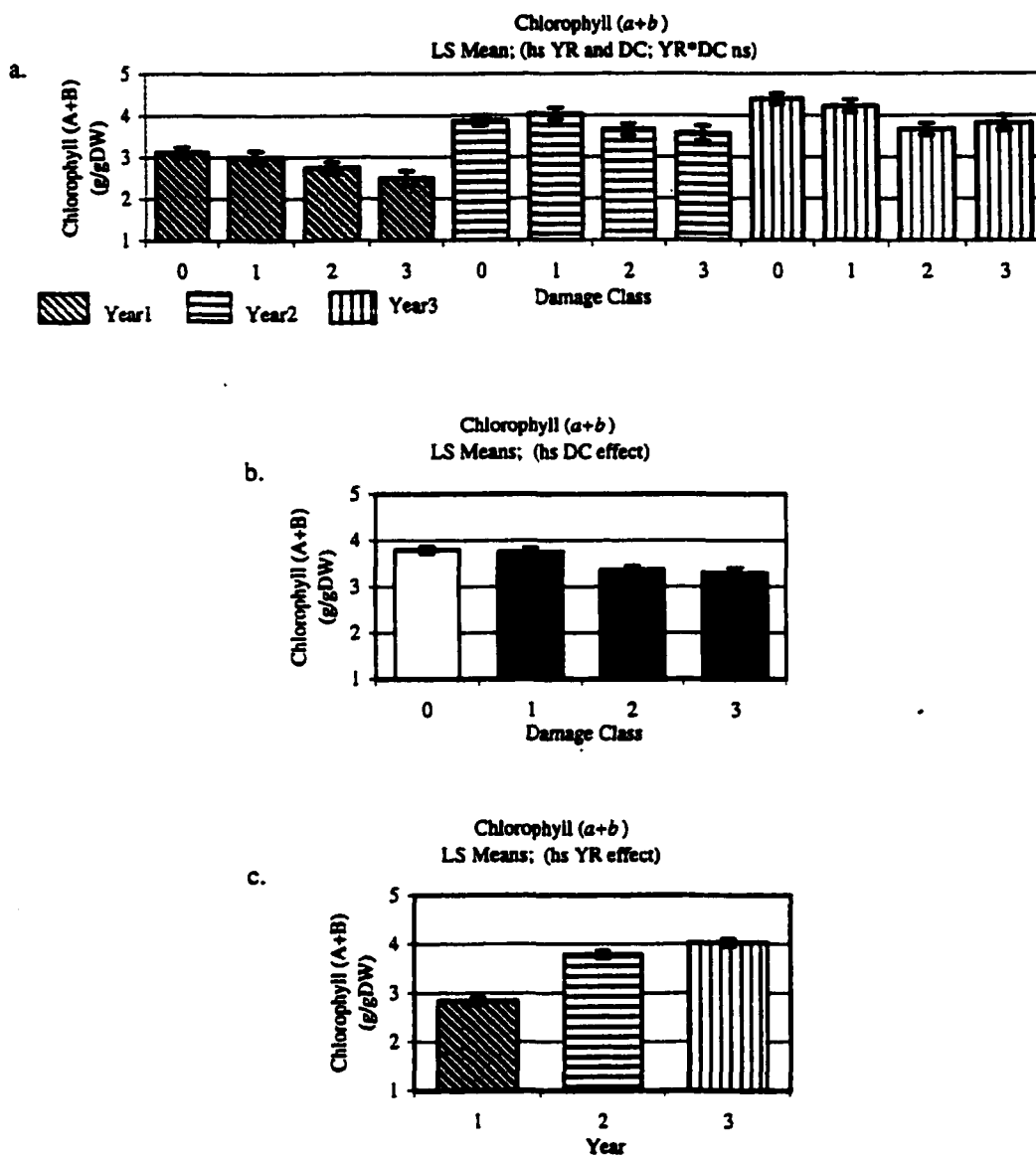


**Figure 4.8.4: Pigments. Chlorophyll ( $a+b$ ):** Least square (LS) means and standard errors are plotted. The effects of (a) damage and age together, (b) damage and (c) age are evaluated.

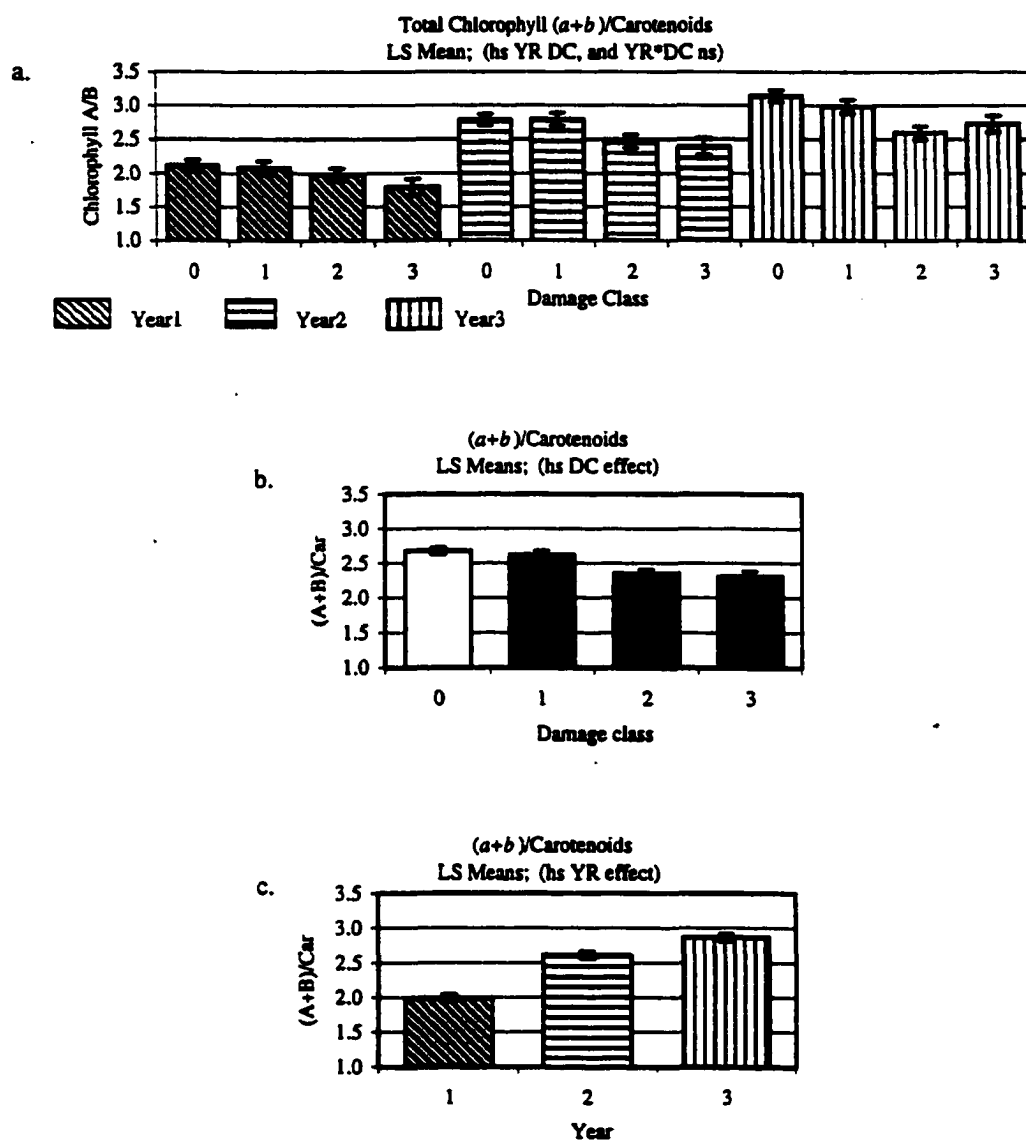


**Figure 4.8.5: Pigments. ( $a+b$ )/Carotenoids: Least square (LS) means and standard errors are plotted. The effects of (a) damage and age together, (b) damage and (c) age are evaluated.**

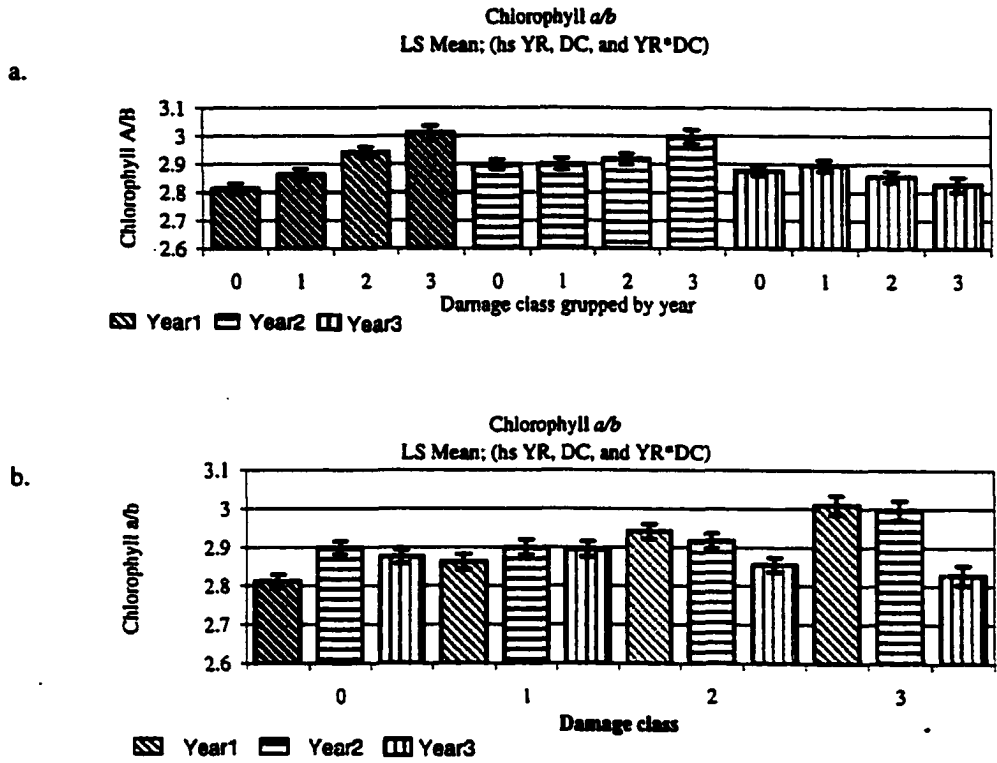


**Figure 4.8.6: Pigments. Chlorophyll *a/b* : Least square (LS) means and standard errors are plotted. The effects of (a) damage and age together and (b) damage are evaluated.**



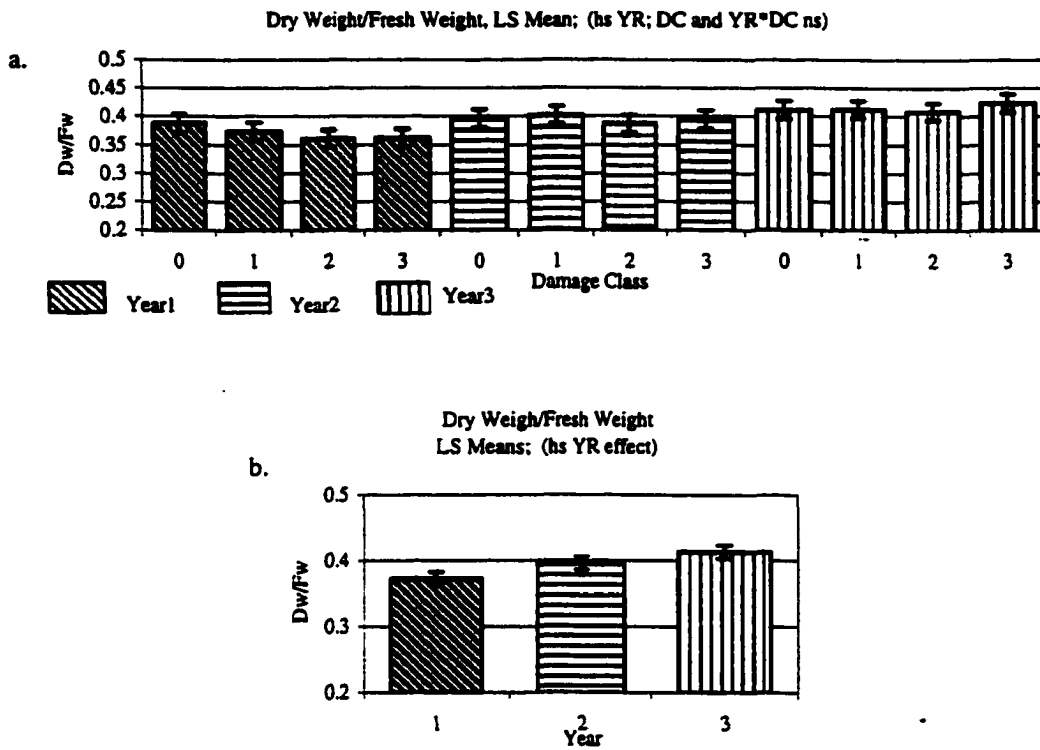


**Figure 4.8.7: Pigments. Dry Weight/Fresh Weight: Least square (LS) means and standard errors are plotted. The effects of (a) damage and age together and (b) damage are evaluated.**

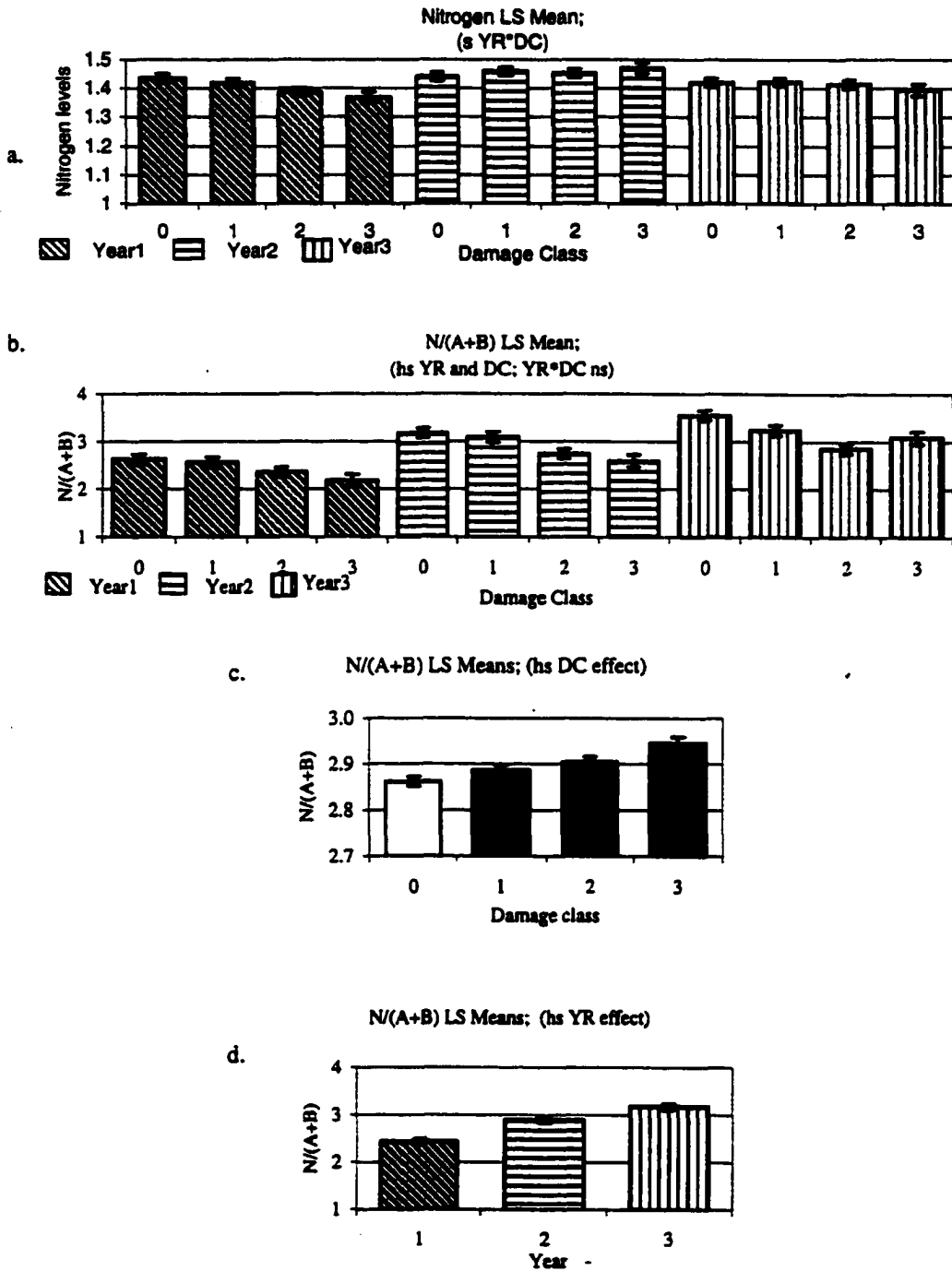


**Figure 4.9: Foliar Constituents - Nitrogen ratio levels: Least square (LS) means and standard errors are plotted. The effects of: Nitrogen (a) damage and age together; (a+b)/N: (b) damage and age together and (c) damage, and (d) age are evaluated.**

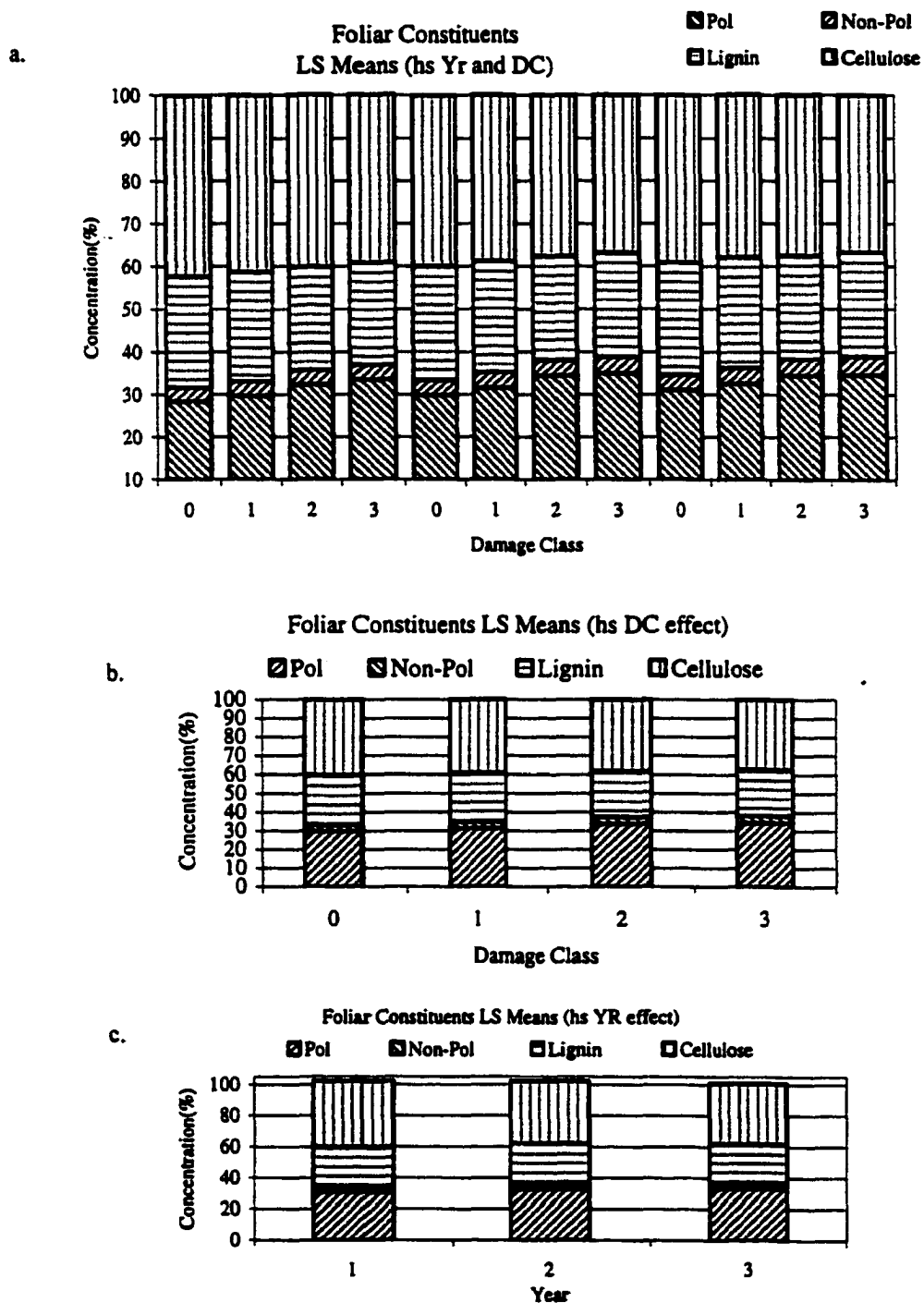


**Figure 4.10: Foliar Constituents - Relative constituents concentrations: Least square (LS) means and standard errors are plotted. the effects of (a) damage and age together, (b) damage and (c) age are evaluated.**

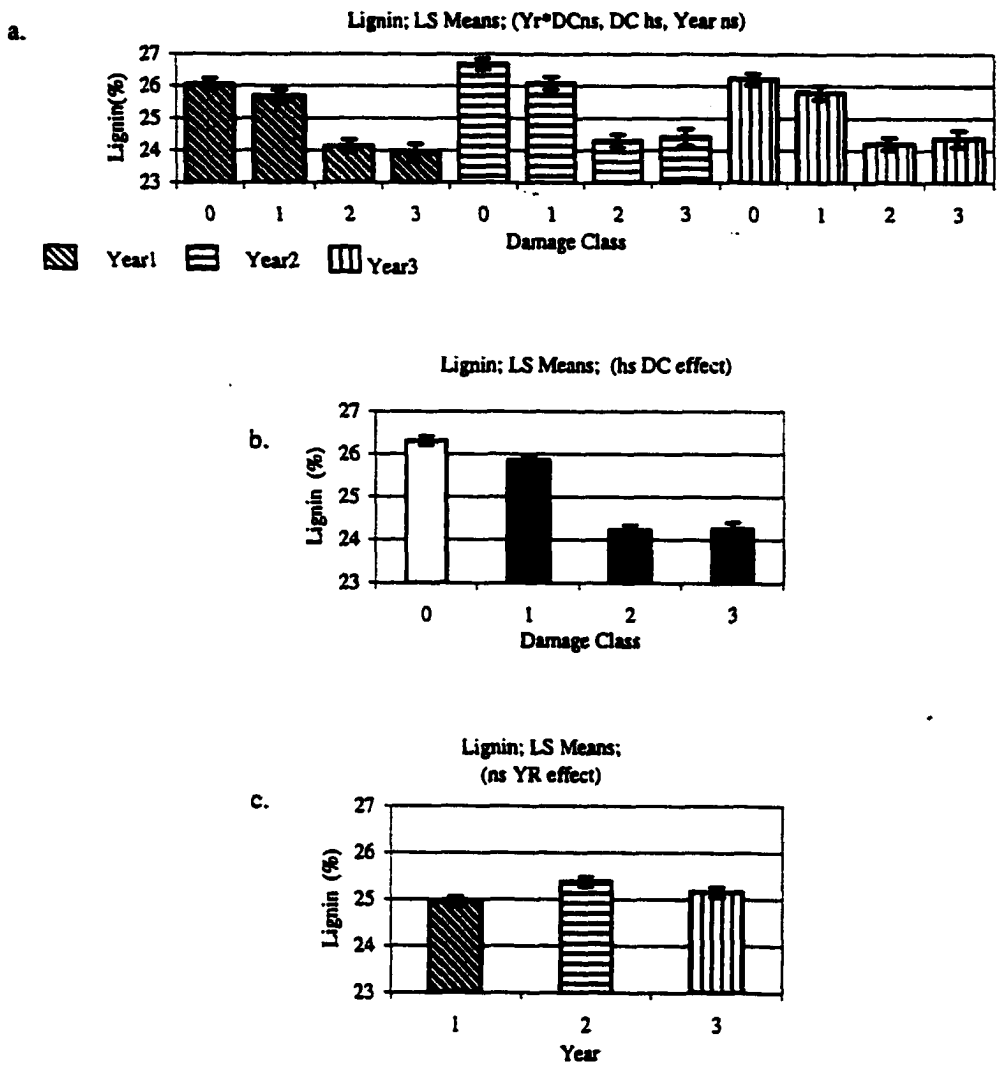


**Figure 4.10.1: Foliar Constituents - Lignin: Least square (LS) means and standard errors are plotted. The effects of (a) damage and age together, (b) damage and (c) age are evaluated.**

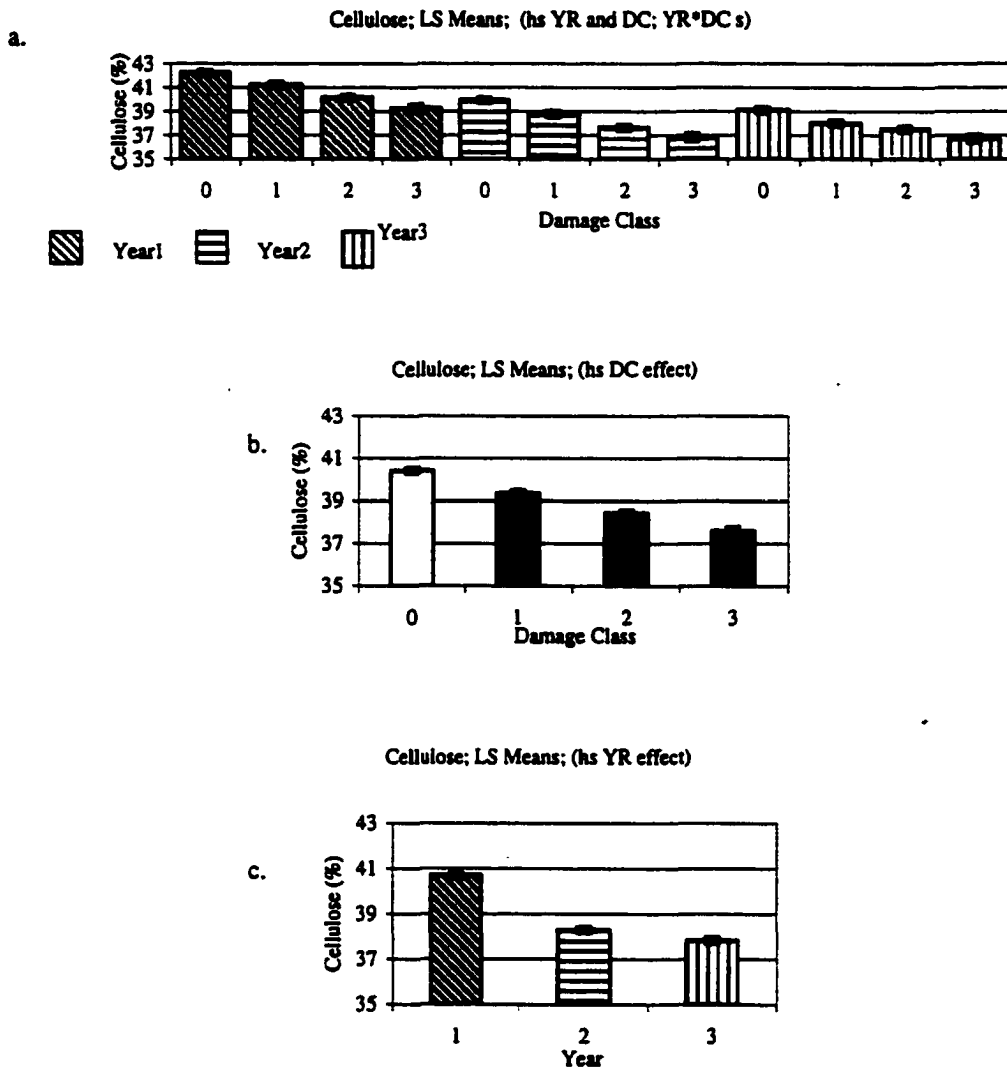


**Figure 4.10.2: Foliar Constituents - Cellulose: Least square (LS) means and standard errors are plotted. The effects of (a) damage and age together, (b) damage and (c) age are evaluated.**

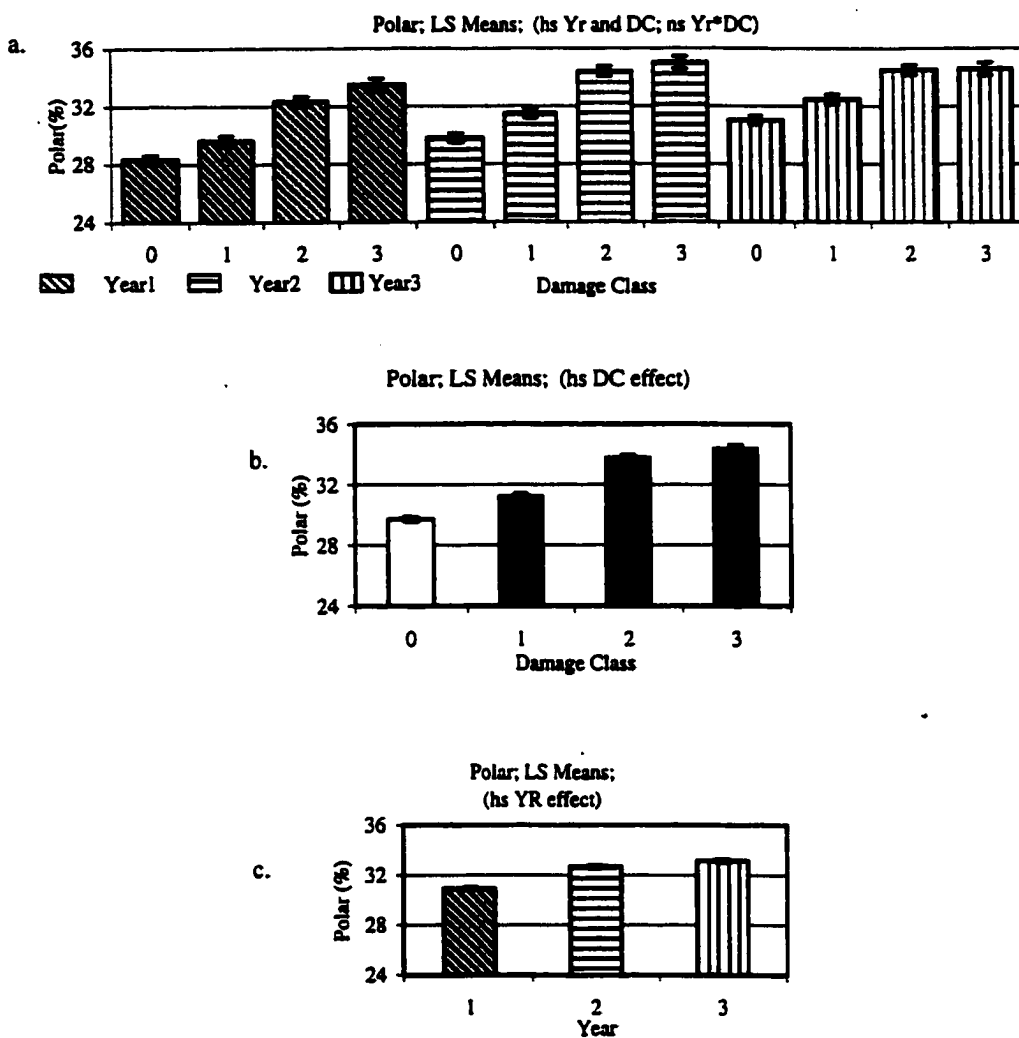


**Figure 4.10.3: Foliar Constituents - Polar: Least square (LS) means and standard errors are plotted. The effects of (a) damage and age together, (b) damage and (c) age are evaluated.**

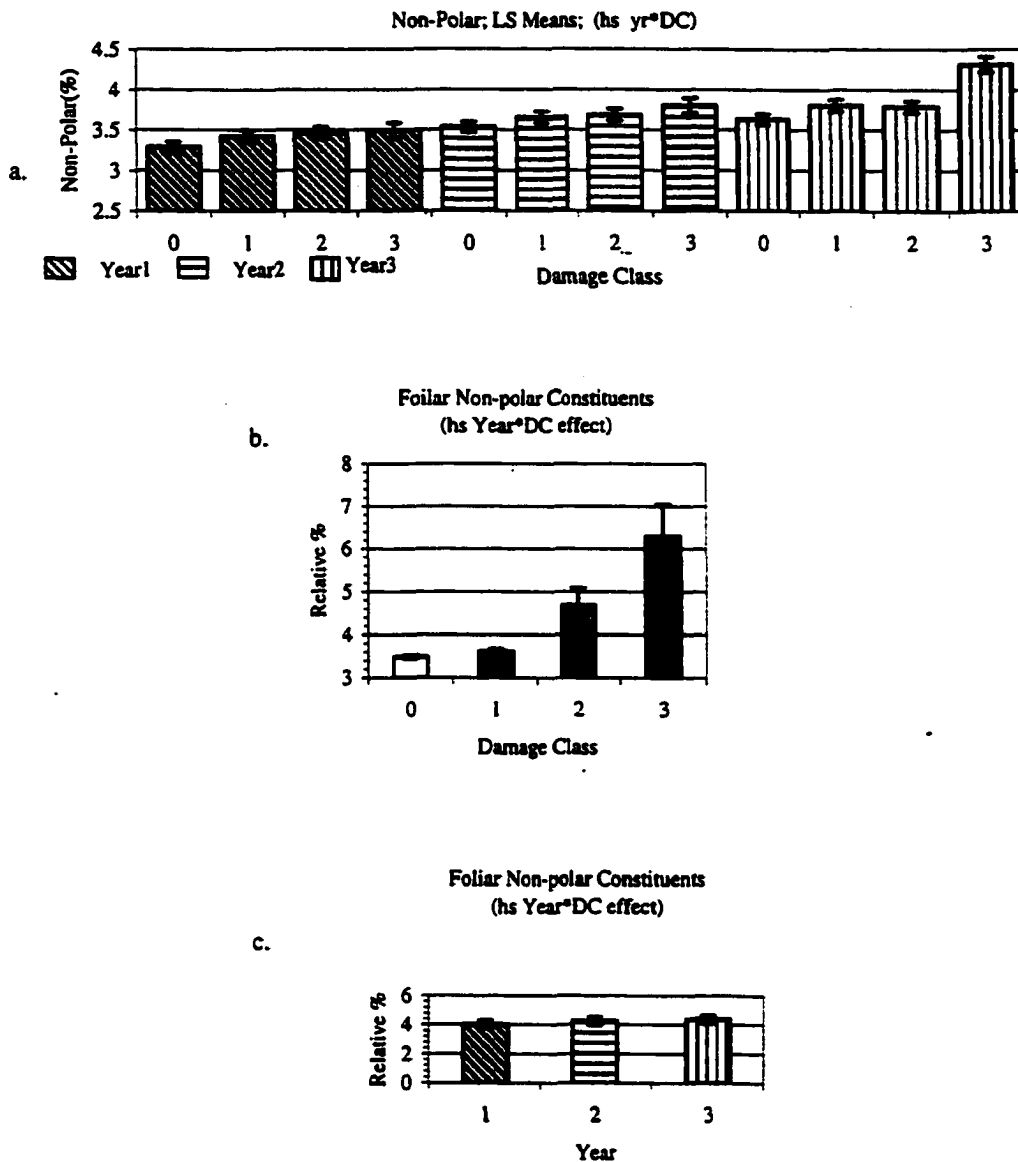


**Figure 4.10.4: Foliar Constituents - Non-Polar: Least square (LS) means and standard errors are plotted. The effects of (a) damage and age together, (b) damage and (c) age are evaluated.**

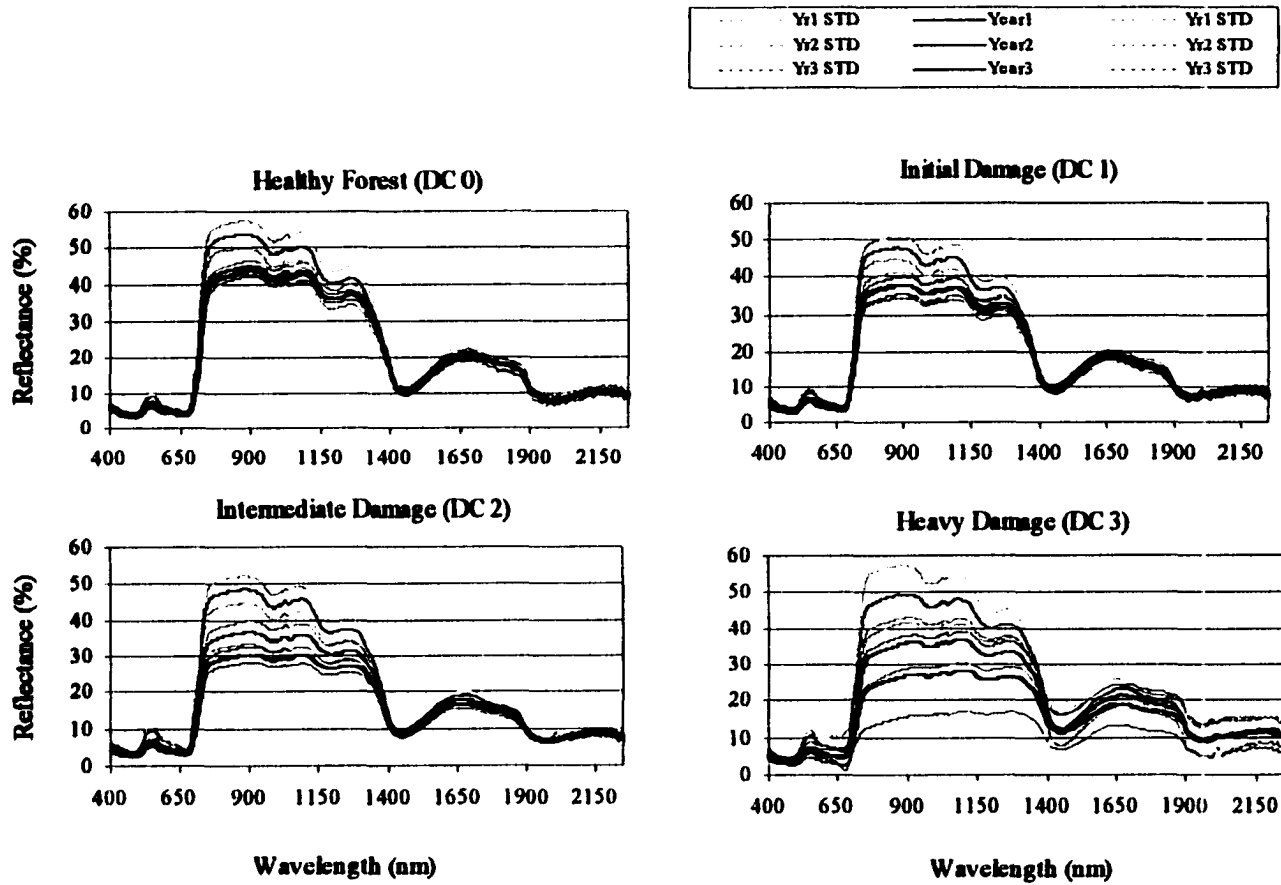


**Figure 4.11: Spectral reflectance of first-, second- and third-year Norway spruce needles by damage classes**



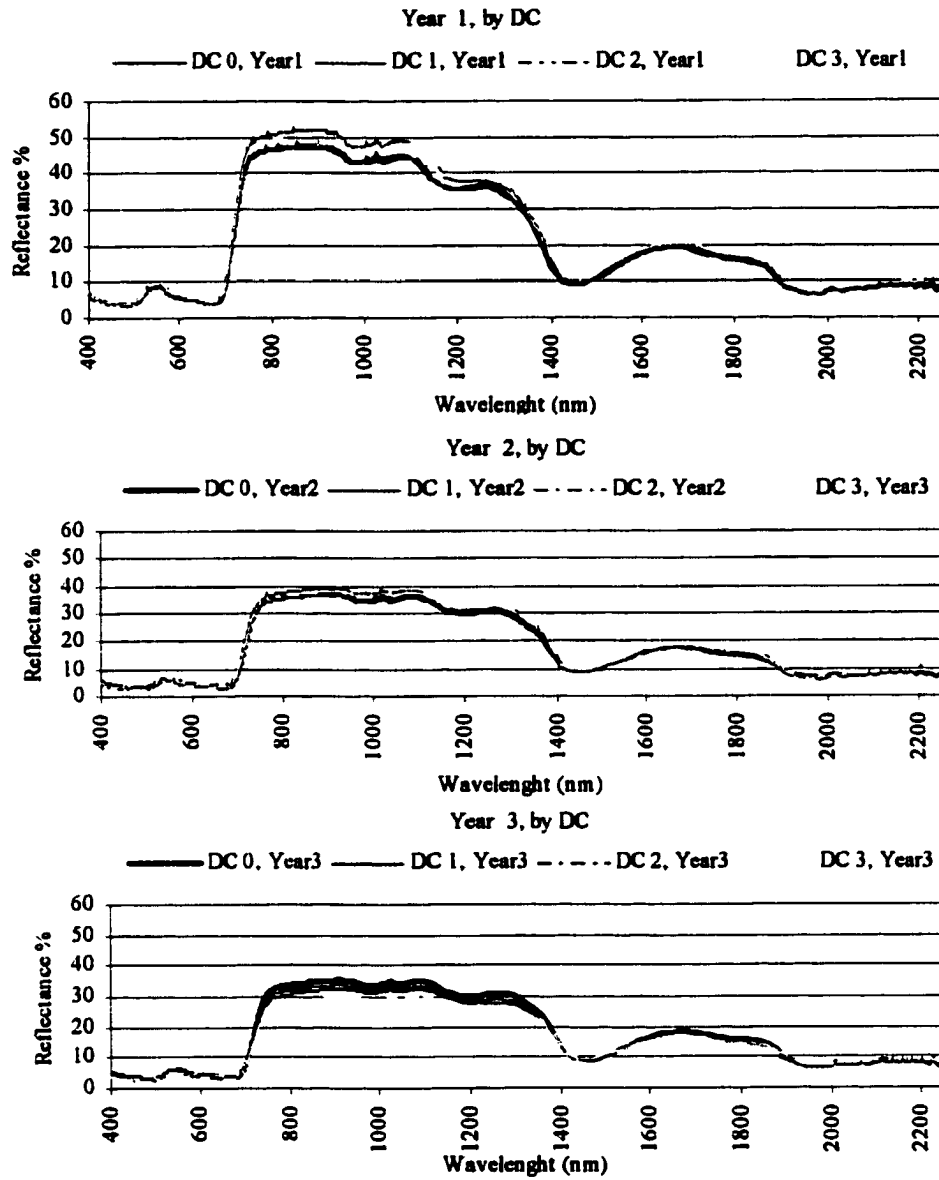
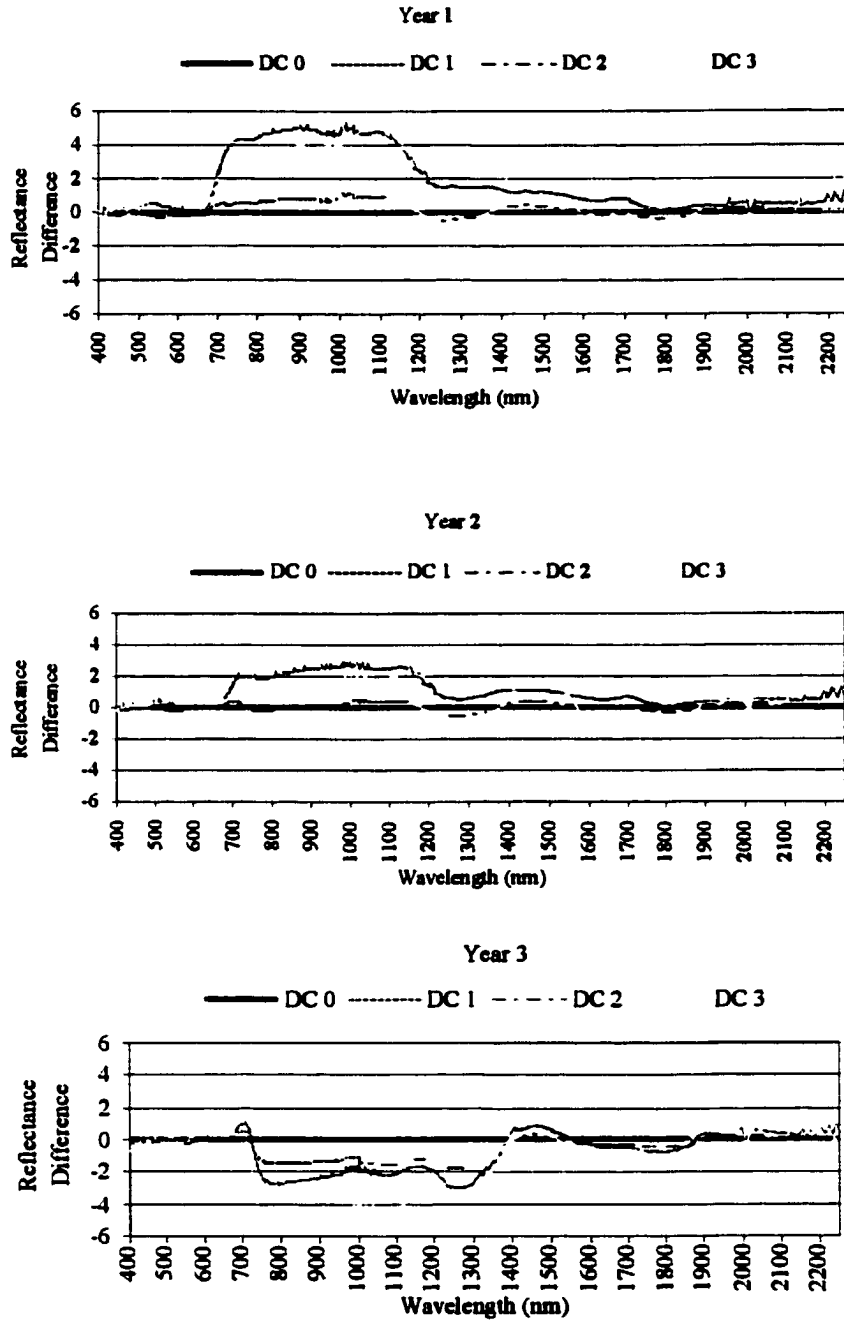
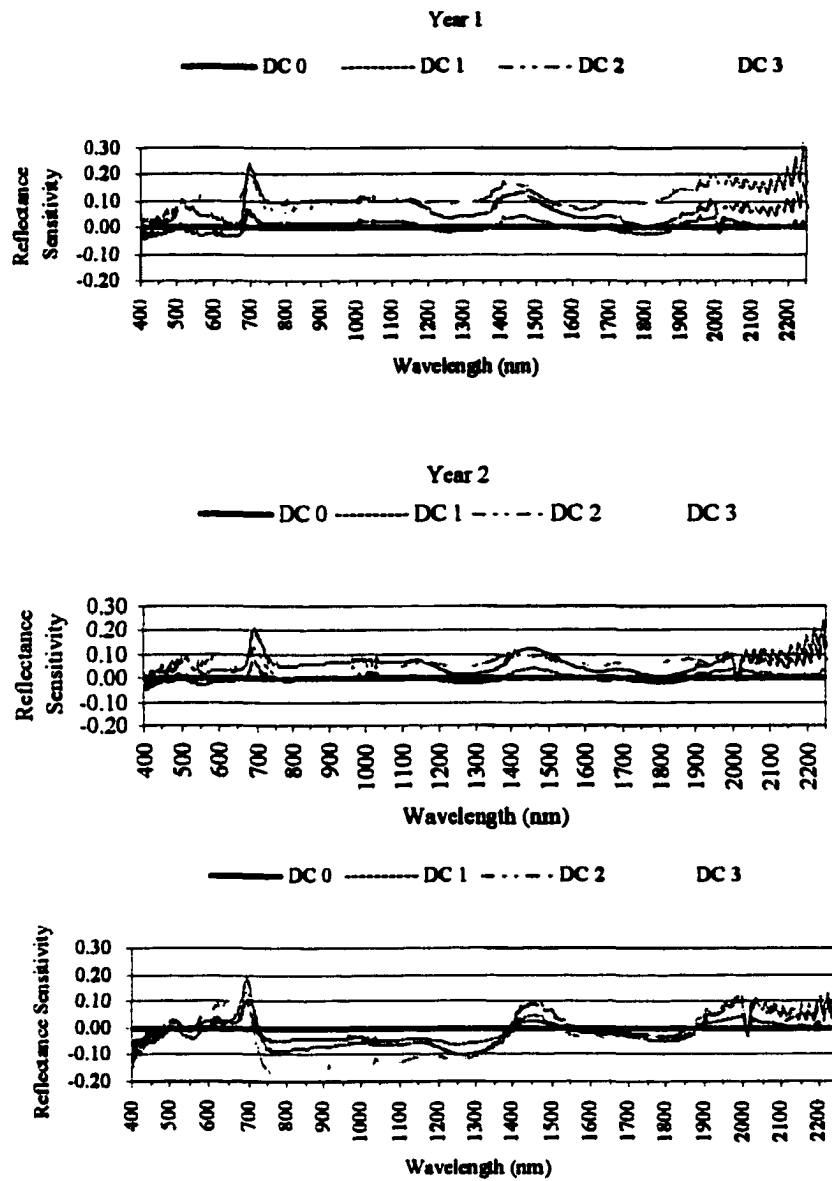


Figure 4.12: Spectral reflectance of DC0, DC1, DC2 and DC3 Norway spruce foliage by age groups.



**Figure 4.13: Spectral reflectance difference of DC0, DC1, DC2 and DC3 Norway spruce foliage by age groups.**



**Figure 4.14: Spectral reflectance sensitivity of DC0, DC1, DC2 and DC3 Norway spruce foliage by age groups.**

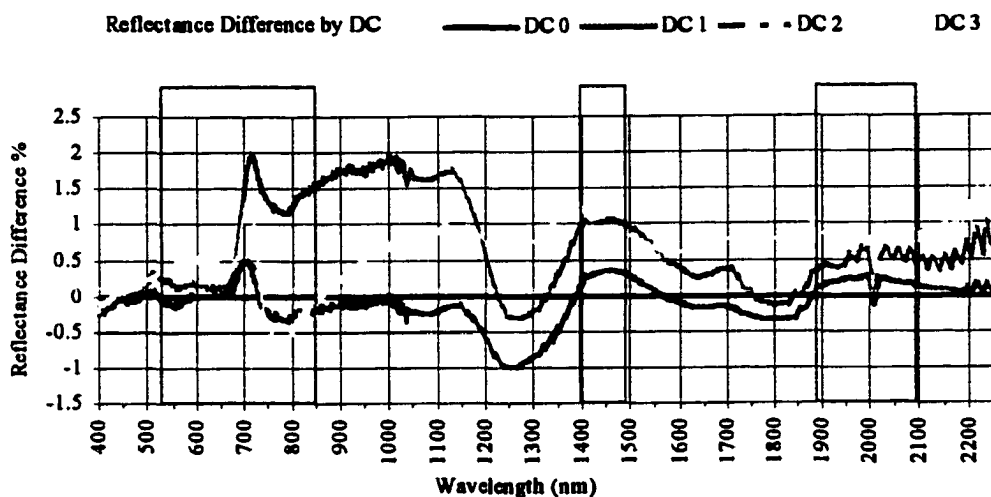


**Figure 4.15 Overall Reflectance difference (averaged spectra across age groups). The regions of significant differences between healthy (DC0) and damaged (DC1-3) are indicated with red boxes.**

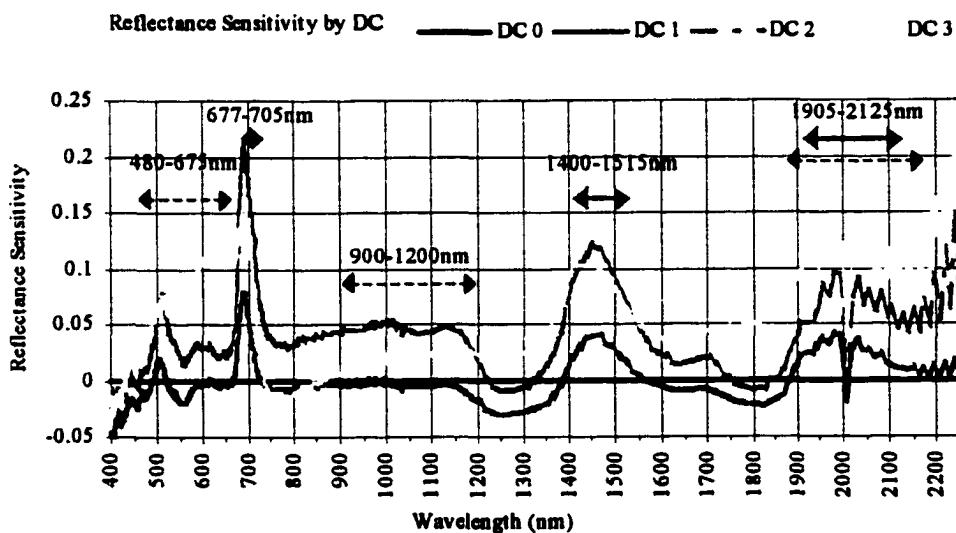


**Figure 4.16 Reflectance Sensitivity (averaged spectra across age groups). The regions of significant differences between DC0 and DC1 are indicated with red. The regions of significant differences between healthy (DC0) and damaged (DC1-3) are indicated with blue.**

## **Chapter 5**

### **SEPARATION OF INITIAL DAMAGE IN NORWAY SPRUCE CANOPIES ALONG A DAMAGE GRADIENT USING HIGH SPECTRAL RESOLUTION AIRBORNE DATA**

#### **5.1 Introduction**

High elevation spruce forest ecosystems are highly sensitive to environmental and climate changes. The Norway spruce forests (*Picea abies* (L.) Karst.) located in the Krusne hory/Erzgebirge Mountains along the northwest border between the former eastern Germany and the Czech Republic (Figure 5.1) have been under a dramatic growth decline since 1965 (Kubikova, 1991). Recent assessments of selected forest stands in this region have identified an apparent ecosystem recovery during the last decade (Entcheva *et al*, 1996). Accurate methods for monitoring forest health conditions on a regional scale are required for making timely and effective management decisions.

Previous research has developed the remote sensing capabilities for assessment of either very broad categories of forest damage on regional scale, or for estimation of a large gradient of forest health on a local scale (Lambert *et al*, 1995; Ardo *et al*, 1997). Using Landsat Thematic Mapper (TM) data and applying a logit regression approach to classify forest damage in the Czech Republic on a regional scale, Lambert *et al*. (1995) were able to discriminate only three major damage categories (healthy, moderate, and heavy damage), while foresters visually recognize a total of five damage classes when

conducting intensive forest ground surveys (Henzlick, 1997). The use of multispectral LandsatTM data does not allow discrimination of the initial damage levels marked by chlorophyll loss. Remote sensing methods allowing for detection of the subtle changes appearing with initial forest damage are currently needed.

When ecosystem health is in decline, many vegetation properties are altered simultaneously. The process of photosynthesis is highly sensitive to environmental stresses, as well as to normal developmental and seasonal changes (Larcher, 1995). Therefore, changes in photosynthetic apparatus and sequential changes in pigment concentration are considered indicative of initial vegetation stress (Carter *et. al.*, 1996; Rock *et. al.*, 1988).

The properties of leaf reflectance spectra are determined by pigment levels, cellular structure, water content and biochemical components (Rock *et. al.*, 1986 and 1988; Martin and Aber, 1997). Changes in the amount of foliar chlorophyll, lignin, cellulose, nitrogen, etc. and water content of the tissue are indicative of change in tree health and produce diagnostic changes in the spectral signatures of vegetation (Rock *et al.*, 1986; Carter *et al.*, 1996). Chlorophyll and carotene concentration change and additional foliar compounds may build within the leaves in response to stress affecting the spectral properties of the foliage (Rock *et al.*, 1986). Foliar chemistry is considered to be a reflection of the growing conditions to which the trees were subjected at the time of needle formation, as cell wall composition is unlikely to change over time as growing conditions degrade or improve (McNulty *et al.*, 1990 and 1991). Thus, monitoring of vegetation vigor based on estimates of chlorophyll levels may allow damage detection in

the early stages of ecosystem stress, while using spectral estimates of foliar chemical constituents may be more indicative of long-term vegetation health.

The early stages of damage in vegetation characterized by subtle reductions in chlorophyll concentrations can be monitored using hyperspectral systems that acquire data along the visible and near-infrared vegetation spectrum, dominated by chlorophyll absorption (Rock, *et al.*, 1988; Miller, *et al.*, 1993; Vogelmann, *et al.*, 1993).

Investigations using both field and airborne spectrometers acquiring spectral data in narrow (1.5-10.0nm wide) bands have produced a large number of ratios/indices correlated with foliar chlorophyll concentrations and indicative of vegetation stress (Rock *et al.*, 1994; Vogelmann *et al.*, 1993; Zarco-Tejada *et al.*, 1999). Canopy optical indices have been shown as bio-indicators of vegetation conditions, inferring from the changes in leaf reflectance data changes in vegetation foliar constituents (pigments and nitrogen, lignin and cellulose content) and amount and structure of foliar biomass (Rock *et al.*, 1986; Chappelle *et al.*, 1992; Vogelmann *et al.*, 1993; Carter, 1994; Datt *et al.*, 1998). Sensitivity analysis of high spectral resolution data have allowed for determination of the band regions most sensitive to vegetation stress (Carter, 1994). Derivative analysis of hyperspectral data was suggested to allow for determination of changes in the shape or position of the spectral features associated with the damage, and also as removing the possible effects of baseline shifts and scatter on the spectra (Miller *et al.*, 1990; Martin, 1994).

Many of the analyses and algorithms developed using high spectral resolution data are based on leaf reflectance measurements, and/or have been developed for assessment of pigment levels on a large region scale. Such algorithms need to be applied to spectra at

the forest stand level and their potential for damage detection at the canopy level needs to be assessed (Datt *et al.*, 1998). Their sensitivity to changes in pigment concentration and foliar chemical constituents occurring with vegetation damage needs to be evaluated.

The main goal of this investigation was to evaluate the potential of airborne hyperspectral remote sensing data for separation of the initial levels of damage in the Norway spruce canopies of the Krusne hory, Czech Republic. The objectives of the research were to:

1. evaluate the optical properties of Norway spruce at the canopy level along a full range of damage conditions using ASAS data, and determine the spectral regions most sensitive to the initial stages of decline for computation of vegetation indices;
2. establish the links between airborne hyperspectral data and forest damage evaluation procedures needed for forest health monitoring by evaluating the relationship of spectral reflectance properties to bio-physiological characteristics from randomly selected ground study sites; and
3. evaluate the potential of high spectral resolution airborne canopy (ASAS) and field foliar (GER2600) reflectance data to provide comparable results at the canopy level for separation of early damage levels and forest health monitoring.

## **5.2 Methods**

The high elevation forests of northwestern Bohemia (Figure 5.1) offer a unique opportunity for study of the full gradient of forest decline conditions due to air-pollution across a homogeneous Norway spruce ecosystem within a limited elevation range (900-1100m). The study areas have been the object of detailed soil and forest surveys and



climate monitoring by the Czech Forest Service (Henzlik, 1997). Some of the stands have been used in the previous Landsat TM forest damage assessments (Lambert *et al.*, 1995).

### **5.2.1 Forest Health Evaluation and Stand Measurements**

Forest physiological condition was assessed using methodology for evaluating the state of crowns of individual trees established by Hildebrandt (Hildebrandt and Gross, 1992). In analogy with terrestrial inventories used by the forest service, five levels were distinguished. Level 0 (DC0) indicates “healthy” - no visible damage symptoms, level 4 (DC4) indicated “dead”. Determination of a health level (damage class) includes evaluation of: (1) crown thinning characteristics: crown type (for spruce brush, comb or plate), form and shape; (2) foliar loss; (3) Presence/absence of chlorosis - yellowing of the needles due to chlorophyll loss; and (4) foliar retention. The remote-sensing discrimination of the initial stages of forest decline is of interest to the current research. Therefore, damage level 4 (dead) stands were excluded from the study, resulting in a classification scheme using 4 levels (Table 5.1). Figure 5.2 presents the extremes of damage conditions (DC0 and DC3) encountered within the present study.

To test the discrimination capabilities of hyperspectral data for initial forest damage detection, forest stands older than 60 years and larger than five hectares which were representative of the full range of forest health (healthy, initial damage, intermediate and heavy damage) along a limited elevational range were selected. For forest field evaluation and measurements within the research areas, 30x30m study sites were randomly selected - a total of 183 sites within the Krusne hory mountains, from which 51 sites for sampling collections (“intensive sites”) and 132 sites for image

classification and validation (“non-intensive sites”). Differentially-corrected GPS coordinates were collected at each plot center. In each of the 183 sites, stand structure and tree damage class was characterized. Within an 11.3m radius circular plot located at the center of the study site, forest stand parameters such as stand density, biomass, basal area (BA), tree diameter at breast height (DBH) and tree height were measured. Table 5.2 represents the full list of field measurements performed. Within each of the 51 intensive sites, five canopy level trees representative of the stand damage level and forest growth parameters were selected. The representative trees were marked permanently with aluminum tags and further used for sampling.

### **5.2.2 Foliar Collections, Spectral Measurements and Laboratory Analyses**

Foliar sampling for spectral measurements and pigment extractions was conducted within the 2 weeks scheduled for the ASAS image acquisition (August 15-28, 1998). One branch from the upper portion of the functional canopy was collected from each of the five representative trees. Because needle retention is a function of the state-of-health, 1st, 2nd and 3rd year needles were collected. Two separate sets of foliar samples were collected from the same branch: (1) one set for VIS/NIR spectral measurements and for determining foliar lignin, cellulose and nitrogen levels, and (2) another set for foliar pigment analysis (e. g. chlorophyll *a* and *b*, carotenoids). The samples for VIS/NIR spectral measurements and foliar chemistry were immediately sealed in plastic bags with wet papertowels, placed in coolers on frozen blue ice, and taken to the laboratory for fresh foliage spectral measurements. Branch samples were analyzed within 2-6 hours of collection. One-, two- and three-year old branch segments were separated and arranged in

non-reflective trays. The samples were then scanned using a GER2600 Visible Infrared Spectrometer (Geophysical Environmental Research Corp., New York)<sup>1</sup> set-up in a laboratory environment under a tungsten light source. To limit the effects of scattering on the spectra, three sets of GER2600 measurements (each measurement averaging six scans) were acquired with the sample rotated 90° after each measurement, averaging the 3 scans for a sample. A total of 15 averaged spectra were obtained for a study site (5 trees, 3 age classes). For comparison to the ASAS canopy level measurements at each wavelength the GER2600 spectra from a study site were averaged to stand level, while the spectral resolution of the GER2600 data was maintained at 2.5nm spectral bandwidth (at half-max full width) in the 300-1050nm spectral region.

After the fresh samples were scanned with the GER2600 spectrometer they were taken to UNH, air-dried, ground in a Wiley mill to 1mm particles and homogenized (Bolster *et al.*, 1996). The samples were dried in a forced air convection oven at 70°C for 15 hours and cooled to room temperature in dessicators. The processed samples were immediately scanned on a NIRSystems 6500 monochromator (NIRSystems Inc., Silver Spring, MD), which covers the 400-2500nm spectral range at 10nm resolution, following procedures described by Bolster *et al.* (1996).

Carbon constituent analyses were performed using a series of extractions following the methods described by Newman *et al.* (1994). The following constituents were isolated: organic non-polar components (fats, waxes and other organic soluble materials), polar extractives (phenols, simple sugars, starch and simple amino acids), cellulose (acid soluble compounds) and lignin. Foliar constituents were quantified as

---

<sup>1</sup> Brand names are cited for clarity and are not intended to imply endorsement.

percentages of the initial sample weight. Therefore the total of foliar lignin, cellulose, polar and non-polar constituents summed to 100%. Standard NIR procedures were used to develop a relationship between the NIR absorption data and the set of samples (Williams and Norris, 1987; Martin, 1994).

Pigment extraction was accomplished at the Department of Plant Physiology at Charles University, Prague. A 5-day procedure was used, ensuring 97% efficiency of pigment extraction (Šolcová, 1999). In this paper the pigment data are analyzed to assess the relationship between pigment levels and ASAS airborne spectral reflectance at a stand level.

### **5.2.3 ASAS Data Acquisition and Processing**

Airborne hyperspectral imagery was acquired using the Airborne Solid-state Array Spectroradiometer (ASAS). The ASAS system is an airborne push-broom imaging radiometer, with a 512 x 62 pixel CCD area array (Figure 5.3). The instrument is maintained and operated by the Laboratory for Terrestrial Physics at the NASA Goddard Space Flight Center (Irons *et al.*, 1991). The instrument produces a 512 pixel wide image strip for 62 spectral bands. The spectral range of ASAS covers 410-1032nm with a spectral resolution of 9.5-11.5nm intervals (half-max, full width), with optimal spectral performance in the 500-900nm region (Russell *et al.*, 1997). Data are recorded as unsigned 16 bit digital numbers and calibrated to radiometric units using laboratory-derived sensor gain coefficients. For this study, ASAS was flown on-board an Antonov AN-2 single engine biplane (Figure 5.3) at 2500m above ground level, producing an approximately 820m swath width, with a 1.5m by 2.00m nominal spatial resolution

(Table 5.3). For this study only nadir data were acquired. To minimize the effects of solar hotspots and canopy shadow, the flight lines were oriented from a northwest to southeast direction. The imagery and data were acquired as close to local solar noon as possible.

Data acquisition was planned for late August 1998. At this time in the Krusne hory the weather is expected to be most stable, and the current year spruce foliage is fully developed and no tree phenological or physiological growth changes are occurring. Although numerous attempts were made, data acquisition occurred on only two dates: August 20 and September 1, between 10:30am and 1pm. Weather conditions were optimal at the beginning of each overflight, but degraded as clouds developed around noon. The western-most study sites (also the healthiest, Figure 5.1. area S1) were flown first, followed by S2 and S3. A total of 17 flight lines were acquired, designed to provide a full coverage of the Krusne hory study areas (Table 5.4; Figure 5.1). Due to the development of both high, cirrus and low cumulous clouds during the acquisition, approximately 25% of the data were of sufficient quality for further analyses. In the current study, data free of the effects of clouds and cloud shadows were used. Although the flight lines were developed to cover the pre-selected on the ground study sites, only 23 sites (10 DC0, 5 DC1, 4 DC2, 4 DC3) were within the cloud-free images. A total of 18 of the 23 sites had been intensively sampled.

Limitations in the calibration path (e.g. sensor sensitivity, stray light and non-solar calibration source color temperature) produces calibration limitations for obtaining at-sensor-radiance (ASR) data in the blue and the NIR above 900nm (Russell *et al.*, 1997), thus a total of 45 calibrated spectral bands covering the 450-900nm spectral region at 10nm intervals were used in the analyzes presented in this study.

To remove atmospheric effects and to perform the at-sensor-radiance (ASR) calibration to reflectance, the Second Simulation of the Satellite Signal in the Solar Spectrum (6S) calibration model was applied (Tanre *et al.*, 1990). The US62 module of the atmospheric model with input conditions for the continental aerosol model was used. Measurements of the atmospheric optical depths were acquired simultaneously with the airborne acquisition using surface-based sun photometers (MICROTOPS II), and used for data calibration. The average aerosol optical thickness measured at the study areas at the time of the overflights was 0.0502 for August 20 and 0.0475 for September 1, 1998. Simultaneously ground spectral data (GER2600, GER Inc.) from both large bright and dark ground targets were acquired. Ground spectral targets included a lime pit, concrete, gravel and asphalt roads and parking lots (Figure 5.4). The ground targets covered approximately 15x20m areas, allowing for the extraction per target of 4-5 pixels free from edge effects. When extracting spectra for the targets from the imagery, the bright calibration targets provided the clearest and strongest spectral data.

Validation of the spectral and radiative transfer calibration was conducted at GSFC during the summer of 1999. To correct for radiometric error in the data, a vicarious hybrid calibration routine was developed that applied both the standard ASAS radiative transfer calibration routine (Kovalick *et al.*, 1994) and the GER2600 measurements from bright ground reflectance targets (Daubney *et al.*, 1999). A comparison of reflectance data for a bright target (Figure 5.4) between the calibrated to reflectance ASAS data and the GER2600 spectral data is shown in Figure 5.5. In the spectral region 490-850nm ASAS data compare well ( $r=0.96$ ,  $r^2=92$ , reflectance range 30-53%) with the onsite GER2600 data. In general, compared to the GER2600 spectra, the ASAS data were 5-10% lower in

magnitude. The lower values in the 450–490nm and 850–900nm region are likely caused by stray light contamination in the array, effecting the radiometric calibration in the blue and portions of the near infrared and causing overcompensation for the radiation levels received in these spectral regions (Russell *et al.*, 1997). The dip-peak feature at 754–764nm of the ASAS data (Figure 5.5) is an artifact due to an atmospheric oxygen absorption feature located at 760nm (Dabney *et al.*, 1999). Due to the location of the oxygen absorption band between the ASAS bands at 754nm and 764nm, an anomalous spectral spike characterizes the 764nm ASAS band. Sharp spectral features, such as the 760nm oxygen absorption band and the accompanying artifact, are among the most reliable indicators of system spectral alignment.

#### **5.2.4 Site Identification on the ASAS Imagery and Extraction of Norway Spruce Canopy Spectra**

Using 1:2500 CIR photography, 1:5000 scale forestry maps with the location of the study sites and field notes, the 23 cloud free field sites were located and marked on the ASAS imagery (Figure 5.4 and Figure 5.5). During field visits to these 23 sites in August 1999, the precise locations of the study sites were confirmed on the imagery.

During the 1998 field campaign, forestry measurements were conducted at the stand level and 5 representative of the canopy trees were sampled (Table 5.2). The 1.5–2m spatial resolution of the ASAS imagery allows for separation of individual tree crowns from within the study sites (Figures 5.4 and 5.5). During the 1999 site location validation process, an attempt was made to identify individual trees in the imagery. This proved to be difficult, and thus to obtain representative spectra for the given study site, reflectance data from 20 to 30 tree crowns were extracted.

An individual tree crown is represented in the imagery by 20 to 25 pixels (5x5 pixels; Figure 5.4c and Figure 5.4d). The spectral variation within individual tree crowns was evaluated by extracting spectral signatures from pixels diagonally across the crown. A first derivative transformation was performed on the spectra extracted from single crowns (Figure 5.7b). The derivative analysis revealed that the shadow within the tree crown causes changes in the amplitude and position of the first derivative (Figure 5.7a and Figure 5.7b). As the amount of shadow within a pixel increases, the noise within the spectra also increases. Extracting spectra from the brightest pixels, located on the sun-lit portion of the crown, produced the least band-to-band variations in reflectance data, while increasing amounts of shadow within a crown increased the noise within the spectra (Figure 5.7a and Figure 5.7b; spectra 1, 4, 5, 6 and 10). The brightest 2 or 3 pixels from the center of a tree crown exhibited the smallest differences among spectra, and therefore, it was decided to extract spectra only from the brightest pixel from within a single tree crown.

Spectra for similar forest age classes, extracted from healthy sites located on opposite southwest and southeast facing slopes, and from DC2 and DC3 sites located on relatively leveled terrain were compared. The differences in stand canopy closure and density associated with damage level resulted in differences in the amount of shadow present within a site. Higher amounts of shadow were present in the healthy forest stands on the steeper terrain that was sloping away from the sun. Likewise, differences were present in DC2 and DC3 sites independent of topographic variation.

Large differences in reflectance amplitude were associated with the amount of shadow present within a tree crown, suggesting that selection of the brightest pixel from



each crown when sampling multiple sites from the same damage level, but from different locations with various slope and exposition, would reduce such effects on the data (Figure 5.7a).

### **5.2.5 ASAS Spectral Analyses**

#### **Spectral properties of Norway spruce canopies by damage class**

The spectral reflectance data extracted from the 23 study sites were analyzed using analyses of variances (ANOVA) to determine the changes occurring in ASAS data for Norway spruce canopy reflectance with ground-based assessments representing increasing damage level. Spectral plots for damage categories were generated, plotting means and standard errors and means and standard deviations. To determine the spectral regions optimal for damage detection, a sensitivity analysis of the canopy reflectance spectra was conducted following the procedure described by Carter *et al.* (1995). The significance level (significant  $p \leq 0.05$ ; highly significant  $p \leq 0.01$ ) of the differences among derivative spectra at each wavelength per damage level was determined by ANOVA and Tukey pair-wise mean comparisons test (*SYSTAT 7.0*; *SPSS Inc.*, 1997).

Considering the possibility for a baseline shift in reflectance data not accounted for with the image calibration and atmospheric correction, a normalization of the spectral data was performed. The ASAS data were normalized to a reflectance minimum at 673nm (the minimum for most of the spectral data at the chlorophyll well) and a reflectance maximum at 744.5nm (the last band before the oxygen absorption feature at 754-764nm, Figure 5.10). To evaluate the potential for damage detection using the normalized red edge reflectance region (680-735nm), the individual normalized ASAS

bands are treated as separate indices - N683, N693, N703.8, N714, N724 and N734.2.

Normalization of the spectral data over a broader range (673nm to 847.2nm) was performed to assess the spectral reflectance properties in the red/NIR region.

To discriminate between overlapping bands and to determine if there are changes in the shape or position of the spectral features associated with the stand damage, a derivative analysis was conducted. The analysis is suggested to remove the possible effects of baseline shifts and scatter within the spectra (Miller *et al.*, 1990; Martin, 1994). The first derivative of reflectance was calculated using the formula:

$$D_{\lambda_i}' = (R_{\lambda_{(i+1)}} - R_{\lambda_{(i-1)}}) / (\lambda_{(i+1)} - \lambda_{(i-1)}),$$

where  $D_{\lambda_i}'$  is the first derivative and  $R_{\lambda_i}$  is the mean reflectance value at  $\lambda_i$  wavelength.

The derivative transformation provides spectral data that is less sensitive to the effects of variable irradiance and background (Lucas *et al.*, 2000). The significance level (significant  $p \leq 0.05$ ; highly significant  $p \leq 0.01$ ) of the differences among derivative spectra at each wavelength per damage level was determined by ANOVA and Tukey pairwise mean comparisons test (SYSTAT 7.0; SPSS Inc., 1997). Mean first derivative spectral plots for damage categories were generated, plotting Least Square (LS) Means and standard errors and LS Means and standard deviations.

### **Spectral indices**

The early stages of damage in vegetation are often characterized by subtle reductions in chlorophyll concentrations, which may be monitored using hyperspectral systems that acquire data in the visible and near-infrared portions of the vegetation spectrum (Rock, *et al.*, 1988; Miller, *et al.*, 1993; Vogelmann, *et al.*, 1993).

Previous investigations have identified a wide range of indices as indicators of vegetation health and physiological properties. We evaluated the potential of the spectral indices used by other investigators to assess damage for Norway spruce stands. Based on our spectral analysis, a few new spectral ratios were also developed. A list of the formulas used for computation of the indices from the ASAS spectra are presented in Table 5.5. The indices are presented in 4 groups based on the spectral bands/regions they cover and the data treatment involved for their calculation.

Investigations using field and airborne spectrometers acquiring spectral data in narrow (1.5-10.0nm wide) bands have produced a large number of analytical techniques correlated with foliar/canopy chlorophyll concentration (e.g. derivative analysis, sensitivity analysis, spectral normalization, Inverted Gaussian Model approach), and optical indices shown as indicators of vegetation conditions (Rock *et al.*, 1986; Chappelle *et al.*, 1992; Vogelmann 1993; Carter, 1994; Datt *et al.*, 1998; Zarco-Tejada *et al.*, 1999).

Band ratios of derivative spectra have also been suggested as strongly related to chlorophyll *a* or total chlorophyll concentrations (Zarco-Tejada *et al.*, 1999). Using the ASAS spectral data, we evaluated derivative indices suggested in the literature such as  $D_{max}/D_{704}$  ( $D_{max}$  is the maximum value of the first derivative in the red edge region,  $D_{max}=R_{slope}$ ) and  $D_{714}/D_{704}$ . We developed the  $D_{max}/D_{714}$  and  $D_{max}/D_{744}$  indices to express differences in the shape of the first derivative curve among damage levels. The red edge wavelength position – Red Edge Inflection Point (REIP<sub>wave</sub>) can be defined as the boundary between chlorophyll absorption in the red wavelengths and leaf scattering in the near-infrared (NIR) wavelengths (Rock *et al.*, 1994; Miller *et al.*, 1990). Previous

research suggests the wavelength position of the red edge inflection point to be of particular importance (Rock *et al.*, 1988; Vogelmann *et al.*, 1993).

An analysis methodology suggested as an indicator of geobotanical stress evaluates the spectral changes in the red edge region (680-750nm) utilizing first derivative spectra and the Inverted Gaussian Model (IGM; Table 5.5). Among the five IGM parameters, the following are considered of main importance for damage detection: (1) the location of the maximum peak of the first derivative at 680-730nm (red edge position – in the literature as  $\lambda\pi$  ( $\lambda\pi=\lambda_0-\sigma$ ), or REIP); (2) the maximum reflectance at the shoulder (720-850nm) ( $R_s$ ); and (3) the minimum reflectance corresponding to the chlorophyll absorption well ( $R_0$ ). Model description and analysis guidelines are provided by Miller *et al.* (1990). The inverted Gaussian model provides a quantitative representation of the red edge reflectance curve, generating the  $R_s$ ,  $R_0$ ,  $\lambda_0$ ,  $\sigma$  and  $\lambda\pi$  parameters strongly related to foliar chlorophyll content (Miller *et al.*, 1990; Zarco-Tejada; 1999). An inverted Gaussian curve was fitted to the data using the equation:

$$R(\lambda)=R_s-((R_s-R_0)\exp(-(\lambda_0-\lambda)^2/2\sigma^2)).$$

The IGM was applied using non-linear least squares mathematical procedure and 14 ASAS bands from the 673-805nm region. For representation of the red edge, the IGM requires initial assumptions of the model parameters based on spectral analysis (Miller *et al.*, 1990). In the current study, the starting IGM parameters were  $\lambda_0=673\text{nm}$ ,  $R_0=5\%$ ,  $\sigma=40\text{nm}$ ,  $R_s=40\%$ .

Many of the algorithms reported in the literature have been developed using leaf reflectance measurements or have been developed for assessment of changes in pigment concentration occurring with vegetation damage. With the current study, such algorithms

are evaluated using spectra acquired at the forest stand level and their potential for damage detection at the canopy level is assessed.

To determine the extent to which the various algorithms provided potential for damage detection, indices calculated using ASAS spectra extracted from healthy (DC0), and damaged (DC1, DC2 and DC3) canopy were compared using ANOVA and Tukey-Kramer means test (Zar, 1996).

The sensitivity of the individual indices to damage was estimated by calculating the relative difference for each damage class from healthy (Carter, 1994) using the formula:

$$\text{Index Sensitivity to DC1} = (\text{IndexDC1} - \text{IndexDC0}) / \text{IndexDC0}.$$

The sensitivity to damage levels DC1, DC2 and DC3 of each index was calculated.

### **5.2.6 Relationship between Reflectance Indices Derived from Canopy Spectra (ASAS data) and Foliar Spectra (GER2600 data)**

To assess the potential of spectral data extracted at foliar and canopy level to provide comparable results, a number of indices computed from ASAS reflectance spectra and GER2600 reflectance and averaged to stand level are compared.

Spectral data from both instruments were available for 18 intensive study sites. Reflectance data recorded by the GER2600 for first, second- and third-year foliage from five representative trees within each site were averaged to represent stand level spectra. The ASAS reflectance spectra extracted from multiple tree canopies within the imagery were averaged to stand level spectra. Using the same band centers for both data types and preserving the spectral resolution of the data spectral indices were computed. To test the hypothesis that there is no statistically significant difference between means for indices

calculated using the GER2600, data and indices calculated from the ASAS spectra was used ANOVA (SYSTAT, SPSS Inc., 1997). Both sensor type effects and stand damage level effects were considered. The differences between means were considered highly significant statistically when  $p < 0.01$  ( $p < 0.05$  significant). The coefficient of determination ( $r^2$ ) indicates the fraction of the variability in an index that could be accounted for by both treatments (i.e. GER2600 vs. ASAS) and damage level.

### **5.3 Results and Discussion**

#### **5.3.1 Canopy Reflectance Properties**

##### **Evaluation of Norway Spruce Canopy Spectral Properties**

Canopy reflectance increased with increase in damage level, with the healthy (DC0) stands having the lowest reflectance across the 450-900nm spectral range (Figure 5.8). The standard deviations of the data around the means were higher for damaged forests as compared to healthy stands (Figure 5.8b), with highest variations for the two intermediate damage levels (DC1 and DC2), followed by DC3. For DC0 and DC1, the variation of the data around the means were maximum at the spectral band 683nm, while for DC2 and DC3, variation was greatest at 673nm and 642nm respectively. This finding indicates a shift toward lower wavelengths of the chlorophyll absorption minima within the spectra with increasing damage level. The trends of increased reflectance and increased variation with increase in damage level are consistent for all study areas. These trends are in contrast to the spectral trends reported for the NIR region using both field and airborne high spectral resolution data acquired for red spruce in decline in New England (Rock *et al.*, 1988).

Using both airborne and field high spectral resolution data Rock *et al.* (1988) reported a decreasing reflectance in the NIR associated with increasing damage levels, and an increasing reflectance in the visible and red edge regions (for red spruce). The difference in the results reported by Rock *et al.* (1988) and those reported here could be explained by changes in solar zenith angle during observations. The healthy stands (DC0) were located on the western-most slopes of the Krusne hory and ASAS was flown over these healthy sites first (about 10:30am) during the days of data acquisition. ASAS acquired data for the damaged stands to the east at times closer to local noon. The sun therefore rose (the solar zenith angle decreased) between the observations of the healthy stands and the observations of the damaged stands approximately two hours later.

Previous studies have established that coniferous forest reflectance is anisotropic (Kimes *et al.* , 1986., Kriebel, 1978, Ranson, *et al.*, 1994, and Russel *et al.*, 1997); that is, canopy reflectance varies as the directions and angle of solar illumination vary. For the present study the view angle of the ASAS sensor was fixed at nadir (0-view zenith angle), but due to the distance between sites (a total of approximately 50km) and the orientation of the flightlines, the solar illumination zenith angle decreased as the sensor was flown from the healthy sites to the damaged sites. The coniferous forest data reported by Kriebel (1978) and by Kimes *et al.* (1994) show an increase in nadir reflectance at all wavelengths as solar zenith angle decreases. Therefore, the observed increase in canopy reflectance with increasing damage in the Krusne hory may be an illumination artifact associated with/or exaggerated by the decreasing solar zenith angle. This illumination effect may be more pronounced than the effect of canopy damage on the magnitude of reflectance. Other factors, such as the increasing amounts of grass (*Calimagrastis spp.* and

*Dechampsia spp.*) in the understory associated with changes in canopy structure with increasing canopy damage may also effect the magnitude of reflectance.

In the visible portion of the spectrum (450-700nm), reflectance maxima and minima occurred in the green region at 551.5nm and in the red region at 673nm, respectively, for all damage levels. The shape of the spectral curve in this region was typical for vegetation spectra acquired from spruce needles by a field spectrometer (Rock *et al.*, 1988), with two minor peaks at 550 and 600nm for the healthy canopy.

With increasing damage level, there was an increasing change in the 770-850 region, with the development of a spectral peak at 820-830nm for the damaged canopies (Figure 5.8). The reflectance maximum in the NIR region (770-900nm) for healthy canopies (DC0) peaked at 847nm with a second minor peak at 774nm. The maximum for DC1 was at 837nm, while for both DC2 and DC3 the peak was at 826nm. These results illustrate an apparent shift towards shorter wavelengths for the reflectance peak occurring with an increase in damage level. Reflectance minima in the NIR occurred for DC0 at 795nm, and at 775 for the remaining damage classes.

Based on ANOVA and Tukey's tests performed at each band, at 580nm and in the regions 680-740nm and 770-870nm, differences among means across damage levels were statistically significant ( $p < 0.01$ ). Reflectance difference peaks occurred in the 683-740nm and 805-878nm regions, with maximums for all damage levels at 724nm and 826nm (Figure 5.9a). Reflectance sensitivity was higher for the more heavily damaged canopies across the whole spectral range. The peaks for DC1 were in the 673-724nm range, while for DC2 and DC3 were broader, in the 581-703 range. This indicates that the bands from these spectral regions have the highest potential for damage level separation



in Norway spruce canopies. For all damage levels, the sensitivity maximum occurred at 683nm (Figure 5.9b). Although differences in the 800-900nm region were large and statistically significant, the sensitivity to damage was low, suggesting low potential for damage separation of this spectral region.

### **Canopy reflectance properties of normalized reflectance spectra**

Normalizing the reflectance data to a minimum at 673nm and a maximum at 744nm allowed for visual evaluation of the reflectance properties in the red edge region, independent of the influence of the spectral amplitude variation. With an increase in damage, a trend of a shift of the reflectance curve toward shorter wavelengths can be seen (Figure 5.10a). In the red edge region, reflectance increased significantly with damage throughout the 683.2-734.2nm region, and was maximal around the middle of the spectral region – at 703.8nm and 714nm.

Normalization of spectral reflectance to 673-847.2nm (Figure 5.10b) provides evidence that NIR reflectance may drop with increasing damage, a drop that may be masked by changes in reflectance magnitude due to BRDF effects (as discussed previously). An increase in reflectance in the 670-710nm region and a decrease in reflectance in the 720-820nm, observed with an increase in damage level, are a typical spectral property of vegetation under stress (Rock *et al.*, 1986; 1988). The normalization approach allows the red edge properties to be used for separation of damage classes based on physiological differences occurring with damage.

### **Derivative analysis**

To study the pattern and precise location of the spectral features of Norway spruce reflectance by damage level a derivative analysis was conducted (Figure 5.11). A major

spectral peak occurred in the 673-744nm region (i.e. the red edge). A secondary peak occurred between 775nm and 850nm (NIR), while a minor spectral feature is seen between 571nm and 600nm (the green peak). The maximum of the red edge peak (REIP) for healthy forest (DC0) was at 724nm, for DC1 and DC3 at 714nm, and for DC2 at 724nm (Figure 5.11a). With increase in damage level, the variation of the data around the means increased, with the least amount of overlap among standard deviations noted in the red edge and the NIR regions (Figure 5.11b).

Statistically significant differences in the derivative spectra with damage class occurred in the 683-744nm and 775-847nm regions ( $p < 0.01$ ). The 683-744nm peak (REIP) has been correlated with pigment levels, while a decrease in chlorophyll *a* and *b* concentrations with increased damage levels have been related to changes in the amount and position of the spectral maximum. For the wavelength position of the derivative there was no significant difference between DC0 and DC1, but they were as a group significantly different from DC2 and DC3 (Figure 5.11a and 5.14b). Based on ANOVA results, there were highly significant differences in amount of derivative maximum between DC0 and DC1, DC2 and DC3 (Figure 5.11a and 5.14b).

The second peak in derivative spectra occurred for DC 0 at 837nm, for DC1 at 805nm, for DC2 at 816nm and for DC3 at 805nm with values of 0.03, 0.09, 0.17 and 0.16 respectively (Figure 5.11). The NIR (770-850nm) region of the spectrum is associated with the leaf and canopy scattering and the amount of forest biomass. There were statistically significant differences between healthy canopies and all damage levels at both 816 and 826nm. A small, but broad shift (approximately 40nm) in derivative peak maxima was observed with increasing damage.

### **5.3.2 Evaluation of Spectral Indices for Separation of Initial Damage Levels**

The current study evaluated the use of high spectral resolution data for separation of damage levels in Norway spruce canopy using a wide range of algorithms (Table 5.5). The coefficients of determination of the spectral indices to damage (Table 5.6a and 5.6b) and the sensitivity of a particular index to individual damage level (Table 5.7a and 5.7b) were used as an indicator for evaluating the detection potential of the algorithms. Figures 5.12, 5.13, 5.14 and 5.15 depict the differences among LS Means by damage level. The statistical significance of the differences among means is depicted by plotting the standard errors of the means as error bars, with non-overlapping error bars representing statistically significant differences ( $p < 0.01$ ).

From all indices evaluated only C2, PRI2, R550/R700 and  $\lambda\pi$  did not differ statistically for healthy and damaged vegetation, or among damage levels (Tables: 5.6a and 5.6b; Figure 5.12 b, 5.12g, 5.13 c and 5.15e).

The following sections report and discuss the results for the indices having higher sensitivity to the decline and statistically significant differences among means per damage level. The indices are organized in five major groups: (1) optical, (2) LandsatTM and Narrow-band, (3) derivative, (4) IGM, and (5) normalized indices.

#### **Optical indices**

The C1 index ratios reflectance at 695nm (strongly sensitive to changes in chlorophyll) and the NIR 760nm (insensitive to pigments) (Figure 5.12a). This ratio has been modified for use with ASAS data to ratio of 695nm to 775nm wavebands, to avoid the 760nm oxygen absorption feature present in the ASAS spectra. The ratio increased

with increase in damage and differed significantly for healthy canopies as compared to DC1, DC2 and D3 ( $r^2=0.93$ ). The sensitivity of the index to damage was relatively strong (0.13), as compared to the remaining indices on the list.

The RE1 index (the average reflectance in the 673-703.8nm region) shows high sensitivity to damage levels 2 and 3 (Figure 5.12i). The index is strongly correlated to damage ( $r^2=0.96$ ), and its sensitivity to DC1 is also relatively high.

The pigment-specific indices RARSa ( $r^2=0.97$ ), RARSb ( $r^2=0.70$ ) and RARSc ( $r^2=0.38$ ), suggested in the literature as indices utilizing bands strongly sensitive to pigment concentration, display a relatively higher sensitivity to DC2 and DC3 when ranked among the other indices, while only RARSc (Figure 5.12p) has a relatively high sensitivity to DC1.

The results suggest a high potential for separation of initial damage levels (DC1) using a number of optical indices incorporating red edge spectral bands, especially the C1 and RE1 optical indices.

#### **LandstaTM and narrow-band ratios**

There was a strong correlation between the NDVI ( $r^2=0.97$ ) and TVI ( $r^2=0.98$ , as calculated from NDVI) indices and damage class (Table 5.6a), the indices decreasing with an increase in damage level. The differences between means from DC0 and DC1 were not significant, while there were highly significant differences among means from DC2, DC3 and the combined group of DC0 and DC1 (Figures 5.13a and 5.13b). This result demonstrates low potential of these indices for detection of the initial levels of damage.

### **Derivative indices**

The derivative indices  $D_{max}/D_{704}$  and  $D_{714}/D_{744}$  have the highest sensitivity when ranked among the other derivative indices. All indices decrease in value with an increase in damage level, except for  $D_{max}/D_{744}$  which increases with an increase in damage (Figures 5.14 d-f).  $D_{max}/D_{704}$ ,  $D_{max}/D_{714}$  and  $D_{714}/D_{704}$  show statistically significant differences among all damage levels, while  $D_{max}/D_{744}$  is able to separate the combined group of DC2 and DC3 from the combined group of DC 0 and DC1.

These results suggest a high potential for separation of early stages of damage for the derivative indices  $D_{max}/D_{704}$ ,  $D_{max}/D_{714}$  and  $D_{714}/D_{704}$ , with the  $D_{max}/D_{704}$  having the highest sensitivity to DC1.

### **Inverted Gaussian Model (IGM) parameters**

From the IGM parameters, the  $R_o$  index (representing the estimated reflectance minimum in the chlorophyll well in the 670-680nm region) had the highest relationship to the decline for all damage levels ( $r^2=0.93$ ).  $R_o$  increases significantly with an increase in damage level (Figure 5.15 a). The index sensitivity to initial damage is 0.59, 7.08 to DC2 and 10.63 to DC3, suggesting a high potential of this index for separation of initial levels of stress as well as of intermediate and heavy damage.

The results demonstrate that  $R_o$  has the highest sensitivity and potential for separation of initial damage level among all evaluated indices.

### **Normalized bands**

Reflectance for the normalized bands increases with an increase in damage level (Figure 5.10a). There were statistically significant differences among normalized spectra throughout the 683.2-734nm region (Table 5.6c). Using only bands 704nm and 714nm,

separation of DC0 from DC1, DC2 and DC3 was possible. It is important to note that the normalized bands show relatively high sensitivity to initial damage (DC1), while their sensitivity to DC2 and DC3 is lower as compared to Ro, RE1 and C1 (Table 5.7c).

#### **Overall comparison among the indices sensitive to stress**

Evaluating the sensitivity and correlation of the indices from the different groups, the overall highest potential for separation of initial damage levels (DC0 and DC1) was demonstrated by Ro. Ro was followed by C1, RE1, N704, Dmax/D704 and the RARSc index.

### **5.3.3 Evaluation of the Effect of the Decline on Forest Stand Parameters and Foliar Chemical Constituents**

Reflectance spectral properties at the canopy level are a function of physiologically-based parameters (e.g. pigment concentrations) and of the forest canopy structure (e.g. stand density, canopy closure, canopy architecture, etc.). Many of the parameters are effected simultaneously by forest damage and therefore it is important in defining the basis for use of the hyperspectral indices as bio-indicators of damage to be familiar with the extent to which the individual canopy parameters are affected by the damage conditions.

#### **Relationships between damage level and forest stand parameters**

The variation of the measured stand parameters with damage level was evaluated (ANOVA, Table 5.8). A relatively low relationship between damage class and forestry parameters was noted. Statistically significant differences with a relatively low relationship to damage level were depicted for forest stand age, canopy closure and elevation.

In relation to damage level, the stand parameters varied. The more heavily damaged stands were relatively younger, they were located at the lower elevations and had lower canopy closure. Since canopy closure was one of the main characteristics evaluated during the field evaluation of forest health, observation of lower canopy closure at the more damaged sites was anticipated. The pattern of more damaged stands being younger could be explained by the less damaged forests living longer and reaching a greater age.

A trend of heavier forest damage occurring at the higher elevations in the Krusne hory had been reported for broad elevational ranges (601-800m and 801-1000m) by previous investigations (Rock *et al.*, 1994; Ardo *et al.*, 1997; Lambert *et al.*, 1995). Our finding of occurrence of forest stands with heavier damage at the lower elevations contradict this reported trend. Within the small (approximately 100m) elevational gradient, the variation of forest damage observed with elevation could be explained by the sites at lower elevations having a closer proximity to the pollution sources, and/or by the pollution air-mass being present longer at the lower protected from winds landscape features.

#### **Relationships between damage level and foliar constituents**

With the current study, insignificant relationships were established between pigment levels (i.e., chlorophyll *a*, *b* and carotenoids) and damage level (Table 5.8). A statistically significant relationship to damage was established for the chlorophyll *a/b* ratio ( $r=0.60$ ; Table 5.8), identifying this ratio as a potential bioindicator of damage in the Krusne hory.

Numerous investigations demonstrate strong relationships between vegetation stress and pigment levels, and consider pigments to be sensitive indicators of plant stress (Rock *et al.*, 1986; Lichtenthaler, 1988). Many of these previous investigations evaluated the initial changes in pigment levels shortly after introducing a new stress agent to vegetation that had been growing under optimal conditions. The long-term effect of the stress factors (in the Czech Republic SO<sub>2</sub> air pollution since 1965-67), and the occurrence of growth recovery during the period 1980-95 (Entcheva *et al.*, 1996), could provide an explanation for the relatively stable pigment levels across the study areas. In addition, forest damage classes represent a combination of stand and individual tree parameters effecting pigment levels in complex ways. This complexity could also account for the lack of a strong direct correlation between damage level and photosynthetic pigments. Depending on the degree of canopy closure, two canopies can have very different foliar pigment concentration per unit of canopy area, while pigment concentration per unit of leaf mass could be similar.

#### **Relationship between damage level and foliar constituents**

Evaluating the relationship between foliar constituents (nitrogen, lignin, cellulose, polar and non-polar compounds, Table 5.8) and damage level, a highly significant relationship was established for non-polar constituents ( $r^2=0.88$ ) and for lignin ( $r^2=0.60$ ). These findings suggest a potential for non-polar constituents and lignin compounds as indicators of damage.

Strong correlations between the non-polar fraction and chlorophyll *a* ( $r=-0.60$ ), chlorophyll *b* ( $r=-0.64$ ) and total chlorophyll were established ( $a+b$ ,  $r=-0.61$ ; Table 5.9).

Non-polar constituents include organic components such as fats, waxes and other



organic-soluble materials, removed by boiling two grams of dried foliage material in dichlormethane for five hours (Newman *et al.*, 1994). During this procedure a large amount of the remaining in the dried foliage pigments are also removed.

Strong relationships were established between lignin, cellulose, polar and non-polar chemical constituents (Table 5.9). Since these constituents are products of the same chemical analysis, which sum to 100%, this relationship was anticipated.

### **5.3.4 Evaluation of the Relationships between Reflectance Indices and Forest Stand Parameters and Foliar Constituents**

#### **Relationship between reflectance indices and forest stand parameters**

Correlation analyses were conducted to evaluate the relationship between all computed hyperspectral indices and the canopy characteristics indicative of forest damage (Tables 5.10a and 5.10b). The results only for the indices sensitive to forest damage (i.e. Ro, C1, RE1, N704, Dmax/D704 and RARSc) are discussed below.

Canopy closure affected significantly most of the spectral indices. A strong correlation was established between canopy closure and C1( $r=-0.62$ ), RE1 ( $r=-0.64$ ) and Dmax/D704 ( $r=0.77$ ). This finding confirms the importance of canopy closure as a stand parameter for linking field damage evaluation to remote sensing assessment of forest condition.

Strong correlations were found between study site elevation and the indices sensitive to damage level: Ro ( $r=-0.72$ ), RARSc ( $r=-0.70$ ), RE1( $r=-0.70$ )(Table 5.10a and 5.10b). The relatively strong relationships between damage level and elevation, and damage level and canopy closure explain their indirect effect on canopy spectral properties and in particular on the indices found to be sensitive to damage.

## **Relationship between reflectance indices and canopy pigments and chemical constituents**

Tables 5.11a and 5.11b depict the correlation between foliar compounds and spectral indices. The results for the indices sensitive to forest damage (i.e. Ro, C1, RE1, N704, Dmax/D704 and RARSc) are discussed below.

The strongest relationship revealed for most indices, was to non-polar foliar compounds: Ro( $r=0.87$ ), C1( $r=0.84$ ), RE1 ( $r=0.88$ ), N704 ( $r=0.71$ ) and Dmax/D704 ( $r=-0.69$ ). A number of indices were also strongly correlated with lignin compounds: C1( $r=-0.69$ ), Ro( $r=-0.67$ ), RE1 ( $r=-0.66$ ), N704( $r=-0.61$ ). A relatively high correlation to polar compounds was exhibited by the indices C1( $r=0.64$ ) and N704( $r=0.61$ ). Considerable relationships were established between chlorophyll level and the indices sensitive to damage: Ro (to chlorophyll:  $a$   $r=-0.61$ ,  $b$   $r=-0.65$  and  $(a+b)$   $r=-0.62$ ) and N704 (to chlorophyll:  $a$   $r=-0.61$ ,  $b$   $r=-0.64$  and  $(a+b)$   $r=-0.62$ ). The RARSc index was found to be strongly related to carotenoid levels ( $r=0.75$ ).

The relationship of the inverted IGM parameters to chlorophyll *a*, chlorophyll *b* and total chlorophyll (Table 5.11b), and of the RARSc to carotenoids (Table 5.11a) have been documented by previous research (Miller *et al.*, 1990; Datt, 1998). Our findings demonstrate strong relationships between the indices sensitive to damage and foliar non-polar and lignin compounds, not previously reported.

These results, combined with the significant effect of damage level on non-polar and lignin levels established earlier, provide the bio-physiological link for use of the reflectance indices sensitive to damage for forest damage evaluation.

### **5.3.5 Relationship between Reflectance Indices Derived from Canopy spectra (ASAS data) and Foliar Spectra (GER2600 data)**

Table 5.12 depicts the relationship between spectral indices derived using ASAS and GER2600 reflectance data. No statistically-significant differences between ASAS and GER2600 means were found for the following indices: C1, V3, NDVI and TVI (Table 5.12; Figures 5.16a-e). A common factor for the ratio indices is their use of one or a few broadly spaced bands in the NIR and in the red region (NIR bands: 744nm, 775nm, 795nm; red edge bands: 673nm, 693nm, 724nm).

The inverted Gaussian model parameter  $R_0$  also compares relatively well, with no statistically significant differences, between ASAS and GER2600 data means (Table 5.12; Figure 5.16d). This result complies with the detailed evaluation of the IGM approach performed by Miller *et al.* (1990), where he reports specification of the red edge parameters within 2nm and relative error of the methodology of less than 15%.

Comparing the GER2600 and ASAS data for individual indices, an apparent trend of higher variation around an overall mean for individual indices within the ASAS data was noted (Figures 5.16a-e). The extracted tree crown spectra (using ASAS data) providing better spectral representation of the within stand variations than the foliar spectra (GER2600 data) is a possible explanation.

Considering the properties of derivative spectra to remove/limit the effects of baseline shifts and scattering on the reflectance spectra, no statistically significant differences were expected between means for the REIP and the derivative indices. The 10nm bandwidth of ASAS data appears to present difficulties for comparing derivative spectra, and limits the possibilities for REIP (REIPwave) position to approximately four

values. The differences in spectral characteristics and resolution between the two sensors (10nm ASAS vs. 2.5nm GER2600) offer a possible explanation for the fact that relatively few spectral indices compared well between instruments. Another explanation may relate to the difference in illumination sources (sun for ASAS vs. tungsten lamp for GER2600).

These results demonstrate that hyperspectral reflectance airborne data extracted at the canopy level (10nm ASAS) and laboratory foliar reflectance measurements (2.5nm GER2600) data can provide similar results for selected red edge and derivative indices.

#### **5.4 Conclusions**

A general trend in Norway spruce canopy spectra of increasing reflectance with increased damage levels was established across the 400-900nm spectral range. This spectral trend in the visible region is typical for vegetation in decline as measured at the foliar level by a field spectrometer, while the increasing reflectance observed in the NIR is in contrast to the pattern observed at the foliar level. This is likely due to sun angle differences related to variation in time-of-day of data collection for the different damage conditions. The higher canopy closure, foliar retention and stand density for the canopy of healthier forests, creating a higher amount of shadow in the canopy of healthier stands and causing a higher overall light absorbency and lower reflectance probably contributes as well.

This study illustrates that hyperspectral data can provide improved damage separation capabilities compared to multispectral broad band data. Using canopy spectra, the red edge spectral region (673-724nm) was identified as presenting the highest potential for separation of the initial levels of damage. This finding corresponds with the

region suggested as most sensitive to stress based on foliar reflectance measurements. Twelve indices were identified as strongly correlated to damage level, from which nine present the most potential for use as bioindicators of the initial level of damage: three optical indices (C1, RE1, RARSc), two derivative indices (D714/D704, Dmax/D704), two modeled parameters product of Inverted Gaussian model application (Rs, Ro) and two normalized red edge bands (N693, N704).

The presence of relatively stable pigment levels across the damage gradient, while the damage levels have a significant effect on the chlorophyll *a/b* ratio and on foliar constituents (non-polar and lignin), suggests the possibility of a recent forest recovery across the damage gradient (a forest health condition in which foliar pigments at the heavily damaged forests have recovered to levels close to the concentrations occurring in healthy forest stands, while foliar chemical constituents reflect the long-term health condition of these forests). This study confirms the high potential of the chlorophyll *a/b* ratio as a bio-indicator of damage, and establishes the high potential for use of foliar chemical compounds as indicators of long-term forest health.

The spectral changes in the canopy reflectance indices sensitive to damage were explained primarily by the change in foliar non-polar and lignin compounds, while the changes in the normalized red edge reflectance bands were associated with changes in both pigment levels and foliar constituents. These relationships establish the bio-physiological basis (link) for the use of these indices as indicators of forest damage. The significant effect of canopy closure on the indices provides a canopy morphological basis for use of these indices as indicators of damage.

Finally, this study demonstrates that using hyperspectral reflectance ratios, canopy reflectance measurements can produce reflectance spectra that closely resemble leaf level reflectance measurements. Five indices providing similar results were identified, from which two (reflectance ratio of 693/775 and the position of the reflectance minimum in the chlorophyll well, as computed by the Inverted Gaussian Model) have shown a high potential for separation of the initial forest damage levels.

The derivative indices were identified as least sensitive to vegetation morphological parameters, therefore providing the best potential for across-forest scales and instruments comparisons. The 10nm spectral resolution of ASAS was found to be marginal for determining the effect of the decline on the derivative indices.

Damage Class	Code	Percent Defoliation (%)	Forest Health Status	
			without chlorosis	with chlorosis
Healthy	0	0 – 10	Healthy	Initial damage
Initial	1	11 – 25	Initial damage	Medium damage
Medium	2	25 – 60	Medium damage	Heavy damage
Severe	3	60 – 99	Heavy damage	Forest ecosystem collapse - Dead
Dead	4	100	Forest ecosystem collapse - Dead	Standing dead forest

**Table 5.1: Forest damage evaluation criteria and damage level assignment**

Data	Acquisition Approach	Study Sites/Samples
ASAS <sup>1</sup> imagery	ASAS, nadir imagery, 60 ~10nm bands	182 sites
GER2600 <sup>2*</sup> calibration spectra	Spectra from ground targets with constant reflectance	6 targets
Field sites total	30x30m sites into 90x90m areas, 42 sites per damage class	182 sites
Forest stand damage class	healthy, initial, intermediate, and heavy damage, control	182 sites
Forest canopy closure	Within 1/10 acre plot, forest densiometer	182 sites
Stand density	Within 1/10 acre plot, prism	182 sites
Stand height	Height of the forest canopy, clinometer	182 sites
Site GPS position	Field visit, Trimble GPS units	182 sites
Photography for site characterization	Photos in the 4 world directions, 35 mm camera	182 sites
Site elevation and map location	Survey maps, GPS units	182 sites
Sites for sampling collections	30x30m sites into 90x90m areas, 12-14 sites per damage class	51 sites (14 DC0, 12 DC1, 14 DC2, and 12 DC3)
Individual trees damage class	healthy, initial, intermediate, and heavy damage, control	51 sites , 5 trees per site, 255 trees
Tree diameter at breast height	Tree diameter at 1.30m height, DBH tape	255 trees
Tree height	Height of the 5 representative trees, clinometer	255 trees
Tree age and growth rate	Cores extracted from 5 trees per stand, instrument borer	246 cores
Spruce foliar samples collection	1 <sup>st</sup> , 2 <sup>nd</sup> and 3 <sup>rd</sup> year of needles samples from 5 trees per site	765 samples
GER2600 spruce foliage spectra	Spectra from 5 representative trees per site	765 samples
Lignin, cellulose and nitrogen levels	Relationship between chemical content and spectral signature	765 samples
Foliar chlorophyll and carotenoids levels	Laboratory extraction and analyses	765 samples

<sup>1</sup> Airborne Solid-state Array Spectrometer (ASAS); NASA, Goddard Space Flight Center

<sup>2</sup> Field spectrometer GER2600, University of New Hampshire

\* The brand names of the instruments used in the investigation are cited for descriptive purposes and are not intended to imply endorsement

**Table 5.2: Data for the study areas in northwest Bohemia, Czech Republic, acquired August 1998**



Flight Parameters	ASAS Specifications
Flight Altitude	2500m agl
Swath Width	820m
Side overlap of flight lines	20%
Nominal spatial resolution	~2m
Number of Bands	62 (45)
Spectral Region	500-850nm

**Table 5.3: Airborne Solid-state Array Spectroradiometer (ASAS) flight parameters, Czech Republic, 1998**

Study Area	Flight Lines	Acquisition Date	Cloud Cover (%)
S1	1, 2, 3, 4, 5, 6	20-Aug	15-20%
S2	7, 8, 9, 10, 11, 12	20-Aug	30-40%
S3	13, 14, 15, 16, 17	01-Sep	60-70%

**Table 5.4: Flight attributes for ASAS nadir data acquisition, Czech Republic, 1998**

Index	Algorithm	Figure
	<b>1. Optical Indices</b>	
C1	$R693/R775$ <sup>1</sup>	11.a
C2	$R693/R500$	11.b
V1	$R744.5/R724$	11.c
V2	$(R731-R724)/(R731+R724)$	11.d
V3	$(R734.2-R744.5)/(R714+R724)$	11.e
PRI1	$(R531.8-R571)/(R531.8+R571)$	11.f
PRI2	$(R551.5-R531.8)/(R551.8+R531.8)$	11.g
PRI3	$(R571-R541.8)/(R571+R541.8)$	11.h
RE1	Average (R673:R703.8)	11.i
RE2	Average (R714:R724)	11.j
RE3	Average (R734.2:R744.5)	11.k
SR	$R744.5/R673$	11.l
SIPI	$(R795.5-R502.2)/(R795-R642.5)$	11.m
RARSa	$R673/R703.8$	11.n
RARSb	$R673/(R652.5 \cdot R703.9)$	11.o
RARSc	$R775/R502.2$	11.p
PSSRa	$(R795.5-R683.2)/(R795+R683.2)$	11.q
PSSRb	$(R795.5-R601.8)/(R795+R601.8)$	11.r
PSSRc	$(R795.5-R502.2)/(R795+R502.2)$	11.s
N <sup>2</sup> 683.2	R683.2 normalized to min. 670nm and max. 744.5nm.	
	<b>2. Landsat TM and Narrow-band Indices</b>	
NDVI	$(R795.5-R673)/(R795+R673)$	12.a
TVI	$(\text{Square root}(\text{NDVI})) \cdot 100$	12.b
R550R700	$R551.5/R703.8$	12.c
R850R700	$R857.5/R693$	12.d
R850R550	$R857.5/R551.5$	12.e
R815R740	$R816.2/R744.5$	12.f
R734R693	$R744.6/R693$	12.g
R734R714	$R744.6/R714$	12.h
R550R600	$R551.5/R601.8$	12.i
	<b>3. Derivative Indices</b>	
REIPwave	Position of D maximum in the 670-730nm region <sup>3</sup>	13.a
REIPslope=Dmax	D maximum in the 670-730nm region	13.b
D714D704	$D714/D703.8$	13.c
DMAXD714	$D_{\text{max}}/D714$	13.d
DMAXD704	$D_{\text{max}}/D703.10$	13.e
DMAXD744	$D_{\text{max}}/D744.5$	13.f
	<b>4. Inverted Gaussian Model (IGM) Parameters</b>	
Rs	R maximum in the 670-850nm region, IGF	14.a
Ro	R minimum in the 670-850nm region, IGF	14.b
$\lambda_0$	Wavelength position of Ro, IGF	14.c
$\sigma$	$(\lambda_0 - \lambda\pi)$ , IGF	14.d
$\lambda\pi$	Wavelength position of Dmax, IGF	14.e

<sup>1</sup> R - reflectance (%); <sup>2</sup> N - normalized reflectance; <sup>3</sup> D - derivative value, product of first derivative transformation of reflectance

**Table 5.5: Bands ratios and algorithms evaluated for stress detection**

Dep Var	n (sites)	F-ratio	p (Pr>F)	r	r <sup>2</sup>
<b>1. Optical Indices</b>					
C1	23	64.32	0.00	0.97	0.93
C2	23	0.29	0.83	0.24	0.06
V1	23	14.22	0.00	0.87	0.75
V2	23	9.05	0.00	0.81	0.66
V3	23	8.46	0.00	0.80	0.64
PR11	23	5.25	0.01	0.73	0.53
PR12	23	0.55	0.66	0.33	0.11
PR13	23	7.07	0.00	0.78	0.60
RE1	23	119.46	0.00	0.98	0.96
RE2	23	40.02	0.00	0.95	0.90
RE3	23	12.69	0.00	0.86	0.73
SR	23	27.69	0.00	0.93	0.86
SI1	23	11.54	0.00	0.84	0.71
RARSa	23	161.18	0.00	0.99	0.97
RARSb	23	10.65	0.00	0.83	0.70
RARSb	23	2.90	0.07	0.62	0.38
PSSRa	23	76.99	0.00	0.97	0.94
PSSRb	23	138.20	0.00	0.98	0.97
PSSRc	23	41.93	0.00	0.95	0.90
<b>2. LandsatTM and Narrow-band Indices</b>					
NDVI	23	165.80	0.00	0.99	0.97
TVI	23	182.16	0.00	0.99	0.98
R550/R700	23	0.29	0.83	0.24	0.06
R850/R700	23	3.91	0.03	0.67	0.46
R850/R550	23	8.80	0.00	0.81	0.65
R815/R740	23	6.83	0.00	0.77	0.59
R734/R693	23	13.42	0.00	0.86	0.74
R734/R714	23	52.84	0.00	0.96	0.92
R550/R600	23	11.72	0.00	0.85	0.72

**Table 5.6a: ASAS indices tested for significant differences among damage levels (ANOVA). Significance of the differences between means for Optical, LandsatTM and Narrow-band Indices.**

Derivative Index	n (sites)	F-ratio	p (Pr>F)	r	r <sup>2</sup>
<b>3. Derivative Indices</b>					
REIPwave	23	12.59	0.001	0.85	0.73
REIPslope	23	11.52	0.000	0.84	0.71
D714/D704	23	43.24	0.000	0.95	0.90
Dmax/D714	23	25.30	0.001	0.92	0.84
Dmax/D704	23	7.88	0.000	0.79	0.63
Dmax/D744	23	4.69	0.02	0.71	0.50
<b>4. Inverted Gaussian Model (IGM) Parameters</b>					
Rs	23	8.61	0.000	0.81	0.65
Ro	23	60.58	0.000	0.96	0.93
λ <sub>0</sub>	23	6.24	0.010	0.76	0.57
σ	23	3.73	0.042	0.67	0.44
λπ	23	0.50	0.691	0.31	0.10

**Table 5.6b: ASAS indices tested for significant differences among damage levels (ANOVA).** Significance of the differences between means for Derivative indices and Inverted Gaussian Model parameters.

Normalized Band	n (sites)	F-ratio	p (Pr>F)	r	r <sup>2</sup>
<b>5. Normalized to 683-734nm</b>					
N683	23	40.98	0.000	0.46	0.21
N693	23	58.58	0.000	0.53	0.28
N704	23	96.36	0.000	0.62	0.39
N714	23	109.28	0.000	0.68	0.46
N724	23	95.26	0.000	0.62	0.39
N734	23	79.20	0.000	0.59	0.35

**Table 5.6c: ASAS indices tested for significant differences among damage levels (ANOVA).** Significance of the differences between means for normalized red edge bands.

Index	Index Sensitivity to Damage Level		
	DC1	DC2	DC3
<b>1. Optical Indices</b>			
C1	0.13	0.70	1.06
C2	-0.08	-0.20	-0.15
V1	-0.03	-0.17	-0.22
V2	-0.06	-0.55	-0.68
V3	-0.07	-0.57	-0.71
PRI1	0.10	-0.64	-0.87
PRI2	-0.59	-0.01	-0.17
PRI3	0.02	-0.50	-0.74
RE1	0.13	1.20	1.88
RE2	0.06	0.56	0.84
RE3	0.01	0.26	0.43
SR	-0.02	-0.46	-0.65
SIPI	-0.01	0.03	0.08
RARSa	-0.02	0.47	0.74
RARSb	-0.01	-0.37	-0.53
RARSc	-0.15	-0.49	-0.61
PSSRa	-0.02	-0.18	-0.28
PSSRb	-0.02	-0.14	-0.17
PSSRc	-0.02	-0.14	-0.17
<b>2. LandsatTM and Narrow-band Indices</b>			
NDVI	-0.01	-0.17	-0.26
TVI	0.00	-0.05	-0.09
R550/R700	-0.03	0.03	-0.06
R850/R700	-0.03	-0.33	-0.51
R850/R550	0.01	-0.22	-0.30
R815/R740	0.03	0.12	0.13
R734/R693	-0.05	-0.36	-0.50
R734/R714	-0.03	-0.17	-0.23
R550/R600	-0.01	-0.18	-0.27

**Table 5.7a: Sensitivity of individual indices to damage level. Sensitivity of Optical indices, LandsatTM and Narrow-band ratios.**

Index	Index Sensitivity to Damage Level		
	DC1	DC2	DC3
<b>3. Derivative Indices</b>			
REIPwave	-0.01	-0.03	-0.02
REIPslope	-0.02	-0.06	-0.09
D714/D704	-0.06	-0.27	-0.33
Dmax/D714	-0.03	-0.15	-0.20
Dmax/D704	-0.10	-0.14	-0.15
Dmax/D744	0.05	0.74	0.60
<b>4. Inverted Gaussian Model (IGM) Parameters</b>			
Rs	0.06	0.36	0.51
Ro	0.59	7.09	10.63
$\lambda_0$	-0.02	-0.01	-0.01
$\sigma$	0.05	0.19	0.22
$\lambda\pi$	0.00	0.00	0.00

**Table 5.7b: Sensitivity of individual indices to damage level. Sensitivity of Derivative indices, Inverted Gaussian Model Parameters and Normalized bands.**

Normalized Band	Band Sensitivity to Damage Level		
	DC1	DC2	DC3
N683.2	0.37	0.57	1.01
N693	0.18	0.36	0.54
N703.8	0.12	0.33	0.46
N714	0.08	0.24	0.31
N724	0.03	0.13	0.17
N734.2	0.02	0.07	0.09

**Table 5.7c: Sensitivity of the normalized bands to damage level (683-734nm spectral region)**

Evaluated Parameter	<i>n</i> (sites)	<i>F</i> -ratio	<i>p</i> ( <i>Pr</i> > <i>F</i> )	<i>r</i>	<i>r</i> <sup>2</sup>
Chlorophyll <i>a</i>	18	0.93	0.455	0.43	0.19
Chlorophyll <i>b</i>	18	1.19	0.356	0.48	0.23
Carotenoids	18	0.41	0.750	0.30	0.09
Chlorophyll ( <i>a+b</i> )	18	0.99	0.429	0.45	0.20
Chlorophyll <i>a/b</i>	18	3.16	0.064	<u>0.66</u>	0.44
( <i>a+b</i> )/Carotenoids	18	0.48	0.235	0.48	0.23
Nitrogen	18	0.89	0.472	0.40	0.16
( <i>a+b</i> )/N	18	1.40	0.290	0.51	0.26
Carotenoids/N	18	0.88	0.485	0.46	0.21
Lignin	18	2.69	0.046	<u>0.60</u>	0.37
Cellulose	18	1.17	0.357	0.45	0.20
Polar	18	1.76	0.200	0.52	0.27
Non-Polar	18	16.44	0.000	<u>0.88</u>	0.78
Tree Height	23	0.21	0.888	0.21	0.04
Tree DBH	23	0.52	0.673	0.32	0.10
Canopy Closure	23	2.71	0.052	<u>0.66</u>	0.43
Total BA	23	1.01	0.419	0.42	0.18
Stand Density	23	0.58	0.635	0.33	0.11
Age	18	4.12	0.027	<u>0.68</u>	0.47
Average BA	23	0.82	0.506	0.39	0.15
Elevation	23	3.81	0.035	<u>0.67</u>	0.45

**Table 5.8: Canopy foliar pigments, chemical compounds and stand parameters tested for significant differences among damage levels (ANOVA)**

Parameter:	<i>a</i>	<i>b</i>	Car	<i>a+b</i>	<i>a/b</i>	N	Lignin	Cellulose	Polar	Non_Polar	Car/N	( <i>a+b</i> )/Car	( <i>a+b</i> )/N	Age
Chlorophyll <i>a</i>	1.00													
Chlorophyll <i>b</i>	<u>0.99</u>	1.00												
Carotenoids (Car)	<u>0.89</u>	<u>0.87</u>	1.00											
<i>a+b</i>	1.00	<u>0.99</u>	<u>0.89</u>	1.00										
<i>a/b</i>	-0.29	-0.42	-0.19	-0.33	1.00									
Nitrogen (N)	0.48	0.49	0.21	0.48	-0.22	1.00								
Lignin	0.51	0.49	0.31	0.51	-0.14	0.53	1.00							
Cellulose	0.30	0.35	0.07	0.31	<u>-0.60</u>	0.45	0.57	1.00						
Polar	-0.39	-0.41	-0.15	-0.39	0.43	-0.50	<u>-0.82</u>	<u>-0.92</u>	1.00					
Non-Polar	<u>-0.60</u>	<u>-0.64</u>	-0.40	<u>-0.61</u>	0.51	-0.57	<u>-0.73</u>	-0.54	0.59	1.00				
Car/N	<u>0.83</u>	<u>0.80</u>	0.92	<u>0.83</u>	-0.14	0.10	0.32	0.15	-0.20	-0.43	1.00			
( <i>a+b</i> )/Car	0.07	0.12	-0.37	0.08	-0.30	0.43	0.33	0.37	-0.39	-0.39	-0.31	1.00		
( <i>a+b</i> )/N	<u>0.94</u>	0.93	0.92	<u>0.94</u>	-0.28	0.15	0.37	0.16	-0.24	-0.47	<u>0.90</u>	-0.09	1.00	
Age	0.17	0.21	0.19	0.18	-0.35	0.28	0.30	0.31	-0.25	-0.55	0.07	-0.06	0.13	1.00
Tree Height	0.22	0.23	0.01	0.22	-0.22	0.29	0.03	0.36	-0.25	-0.12	0.21	0.34	0.14	-0.10
Tree DBH	-0.02	0.02	-0.19	-0.01	-0.40	-0.04	0.10	0.52	-0.36	-0.28	0.00	0.36	0.02	0.40
Canopy Closure	-0.07	-0.02	-0.33	-0.06	-0.31	0.40	0.42	0.47	-0.42	<u>-0.63</u>	-0.27	<u>0.60</u>	-0.20	<u>0.61</u>
Total BA	0.16	0.18	-0.12	0.16	-0.20	0.52	0.58	0.49	<u>-0.61</u>	-0.38	-0.12	0.59	-0.02	0.09
Stand Density	0.09	0.09	-0.18	0.09	-0.07	0.48	0.47	0.34	-0.45	-0.35	-0.10	0.58	-0.09	0.04
Average BA	0.04	0.07	0.06	0.05	-0.25	-0.23	0.10	0.24	-0.24	0.07	-0.03	-0.07	0.15	0.02
Elevation	0.44	0.50	0.43	0.46	-0.56	0.19	0.33	0.02	-0.08	<u>-0.68</u>	0.34	0.13	0.46	0.44

Parameter:	Tree Height	Tree DBH	Canopy Closure	Total BA	Stand Density	Average BA	Elevation
Tree DBH	<u>0.60</u>	1.00					
Canopy Closure	0.16	0.54	1.00				
Total BA	0.18	0.22	0.50	1.00			
Stand Density	0.24	0.24	0.52	<u>0.93</u>	1.00		
Average BA	-0.03	0.05	-0.15	-0.28	-0.58	1.00	
Elevation	-0.15	0.00	0.30	0.05	0.05	-0.09	1.00

**Table 5.9: Correlation between stand parameters, foliar pigments and chemical constituents for the ASAS study areas**



Parameters	Canopy Closure	Elevation	Age	Tree Height	Tree_DBH	Total_BA	Stand Density
<b>Optical Indices</b>							
C1	-0.62	-0.58	-0.50	-0.19	-0.42	-0.41	-0.35
C2	-0.38	0.61	0.10	-0.41	-0.35	-0.29	-0.28
V1	0.64	0.39	0.42	0.28	0.48	0.47	0.42
V2	-0.60	-0.32	-0.32	-0.27	-0.42	-0.49	-0.45
V3	-0.60	-0.31	-0.33	-0.28	-0.43	-0.48	-0.45
PRI1	0.82	0.54	0.69	0.16	0.65	0.25	0.28
PRI2	-0.35	-0.22	-0.14	0.34	-0.06	0.27	0.14
PRI3	-0.78	-0.62	-0.75	-0.18	-0.60	-0.26	-0.25
RE1	-0.64	-0.70	-0.54	-0.10	-0.38	-0.39	-0.35
RE2	-0.67	-0.72	-0.55	-0.03	-0.38	-0.39	-0.36
RE3	-0.64	-0.78	-0.55	0.10	-0.30	-0.33	-0.33
SR	0.62	0.60	0.52	0.20	0.44	0.38	0.36
SIPI	-0.80	-0.36	-0.50	-0.42	-0.60	-0.44	-0.45
RARSa	-0.59	-0.75	-0.54	-0.12	-0.38	-0.35	-0.30
RARSb	0.67	0.60	0.56	-0.02	0.41	0.34	0.34
RARSc	-0.08	0.70	0.32	-0.24	-0.10	-0.06	-0.07
PSSRa	0.60	0.64	0.49	0.17	0.39	0.41	0.37
PSSRb	0.58	0.66	0.53	0.12	0.39	0.36	0.29
PSSRc	0.37	0.76	0.45	-0.05	0.18	0.27	0.20
<b>LandsatTM and Narrow-band indices</b>							
NDVI	0.61	0.67	0.51	0.15	0.38	0.39	0.34
TVI	0.61	0.67	0.51	0.15	0.38	0.39	0.34
R550/R700	0.18	-0.31	-0.16	0.37	0.02	0.36	0.39
R850/R700	0.45	0.24	0.26	0.27	0.34	0.41	0.40
R850/R550	0.36	0.50	0.39	0.00	0.26	0.21	0.20
R815/R740	-0.68	-0.53	-0.62	-0.32	-0.68	-0.35	-0.24
R734/R693	0.60	0.41	0.46	0.28	0.47	0.42	0.38
R734/R714	0.71	0.60	0.60	0.17	0.51	0.41	0.35
R550/R600	0.62	0.50	0.53	0.27	0.40	0.45	0.37

**Table 5.10a: Correlation between ASAS spectral indices and forest stand parameters**

Parameters	Canopy Closure	Elevation	Age	Tree Height	Tree DBH	Total BA	Stand Density
<b>Derivative Indices</b>							
REIPwave	0.38	0.33	-0.01	0.31	0.18	0.24	0.32
REIPslope	-0.26	-0.58	0.02	0.10	0.07	-0.03	-0.16
D714/D704	0.41	0.30	0.00	0.28	0.19	0.11	0.22
Dmax/D714	0.54	0.38	0.15	0.35	0.33	0.22	0.31
Dmax/D704	0.77	0.50	0.43	0.20	0.45	0.19	0.32
Dmax/D744	-0.19	-0.07	0.15	-0.20	0.01	-0.19	-0.16
<b>Inverted Gaussian Model Parameters</b>							
Rs	-0.48	-0.82	-0.39	-0.31	-0.33	-0.35	-0.34
Ro	-0.56	-0.72	-0.47	-0.32	-0.37	-0.40	-0.36
$\lambda_0$	0.40	0.59	0.27	0.57	0.32	0.38	0.36
$\sigma$	-0.50	-0.61	-0.49	-0.04	-0.40	-0.20	-0.06
$\lambda\pi$	-0.15	-0.07	-0.27	0.53	-0.12	0.17	0.30
<b>Normalized Bands</b>							
N683.2	-0.34	-0.27	-0.20	<u>-0.70</u>	-0.36	-0.54	-0.55
N693	-0.37	-0.38	-0.25	<u>-0.67</u>	-0.39	-0.50	-0.54
N703.8	-0.49	-0.46	-0.36	-0.59	-0.46	-0.55	-0.55
N714	-0.48	-0.42	-0.31	-0.58	-0.45	-0.56	-0.56
N724	-0.52	-0.45	-0.34	-0.53	-0.46	-0.56	-0.56
N734.2	-0.48	-0.40	-0.28	-0.59	-0.44	-0.59	-0.58

**Figure 5.10b: Correlation between ASAS spectral indices and forest stand parameters**

Parameters:	<i>a</i>	<i>b</i>	Car	( <i>a+b</i> )	<i>a/b</i>	N	Lignin	Cellulose	Polar	Non Polar	Car/N	( <i>a+b</i> )/Car	( <i>a+b</i> )/N
Optical Indices													
C1	-0.52	-0.55	-0.38	-0.53	0.51	-0.27	-0.69	-0.60	0.64	0.84	-0.48	-0.29	-0.50
C2	0.40	0.40	<u>0.65</u>	0.40	-0.09	-0.28	-0.07	-0.48	0.39	-0.14	0.54	-0.43	0.58
V1	0.42	0.44	0.26	0.42	-0.43	0.26	<u>0.68</u>	<u>0.69</u>	<u>-0.71</u>	<u>-0.73</u>	0.39	0.31	0.39
V2	-0.36	-0.38	-0.21	-0.37	0.38	-0.22	<u>-0.63</u>	<u>-0.66</u>	<u>0.68</u>	<u>0.64</u>	-0.36	-0.29	-0.34
V3	-0.36	-0.38	-0.21	-0.36	0.37	-0.22	<u>-0.63</u>	<u>-0.66</u>	<u>0.68</u>	<u>0.64</u>	-0.36	-0.29	-0.33
PRI1	0.19	0.24	0.05	0.21	-0.46	0.18	0.48	0.51	-0.46	<u>-0.74</u>	0.12	0.33	0.18
PRI2	0.32	0.29	0.38	0.31	-0.05	0.28	0.36	0.36	-0.47	-0.02	0.40	-0.30	0.24
PRI3	-0.23	-0.28	-0.11	-0.24	0.52	-0.26	-0.51	-0.49	0.46	<u>0.77</u>	-0.14	-0.27	-0.20
RE1	-0.47	-0.52	-0.35	-0.48	0.58	-0.27	-0.66	-0.55	0.59	<u>0.88</u>	-0.42	-0.30	-0.46
RE2	-0.38	-0.44	-0.27	-0.40	0.59	-0.22	-0.62	-0.53	0.55	<u>0.85</u>	-0.33	-0.30	-0.38
RE3	-0.26	-0.32	-0.19	-0.27	0.60	-0.15	-0.52	-0.43	0.44	<u>0.79</u>	-0.24	-0.25	-0.27
SR	0.48	0.52	0.37	0.49	-0.51	0.24	0.65	0.58	-0.61	<u>-0.81</u>	0.48	0.25	0.48
SIPI	-0.36	-0.39	-0.13	-0.37	0.46	-0.43	-0.58	-0.70	0.64	<u>0.81</u>	-0.27	-0.44	-0.25
RARSa	-0.54	-0.59	-0.42	-0.56	0.60	-0.29	-0.66	-0.52	0.56	<u>0.90</u>	-0.48	-0.30	-0.54
RARSb	0.24	0.29	0.19	0.26	-0.49	0.08	0.52	0.50	-0.49	<u>-0.72</u>	0.29	0.18	0.28
RARSc	0.56	0.57	<u>0.75</u>	0.56	-0.26	-0.14	0.24	-0.10	0.02	-0.45	<u>0.72</u>	-0.34	<u>0.71</u>
PSSRa	0.53	0.57	0.40	0.54	-0.54	0.29	0.70	0.59	-0.63	<u>-0.86</u>	0.49	0.27	0.51
PSSRb	0.55	0.58	0.43	0.56	-0.52	0.23	0.68	0.53	-0.59	<u>-0.85</u>	0.50	0.25	0.56
PSSRc	0.60	0.63	0.56	0.61	-0.50	0.14	0.63	0.36	-0.46	<u>-0.78</u>	0.59	0.12	0.65
LandsatTM and Narrow-band indices													
NDVI	0.54	0.58	0.40	0.55	-0.56	0.29	0.68	0.56	-0.60	<u>-0.88</u>	0.48	0.30	0.52
TVI	0.54	0.58	0.40	0.55	-0.56	0.29	0.68	0.56	-0.60	-0.88	0.48	0.30	0.52
R550/R700	-0.15	-0.15	-0.21	-0.15	-0.07	0.36	0.16	0.50	-0.43	-0.02	-0.08	0.04	-0.33
R850/R700	0.34	0.36	0.28	0.35	-0.32	0.18	0.54	0.63	-0.63	-0.55	0.45	0.10	0.33
R850/R550	0.52	0.53	0.52	0.53	-0.29	-0.02	0.49	0.34	-0.39	-0.63	0.63	0.02	0.61
R815/R740	-0.34	-0.40	-0.12	-0.35	0.60	-0.30	-0.58	-0.57	0.57	0.74	-0.13	-0.46	-0.30
R734/R693	0.44	0.46	0.32	0.45	-0.43	0.25	0.65	0.66	-0.68	-0.73	0.45	0.21	0.42
R734/R714	0.47	0.51	0.32	0.48	-0.51	0.27	0.68	0.59	-0.62	-0.86	0.39	0.32	0.45
R550/R600	0.34	0.40	0.24	0.36	-0.60	0.41	0.67	0.73	-0.73	-0.77	0.29	0.20	0.25

**Table 5.11a: Correlation between ASAS spectral indices and canopy foliar constituents**

Index	Significance of effects	F-ratio	p	r	Index	Significance of effects	F-ratio	p	r
<b>1. Optical Indices</b>					<b>2. LandsatTM and Narrow-band Indices</b>				
C1	Sensor DC	0.45 11.76	<u>0.506</u> 0.000	0.74	NDVI	System DC	0.06 24.93	<u>0.811</u> 0.000	0.85
C2	Sensor DC	22.75 0.28	0.000 0.839	0.67	TVI	Sensor DC	0.04 26.58	<u>0.846</u> 0.000	0.86
V1	Sensor DC	3.70 1.32	0.064 0.285	0.45	R850R700	Sensor DC	200.68 2.90	0.000 0.052	0.94
V2	Sensor DC	8.51 6.70	0.007 0.001	0.70	R850R550	Sensor DC	36.57 7.00	0.000 0.001	0.82
V3	Sensor DC	2.09 6.51	<u>0.159</u> 0.002	0.65	<b>3. Derivative Indices</b>				
PRI1	Sensor DC	67.56 3.93	0.000 0.018	0.86	REIPwave	Sensor DC	11.94 7.35	0.002 0.001	0.73
PRI2	Sensor DC	15.46 0.67	0.000 0.577	0.61	REIPslop	Sensor DC	454.66 3.42	0.000 0.030	0.97
PRI3	Sensor DC	70.84 5.93	0.000 0.003	0.87	D714/D704	Sensor DC	16.82 9.30	0.000 0.000	0.78
RE1	Sensor DC	111.12 11.79	0.000 0.000	0.92	Dmax/D714	Sensor DC	12.18 9.45	0.002 0.000	0.77
RE2	Sensor DC	136.60 9.42	0.000 0.000	0.92	Dmax/D744	Sensor DC	34.14 3.02	0.000 0.046	0.78
RE3	Sensor DC	196.36 5.33	0.000 0.005	0.94	<b>4. Inverted Gaussian Model Parameters</b>				
SR	Sensor DC	127.93 9.49	0.000 0.000	0.92	Rs	Sensor DC	198.43 4.20	0.000 0.014	0.94
SIPI	Sensor DC	1412.29 2.43	0.000 0.086	0.99	Ro	Sensor DC	2.86 13.50	<u>0.102</u> 0.000	0.78
RARSa	Sensor DC	917.83 5.10	0.000 0.006	0.93	$\lambda_0$	Sensor DC	101.00 5.79	0.000 0.003	0.90
RARSb	Sensor DC	829.49 3.30	0.000 0.034	0.91	$\sigma$	Sensor DC	15.98 3.35	0.000 0.033	0.68
RARSc	Sensor DC	11.10 2.02	0.037 0.133	0.62	$\lambda\pi$	Sensor DC	12.61 0.97	0.001 0.420	0.59

**Table 5.12: Relationship between spectral indices computed using ASAS and GER2600**

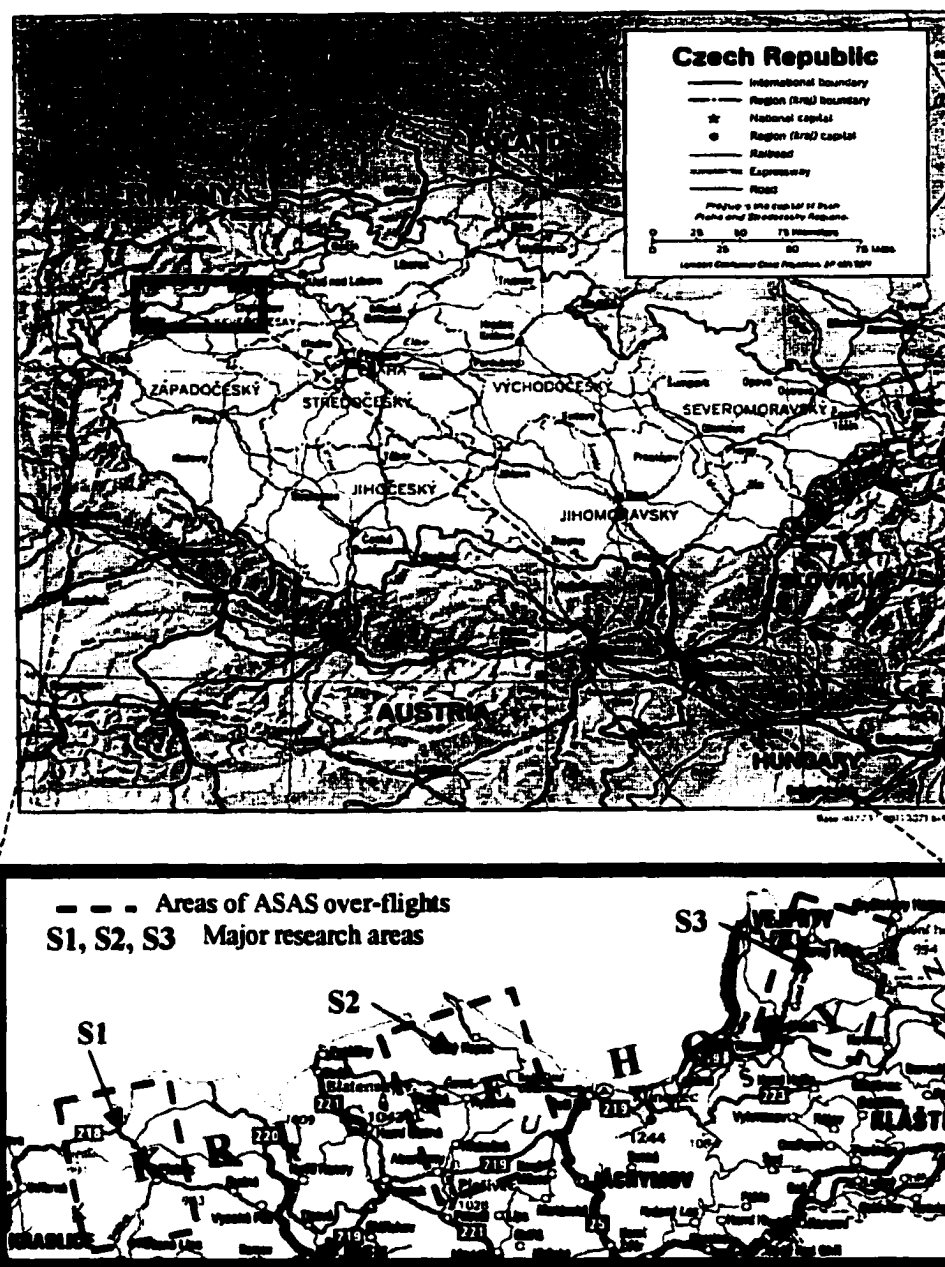
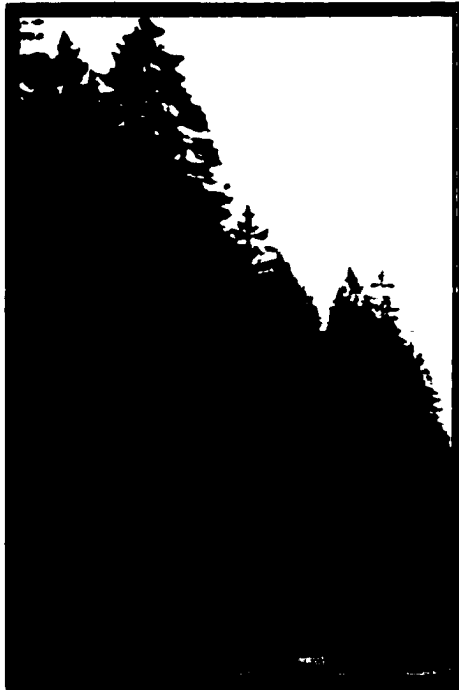
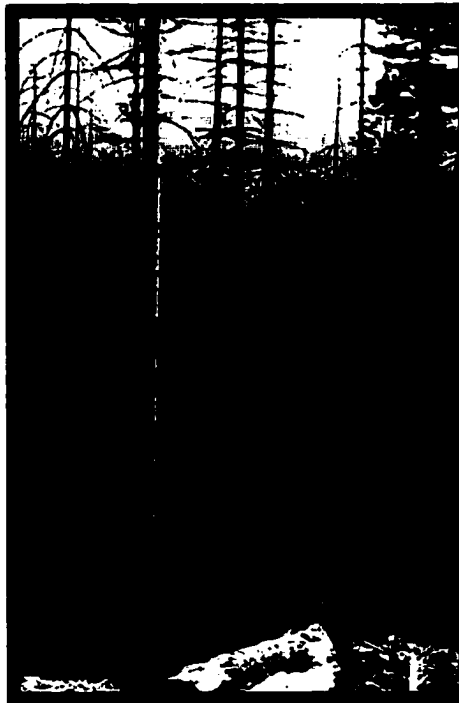


**Figure 5.1: Location of the study areas in the Krušné hory: Norway spruce forests representing the full range of forest health conditions due to  $\text{SO}_2$  pollution.**

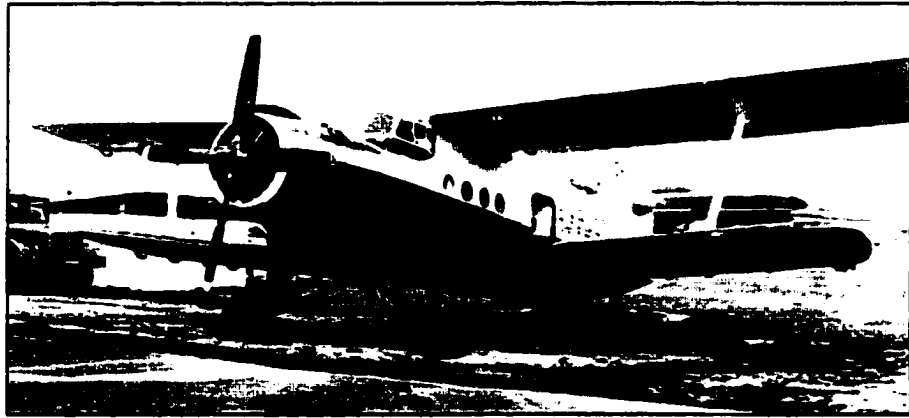


**a. Healthy Forest (DC0),  
Czech Republic**



**b. Heavily Damaged Forest  
(DC3), Czech Republic**

**Figure 5.2: Extreme forest health conditions encountered during the present study.**

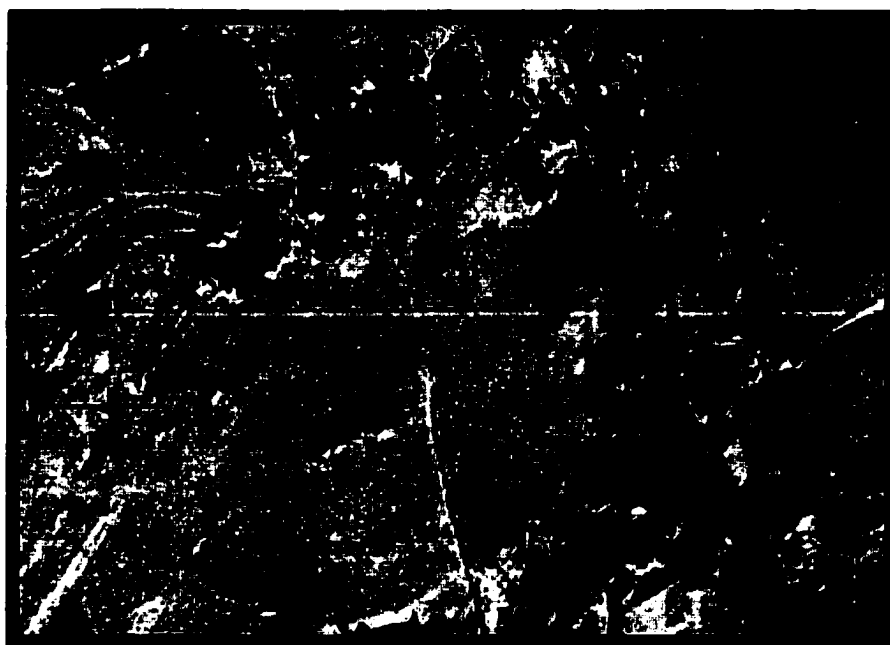


a. An Antonov2 single engine bi-plane used for the airborne acquisition of ASAS high spectral resolution imagery for the Krusne hory, Czech Republic, 1998.



b. The Airborne Solid-state Array Spectroradiometer (ASAS) on board the Antonov2.

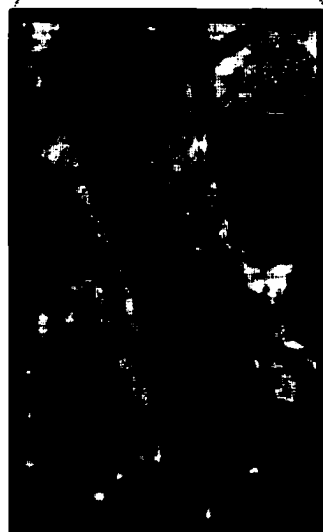
**Figure 5.3: High spectral resolution nadir data acquisition for the study sites. Data were acquired using the Airborne Solid-state Array Spectrometer flown on board the Antonov2 airplane.**



a. ASAS - R805.8,G703.8,B601.8nm; Prebuz, Krusne Hory, Czech Republic 1998



b. Bright (lime pit) ground calibration target

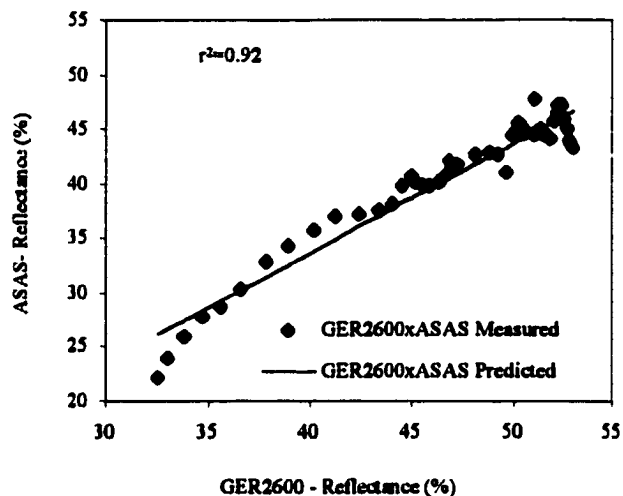


c. Dark (asphalt) ground calibration targets

**Figure 5.4: Ground calibration of the ASAS data.** For calibration of the ASAS data, ground spectra from bright (b) and dark (c) targets were collected.



a. GER2600 versus ASAS - Line Fit Plot



b. Comparison Between GER2600 and ASAS Spectra

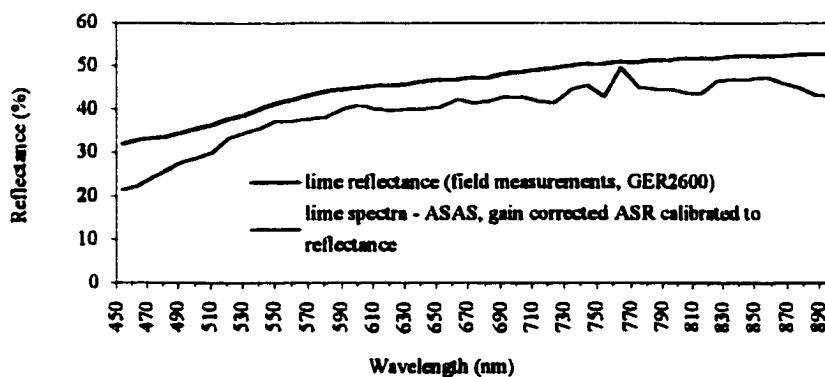


**Figure 5.5: Evaluation of ASAS radiometric calibration. ASAS reflectance spectra and GER2600 reflectance spectra for a bright (lime pit) ground calibration target were compared (ASR - at sensor radiance).**

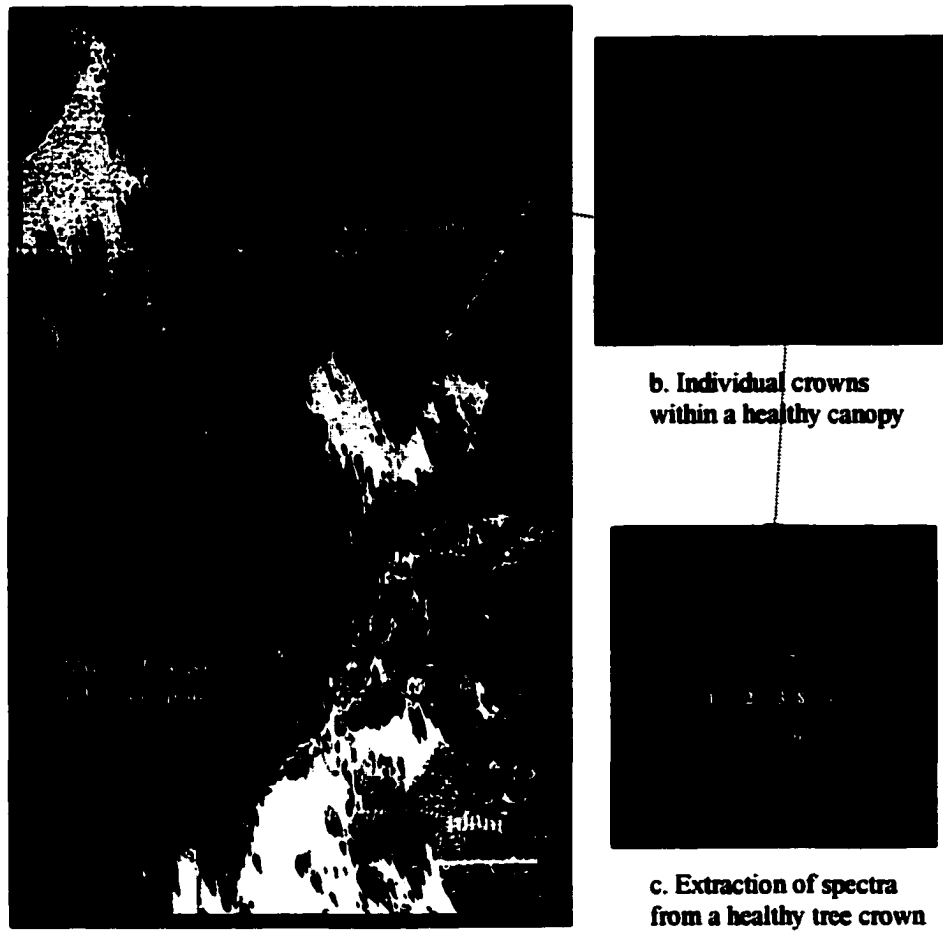


**Figure a:** ASAS image with location of DC0 and DC1 study sites.  
 Displayed are bands: R805.8, G703.8, B601.8

**Figure 5.6 (a-c):** Extraction of reflectance spectra for Norway spruce canopies from individual tree crowns (healthy DC0 and initial damage DC1). Spectra were extracted from the brightest pixel within a tree crown (Fig. 6 c. pixel 3 = 8 above). Note the presence of heavy shadowing within a tree crown and within the canopy of the healthy stand, possibly due to the time of day (10:30am, local time) of the overflight

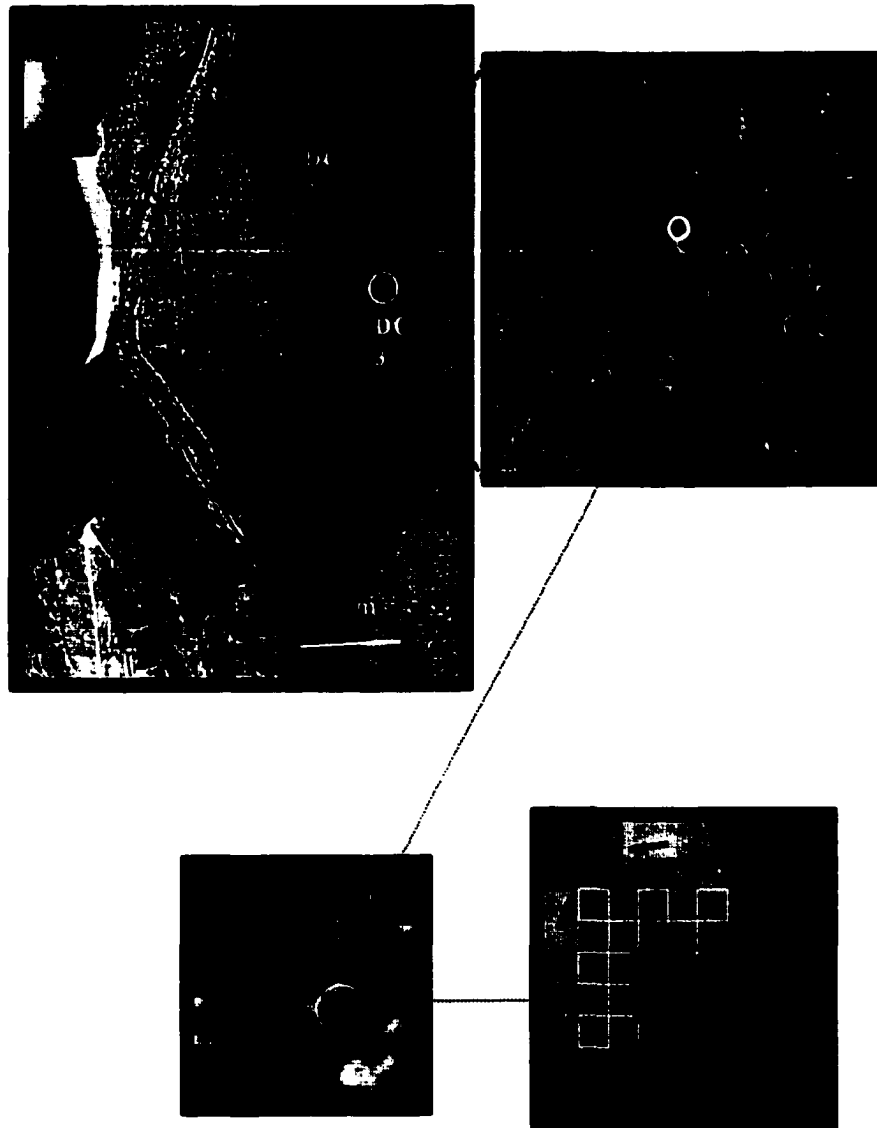


**Figure 5.6d: Extraction of reflectance spectra from individual tree crowns (intermediate DC2 and severe DC3 damage). For each stand, spectra were extracted for 20-30 crowns, from the brightest pixels within a tree crown (in blue above). Note the relatively lower level of shadow within the crowns of a heavily damaged stand, possibly due to the higher sun angle related to time of day (12:30pm, local time) of data acquisition.**

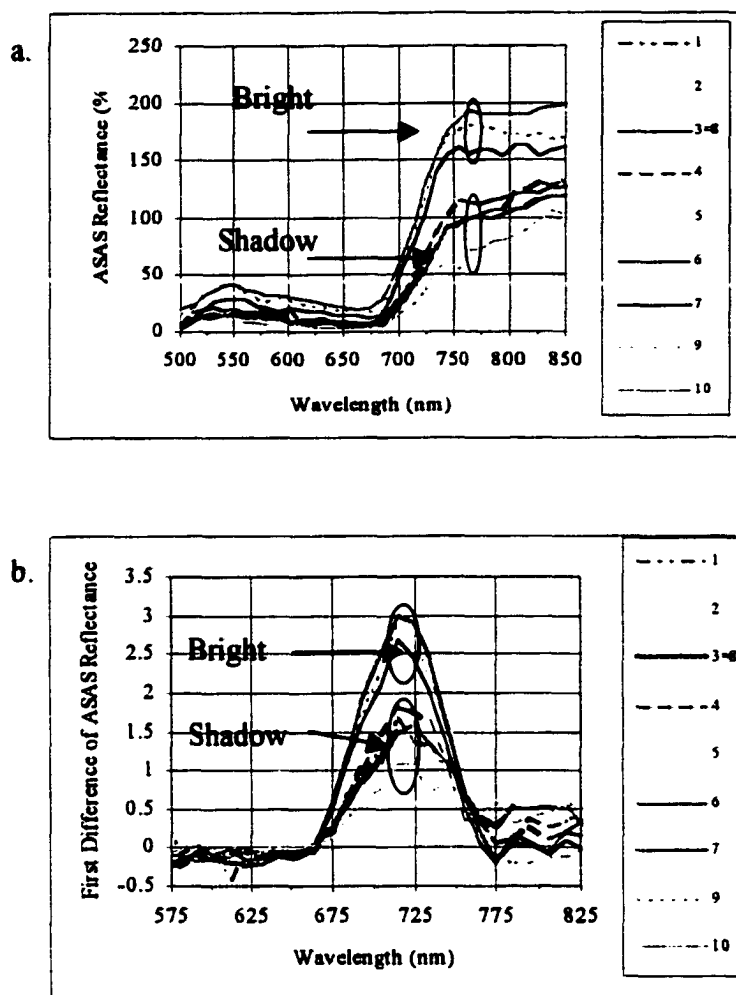


**Figure 5.7 (a,b): ASAS spectra extracted from individual tree crown: (a) Reflectance, (b) First derivative transformation of reflectance ( $\lambda'$ ). The number from 1-10 assigned to each spectral curve refer to the numbered pixels in Figure 5.6.c.**

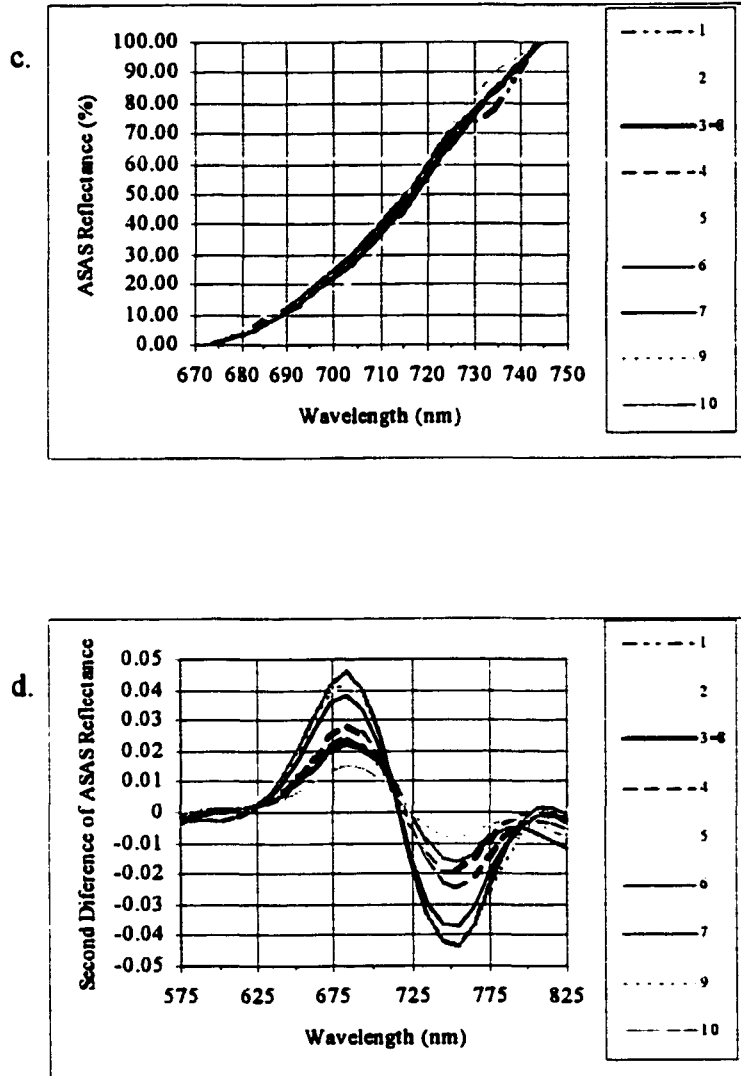


**Figure 5.7 (c,d): ASAS spectral extracted from tree crown: (c) Reflectance Normalized to 670-750nm region; (d) Second derivative of reflectance. The number from 1-10 assigned to each spectral curve refer to the numbered pixels in Figure 5.6.c.**

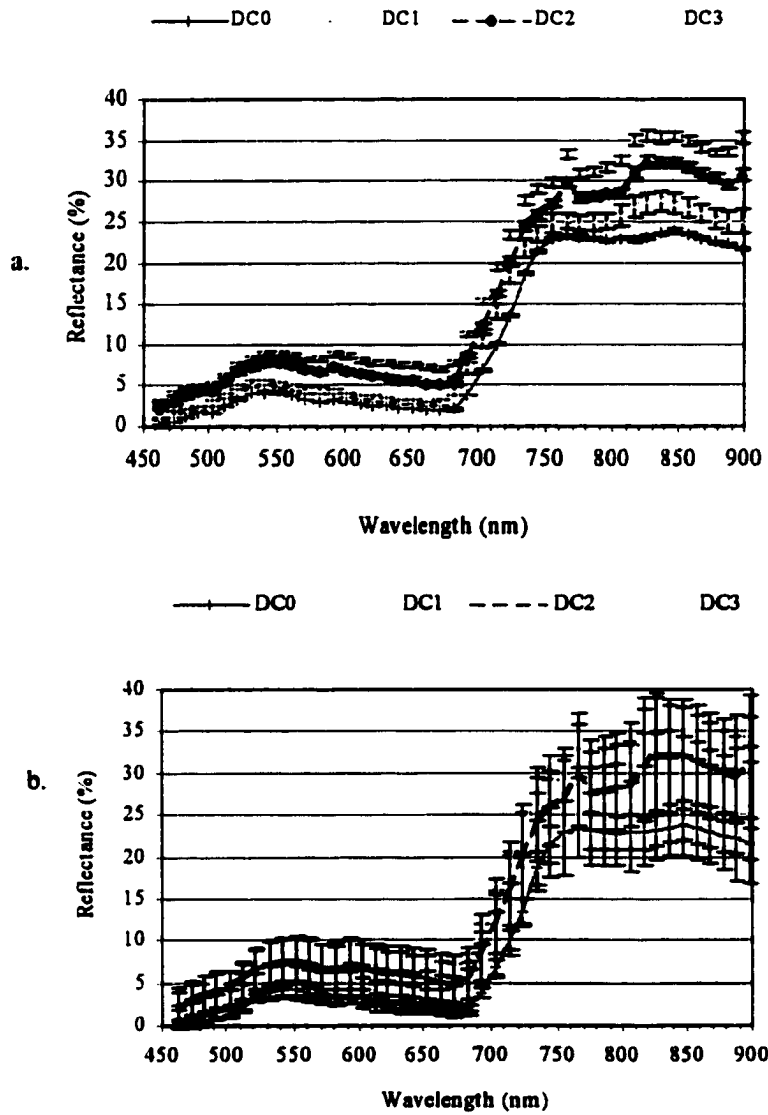


**Figure 5.8: Reflectance of Norway spruce forest canopy.** Least square means (ANOVA) and standard errors (a), and means and standard deviations (b) are plotted for ASAS data acquired for the full range of damage (DC0-DC3) across the Krusne hory, Czech Republic.

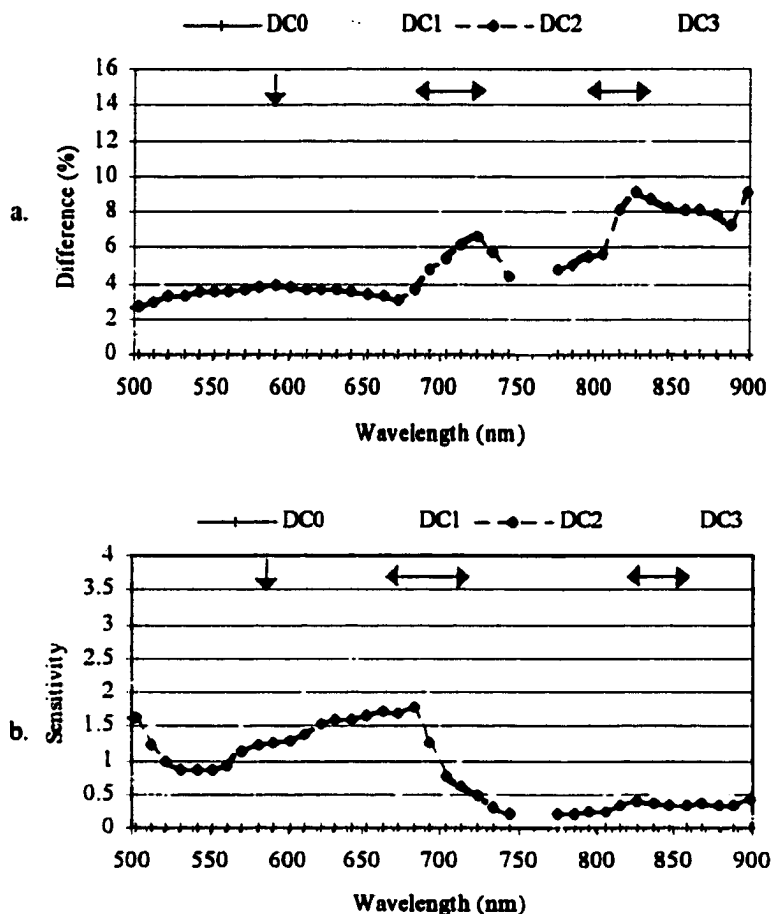


**Figure 5.9: Reflectance Sensitivity of Norway Spruce Forest Canopy.** Reflectance difference (a.) was computed by subtracting mean reflectance of healthy from that of each level of damaged canopy. Reflectance sensitivity to damage (b.), or the relative change in reflectance was computed by dividing the reflectance difference by mean reflectance of the healthy leaves. The red arrows indicate the regions for which differences were significant according to ANOVA ( $p < 0.05$ ) and Tukey-Kramer's test.

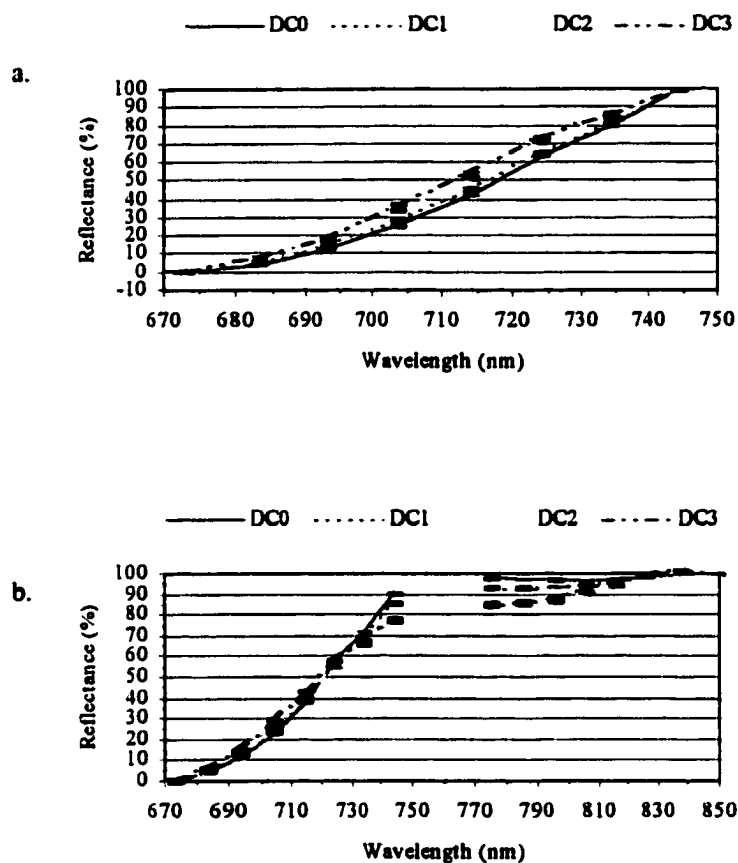


**Figure 5.10: Normalization of ASAS spectra.** To evaluate reflectance properties in the red edge region ASAS reflectance spectra were normalized to 670nm minimum and 744nm maximum (a) and to 670-850nm wavelengths (b).



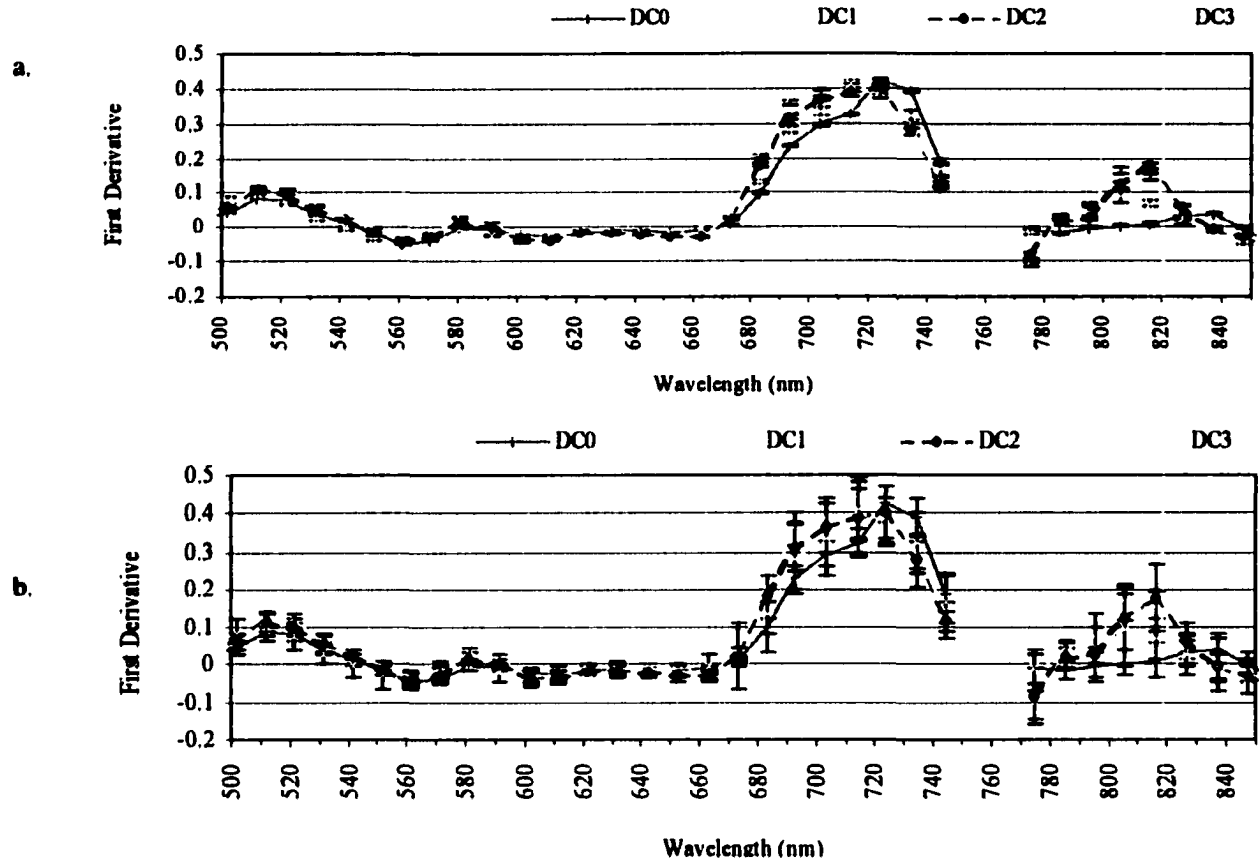


**Figure 5.11: First derivative transformation of ASAS reflectance spectra. Least square (LS) Means and standard errors (a) and LS Means and standard deviations(b) are plotted (ANOVA).**

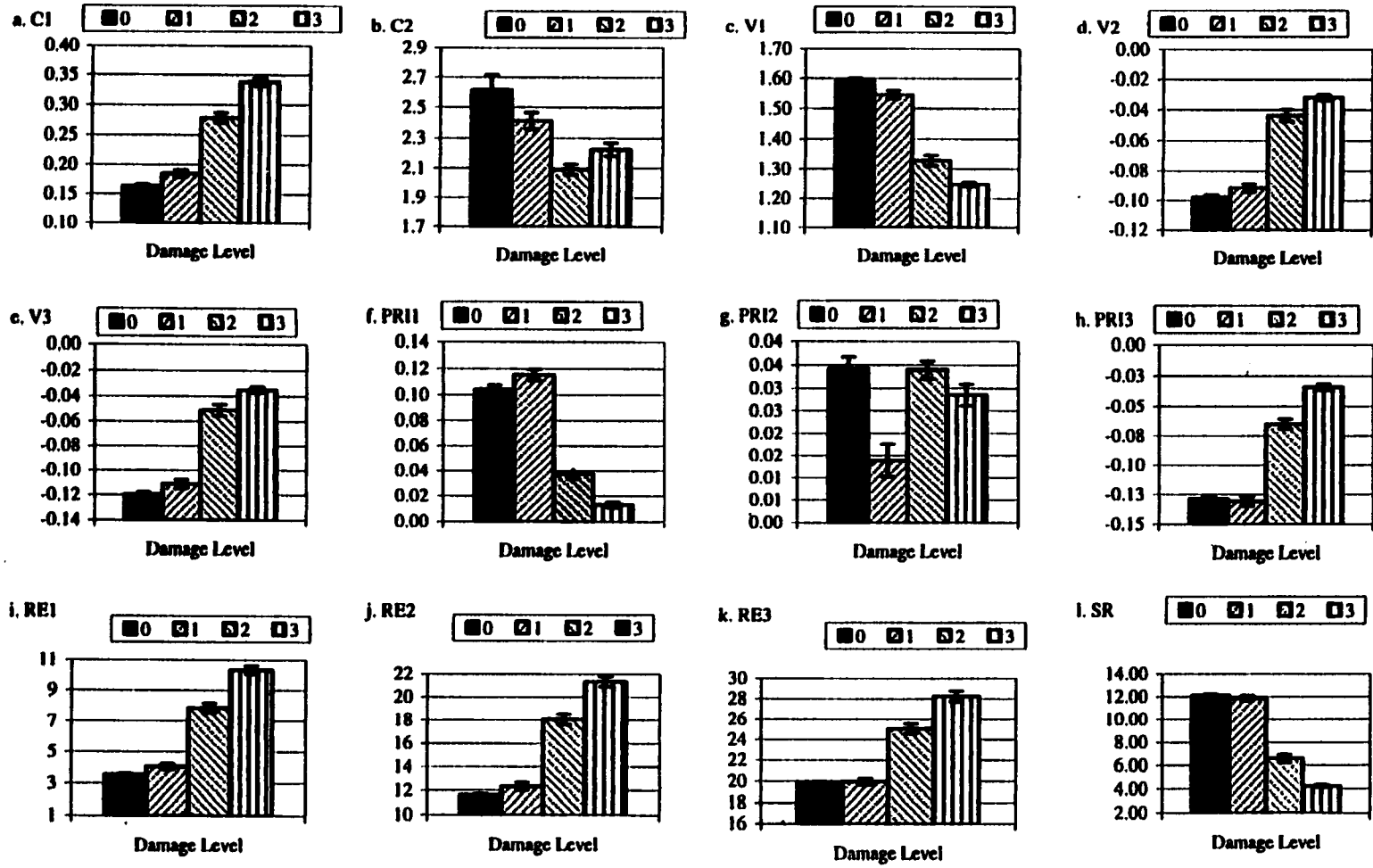


**Figure 5.12(a-l):** Optical indices computed using high spectral resolution ASAS data. To illustrate the significance of the differences occurring with damage levels, least square means and standard errors are plotted (ANOVA). The indices use bands from the visible, red edge and NIR regions.

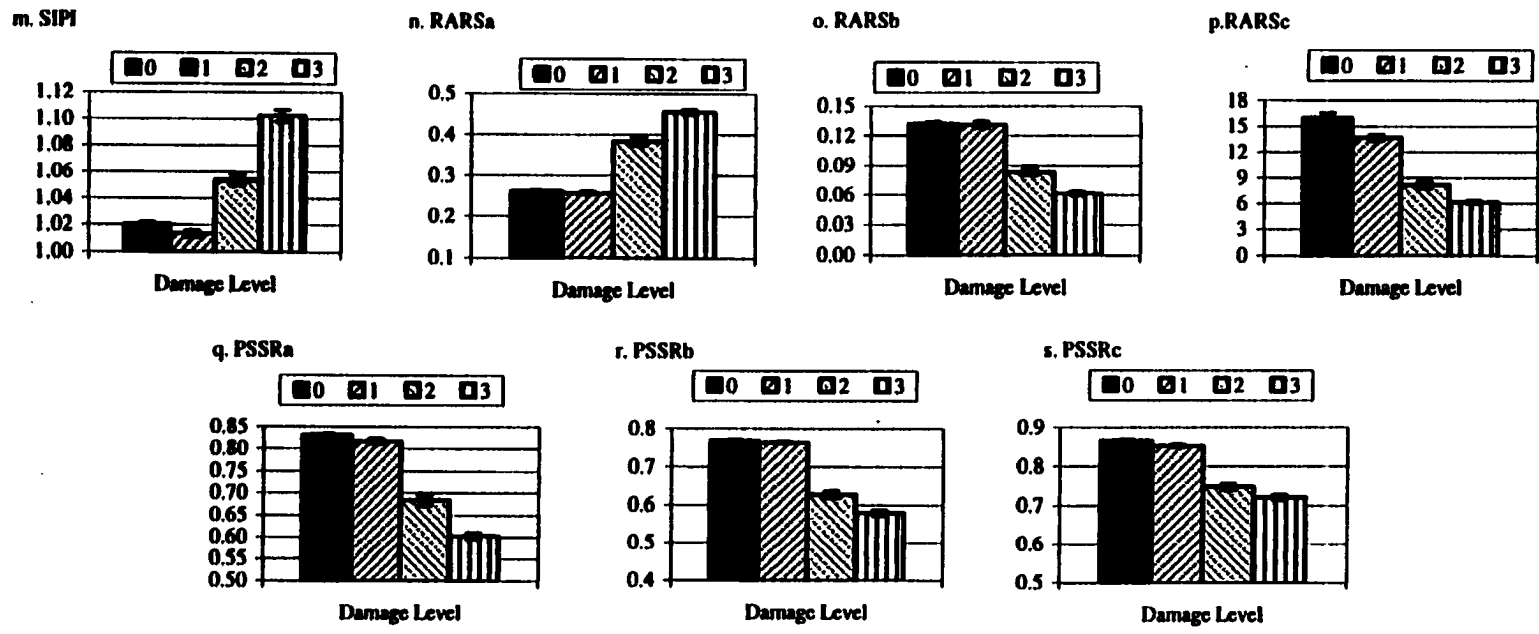


**Figure 5.12(m-s): Optical indices computed using high spectral resolution ASAS data. To illustrate the significance of the differences occurring with damage levels, least square means and standard errors are plotted (ANOVA). The indices use bands from the visible, red edge and NIR regions.**

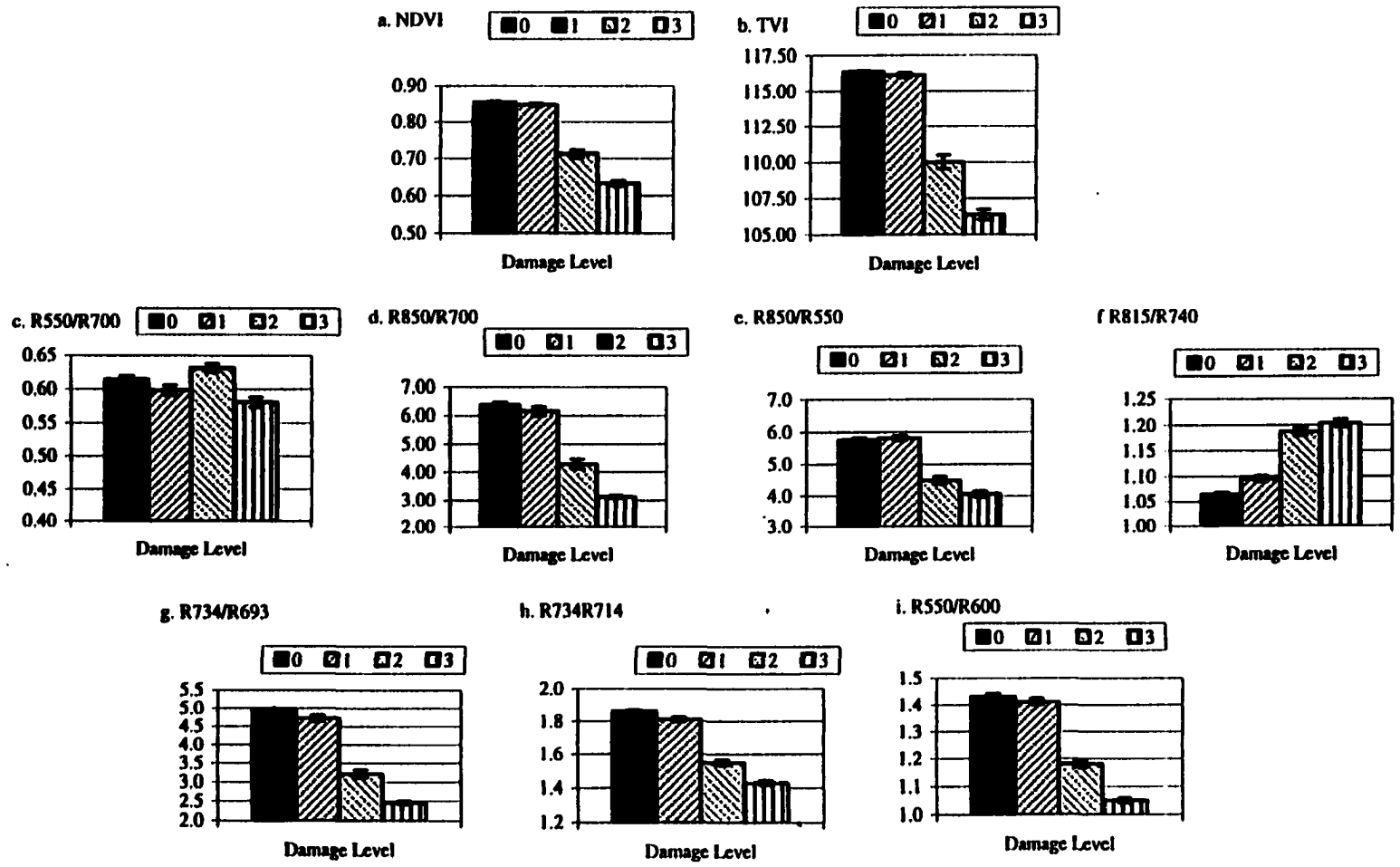


**Figure 5.13(a-1):** Landsat TM and Narrow-band ratios computed using high spectral resolution ASAS data. To illustrate the significance of the differences occurring with damage levels, least square means and standard errors are plotted (ANOVA).

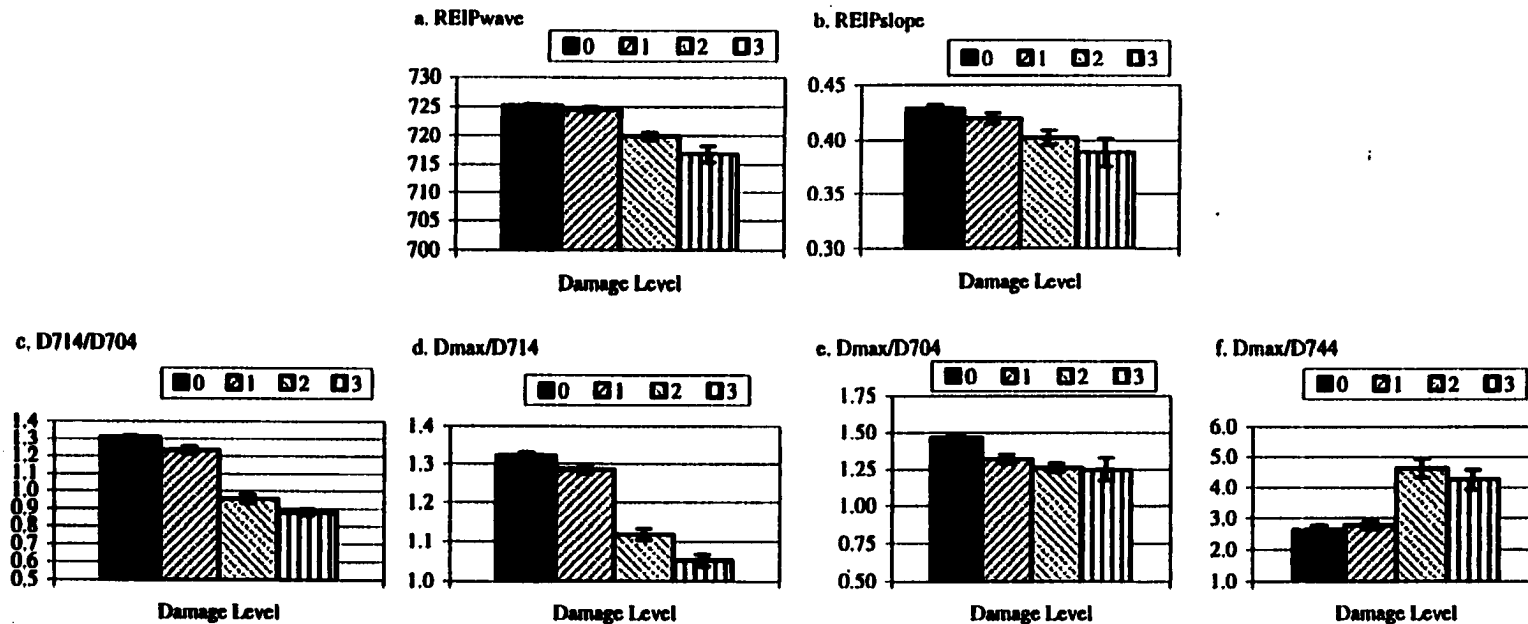


**Figure 5.14(a-f): Derivative indices computed using high spectral resolution ASAS data. To illustrate the significance of the differences occurring with damage levels least square means and standard errors are plotted (ANOVA).**

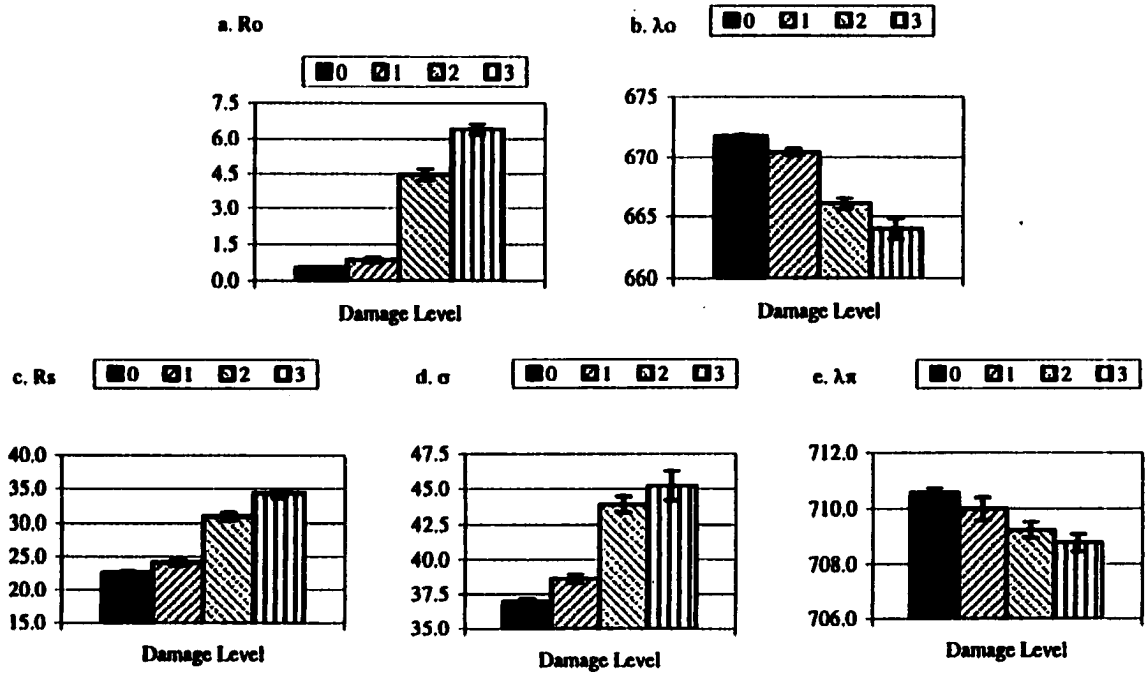


**Figure 5.15(a-e): Inverted Gaussian Model (IGM) parameters computed using high spectral resolution ASAS data. To illustrate the significance of the differences occurring with damage levels, least square means and standard errors are plotted (ANOVA).**

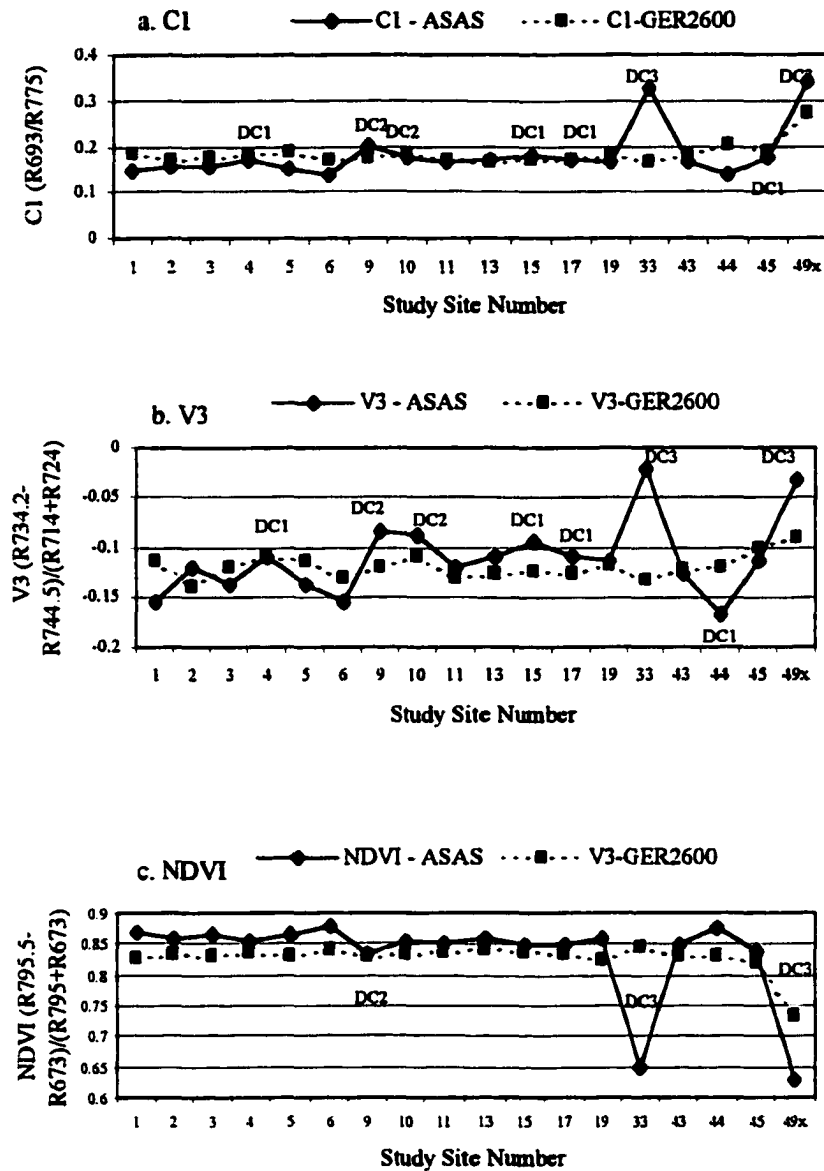


**Figure 5.16: Comparison of indices for the same study sites computed using canopy ASAS and foliar GER2600 reflectance data. (a) C1, (b) V3, (d) NDVI.**

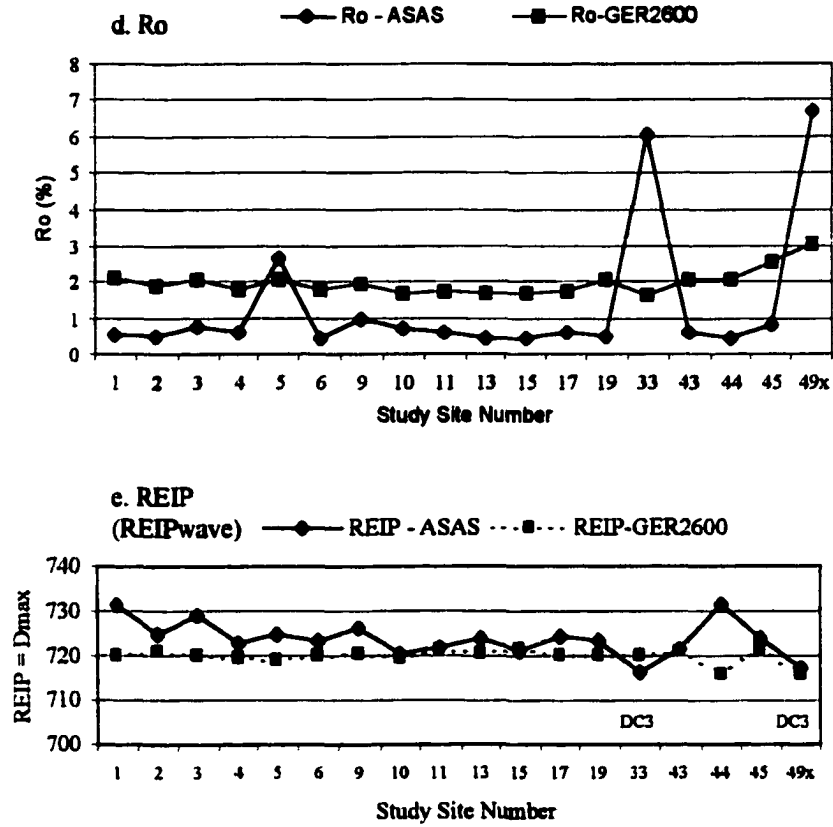


**Figure 5.16: Comparison of indices for the same sites computed using canopy ASAS and foliar GER2600 reflectance data. (d) Ro and (e) REIP (REIPwave).**



## **Chapter 6**

### **CONCLUSIONS**

The goal of the present study was to develop the means for forest stress detection and monitoring of initial forest damage levels. Since vegetation spectral properties are closely tied to foliar pigment and structural chemical content, remote sensing methods using spectral indicators sensitive to the changes in foliar bio-physiological properties characteristic of damage will provide the necessary tools for separation of initial levels of forest damage.

In chapter 3, we present a preliminary assessment of the potential of a video-based Narrow Band Imaging Camera (NBIC) system for forest damage detection at the foliar and canopy levels. The results from this work demonstrate that the NBIC allows for the visualization of the foliar spectral changes occurring with initial damage in Norway spruce. An inter-comparison of instruments (NBIC and GER2600) using foliar and canopy measurements demonstrated that band ratios performed better than individual bands. Band ratios computed from the 10nm narrow band reflectance provided similar results to that obtained by a GER2600 spectrometer.

Chapter 4 presents the results from an evaluation of Norway spruce foliar spectral and biochemical properties from a full range of damage conditions. Based on dendrochronological evaluation of tree yearly increment growth for the study sites, an apparent decline in forest growth began during 1965-67, affecting all spruce forests in the area of Krusne hory (including the healthy DC0). An apparent

recovery began during the mid 1980s, when a trend of increasing yearly tree increment growth was observed for all damage classes (including DC3). This trend suggests that with the current study we are possibly addressing tree physiology in a stage of forest recovery, or the long-term effect of the decline after the main stress factors have been reduced.

The analysis of foliar pigments, structural chemical constituents and field spectrometer data presented in chapter 4 demonstrate that high spectral resolution foliar measurements provide a remote sensing tool for forest health evaluation by separating foliage from healthy forests from forests with initial damage. Based on Norway spruce foliar measurements, the 680-740nm spectral region demonstrates the highest potential for separation of initial damage level. Among the spectral indices from the first-, second and third-year needles, third-year needle reflectance indices demonstrated the highest potential for separation of the damage levels. Based on foliar field reflectance measurements for third-year needles, derivative spectral indices from the red edge region were most strongly correlated to damage level (V4, REIPslope and Dmax/D704), followed by the indices ratioing a highly sensitive to the decline band (around 700nm, or 570nm; PRI1, PRI3, GM2) to insensitive to damage bands (e. g. 750nm, 530nm), and the Inverted Gaussian Parameter Ro. The first six indices were strongly correlated to damage class, while the Ro index exhibited the highest relative change (sensitivity) from healthy to initial damage level among all indices.

Analysis of chlorophyll and carotenoid pigment data indicated relatively stable pigment levels across the damage gradient. This finding corresponds with the apparent recovery in forest growth observed since the mid 1980s in the Krusne hory, and suggests

that pigment levels appear to be less indicative of the long-term effects of the pollution decline and more responsive to the short-term changes in the environment.

This study established a strong correlation to damage for the foliar chemical constituents (lignin, cellulose, polar and non-polar compounds). The more damaged needles exhibited a significant increase in foliar polar compounds (tannins, sugars and starch) and a lower needle lignification and relative cellulose levels. Foliar structural chemical compounds (e.g. polar and lignin) appear to be effective indicators of the long-term environmental conditions. The highest correlation revealed was between damage level and polar compounds, suggesting a high potential for use of these constituents as bio-indicators of stress. Since cellulose and lignin are cellular structural components and unlikely to change in response to an environmental change, the polar constituents are thus more valuable as stress indicators.

The strong correlation between the high spectral resolution indices sensitive to damage and the sensitive foliar chemical constituents (e.g. polar constituents) provides the link between foliar physiological properties and the reflectance indices, and forms the basis for use of the indices as bioindicators of forest decline.

Chapter 5 presents analysis of ASAS data conducted to assess the potential of airborne high spectral resolution data for separation of initial damage levels. Canopy hyperspectral data were able to separate healthy from initially damaged canopies, and therefore provide improved damage separation capabilities as compared to multispectral, narrow and broad band systems. The 673-724nm spectral region was identified as having maximum sensitivity to initial damage. This region corresponds with the spectral region most sensitive to damage as identified on the basis of the foliar reflectance measurements

made in the laboratory. Twelve indices were identified as useful for separation of damage classes, from which six – four optical indices, one derivative index (incorporating reflectance from the red edge region) and one of the normalized red edge bands, are presenting the most potential for use as bio-indicators of the initial level of damage.

Finally, by a direct comparison between ASAS canopy spectral measurements and foliar (field/laboratory) spectral measurements, this study demonstrates that using hyperspectral reflectance ratios, canopy reflectance measurements can produce reflectance spectra that resemble leaf level reflectance measurements closely. Five indices were identified as providing similar results, from which two (reflectance ratio of  $R_{693}/R_{775}$  and the position of the reflectance minimum in the chlorophyll well ( $R_o$ ), as computed by the Inverted Gaussian Model) have shown a high potential for separation of the initial forest damage levels.

## REFERENCES

- Aber, J.D., Driscoll C., Federer A., Lathrop R., Lovett G., Melillo J., Steudler P. and Vogelmann, J. 1993. A strategy for the regional analysis of the effects of physiological and chemical climate change on biogeochemical cycles in northeastern (U.S.) forests. *Ecol. Modeling*, 67, 37-46.
- Aber, J.D., Reich P.B. and Goulden, M.L. 1986. Extrapolating leaf CO<sub>2</sub> exchange to the canopy: a generalized model of forest photosynthesis compared with measurements by eddy correlation. *Oecologia*, 106:257-265.
- Abrahamsen, Stuanes, A. and Tveite, B. 1993. Long-term experiments with acid rain in Norwegian forest ecosystems. *Ecological Studies 104*. Springer-Verlag, New York.
- ACCP, 1994. Accelerated Canopy Chemistry Program: Final Report Presented to EOS-IWG, 19 October 1994.
- Alscher, R. and Cumming, J. 1990. Stress responses in plants: Adaptation and acclimation mechanisms. In: *Plant Biology*, 12. John Wiley and Sons, Inc.
- Ardo, J, Lambert N., Henzlik V. and Rock, B.N. 1997. Satellite-based estimations of coniferous forest cover changes: Krusne hory, Czech Republic 1972-1989. *Ambio*, 26, 3:158-166.
- Blackburn, G.A. 1998. Quantifying chlorophylls and carotenoids at leaf and canopy scales: an evaluation of some hyperspectral approaches. *Remote Sens. Environ.*, 66:273-285.
- Bolster, K.L., Martin M.E. and Aber, J.D. 1996. Determination of carbon fraction and nitrogen concentration in tree foliage by near infrared reflectance: a comparison of statistical methods. *Can. J. For. Res.*, 26:590-600.
- Bonham-Carter, G.F. 1988. Numerical procedures and computer program for fitting and inverted Gaussian model to vegetation reflectance data. *Computer & Geosciences*, 14:339-356.
- Booker, F.L., Anttonen S. and Heagle, A.S. 1996. Catechin, proanthocyanidin and lignin contents of loblolly pine (*Pinus taeda*) needles after chronic exposure to ozone. *New Phytologist*, 132:483-492.

- Boudet, A., Lapiere C., and Grima-Pettenati, J. 1995. Biochemistry and molecular biology of lignification. *New Phytologist*, 129: 203-236.
- Buil, K. 1991. CCD Astronomy. Willmann-Bell, 321.
- Buschmann, C. and Nagel, E. 1993. In vivo spectroscopy and internal optics of leaves as basis for remote sensing of vegetation. *Int. J. Remote Sensing*, 14: 711-722
- Carter, G.A. 1993. Responses of leaf spectral reflectance to plant stress. *Am. J. Bot.*, 80: 239-243.
- Carter, G.A. 1994. Ratios of leaf reflectance in narrow wavebands as indicators of plant stress, *Int. J. Remote Sensing*, 15, 3:697-703.
- Carter, G.A., Dell T.R. and Cibula, W.G. 1996. Spectral reflectance characteristics and digital imagery of a pine needle blight in the southern U.S. *Can. J. For. Res.*, 26:402-407.
- Carter, G.A. and Miller, R. L. 1994. Early detection of plant stress by digital imaging within narrow stress-sensitive wavebands. *Remote Sens. Environ.*, 50: 295-302.
- Carter, G.A., Rebeck J. and Percy, K. 1995. Leaf optical properties in *Liriodendron tulipifera* and *Pinus strobus* as influenced by increased atmospheric ozone and carbon dioxide. *Can. J. For. Res.*, 25: 4-7-412.
- Chappelle, E. W., Kim M. S. and McMurtrey, J. E. 1992. Ratio analysis of reflectance spectra (RARS): an algorithm for the remote estimation of the concentrations of chlorophyll a, chlorophyll b, and carotenoids in soybean leaves. *Remote Sens. Environ.*, 39: 239-247.
- Cibula, W. G. and Carter, G. A. 1992. Identification of a far-red reflectance response to ectomycorrhizae in slash pine. *Int. J. Remote Sens.*, 13, 925-932.
- Cibula, W. and Nyquist, M. 1987. Use of topographic and climatological models in a geographical data base to improve Landsat MSS classification for Olympic National park. *Photogram. Engin. and Remote Sens.*, 53, (1), 925-932.
- Ciolkosz, A. and Zawila-Niedzwiecki, T. 1990. Remotely sensed data and limitation of forest productivity in Poland. *Nature and Resources*, 26:41-44.
- Cook, E. and Kairiukstis, L. 1992. *Methods of dendrochronology*. Kluwer Academic Publishers, the Netherlands, 394.
- Curran, P.J. 1989. Remote sensing of foliar chemistry. *Remote Sens. Environ.*, 30:271-278.

- Curran, P. J., Dungan J. L. and Gholz, H.L. 1990. Exploring the relationship between reflectance red edge and chlorophyll content in slash pine. *Tree Physiology*, 7: 33-48.
- Dabney, P.W., Kovalick W. M., Bur M.J., Russell C.A., Tierney M.R. and Irons, J.R. Inter-comparison of sensor calibration techniques for the advanced solid-state array spectroradiometer (ASAS) as a performance validation tool. *In press*.
- Datt, B. 1998. Remote sensing of chlorophyll a, chlorophyll b, chlorophyll a+b, and total carotenoid content in eucalyptus leaves. *Remote Sens. Environ.*, 66: 111-121.
- Delkov, N. 1984. *Dendrology*. Zemizdat, Sofia, 305.
- Demetrides-Shah T., Steven M. and Clark, J. 1990. High resolution derivative spectra in remote sensing. *Remote Sens. Environ.*, 33, 55-64.
- Entcheva, P., Rock B.N., Lauten G. and Cibula, W. 1996. Remote sensing assessment of forest health in the Bohemian forests of central Europe. In: *Global Networks for Environmental Information, ECO-INFORMA '96*, Environmental Research Institute of Michigan, Ann Arbor, MI, 11:785-790.
- Everitt J., Lulla K., Escobar D. and Richardson, A. 1990. Aerospace Video Imaging Systems for Rangeland Management. *Photogram. Engin. and Remote Sens.*, 56, 3.
- Ferry, J. and Ward, H. 1959. *Fundamentals of plant physiology*, The MacMillan Company, New York, 288.
- Gates, D. M. 1980. *Biophysical ecology*. Springer-Verlag, New York, NY.
- Gates, D. M., Tibbals E. C. and Kreith, F. 1965. Radiation and convection for Ponderosa pine. *Am. J. Bot.* 52: 66-71.
- Gitelson, A.A and Merzlyak, M.N. 1994. Spectral reflectance changes associated with autumn senescence of *Aesculus hippocastanum* L. and *Acer platanoides* L. leaves. Spectral features and relation to chlorophyll estimation. *J. Plant Physiol.*, 143:286-292.
- Gruber, F. 1994. Morphology of coniferous trees: Possible effects of soil acidification on the morphology of Norway spruce and silver fir. In: *Effects of acid rain on forest processes*. Wiley-Liss, Inc., New York, 720.
- Henzlik, V. 1997. Personal Conversation of B.N. Rock and P.K. Entcheva.
- Hildebrandt, G. and Gross, C. editors 1992. *Manual for remote sensing forest health status assessment*. Walpot S.A. Publishers, Belgium, 350.

- Horler, D.N.H., Dockray M., Barber J., and Barringer, A.R. 1983. Red edge measurements for remotely sensing plant chlorophyll content. *Adv. Space Research*, 3: 273-277.
- Hoshizaki, T., Rock B.N. and Wong, S.K.S. 1988. Pigment analysis and spectral assessment of spruce trees undergoing forest decline in the United States and Germany. *GeoJournal*, 17: 173-178.
- Hosley, N. 1936. *Norway spruce in the north-eastern United States*. Harvard Forest, Petesham, MA, Bulletin 19, 60.
- Hunt, E. R. and Rock, B. N. 1989. "Detection of changes in leaf water content using near- and middle-infrared reflectance." *Remote Sens. Environ.*, 30: 43-54.
- Hyink, D. and Zedaker, S. 1987. Stand dynamics and the evaluation of forest decline. *Tree Physiology*, 3, 19-26.
- Irons, J.R., Ranson K.J., Williams D.L., Irish R. R., and Huegel, F. G. 1991. An off-nadir-pointing imaging spectroradiometer for terrestrial ecosystem studies. *IEEE Trans. Geosci. Remote Sens.*, 29, 66-74.
- Jensen, J. 1996. *Introductory digital image processing*. Prentice-Hall, Inc, New Jersey, 307.
- Kimes, D.S., Newcomb W. W., Nelson R.F., and Schutt, J.B. 1986. Directional reflectance distributions of a hardwood and pine forest canopy. *IEEE Transactions on Geoscience and Remote Sensing*, GE-24: 281 - 293.
- Klusterska, I. 1991. Bohemian problem bared. *Acid News*, 1:1-4.
- Klimont, Z., Amann M., Cofala J., Gyarfás K., Laassen G., and Scopp, W. 1993. *Emission of air pollutants in the region of Central Europe Initiative*. IIASA, Laxenburg, Austria.
- Kovalick, W.M., Graham D.W and Burr, M.C. 1994. Data processing and calibration of the Advanced Solid-state Array Spectrometer. *Proceedings of the IEEE Trans. Geosci. Remote Sensing Symposium*, 3: 1652-54.
- Kozłowski ,T. and Pallardy, S. 1997. *Physiology of woody plants*. Academic Press, San Diego.
- Krahl-Urban, B., Papke H., Peters K. and Schimansky, C. 1988. *Forest decline: Cause-effect research in the United States of North America and Federal Republic of Germany*. By: Assessment Group for Biology, Ecology and Energy of the Julich Nuclear Research Center, for US EPA and German Ministry of Research and Technology.



- Kriebel, K. T. 1978. Measured spectral bidirectional reflectance properties of for vegetation surfaces. *Applied Optics*, 17, 2:253-259.
- Kubelka, L., Krasek A., Ybar V., Baldalik V. and Slodicak, M. 1993. *Forest regeneration in the heavily polluted NE Krusne hory Mountains*. Czech Ministry of Agriculture, Prague.
- Kubikova, J. 1991. Forest dieback in Czechoslovakia. *Vegetatio*, 93:101-108.
- Kupiec, J.A. and Curran, P. J. 1994. Remote sensing of foliar chemistry: Moving from the leaf to the canopy. in: ACCP Report 32, 16.
- Lambert, N.J. 1993. Spectral characterization and classification of forest damage in Norway spruce stands in the Czech Republic using Landsat Thematic Mapper data. Masters Thesis, University of New Hampshire, Durham, NH, U.S.A.
- Lambert, N.J., Ardo J., Rock B.N. and Vogelmann, J.E. 1995. Spectral characterization and regression based classification of forest damage in Norway spruce stands in the Czech Republic using Landsat Thematic Mapper data. *Int. J. Remote Sens.* 16: 1261-1287.
- Lange, O., Herber U., Schulze D. and Ziegler, H. 1989. Atmospheric pollutants and plant metabolism. In: *Forest decline and air pollution: A study of spruce (Picea abies) on acid soils*. Ecological studies 77. Springer-Verlag, New York.
- Larcher, W. 1995. *Physiological plant ecology*. Third edition. Springer-Verlag, New York, 506.
- Lee, T. 1995. Physiological ecology. *Personal communication*.
- Lesproject, 1988. *Forestry assessments*. 250 01 Brandys n/L., Zamek, Czech Republic, 507.
- Lichtenthaler, H.K. 1988. *Appications of chlorophyll fluorescence in photosynthesis research, stress physiology, hydrology and remote sensing*. Kluwer Academic Publishers, Dordrecht, The Netherlands, 366.
- Lillesand, T. and Kiefer, R. 1994. *Remote sensing and image interpretation*. Wiley & Sons, New York, 750.
- Lowe, J., Oswald B., Coleman T., Tadese W., Everitt J., Escobar D. and Davis, M. 1995. Comparison of Conventional Grown Sampling and Remote Sensing Techniques for Mapping Forest Vegetation. In: *Proceeding of ACSM/ASPRS Annual Convention & Exposition on Remote sensing and photogrammetry*, 31.

- Lucas, N.S., Curran P.J., Plummer S.E. and Danson, F.M. 2000. Estimating the stem carbon production of a coniferous forest using an ecosystem model driven by the remotely sensed red edge. *Int. J. Remote Sens.*, 21, 4:619-631.
- Materna, J. 1989. Air pollution and forestry in Czechoslovakia. *Environ. Monit. Assess.* 12, 227-235.
- Martin, M.E. and Aber, J.D. 1997. High Spectral Resolution Remote Sensing of Forest Canopy Lignin, Nitrogen, and Ecosystem Processes. *Ecological Applications*, 7(2), 431-443.
- Martin, M. 1994. Measurements of foliar chemistry using laboratory and airborne high spectral resolution visible and infrared data. PhD Thesis, University of New Hampshire, Durham.
- McNulty, S.G., Aber J.D., McLellan T.M. and Katt, S.M. 1991. Nitrogen cycling in high elevation forests in the northeastern U.S. in relation to nitrogen deposition. *Ambio*, 19:38-40.
- Merzlyak, M.N., Gitelson A.A. and Zur, Y. 1999. Remote sensing detection of leaf senescence. Presented at the 21<sup>st</sup> Canadian Symposium on Remote sensing, Ottawa, Ontario, Canada 21-24 June.
- Miller, J. R., Hare E. W. and Wu, J. 1990. Quantitative characterisation of the vegetation red edge reflectance. 1: An Inverted-Gaussian reflectance model. *Int. J. Remote Sens.*, 11(10): 1755-1774.
- Miller, J.R., Freemantle J.R., Belanger M.J., Elvidge C.D., and Boyer, M.G. 1993. Potential for Determination of leaf chlorophyll content using AVIRIS. *Proceedings of the 1993 Airborne Visible/Infrared Imaging Spectrometer (AVIRIS) Workshop*. Jet Propulsion Laboratory, Pasadena, CA, 72-77.
- Miller, R., Carter G., Sheehy J., Rock B., Entcheva P. and Albrechtova, J. 1999. Monitoring initial forest recovery in the Krusne hory, Czech Republic, using ground and airborne multispectral digital cameras. Presented at the Fourth International Airborne Remote Sensing Conference and Exhibition/21 Canadian Symposium on Remote Sensing, Ottawa, Ontario, Canada, June.
- Monsteller, F. and Tukey, J.W. 1977. *Data analysis and regression*. Addison-Wesley Publishing Company, Inc. Reading, MA.
- Mooney H., Winner W. and Pell, E. 1991. *Response of plants to multiple stresses*. Academic Press, San Diego.
- Moss, D.M. and Rock, B.N. 1991. Analysis of Red Edge Spectral Characteristics and total Chlorophyll Values for Red Spruce (*Picea rubens*) Branch Segments From Mt.

- Moosilauke, NH, USA. In *Proceedings of the Annual International Geoscience and Remote Sensing Symposium (IGRASS'91)*, Helsinki, Finland, June 3-6.
- Moss, D.M., Rock B.N, Bogle A.L. and Bilkova, J. 1998. Anatomical evidence of the development of damage symptoms across a growing season in needles of red spruce from central New Hampshire. *Environmental Experimental Botany*, 39:247-262.
- Munden, R., Curran P. J. and Catt, J.A. 1994. The relationship between red edge and chlorophyll concentration in the Broadbalk winter wheat experiment at Rothamsted. *Int. J. Remote Sensing*, 15: 705-709.
- NAPAP, 1990. *State of science and technology*. National Acidic Precipitation Assessment Program, 1990. Integrated Report; 3; 556.
- Neale, C., Vest G. and O'Neil, M. 1995. Monitoring Stream Bank Erosion Using Multispectral Video Imagery in GIS. In: *Proceeding of ACSM/ASPRS Annual Convention & Exposition on Remote Sensing and Photogrammetry*, 210-223.
- Newman, S.D., Soulia M.E., Aber J.D., Dewey B. and Ricca, A. 1994. Analyses of forest foliage: Laboratory procedures for proximate carbon fractionation and nitrogen determination. *J. Near Infrared Spectrosc.*, 2:5-14
- Oven, P. and Torelli, N. 1994. Wound response to bark in healthy and declining silver firs (*Abies alba*). *IAWA Journal* 15: 407-415.
- Pickup, G., Chwings V. and Pearce, A. 1995. Procedures for correcting high resolution airborne video imagery. *Int. J. Remote Sensing*, 16:1647-1662.
- Randson, K. J., Irons J. R. and Daughtry, C. S. 1991. Surface Albedo from Bidirectional Reflectance. *Remote Sens. Environ.*, 35:201-211.
- Rock, B.N. and Ardo, J. 1993. The use of satellite remote sensing for the study of forest decline in the United States and Europe. In *Optics for the Protection of Man and Environment Against Natural and Technological Disasters*, Elsevier Science, B.V., 49-58.
- Rock, B.N., Defeo N. and Vogelmann, J.E. 1987. Final report vegetation survey pilot study: detection and quantification of forest decline damage using remote sensing techniques. *JPL Document D-4669*, Jet Propulsion Laboratory, Pasadena, CA.
- Rock, B.N., Greczynski J., Moss D.M. and Zawila-Niedzwiecki, T. 1992. Spectral characterization of forest decline damage in branch segments of Norway spruce (*Picea abies*) in the Sudety Mountains of Poland. *Proc. of Am. Soc. Photogrammetry and Remote Sens.*, 1:271-279.

- Rock, B. N., Hoshizaki T. and Miller, J. R. 1988. Comparison of *in situ* and airborne spectral measurements of the blue shift associated with forest decline. *Remote Sens. Environ.*, 24:109-127.
- Rock, B.N., Lambert N., Ardo J, and Henzlik, V. 1994. The use of satellite remote sensing for forest monitoring. *Optics in Life Sciences (OWLS III): Optical Methods in Biomedical and Environmental Sciences*. Edited: Ohzu, H. and Komatsu, S., Elsevier Science Publishers, B.V., 261-264.
- Rock, B.N., Skole D. L. and Choudhury, B.J. 1993. Monitoring vegetation change using satellite data. In: *Vegetation Dynamics and Global Change*. A.M. Solomon and H.H. Shugart editors. Chapman & Hall, New York and London, 153-167.
- Rock, B.N., Vogelmann J.E., Williams D.L., Vogelmann A.F., and Hoshizaki, T. 1986. Remote detection of forest damage. *BioScience*, 36:439-445.
- Russell, C.A., J. R. Irons and Dabney, P. 1997. Bidirectional reflectance of selected BOREAS sites from multiangle airborne data. *J. Geophys Res.*, 102, D24: 29.505-29.516.
- Russell, C.A., Walthall C.L., Irons J.R. and Brown de Colstoun, E.C. 1995. Comparison of airborne and surface spectral bidirectional reflectance factors, spectral hemispherical reflectance and spectral vegetation indices. *J. Geophys. Res.* 100 (012): 25, 509-25, 522.
- Schulze, E., Oren R. and Lange, O. 1989. Processes leading to forest decline: A synthesis. In: *Forest decline and air pollution: A study of spruce (Picea abies) on acid soils. Ecological studies 77*. Springer-Verlag, New York, 475.
- Smith, H. 1990. *Air pollution and forests: Interactions between air contaminants and forest ecosystems*. Springer-Verlag, New York, 580.
- Solcova, B. (1999). Detekce poskození jehlic smrku ztepilého (*Picea abies* (L.) Karst.) v Krusných horách a na Sumave: analýza fotosyntetických pigmentů a anatomická analýza. [in Czech] Detection of damage of Norway spruce (*Picea abies* (L.) Karst.) needles: analysis of photosynthetic pigments and anatomical analysis. M. S. Thesis, Department of Plant Physiology, Faculty of Science, Charles University, Prague.
- Soukupova, J., Rock B.N. and Albrechtova, J. 2000. Spectral characteristics of lignin and soluble phenolics in the near infrared – a comparative study. *In press*.
- SPSS Inc., 1997. SYSTAT 7.0: *Statistics*, 751.
- Tanre, D., Deuze J. L., Herman M., Santer R. and Vermote, E. 1990. Second simulation of the satellite signal in the solar spectrum – 6S code. In: *Proceedings of the 10<sup>th</sup>*

*annual International Geoscience and Remote Sensing Symposium, I. IEEE Int. Geosci. And Remote Sens., New York, 187.*

- Vogelmann, A.F. and Rock, B.N. 1988. Anatomy of red spruce needles from forest decline sites in Vermont. *Environmental and Experimental Botany*, 28:19-26.
- Vogelmann, J.E. and Rock, B.N. 1986. Assessing forest decline in coniferous forests of Vermont using NS-001 Thematic Mapper Simulator data. *Int. Journ. Remote Sens.*, 10:1303-1321.
- Vogelmann, J.E., Rock B.N. and Moss, D.M. 1993. Red edge spectral measurements in sugar maple leaves. *Int. Journ. Remote Sens.*, 14:1563-1575.
- Waring, R.H. and Running, S.W. 1998. *Forest Ecosystems: Analysis at Multiple Scales*. Academic Press, Harcourt Brace & Company, San Diego: Academic Press, California, 370.
- Wellburn, A.R. 1994. The spectral determination of chlorophyll *a* and *b*, as well as total carotenoids, using various solvents with spectrophotometers of different resolution. *Journal of Plant Physiology*, 144:307-313.
- Wessman, C., Nel E. and Shapiro, A. 1994. Forest canopy chemistry as determined by Curve Fitting of Endmember Spectra. ACCP, 1994.
- Williams, P. and Norris, K. 1987. *Near-infrared technology in the agricultural and food industries*. American Association of Cereal Chemists, St. Paul, Minnesota, 330.
- Wood E., Tappan G. and Jacobs, D. 1995. Monitoring Senegal's natural resources using airborne videography. In: *Proceeding of ACSM/ASPRS Annual Convention & Exposition on Remote sensing and Photogrammetry*, 315-321.
- Zar, J. 1996. *Biostatistical Analysis*. Prentice Hall, Inc. Publishing, New Jersey, 750.
- Zarco-Tejada, P.J., Miller J.R., Mohammed G.H., Noland T.L. and Sampson, P.H. 1999. Optical indices as bio-indicators of forest condition from hyperspectral CASI data. *Presented at the 19<sup>th</sup> symposium of the European Association of Remote Sensing Laboratories (EARSeL), Valladolid, Spain, 31 May – 2 June.*

## **APPENDIX**

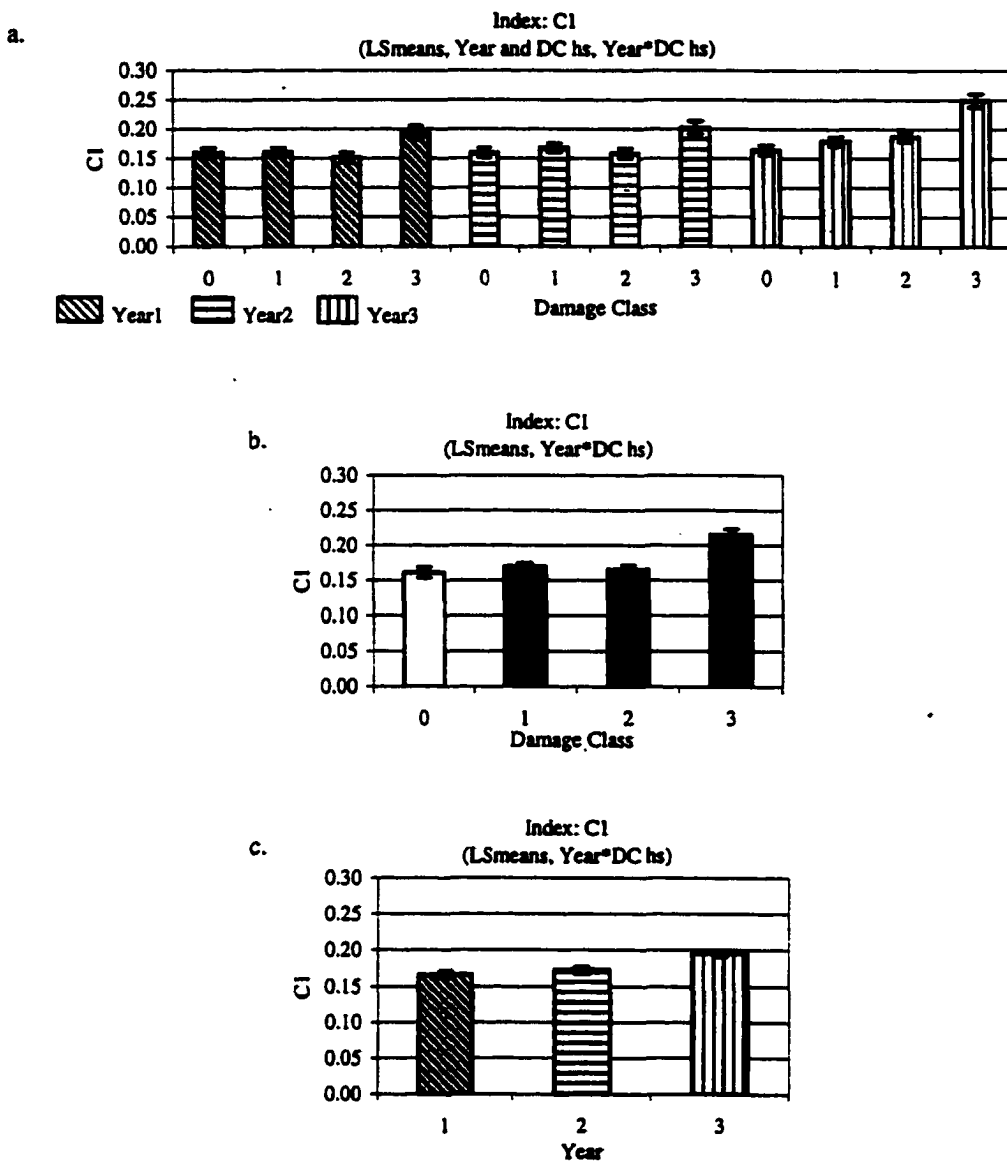


**Figure: A.1.1: Narrow Band Indices (2.5nm). C1 (R693/R775).**  
 Least square (LS) means and standard errors are plotted. The effects of (a) damage and age together, (b) damage and (c) age are evaluated.

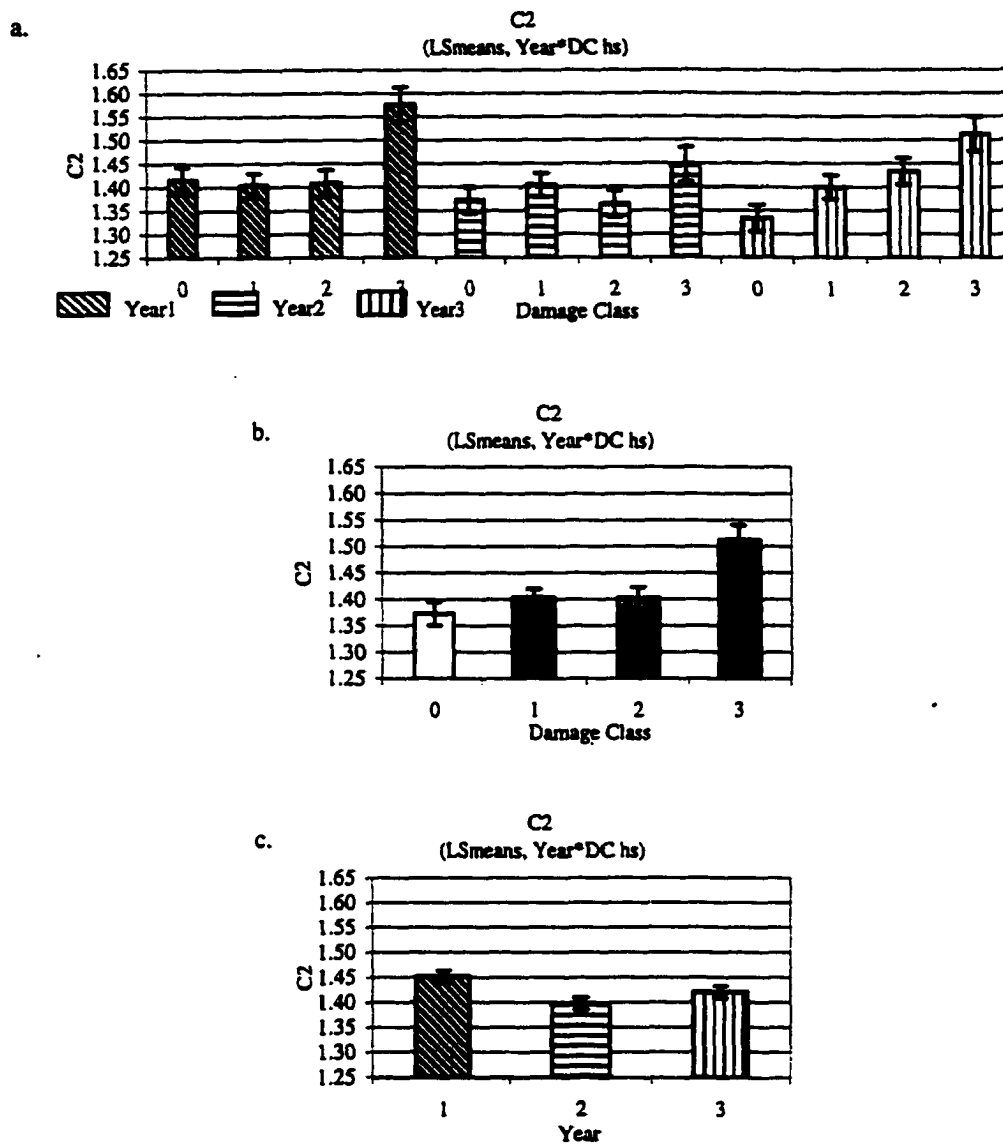


**Figure: A.1.2: Narrow Band Indices (2.5nm). C2 (R693/R420).**  
 Least square (LS) means and standard errors are plotted. The effects of (a) damage and age together, (b) damage and (c) age are evaluated.



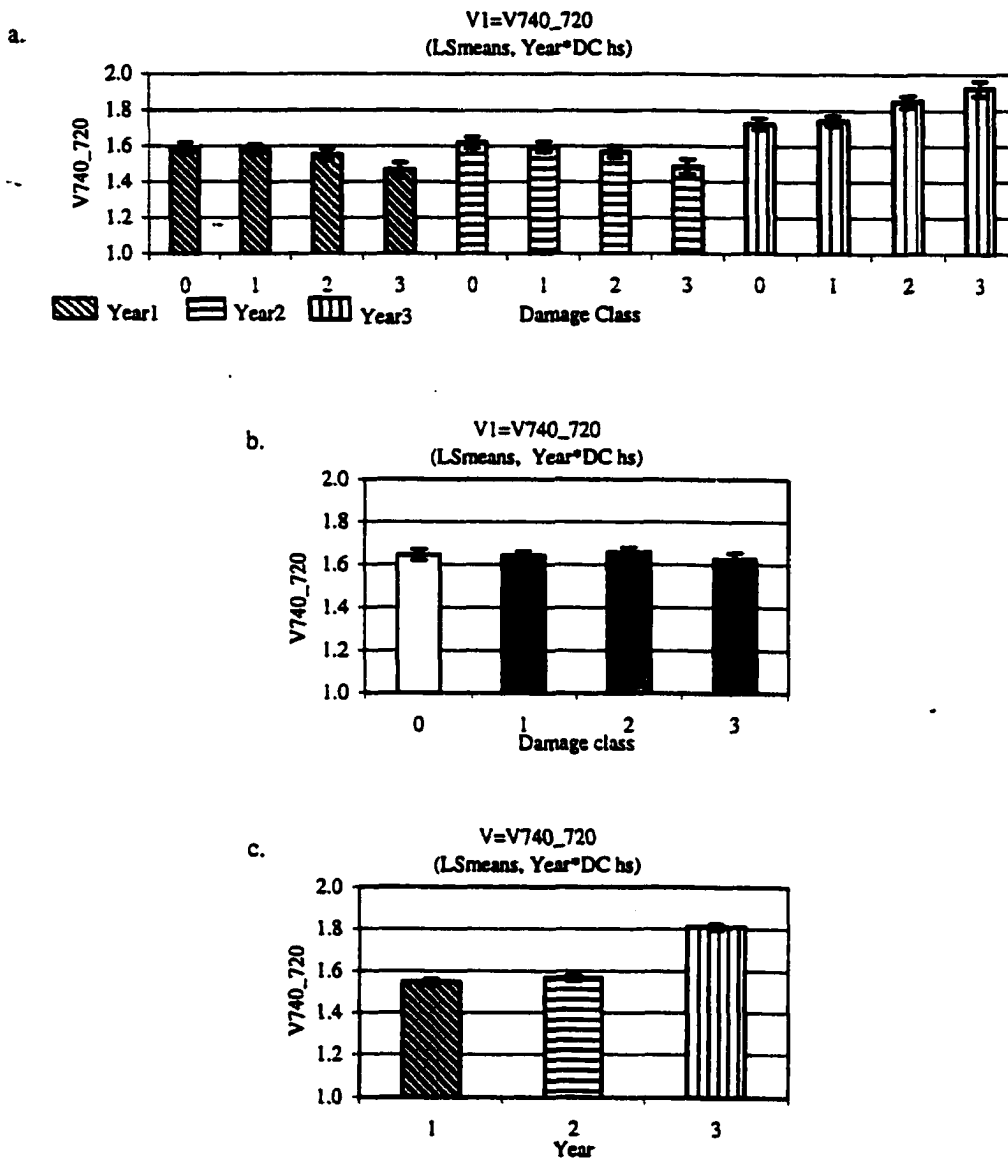


**Figure: A.1.3: Narrow Band Indices (2.5nm). V1 (R740/R720).**  
Least square (LS) means and standard errors are plotted. The effects of (a) damage and age together, (b) damage and (c) age are evaluated.

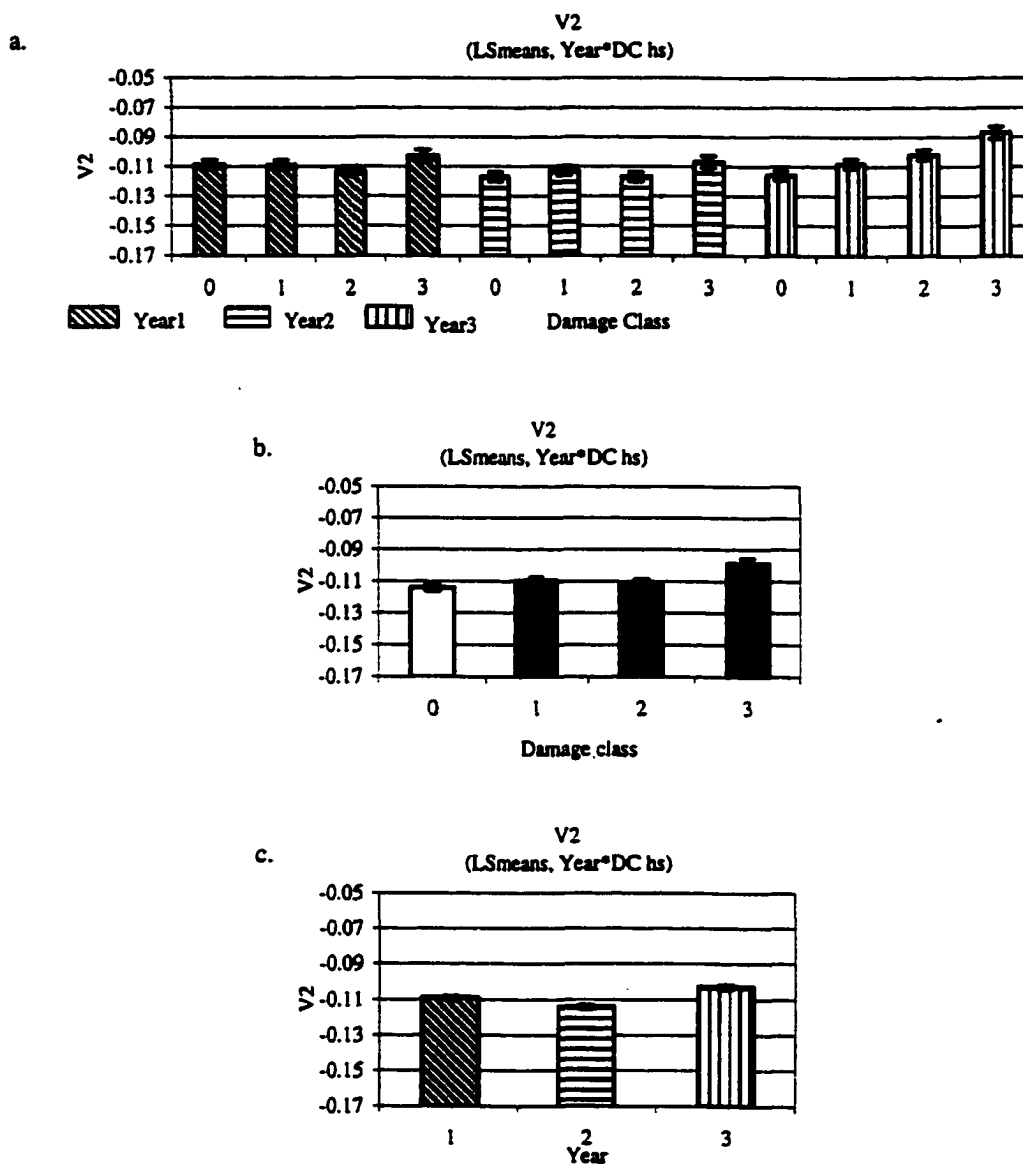


**Figure: A.1.4: Narrow Band Indices (2.5nm). V2 ((R734-R747)/(R715+R726)).** Least square (LS) means and standard errors are plotted. The effects of (a) damage and age together, (b)-damage and (c) age are evaluated.

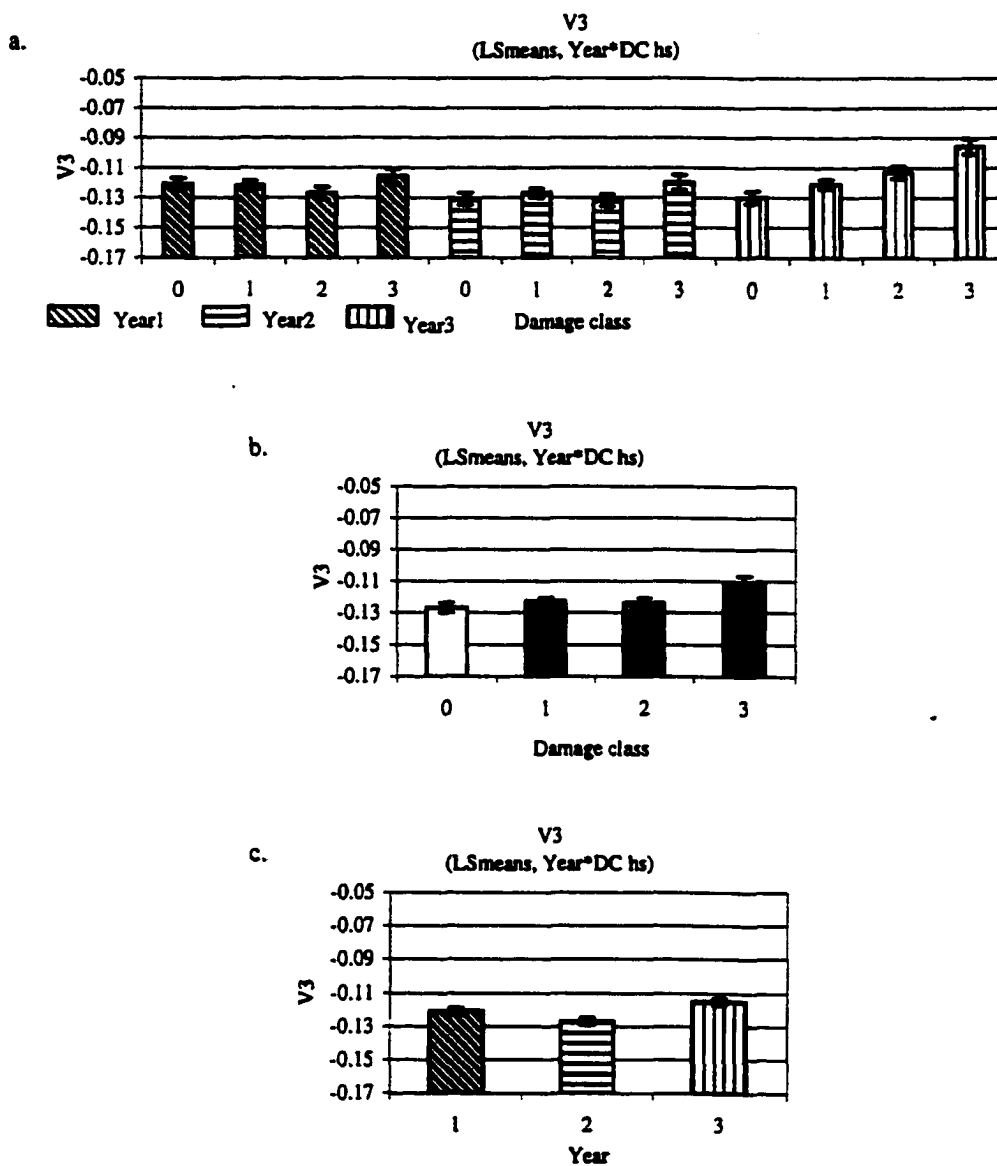


**Figure:A.1.5: Narrow Band Indices (2.5nm). V3 ((R734-R747)/(R715+R720)).** Least square (LS) means and standard errors are plotted. The effects of (a) damage and age together, (b) damage and (c) age are evaluated.

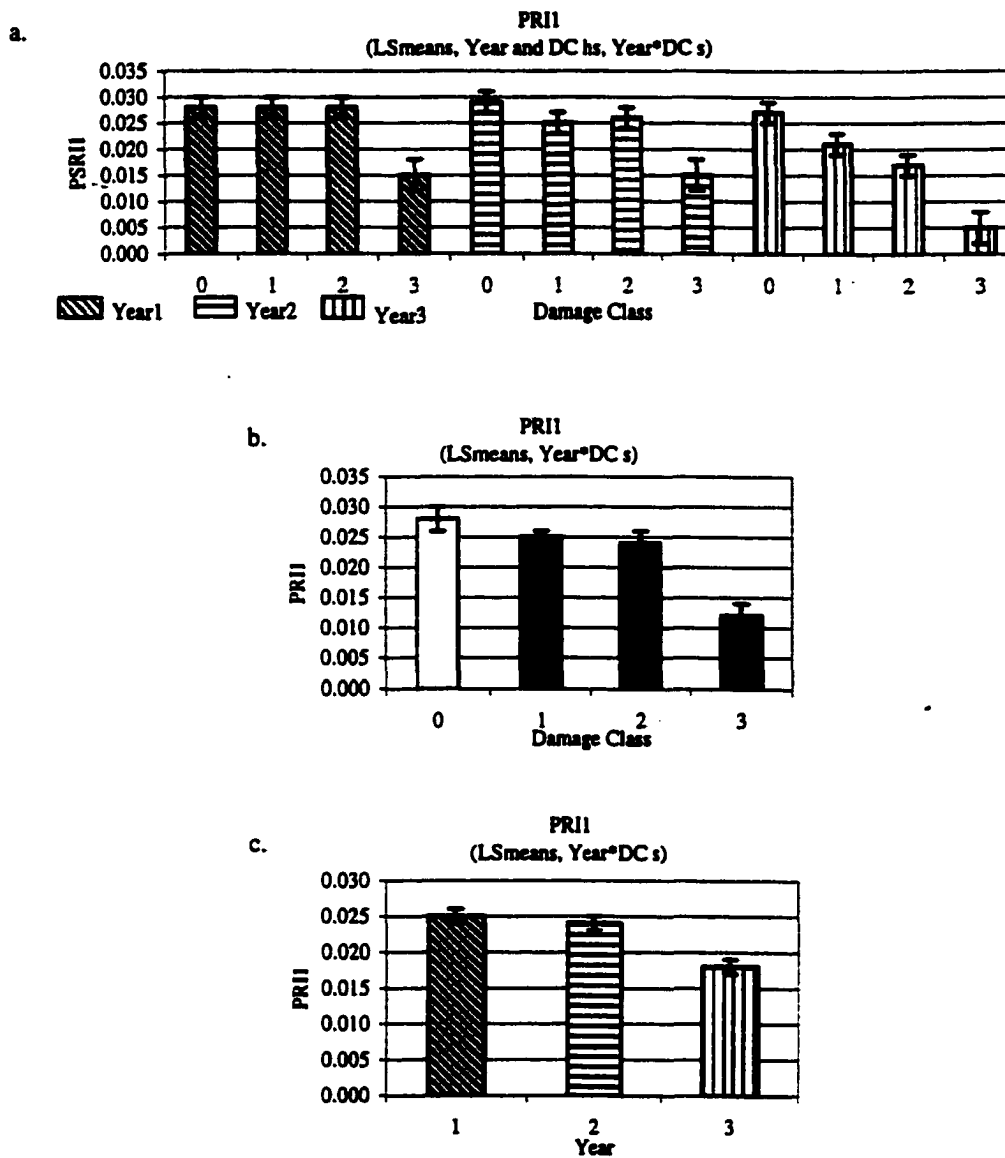


**Figure:A.1.6: Narrow Band Indices (2.5nm). PRII  $((R530-R570)/(R530+R570))$ . Least square (LS) means and standard errors are plotted. The effects of (a) damage and age together, (b) damage and (c) age are evaluated.**

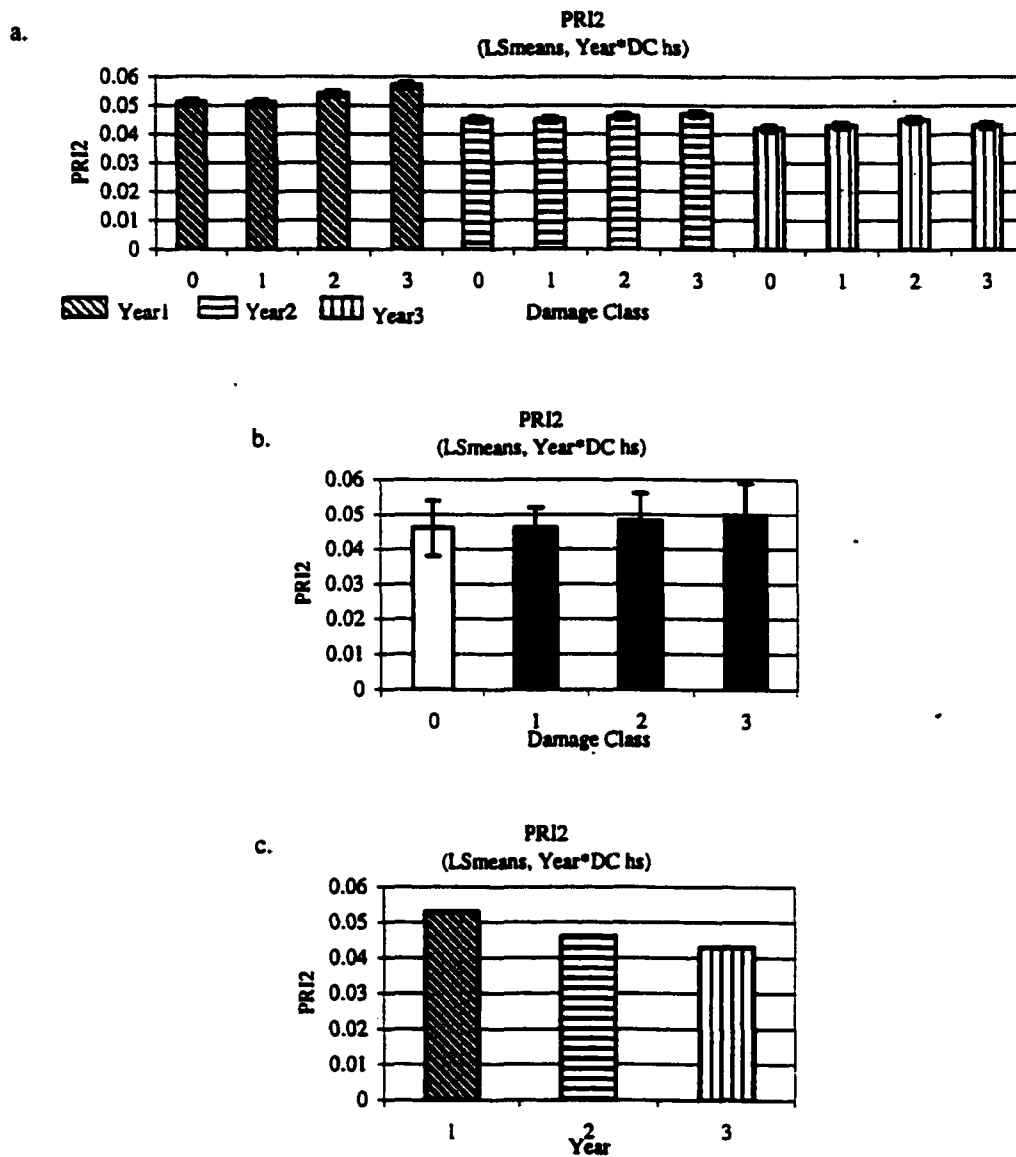


**Figure: A.1.7: Narrow Band Indices (2.5nm). PRI2 ((R550-R530)/(R550+R530)).** Least square (LS) means and standard errors are plotted. The effects of (a) damage and age together, (b) damage and (c) age are evaluated.

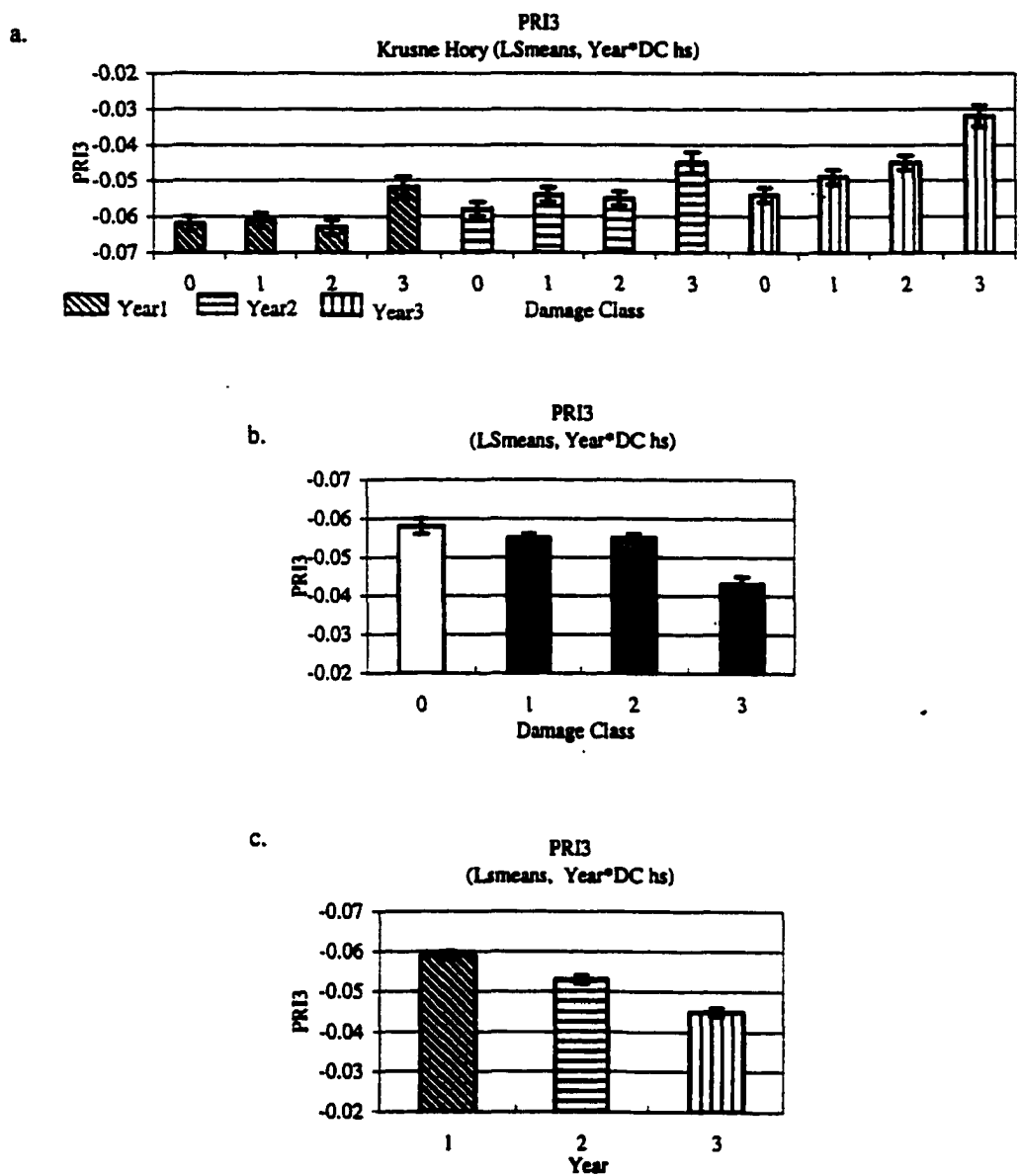


**Figure: A.1.8: Narrow Band Indices (2.5nm). PRI3 ((R570-R540)/(R570+R540)).** Least square (LS) means and standard errors are plotted. The effects of (a) damage and age together, (b) damage and (c) age are evaluated.

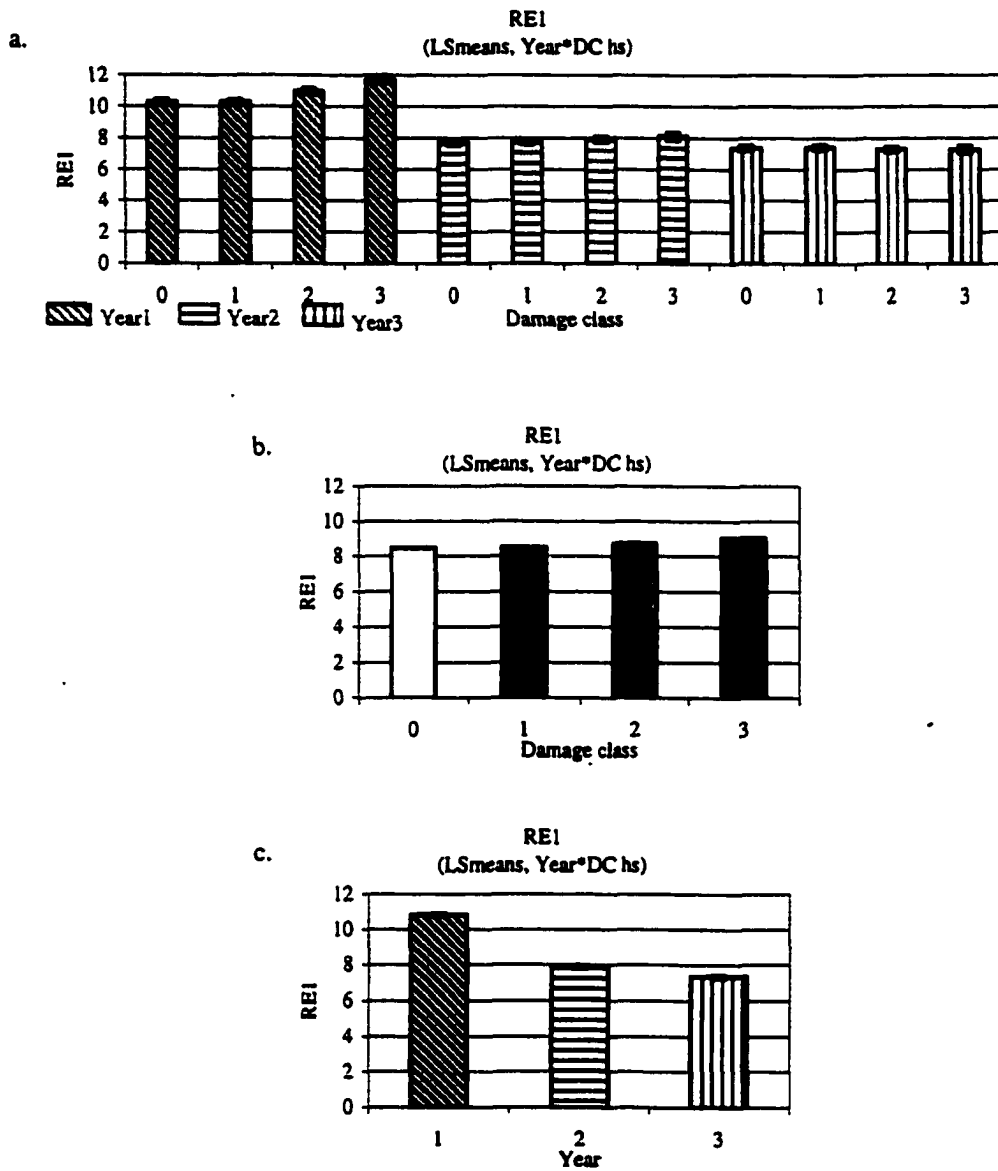


**Figure:A.1.9: Narrow Band Indices (2.5nm). REI (Average R(675...705)).** Least square (LS) means and standard errors are plotted. The effects of (a) damage and age together, (b) damage and (c) age are evaluated.

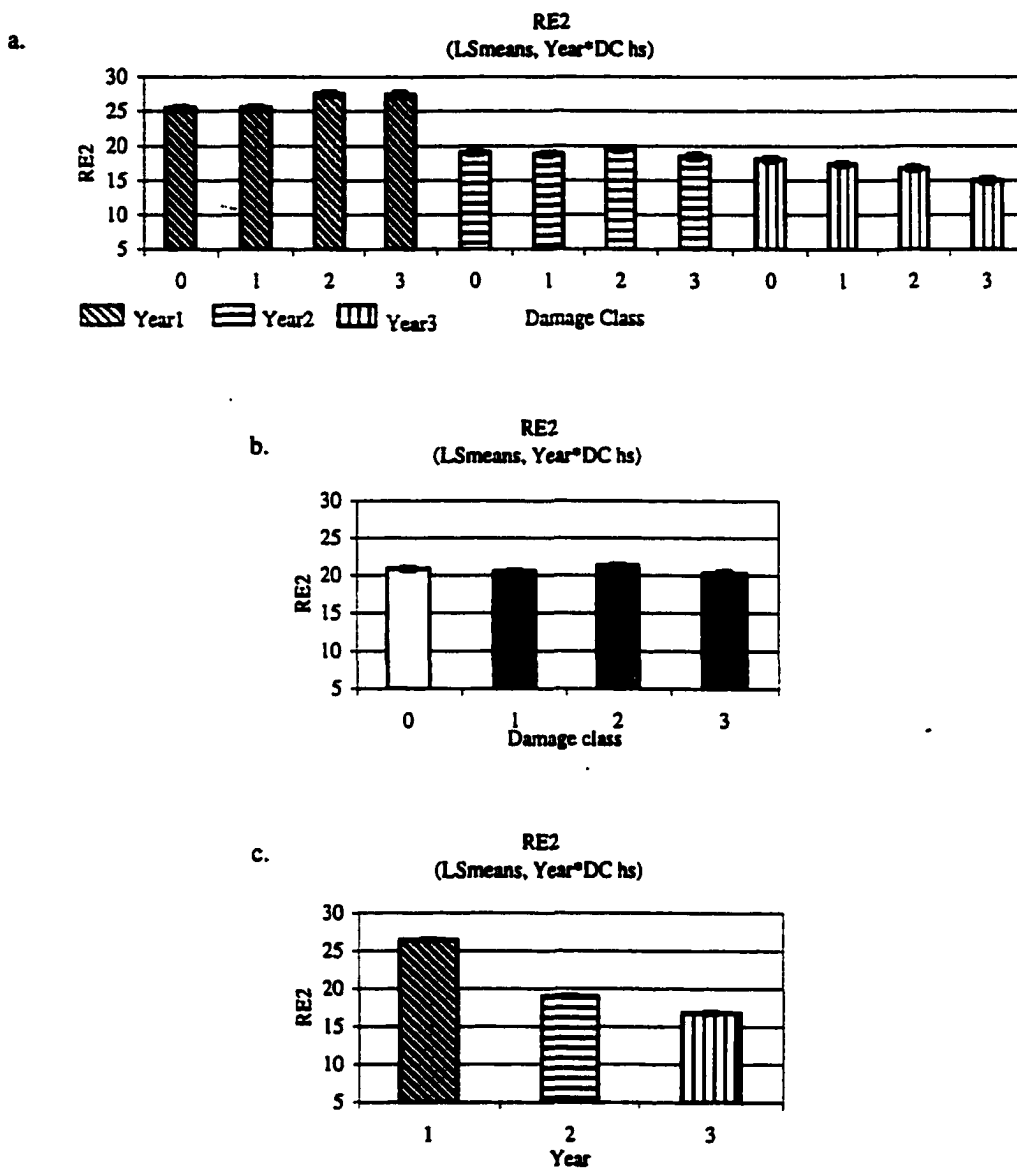


**Figure: A.1.10: Narrow Band Indices (2.5nm). RE2 (Average R(714...725)).** Least square (LS) means and standard errors are plotted. The effects of (a) damage and age together, (b) damage and (c) age are evaluated.



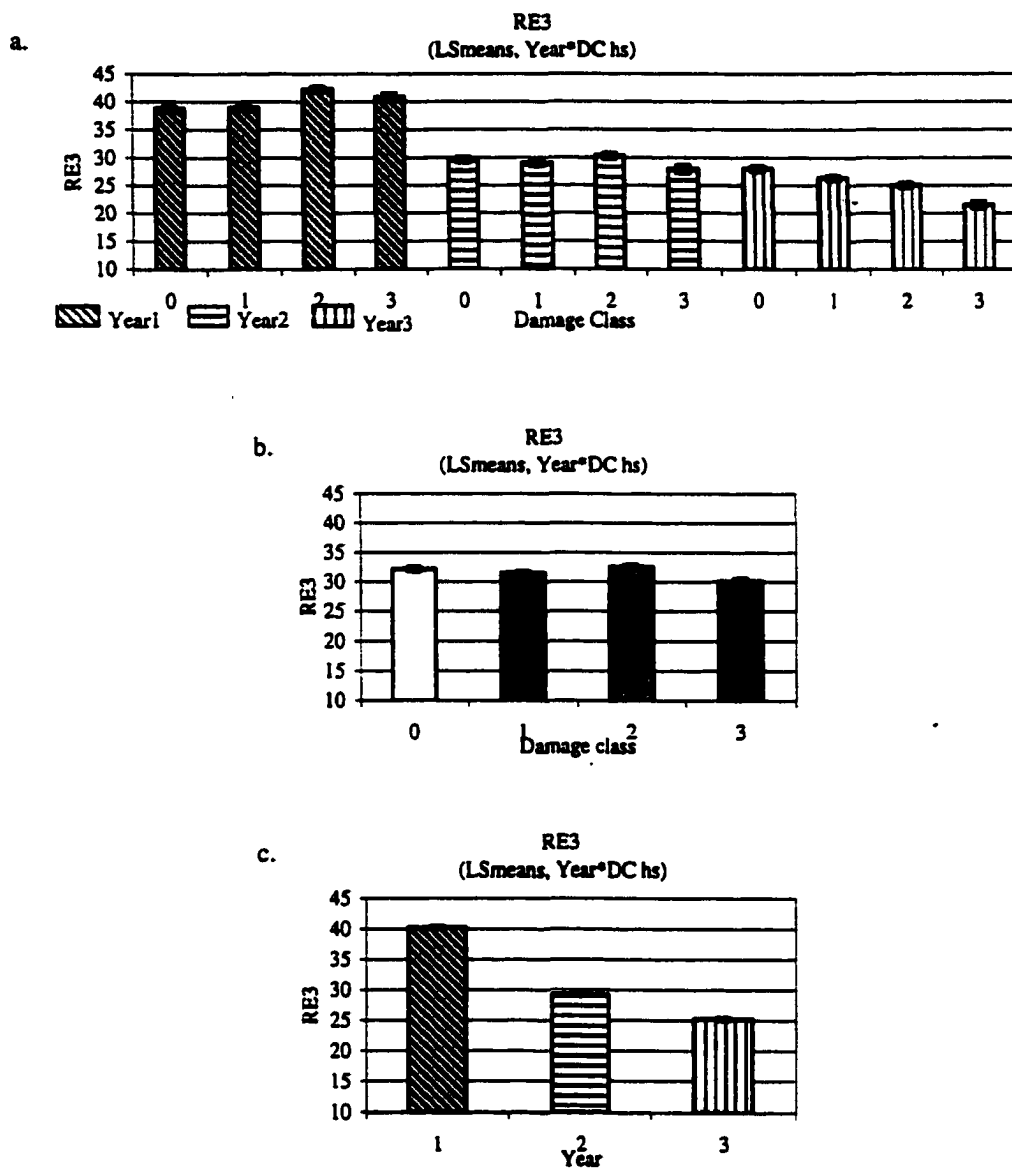


**Figure: A.1.11: Narrow Band Indices (2.5nm). RE3 (Average R(730...745)).** Least square (LS) means and standard errors are plotted. The effects of (a) damage and age together, (b) damage and (c) age are evaluated.

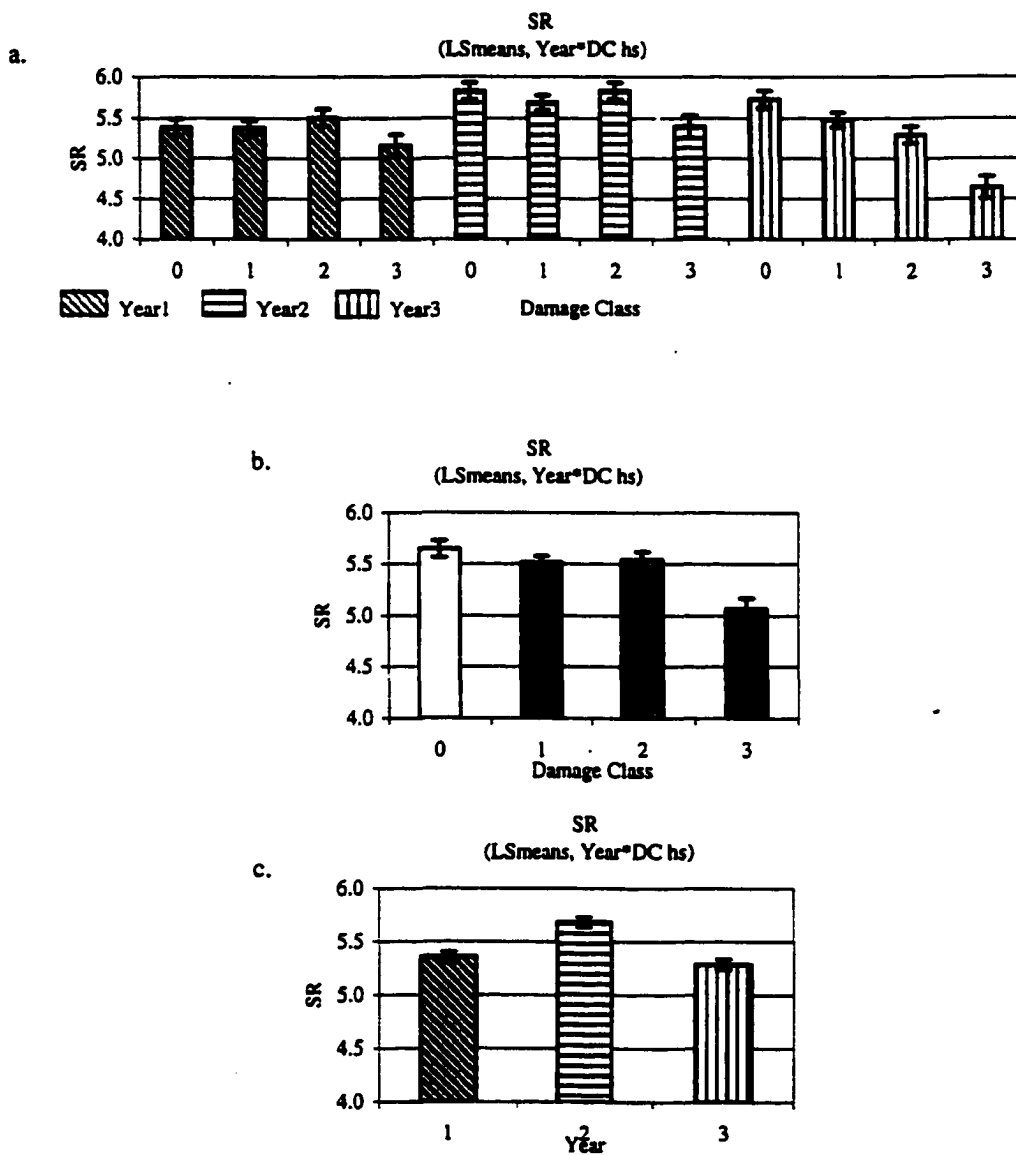


**Figure: A.1.12: Narrow Band Indices (2.5nm). SR (R775/R675).**  
Least square (LS) means and standard errors are plotted. The effects of (a) damage and age together, (b) damage and (c) age are evaluated.

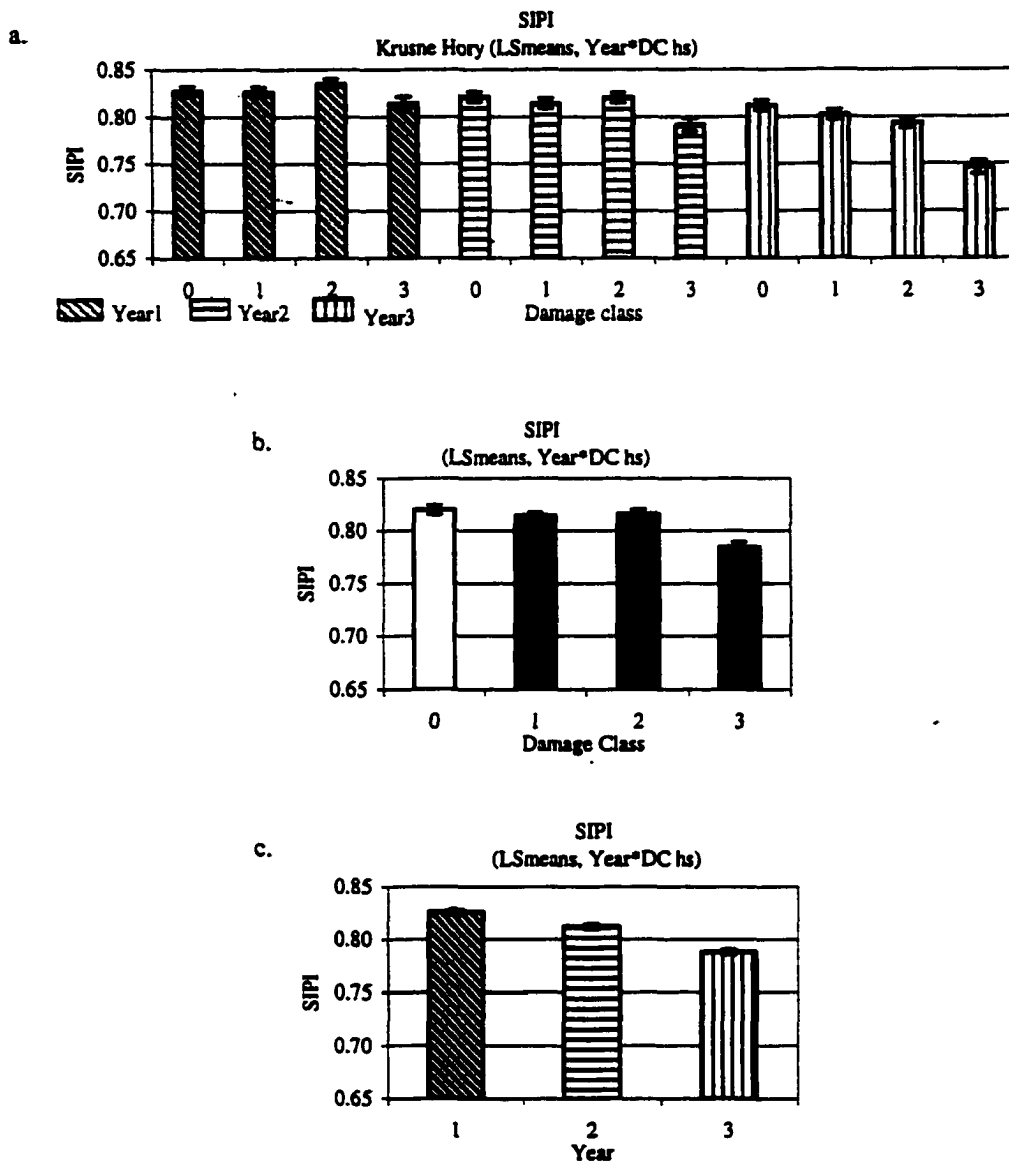


**Figure: A.1.13: Narrow Band Indices (2.5nm).SIPI ((R800-R450)/(R800-R650)).** Least square (LS) means and standard errors are plotted. The effects of (a) damage and age together, (b) damage and (c) age are evaluated.

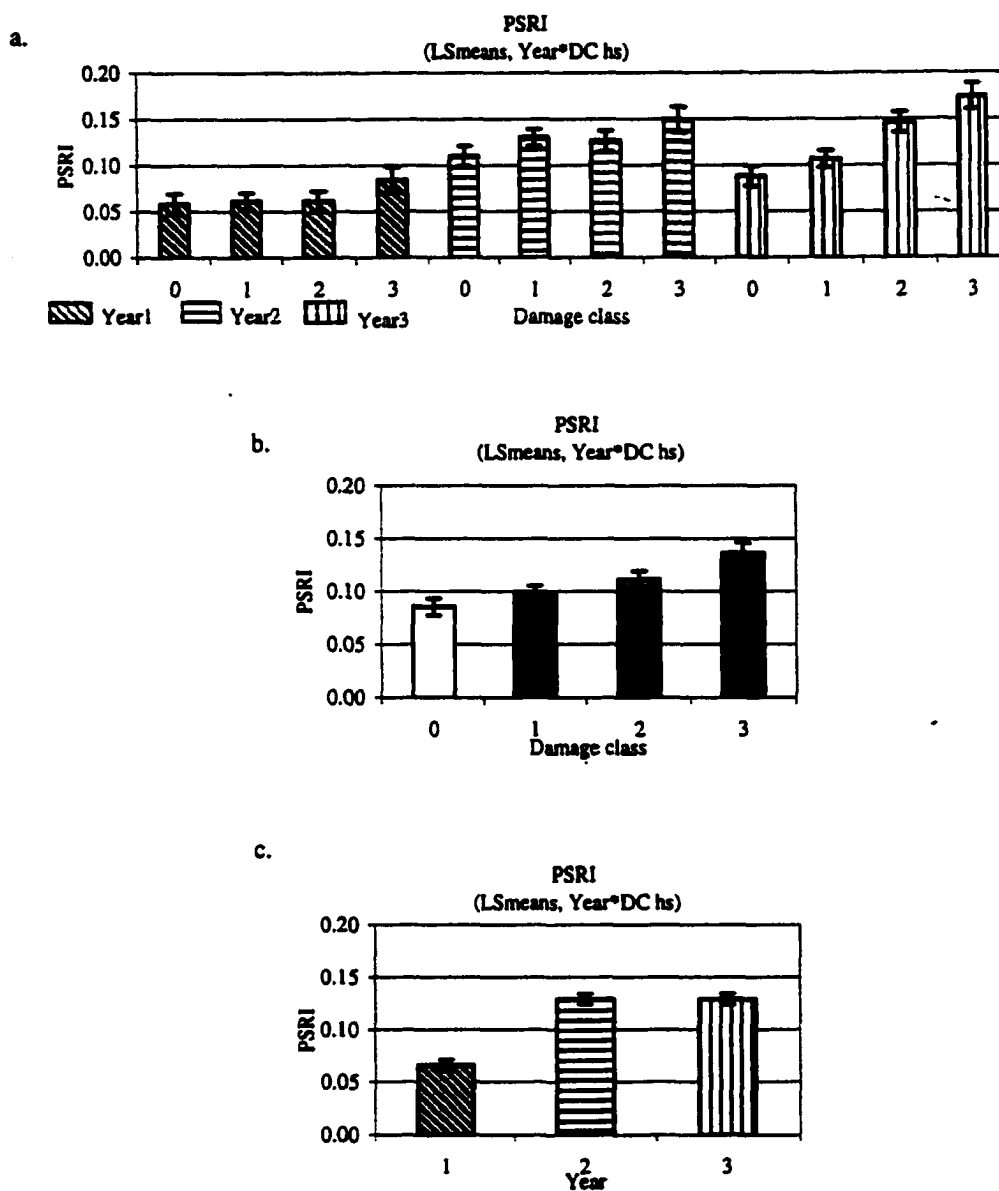


**Figure: A.1.14: Narrow Band Indices (2.5nm). PSRI ((R680-R500)/750).** Least square (LS) means and standard errors are plotted. The effects of (a) damage and age together, (b) damage and (c) age are evaluated.

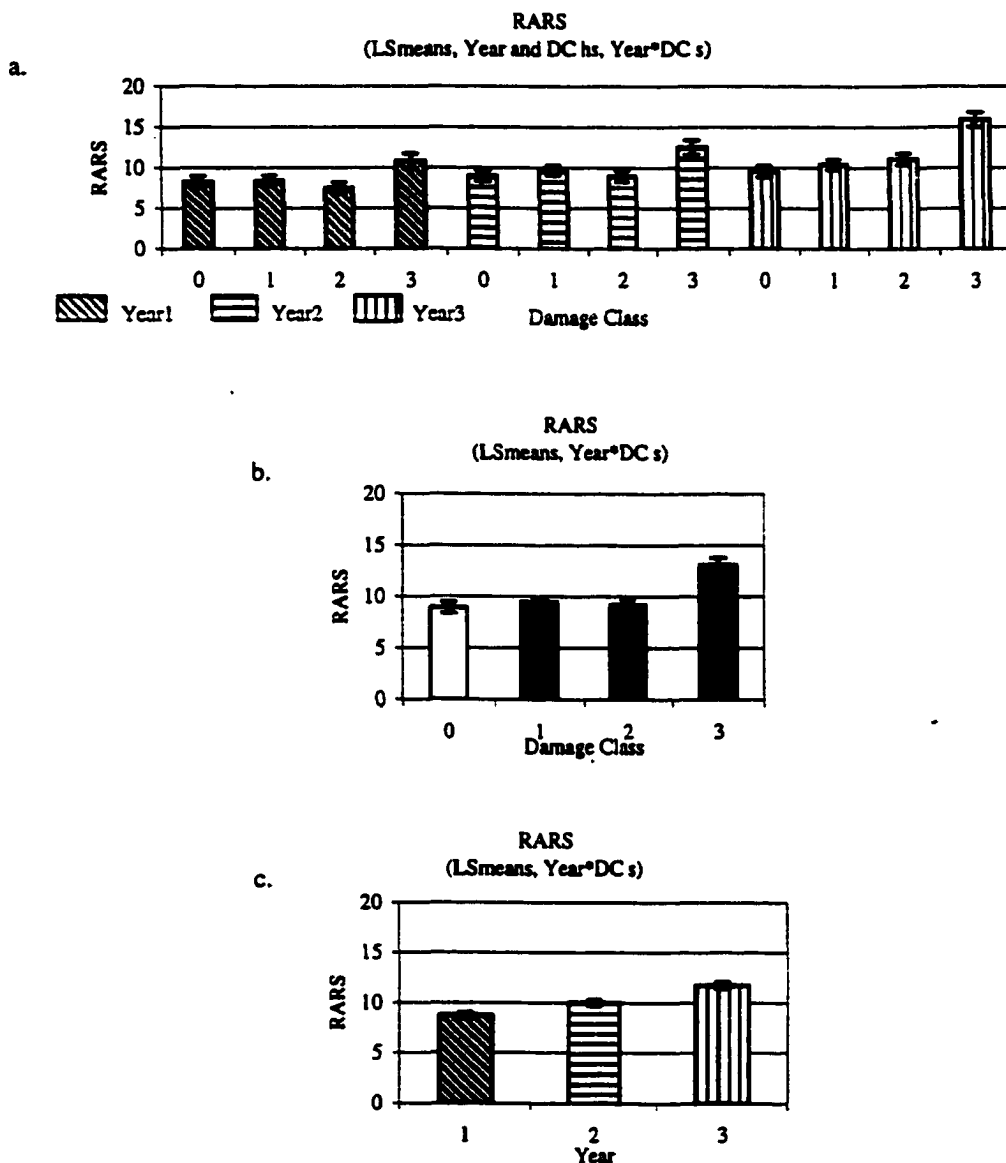


**Figure: A.1.15: Narrow Band Indices (2.5nm). RARS (R800/R670).**  
 Least square (LS) means and standard errors are plotted. The effects of (a) damage and age together, (b) damage and (c) age are evaluated.

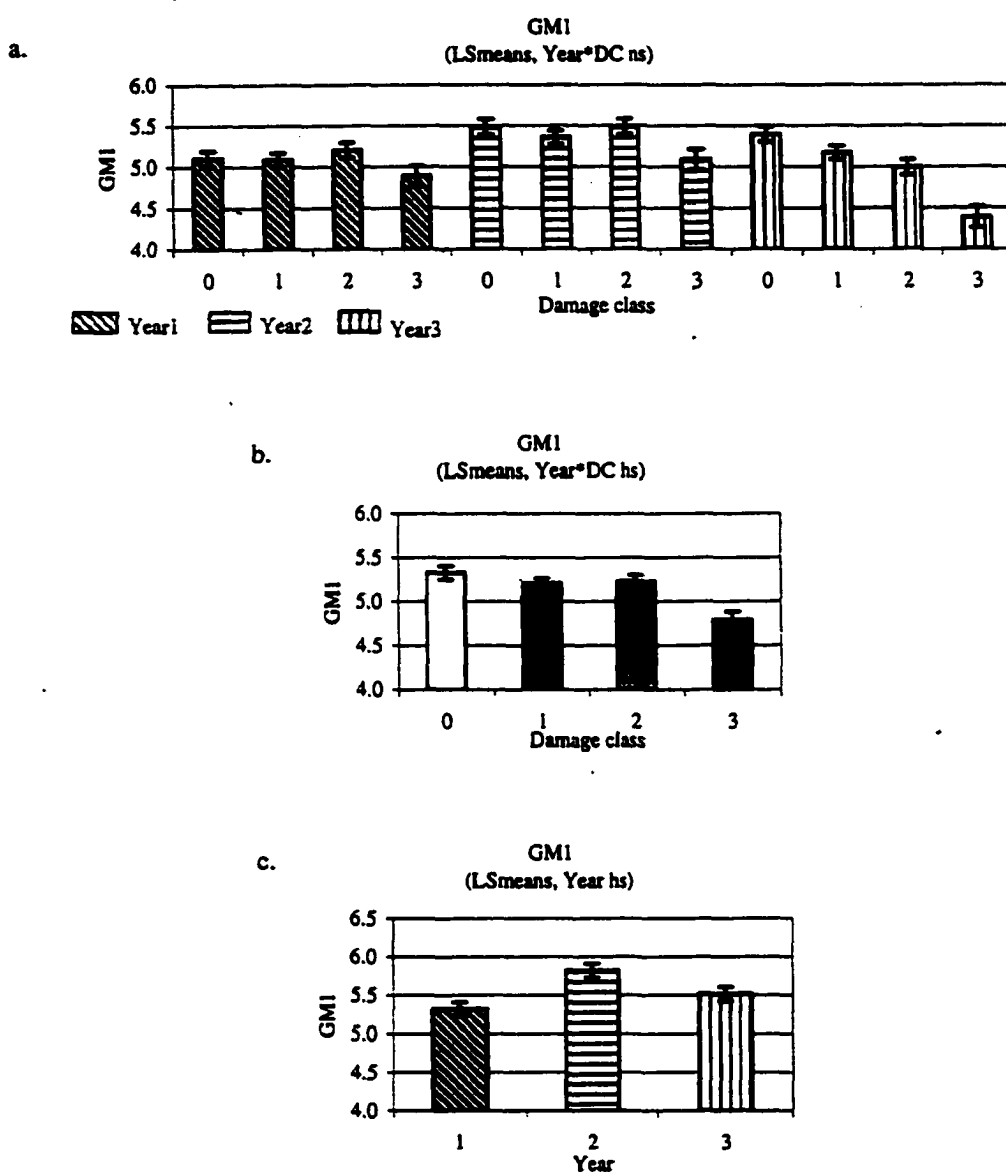


**Figure: A.1.16: Narrow Band Indices (2.5nm). GM1 (R750/R550).**  
Least square (LS) means and standard errors are plotted. The effects of (a) damage and age together, (b) damage and (c) age are evaluated.

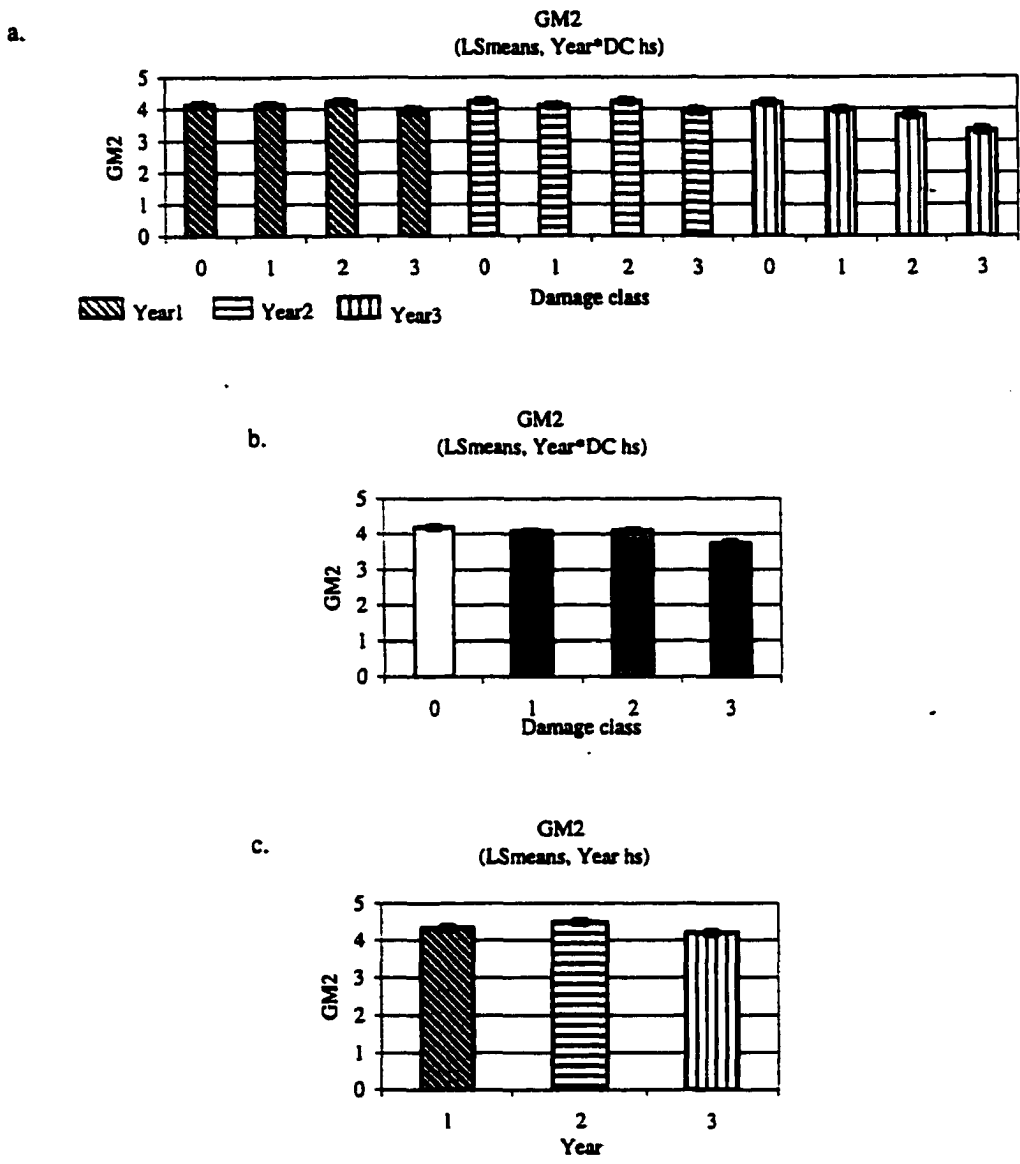


**Figure: A.1.17: Narrow Band Indices (2.5nm). GM2 (R750/R700).**  
 Least square (LS) means and standard errors are plotted. The effects of (a) damage and age together, (b) damage and (c) age are evaluated.

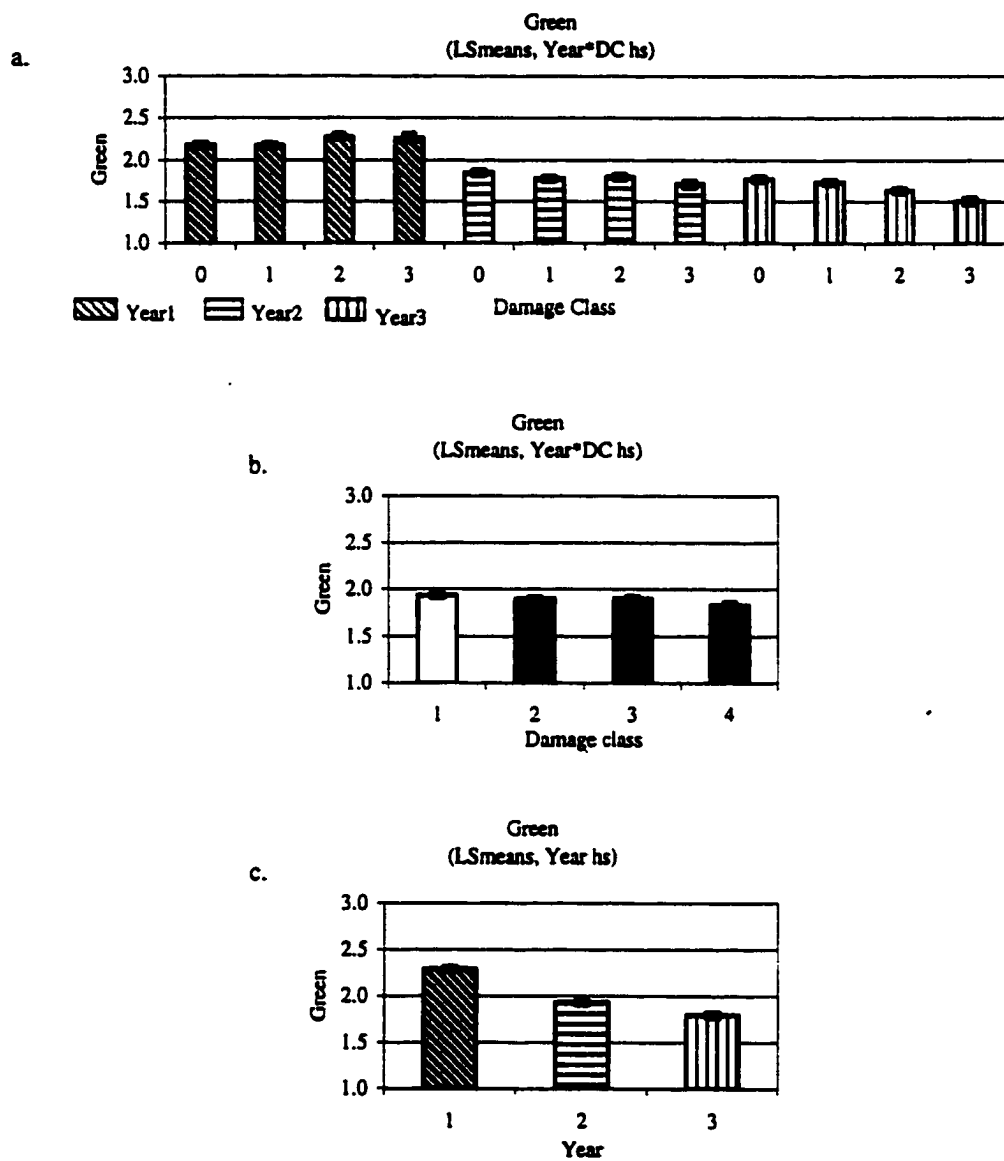


**Figure: A.1.18: Narrow Band Indices (2.5nm). Green (R554/R675).** Least square (LS) means and standard errors are plotted. The effects of (a) damage and age together, (b) damage and (c) age are evaluated.



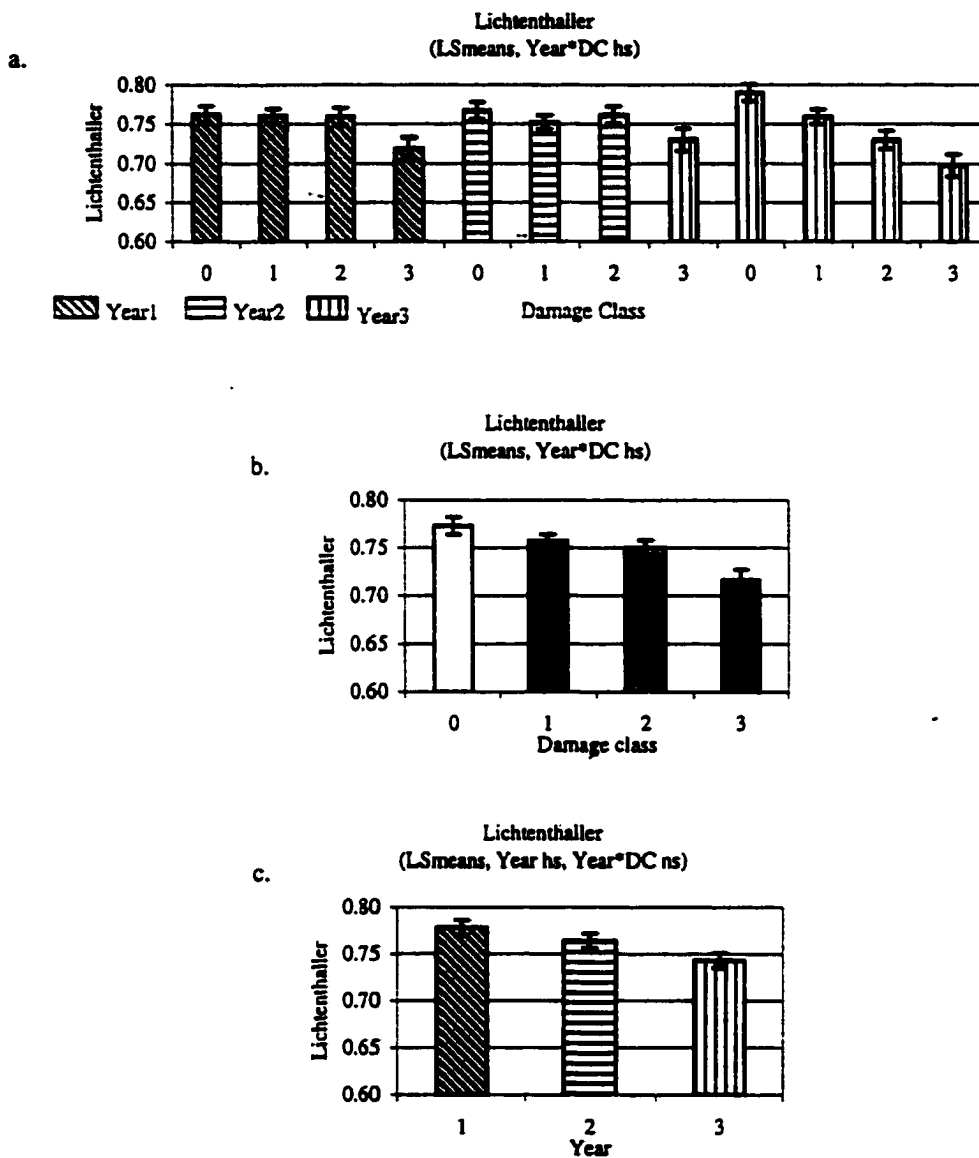


**Figure: A.1.19: Narrow Band Indices (2.5nm). Lichtenthaler (R440/R690).**  
Least square (LS) means and standard errors are plotted. The effects of (a) damage and age together, (b) damage and (c) age are evaluated.

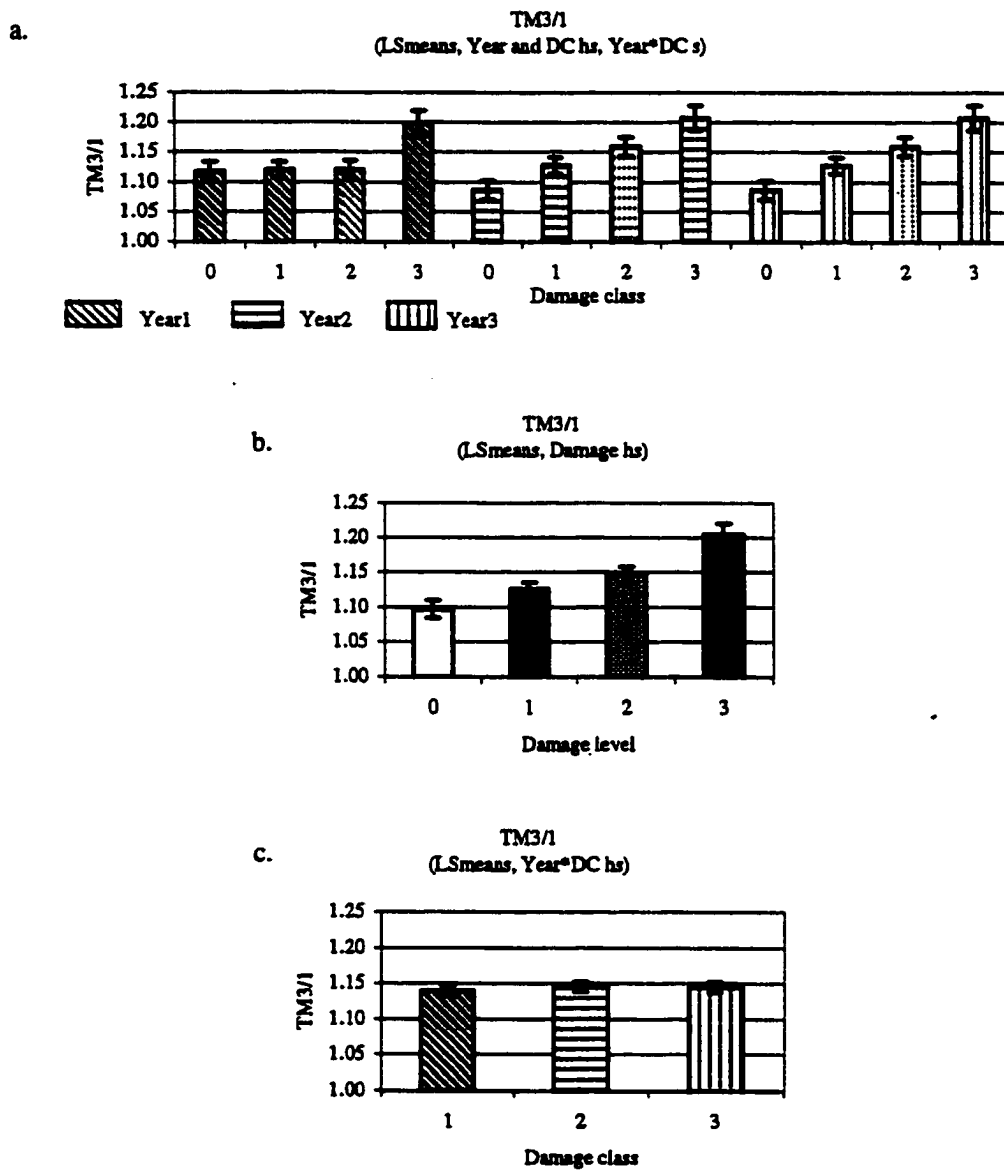


**Figure: A.2.1: Broad Band Indices.  $TM3/1$  (Average  $R(620...690)$ )/(Average  $R(450...520)$ ).** Least square (LS) means and standard errors are plotted. The effects of (a) damage and age together, (b) damage and (c) age are evaluated.

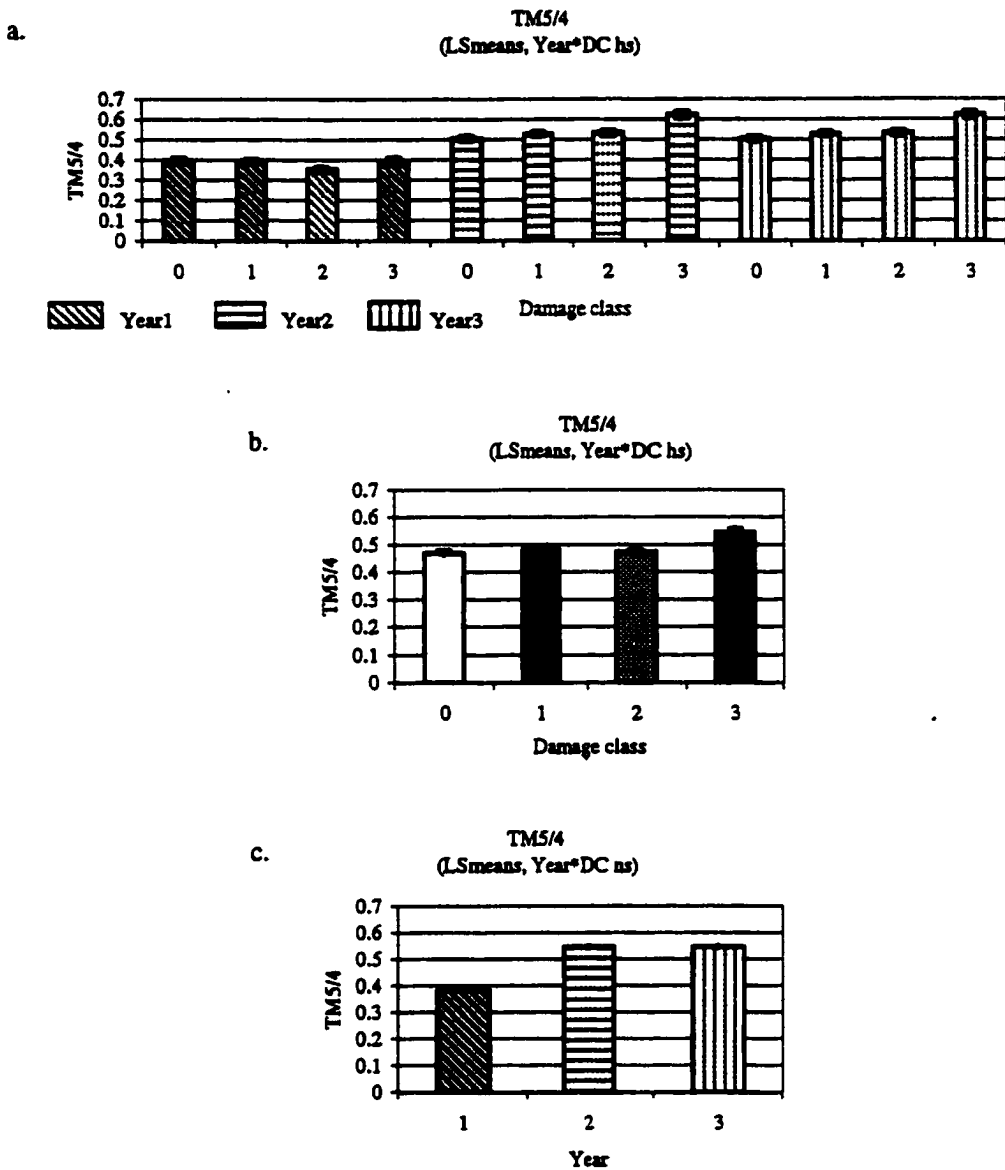


**Figure: A.2.2: Broad Band Indices.  $TM5/TM4$  (Average  $R(1150...1750)$ )/(Average  $R(760...900)$ ).** Least square (LS) means and standard errors are plotted. The effects of (a) damage and age together, (b) damage and (c) age are evaluated.

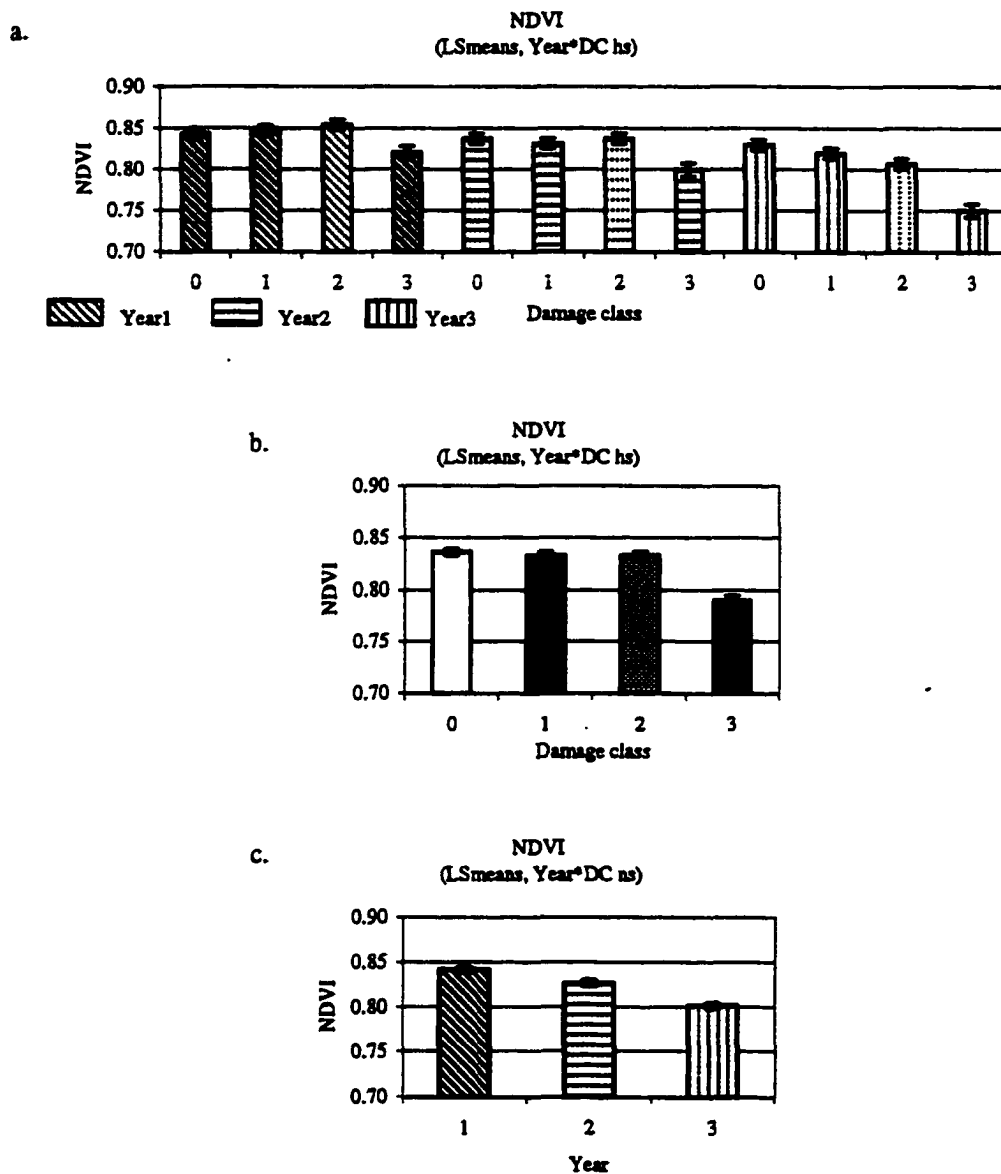


**Figure: A.2.3: Broad Band Indices. NDVI ((TM4-TM3)/(TM4+TM3)).** Least square (LS) means and standard errors are plotted. The effects of (a) damage and age together, (b) damage and (c) age are evaluated.

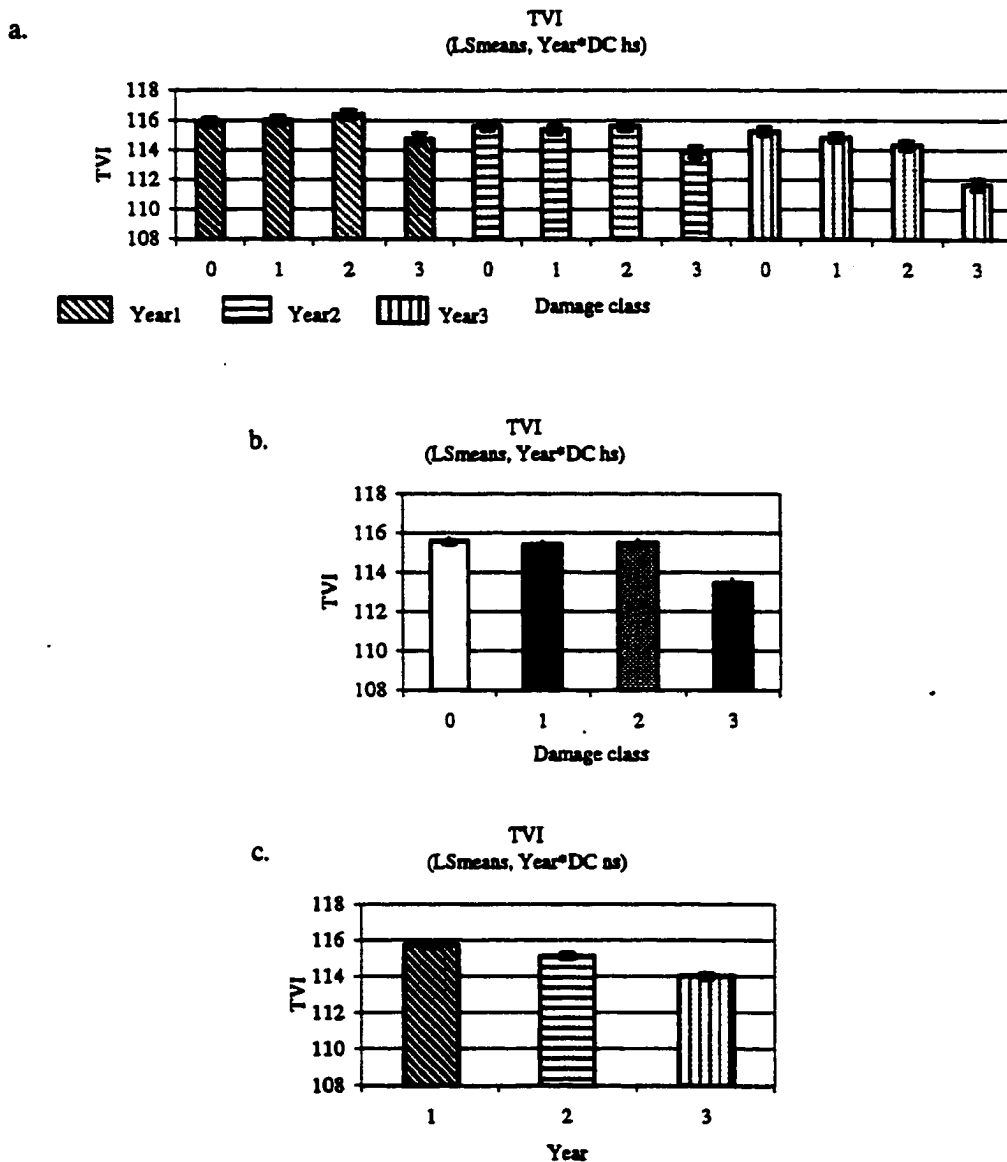


**Figure: A.2.4: Broad Band Indices. TVI (SQRT ((NDVI+0.5)\*100)).** Least square (LS) means and standard errors are plotted. The effects of (a) damage and age together, (b) damage and (c) age are-evaluated.

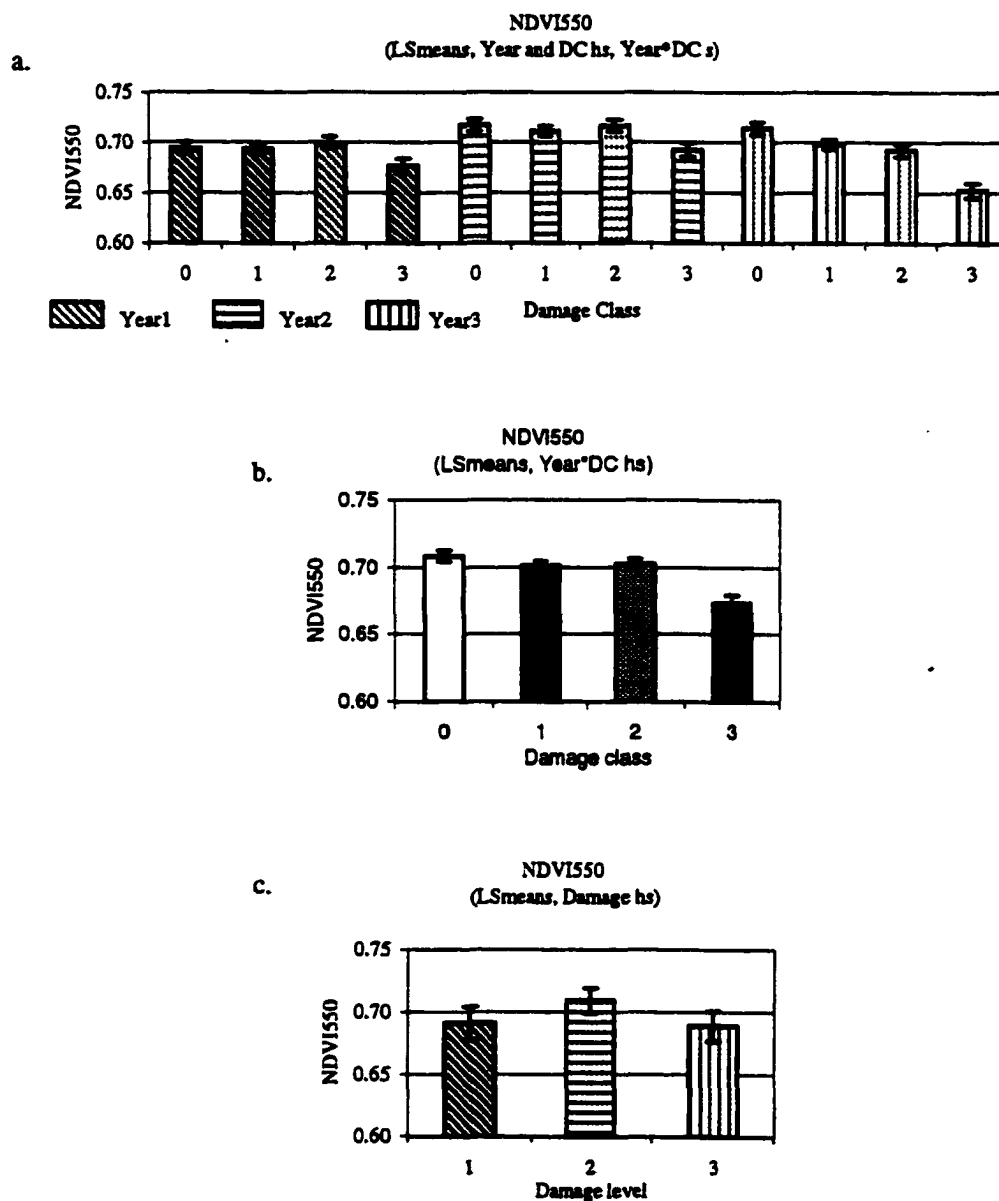


**Figure: A.2.5: Broad Band Indices. NDVI550 ((TM4-R550)/(TM4+R550)).** Least square (LS) means and standard errors are plotted. The effects of (a) damage and age together, (b) damage and (c) age are evaluated.

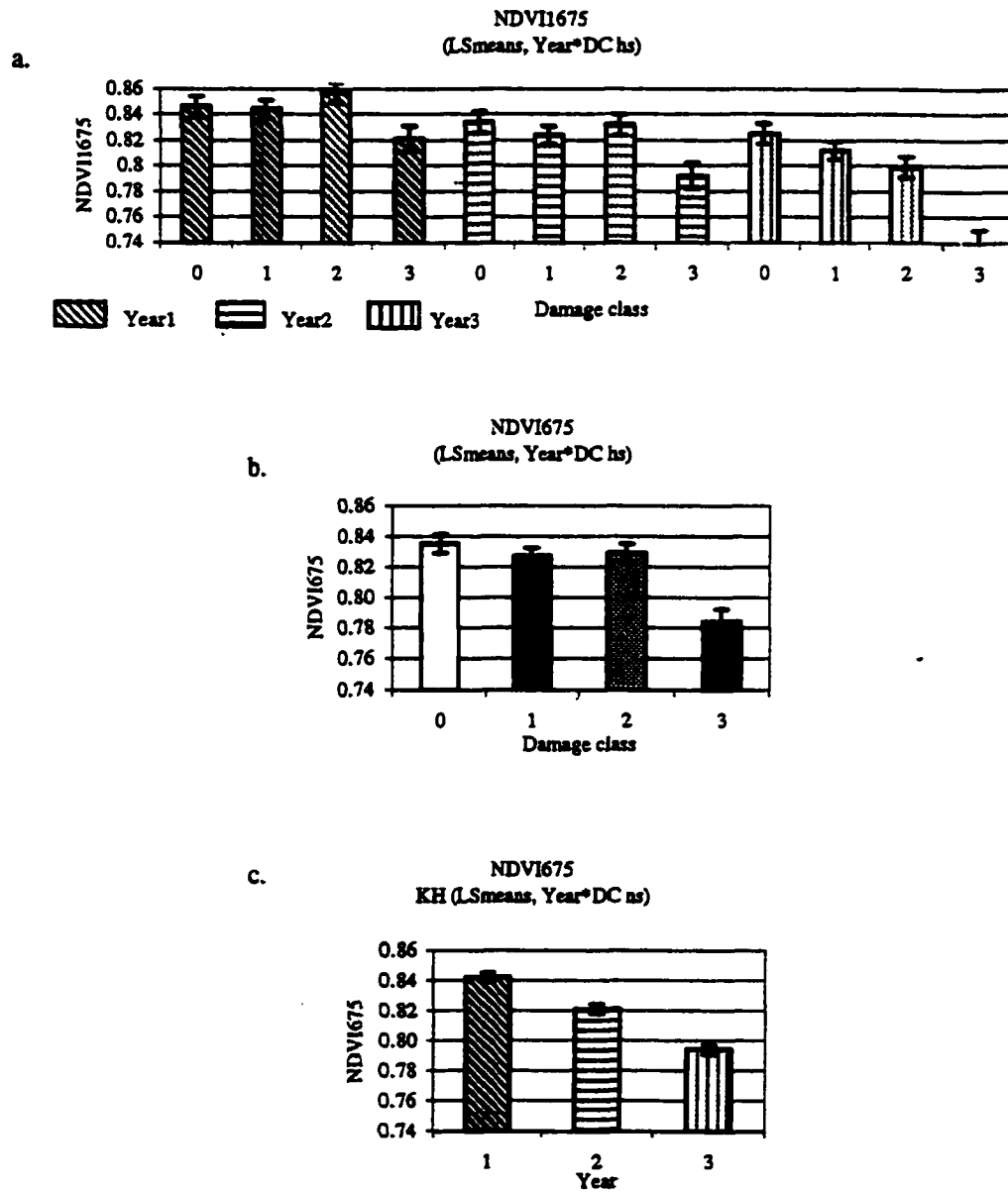


**Figure: A.2.6: Broad Band Indices. NDVI675 ((TM4-R675)/(TM4+R675)).** Least square (LS) means and standard errors are plotted. The effects of (a) damage and age together, (b) damage and (c) age are evaluated.

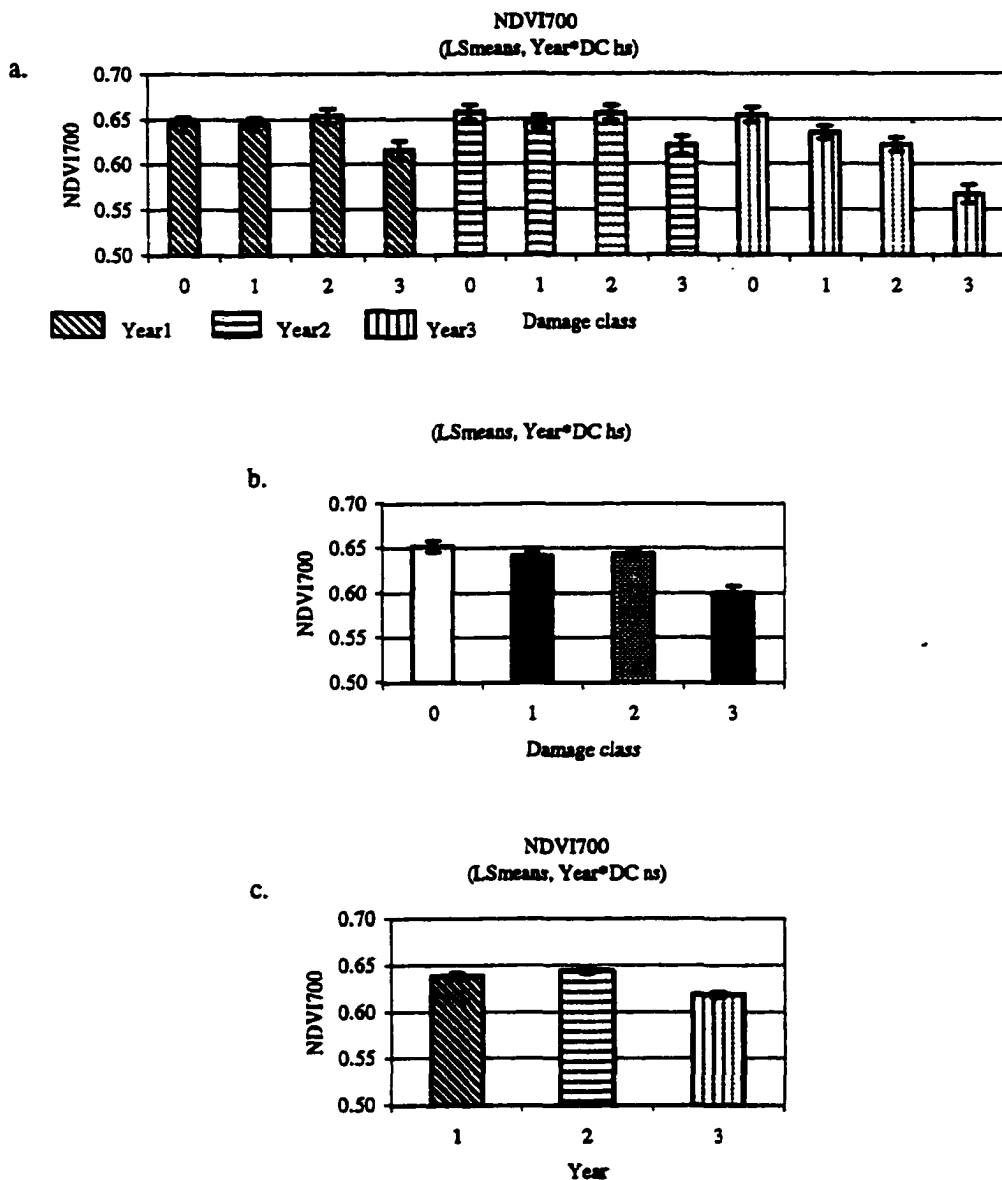


**Figure: A.2.7: Broad Band Indices. NDVI700 ((TM4-R700)/(TM4+R700)).**  
Least square (LS) means and standard errors are plotted. The effects of (a) damage and age together, (b) damage and (c) age are evaluated.



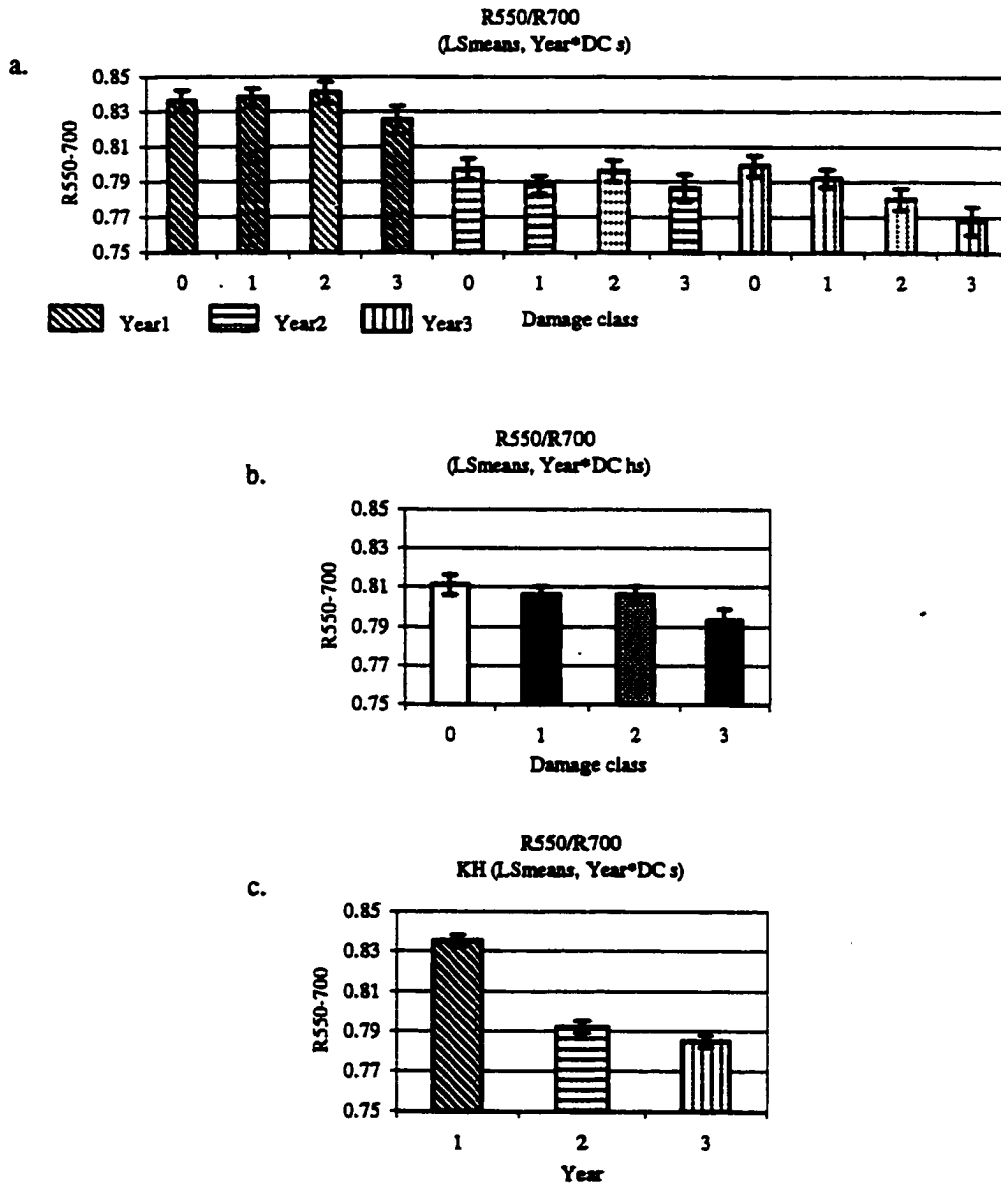


**Figure: A.2.8: Narrow Band Ratios. R550/R700 (R550/R700).** Least square (LS) means and standard errors are plotted. The effects of (a) damage and age together, (b) damage and (c) age are evaluated.

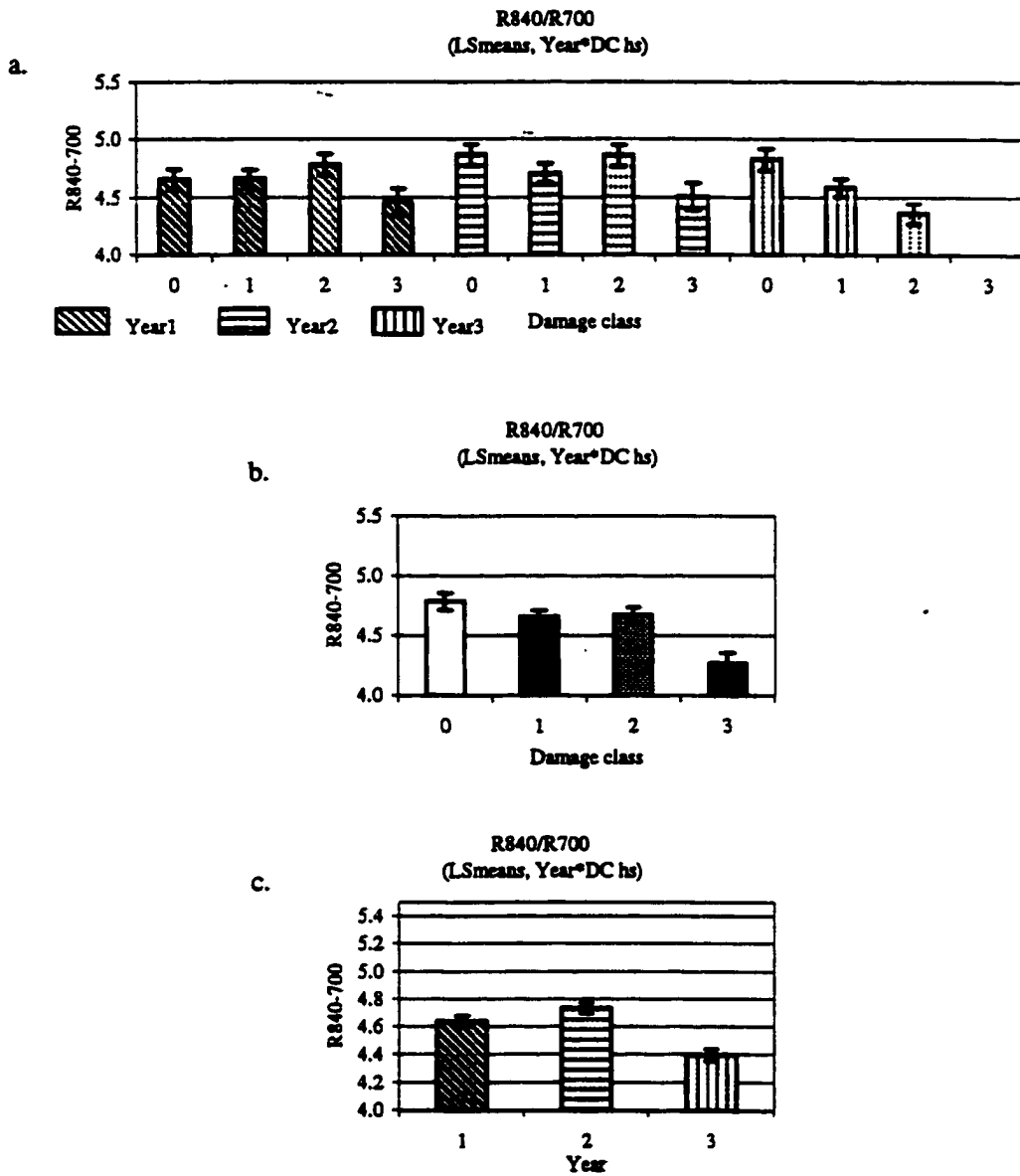


**Figure: A.2.9: Narrow Band Ratios. R840/R700 (R840/R700).**  
Least square (LS) means and standard errors are plotted. The effects of (a) damage and age together, (b) damage and (c) age are evaluated.

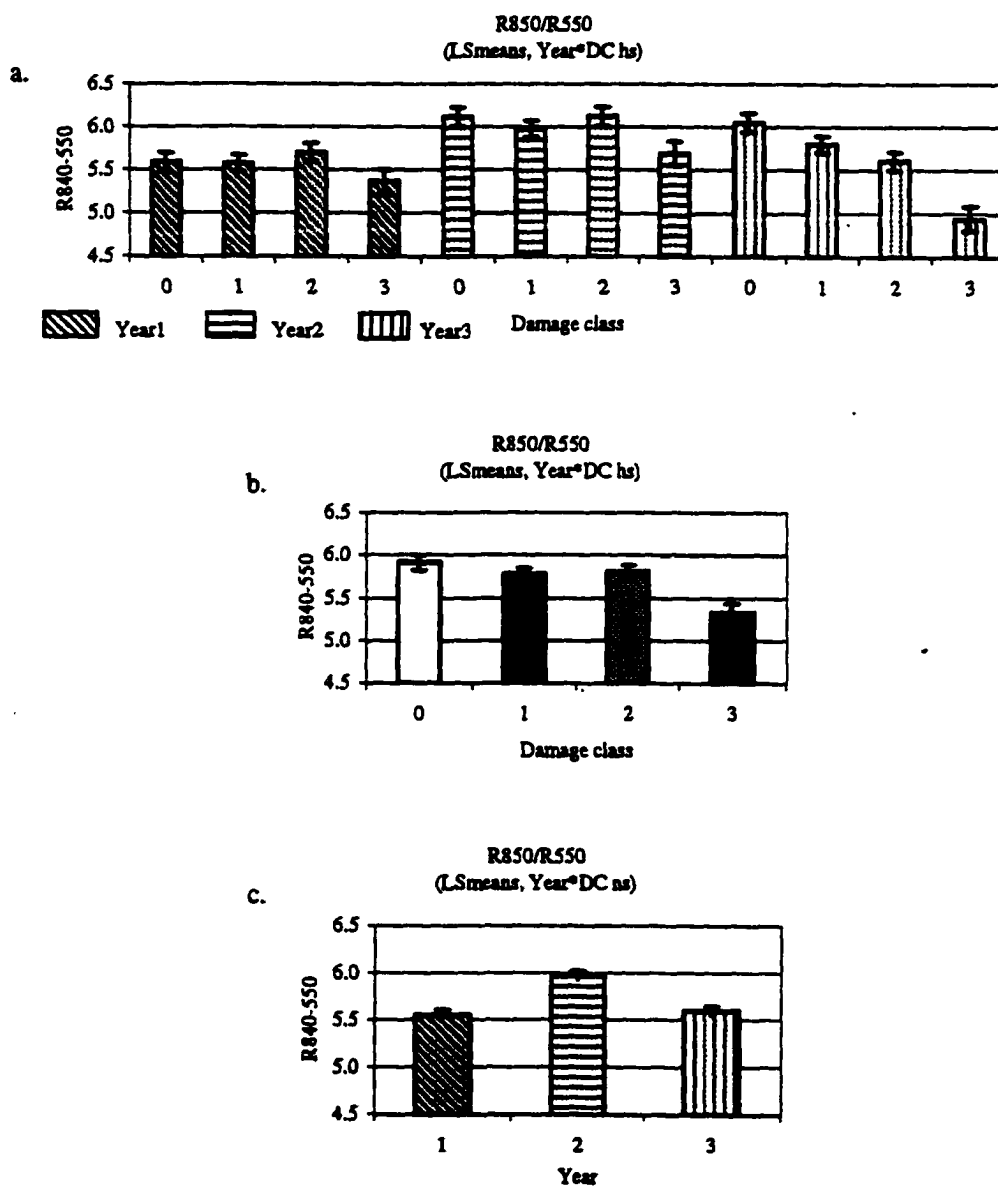


**Figure A.2.10: Narrow Band Ratios, R850/R550 (R850/R550).**  
Least square (LS) means and standard errors are plotted. The effects of (a) damage and age together, (b) damage and (c) age are evaluated.

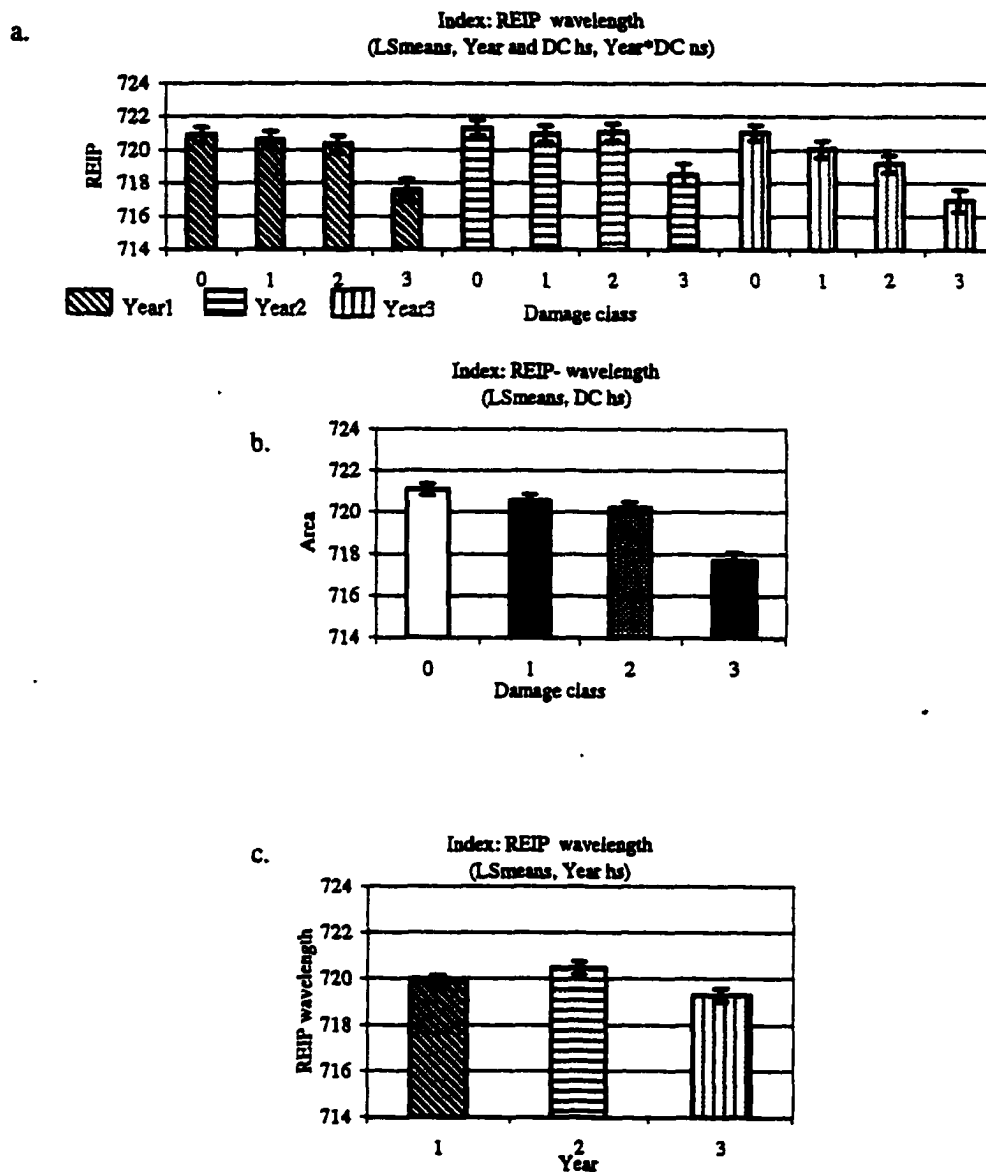


**Figure: A.3.1: Derivative indices. REIPwave** (Position of  $D'$  maximum in the 670-730nm region Least square (LS)means and standard errors are plotted. The effects of (a) damage and age together, (b) damage and (c) age are evaluated.

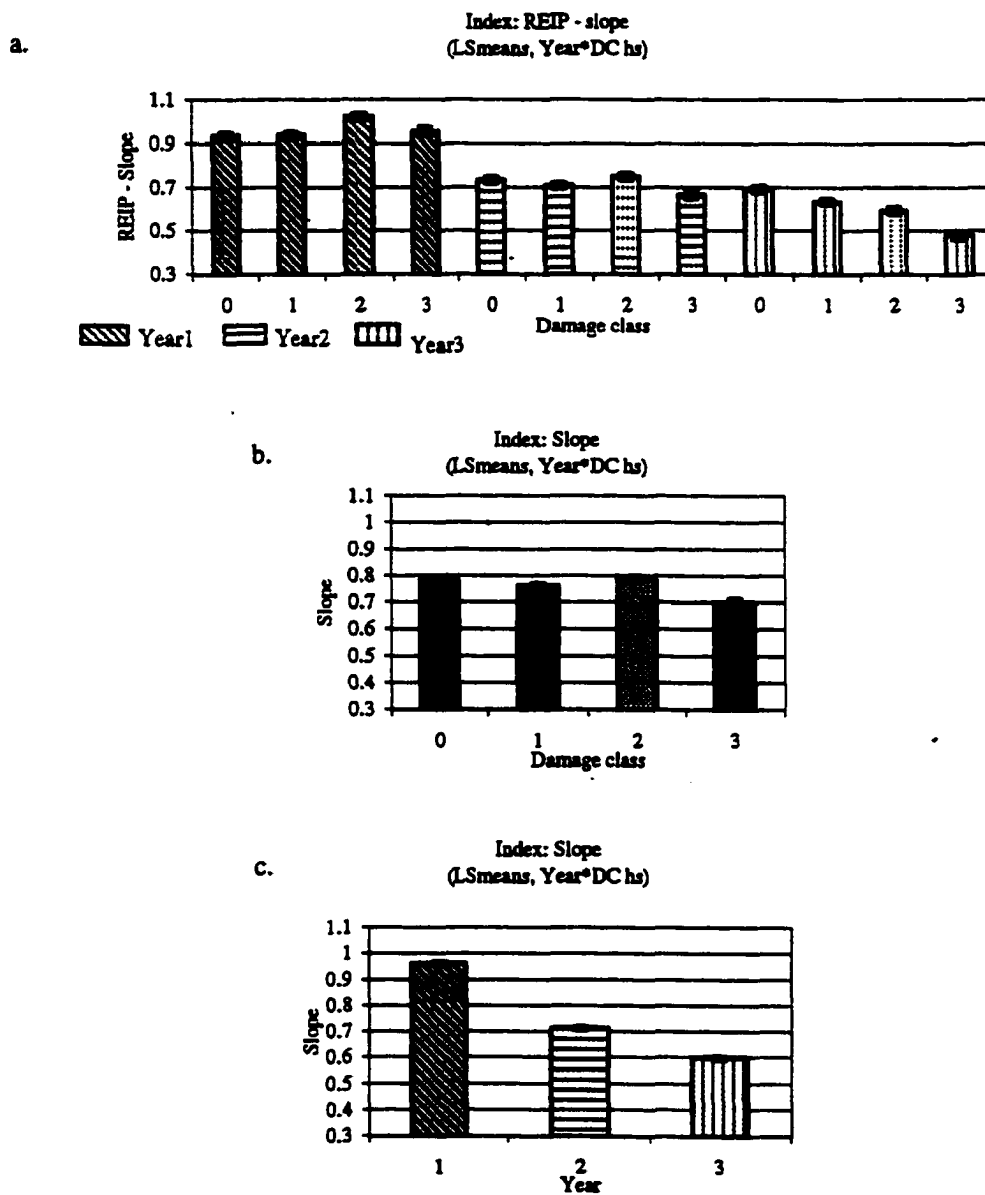


**Figure: A.3.2: Derivative indices. REIP<sub>slope</sub>=D<sub>max</sub> (D maximum in the 670-730nm region). Least square (LS)means and standard errors are plotted. The effects of (a) damage and age together, (b) damage and (c) age are evaluated.**

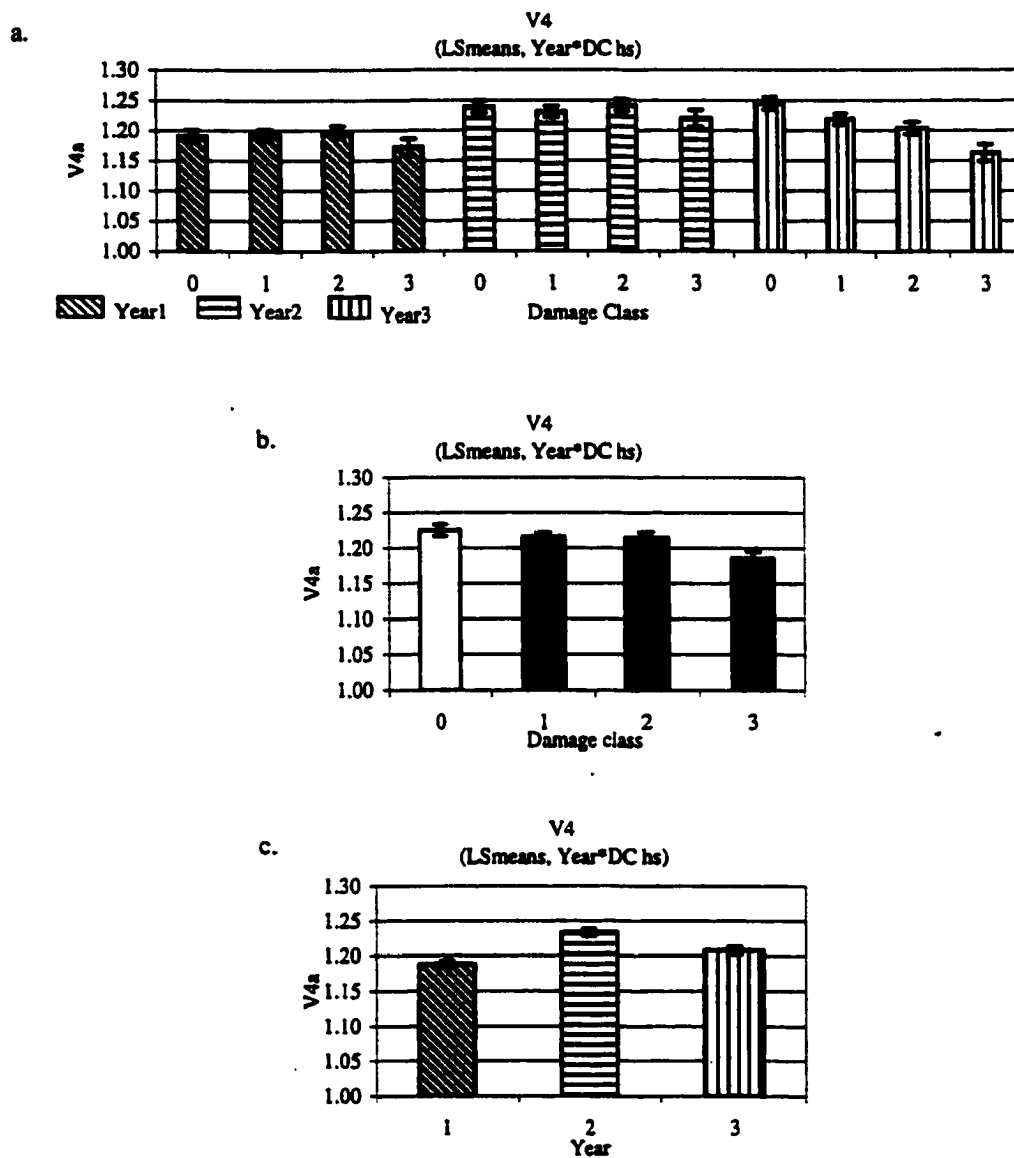


**Figure:A.3.3: Narrow Band Indices (2.5nm). V4 (D715/D705).**

Least square (LS) means and standard errors are plotted. The effects of (a) damage and age together, (b) damage and (c) age are evaluated.

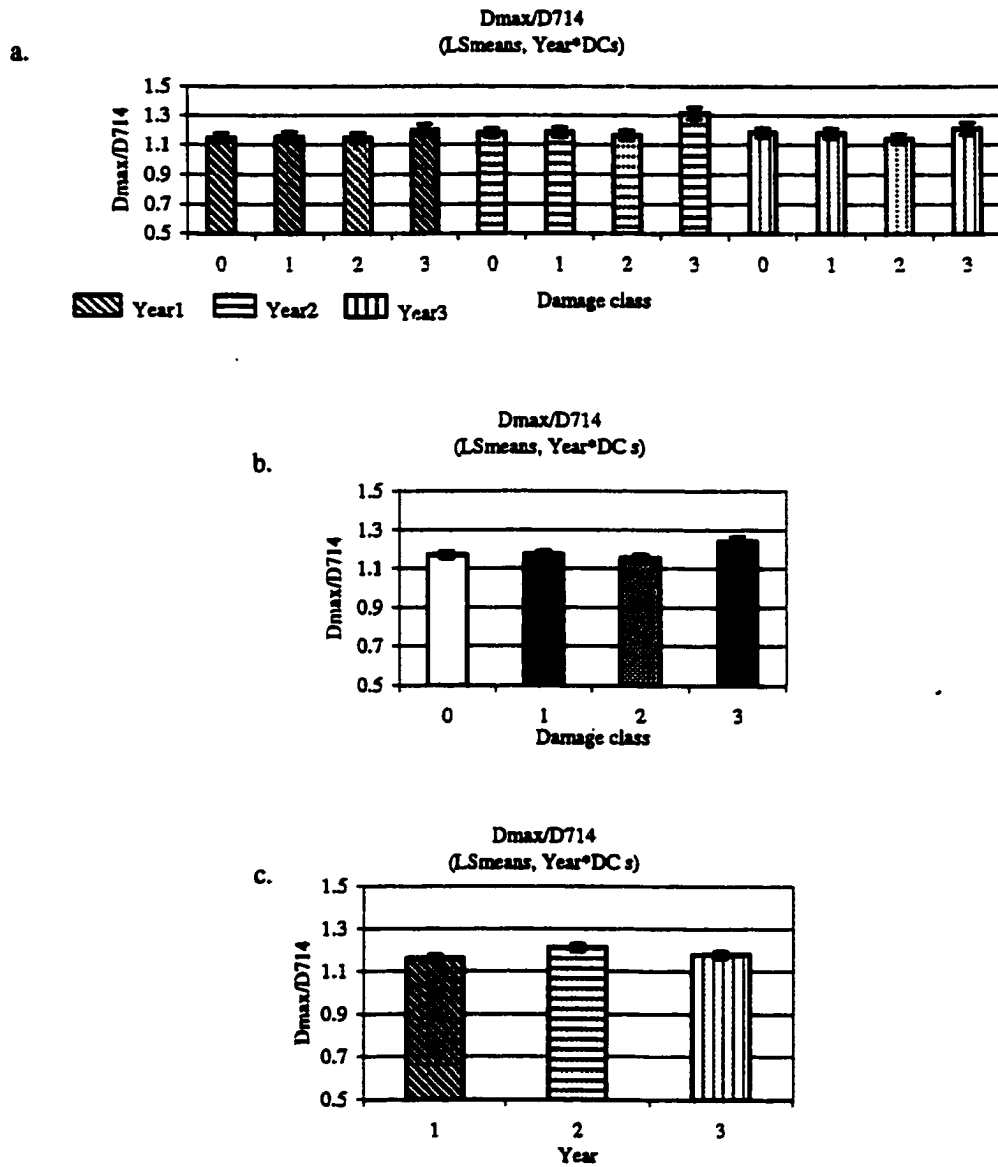


**Figure: A.3.4: Derivative indices. Dmax/D714 (Dmax/D714). Least square (LS) means and standard errors are plotted. The effects of (a) damage and age together, (b) damage and (c) age are evaluated.**

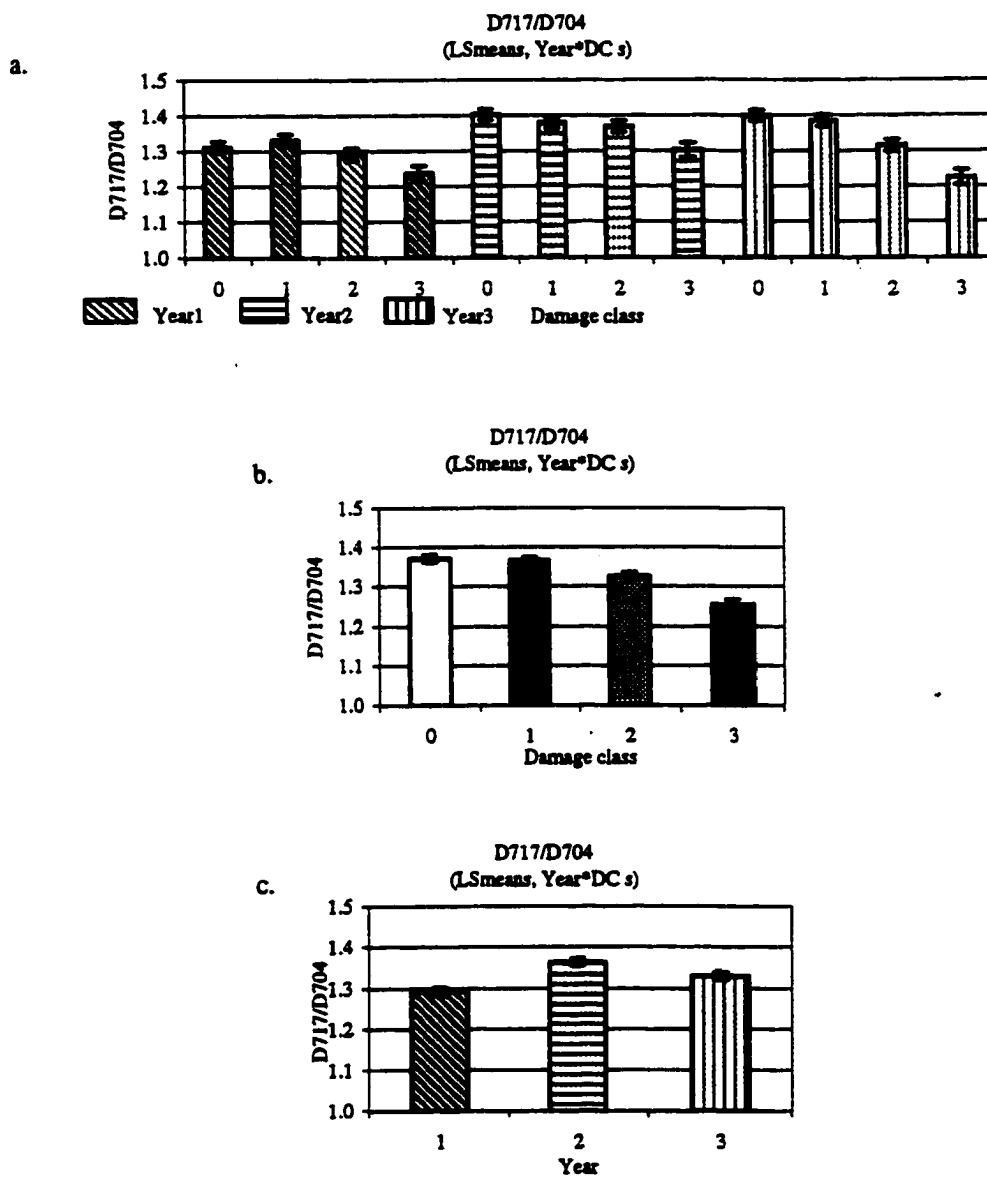


**Figure: A.3.5: Derivative indices. D717/D704 (D717/D704).** Least square (LS) means and standard errors are plotted. The effects of (a) damage and age together, (b) damage and (c) age are evaluated.



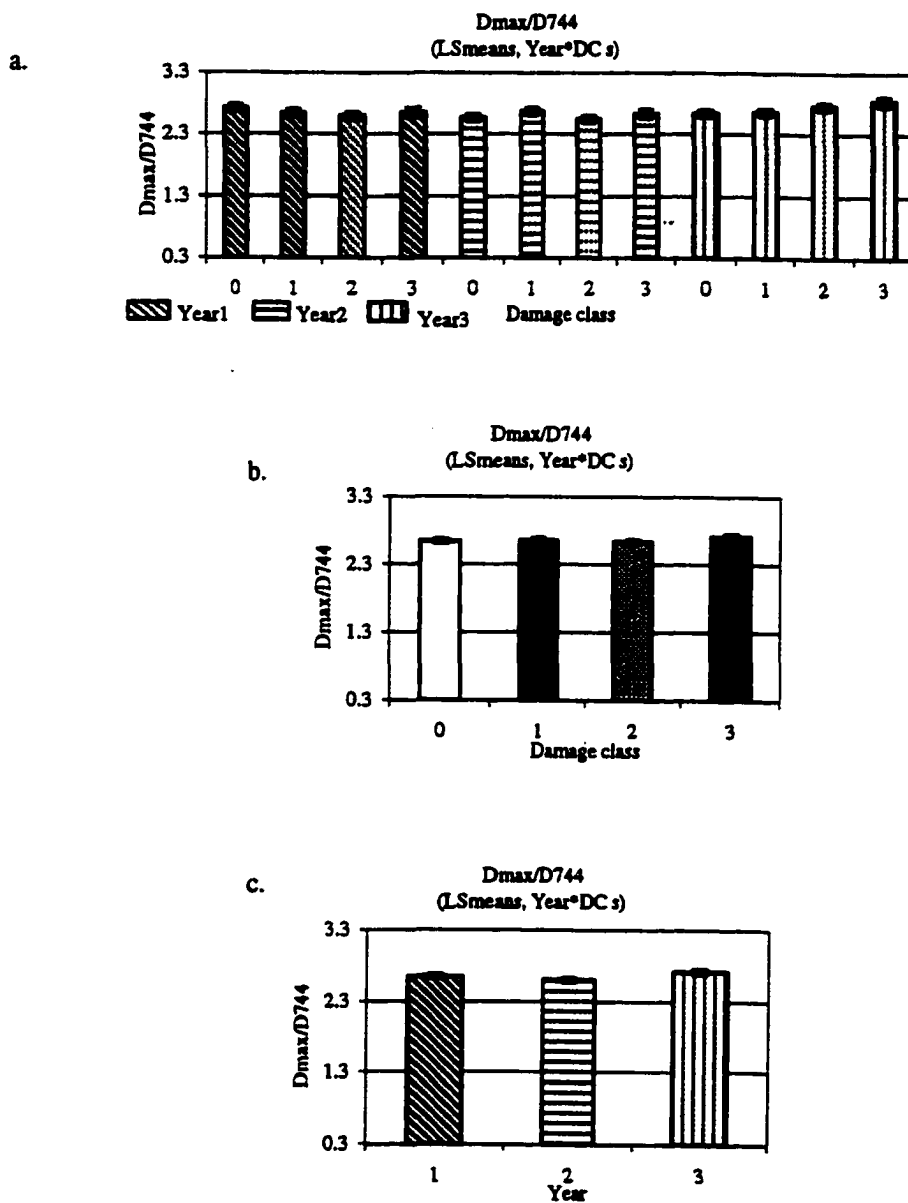


**Figure: A.3.6: Derivative indices.  $D_{max}/D_{744}$  ( $D_{max}/D_{744}$ ). Least square (LS) means and standard errors are plotted. The effects of (a) damage and age together, (b) damage and (c) age are evaluated.**

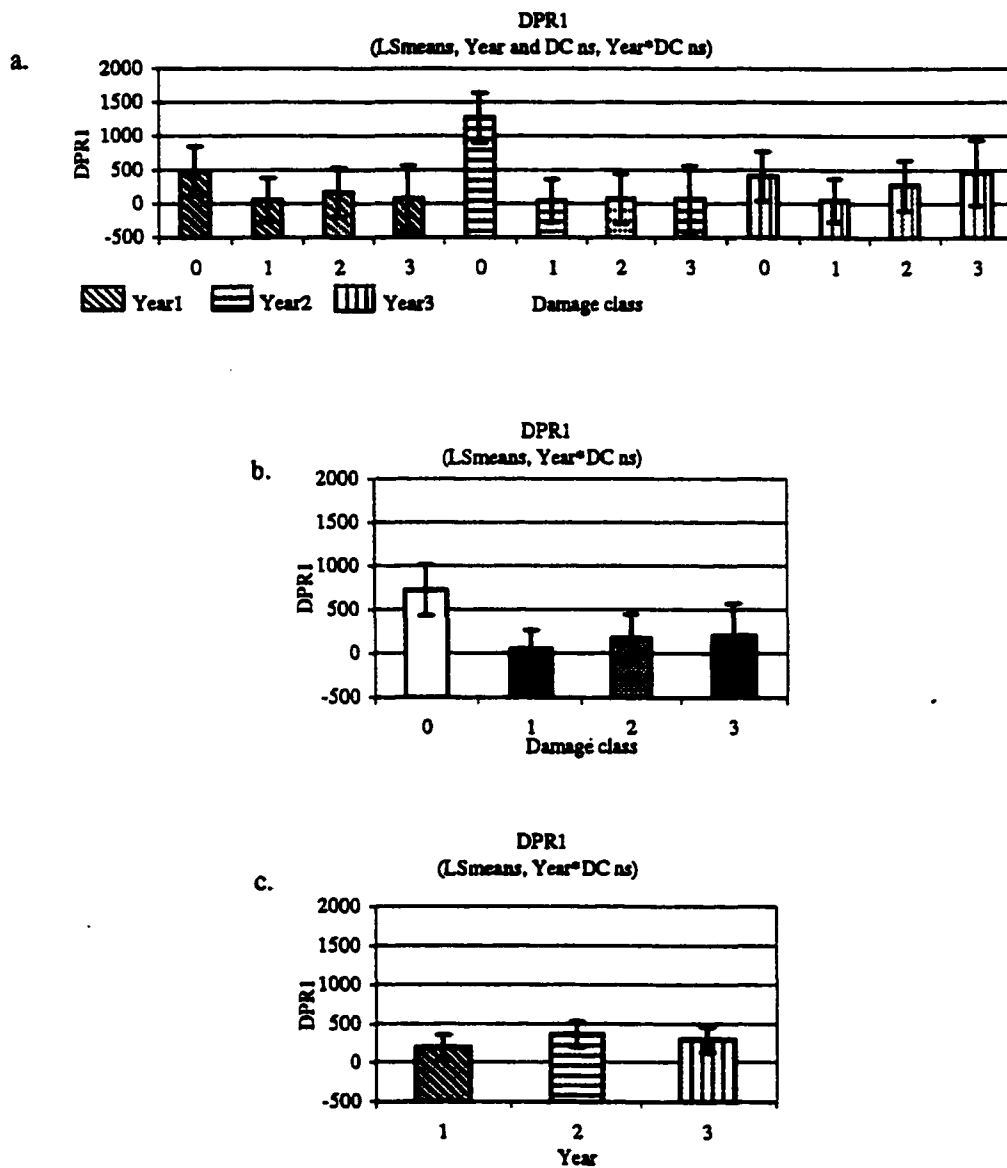


**Figure: A.3.7: Derivative indicas. DPR1 ( $D\lambda_0/D(\lambda_0+12)$ ).** Least square (LS) means and standard errors are plotted. The effects of (a) damage and age together, (b) damage and (c) age are evaluated.

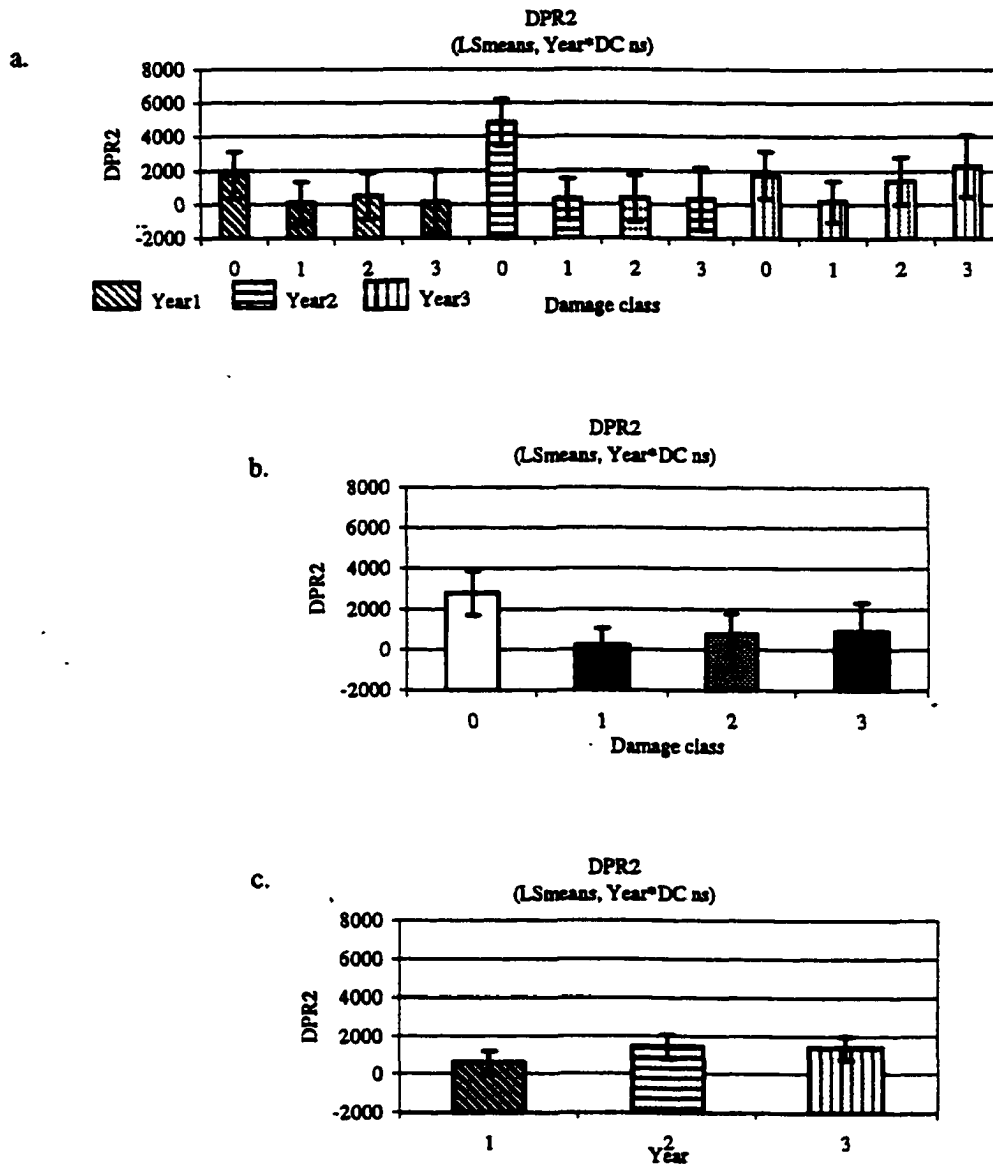


**Figure: A.3.8: Derivative indices. DPR2 ( $D\lambda_0/D(\lambda_0+22)$ ). Least square (LS) means and standard errors are plotted. The effects of (a) damage and age together, (b) damage and (c) age are evaluated**

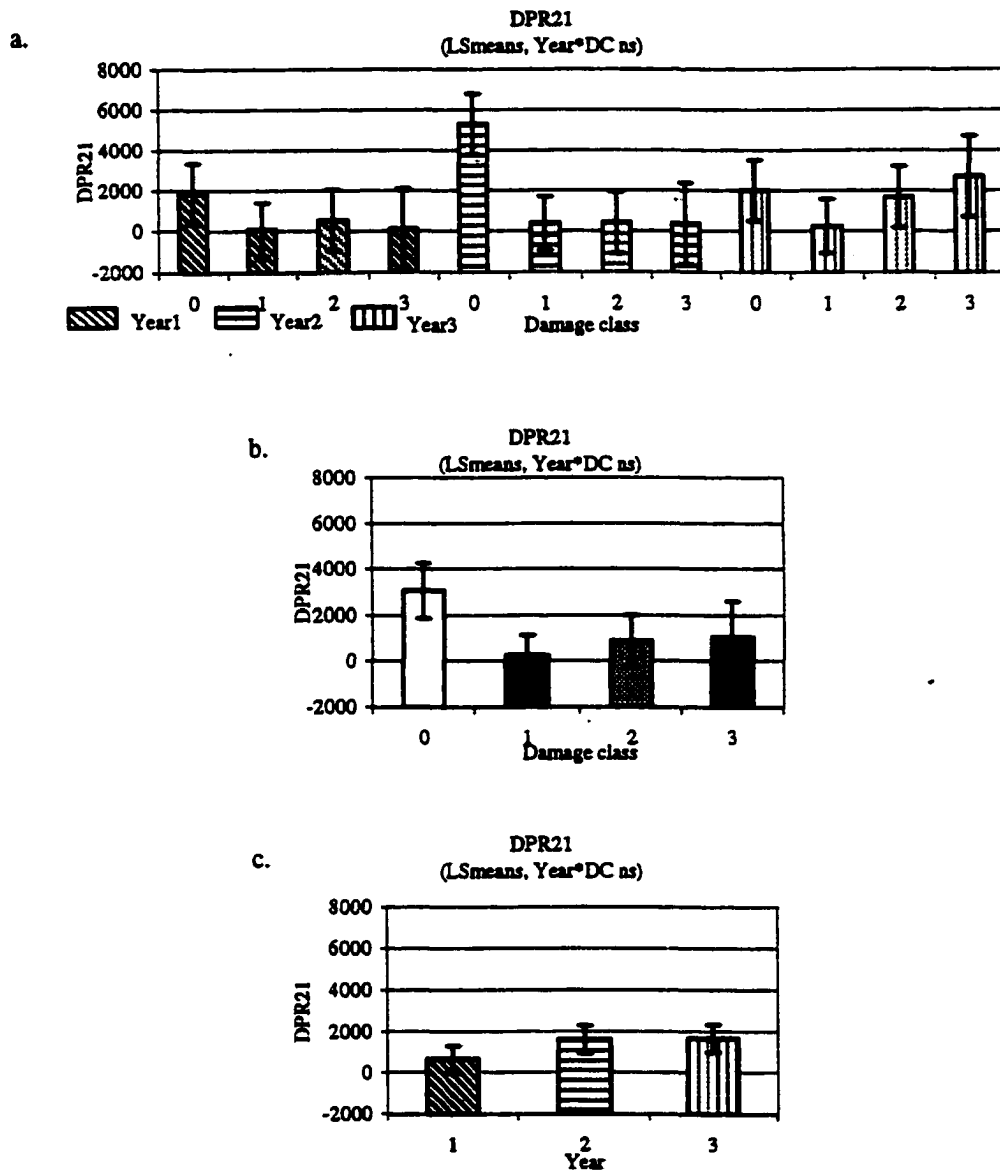


**Figure: A.3.9: Derivative indices. DPR21 ( $D\lambda_0/D703$ ). Least square (LS) means and standard errors are plotted. The effects of (a) damage and age together, (b) damage and (c) age are evaluated.**

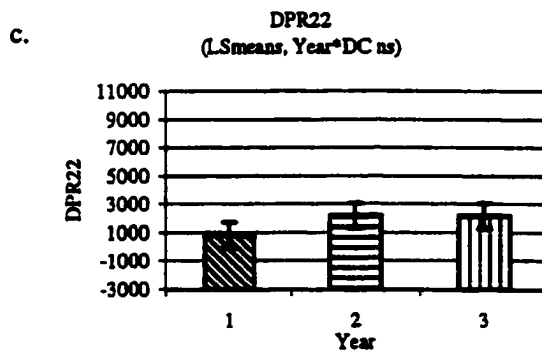
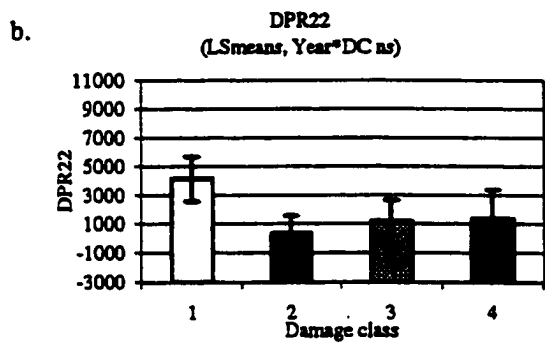
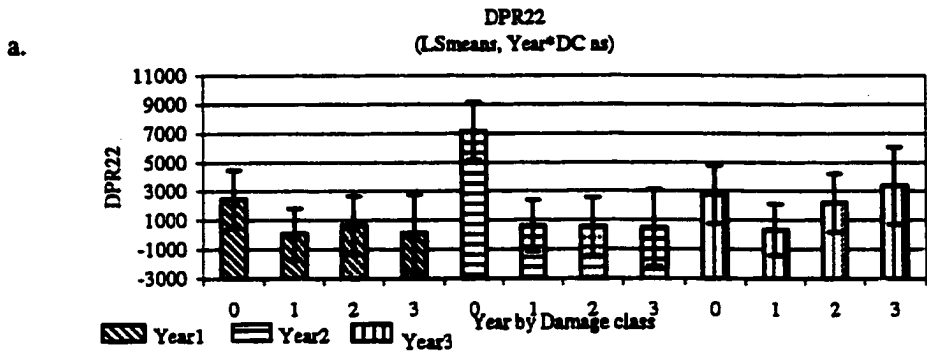


**Figure: A.3.10: Derivative indices. DPR22 ( $D\lambda_0/D720$ ). Least square (LS) means and standard errors are plotted. The effects of (a) damage and age together, (b) damage and (c) age are evaluated.**

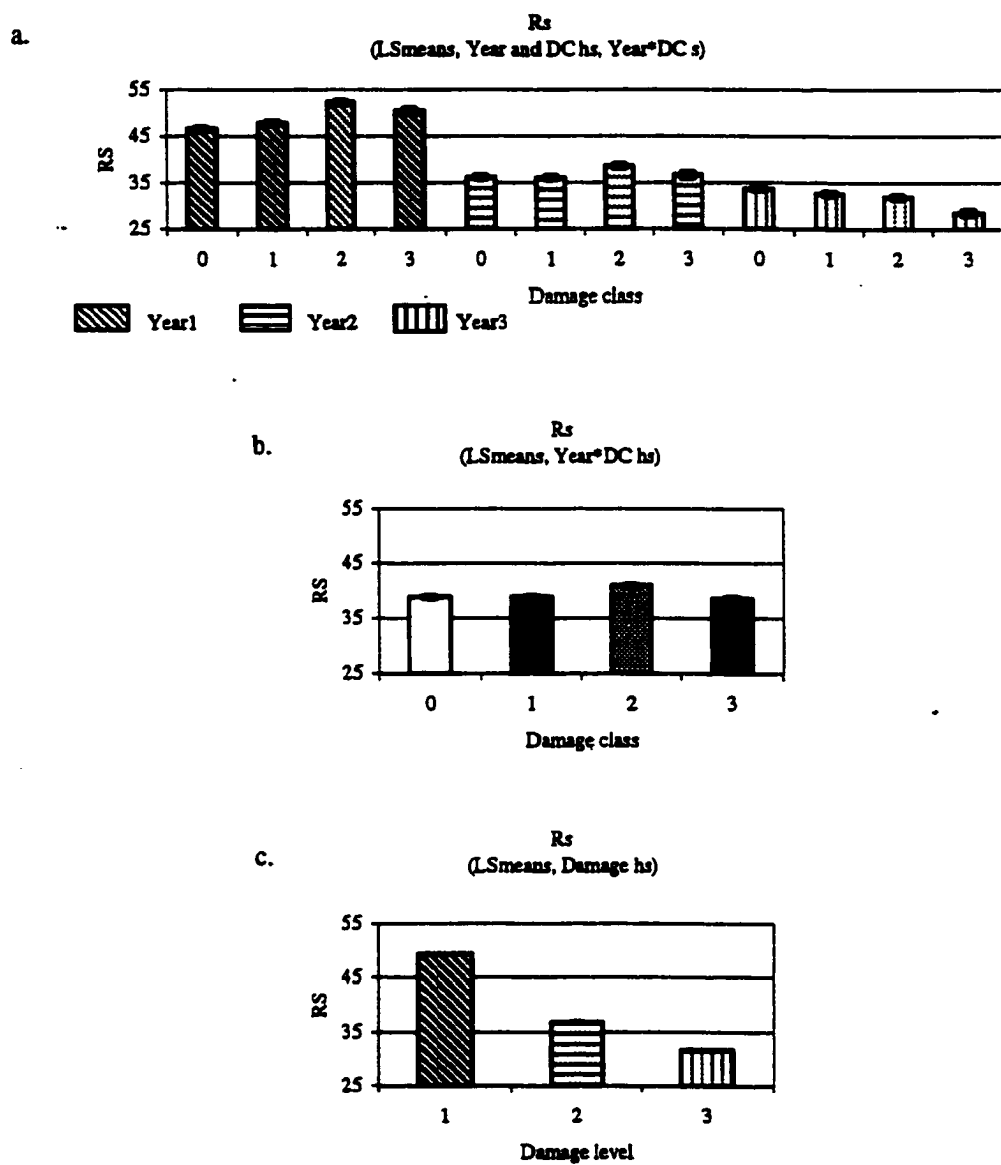


**Figure: A.4.1: IGM indices.  $R_s$  (R maximum in the 670-850nm region). Least square (LS) means and standard errors are plotted. The effects of (a) damage and age together, (b) damage and (c) age are evaluated.**

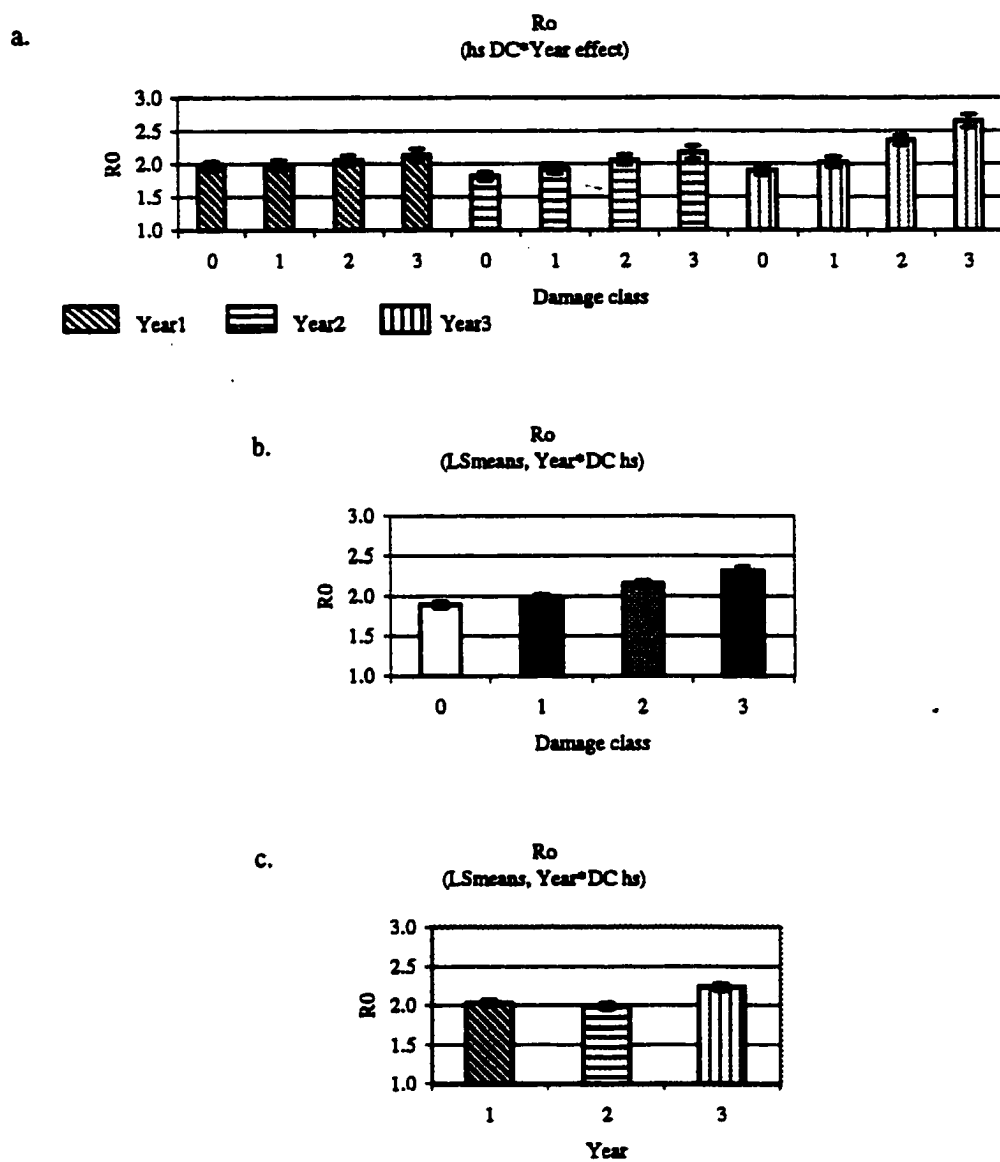


**Figure: A.4.2: IGM indices.  $R_o$  (R minimum in the 670-850nm region). Least square (LS) means and standard errors are plotted. The effects of (a) damage and age together, (b) damage and (c) age are evaluated.**

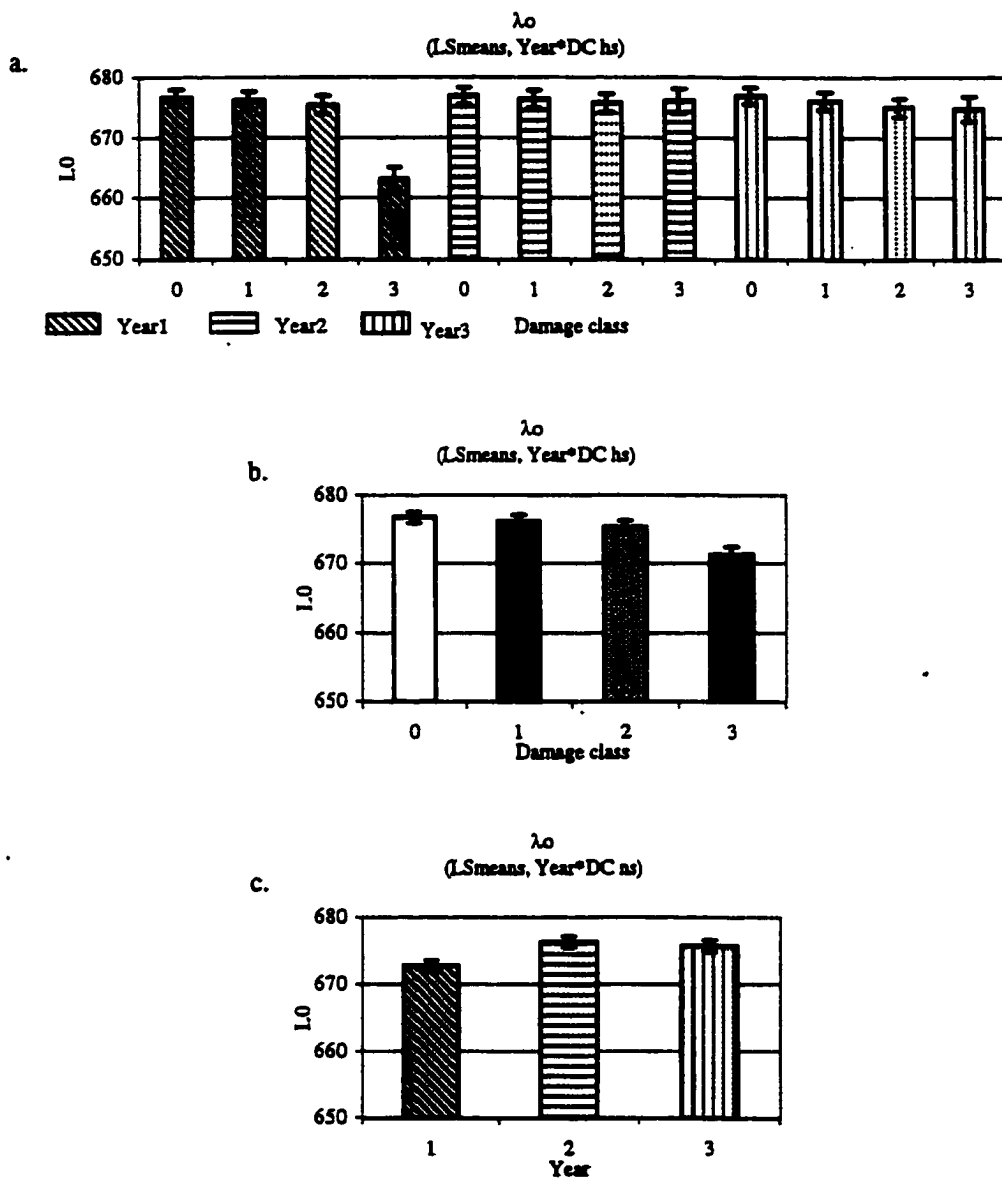


**Figure: A.4.3: IGM indices.  $\lambda_0$ (Wavelength position of R0). Least square (LS) means and standard errors are plotted. The effects of (a) damage and age together, (b) damage and (c) age are evaluated.**



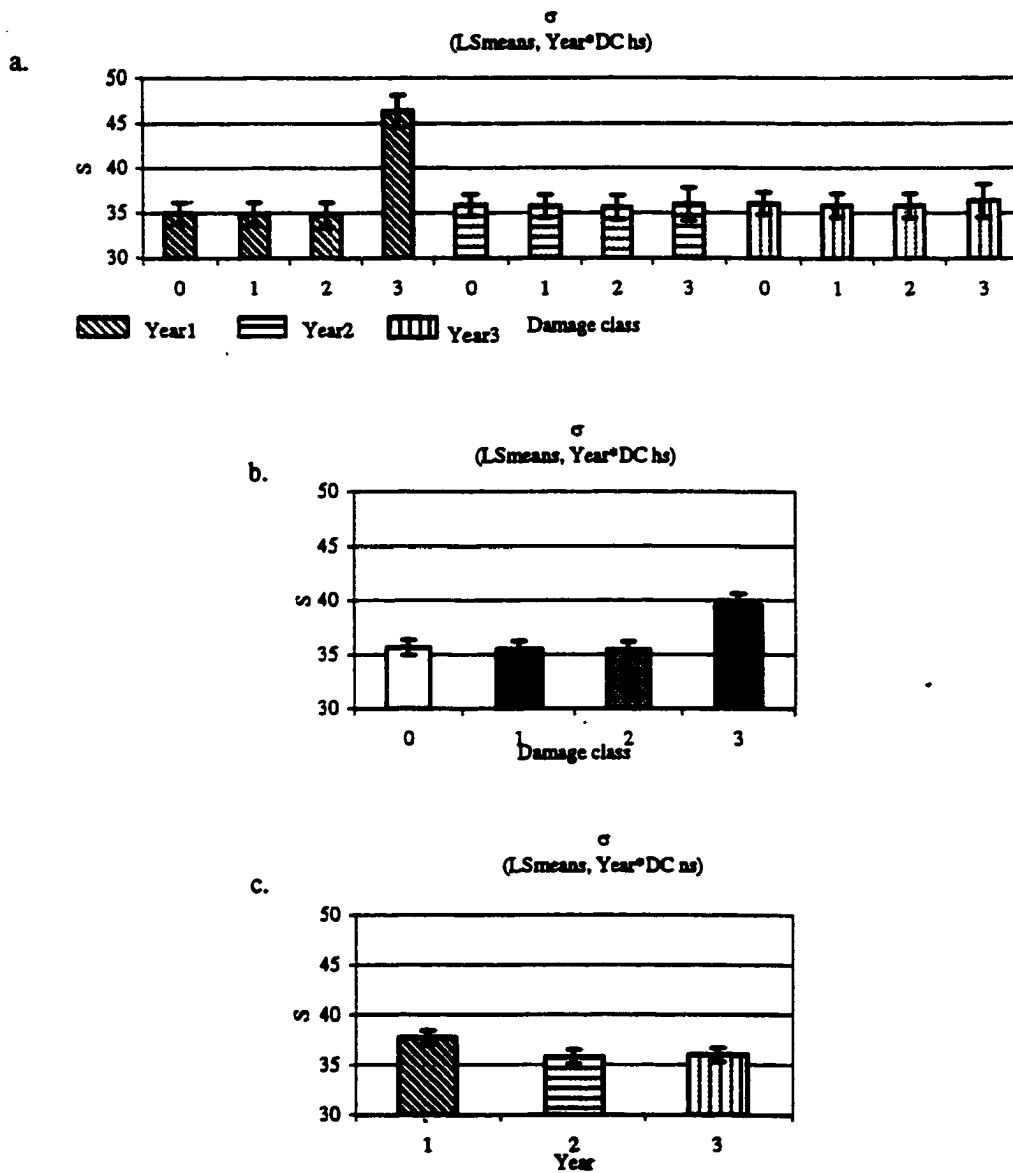


**Figure: A.4.4: IGM indices.  $\sigma$  ( $\lambda_0 - \lambda_\pi$ ). Least square (LS) means and standard errors are plotted. The effects of (a) damage and age together, (b) damage and (c) age are evaluated.**

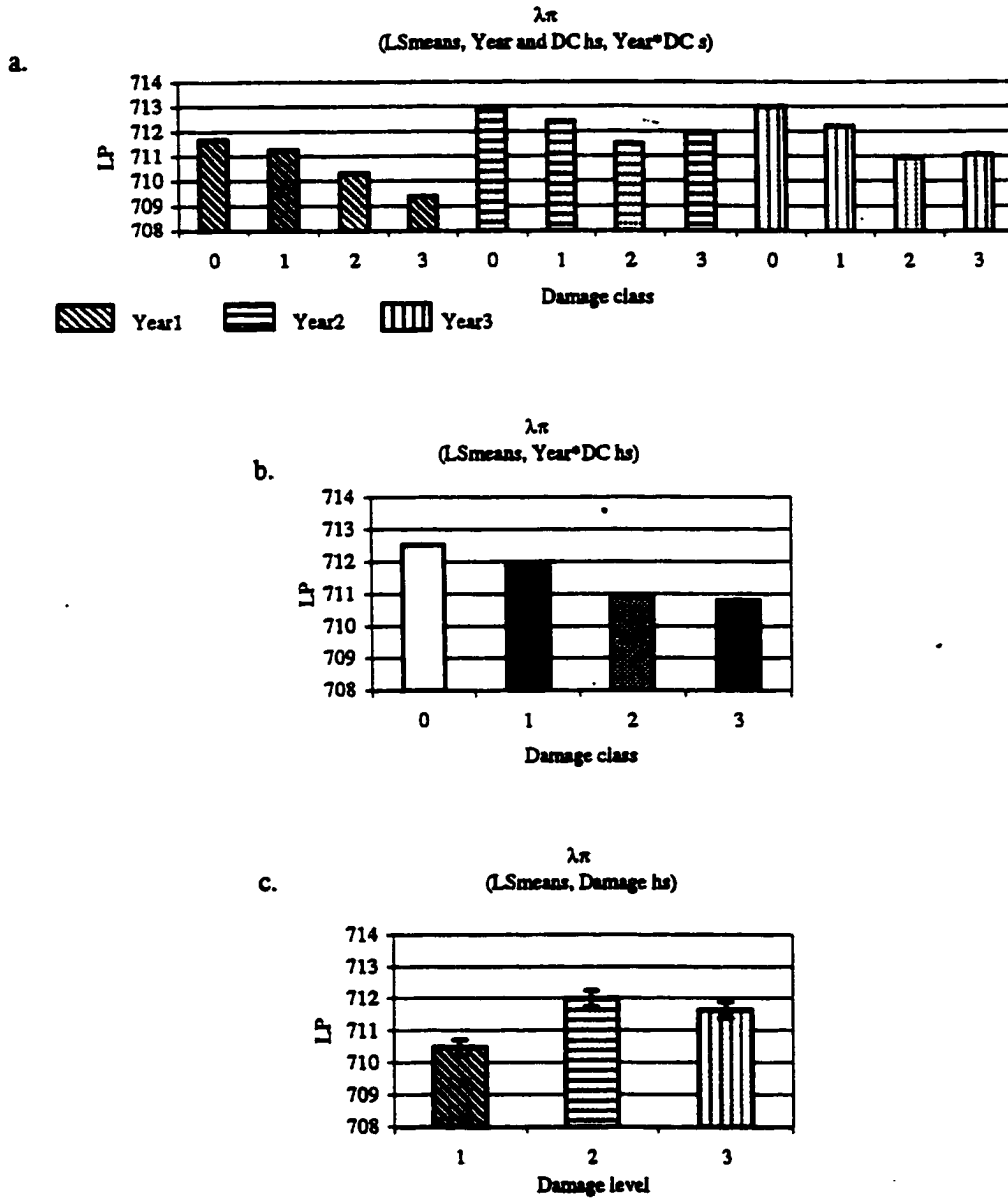


**Figure: A.4.5: IGM indices.  $\lambda\pi$  (Wavelength position of Dmax). Least square (LS) and standard errors are plotted. The effects of (a) damage and age together, (B) damage and (c) age are evaluated.**

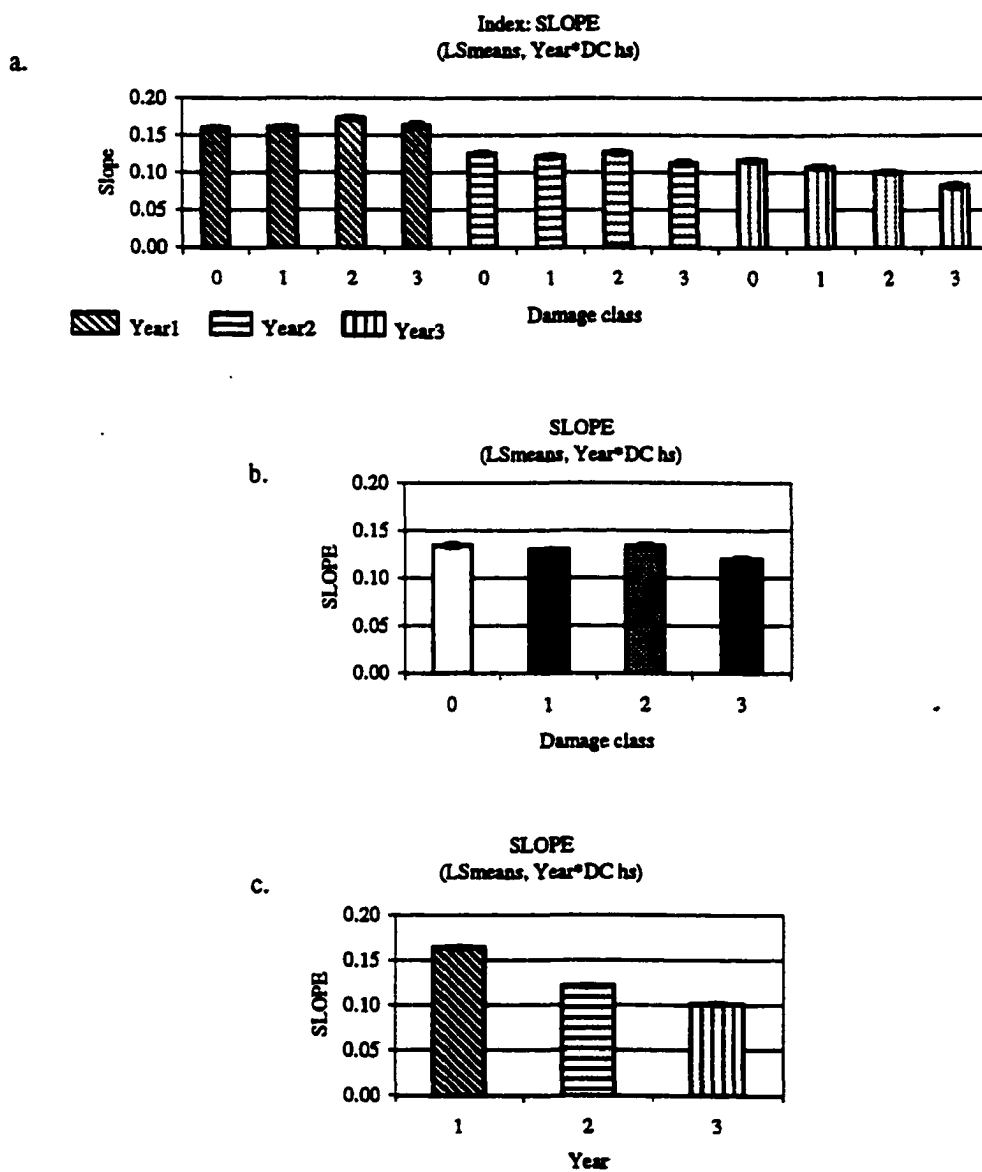


**Figure: A.5.1: Area indices. Slope (Slope of the line connecting the green and the NIR peak). Least square (LS)means and standard errors are plotted. The effects of (a) damage and age together, (b) damage and (c) age are evaluated.**

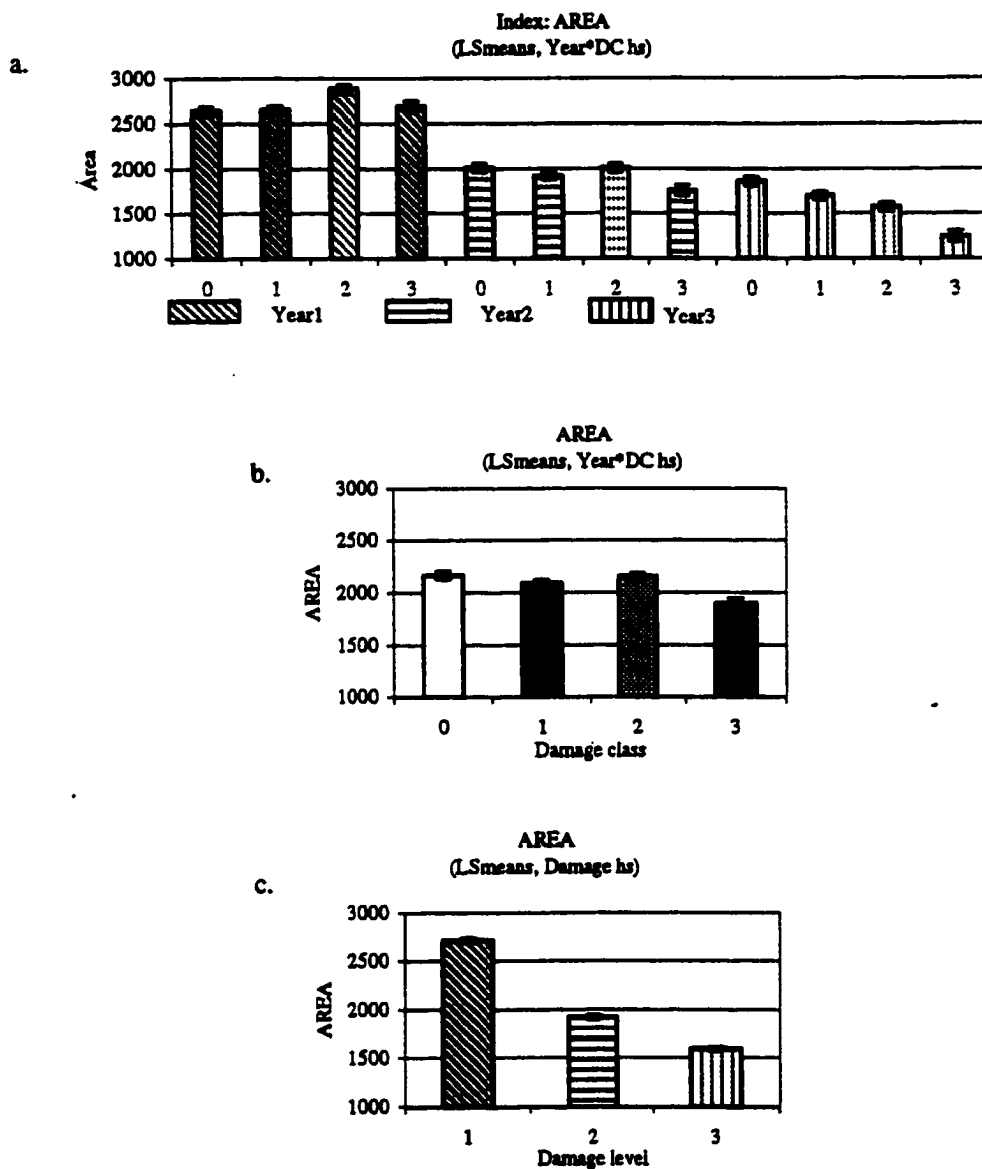


**Figure: A.5.2: Area indices.** Area (Area between the vegetation curve and the line in "Slope"). Least square (LS)means and standard errors are plotted. The effects of (a) damage and age together, (b) damage and (c) age are evaluated.

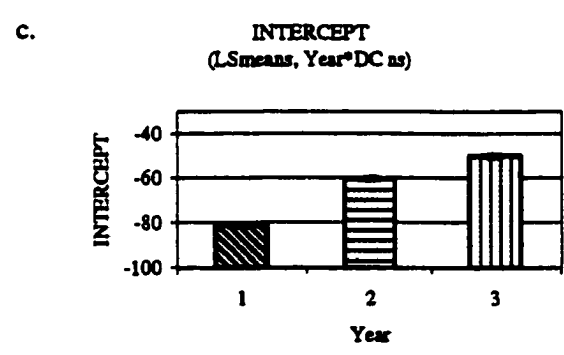
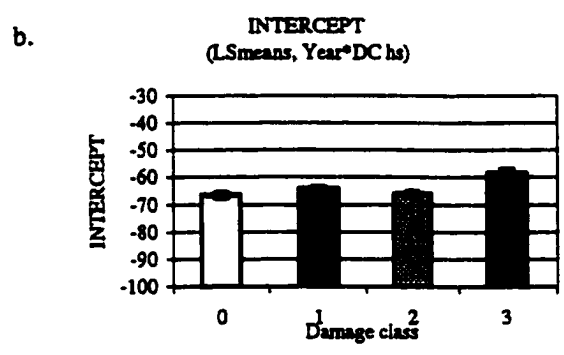
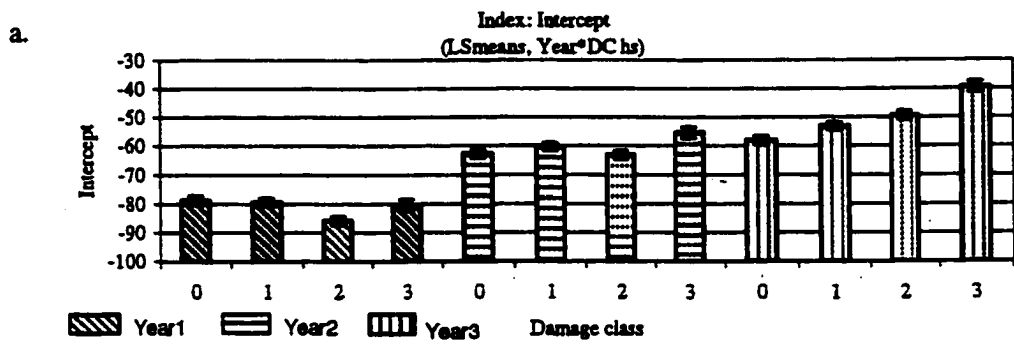


**Figure: A.5.3: Area indices. Intercept (Product for the Area calculation).** Least square (LS)means and standard errors are plotted. The effects of (a) damage and age together, (b) damage and (c) age are evaluated.

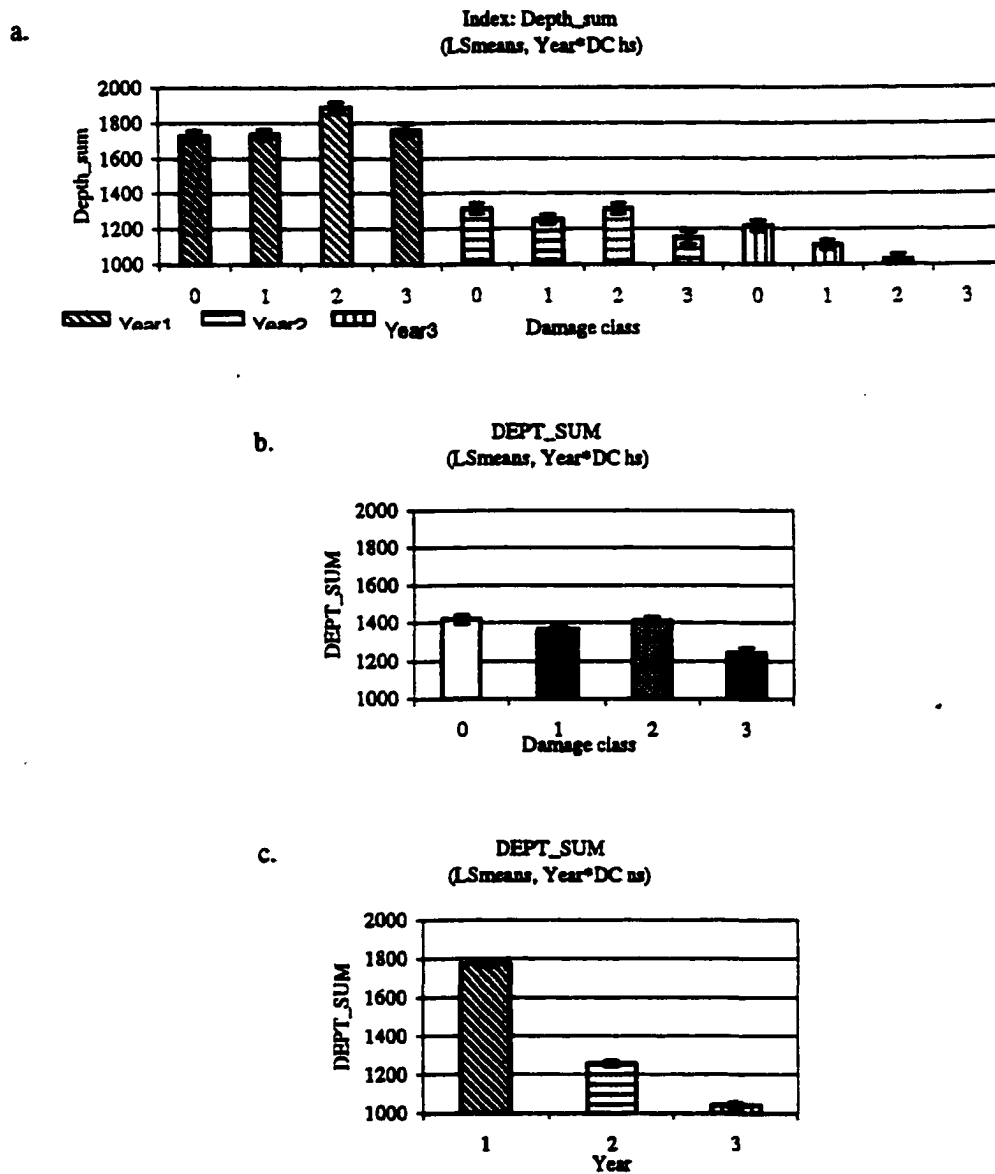


**Figure: A.5.4: Area indices. Dept\_sum (Product for the Area calculation). Least square (LS)means and standard errors are plotted. The effects of (a) damage and age together, (b) damage and (c) age are evaluated.**

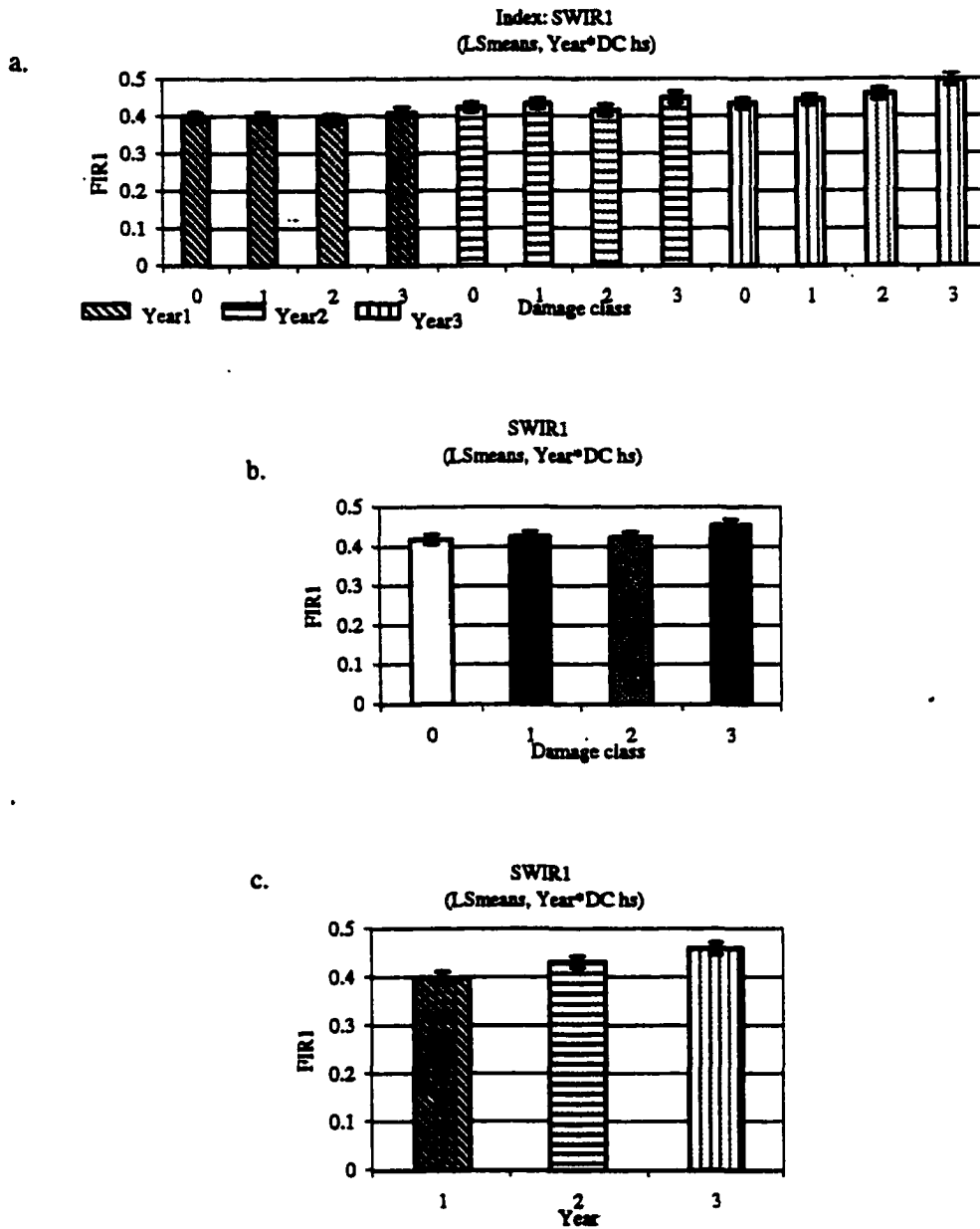


**Figure: A.6.1:SWIR indices. SWIR1 (R1365/R1455). Least square (LS) means and standard errors are plotted. The effects of (a) damage and age together, (b) damage and (c) age are evaluated.**

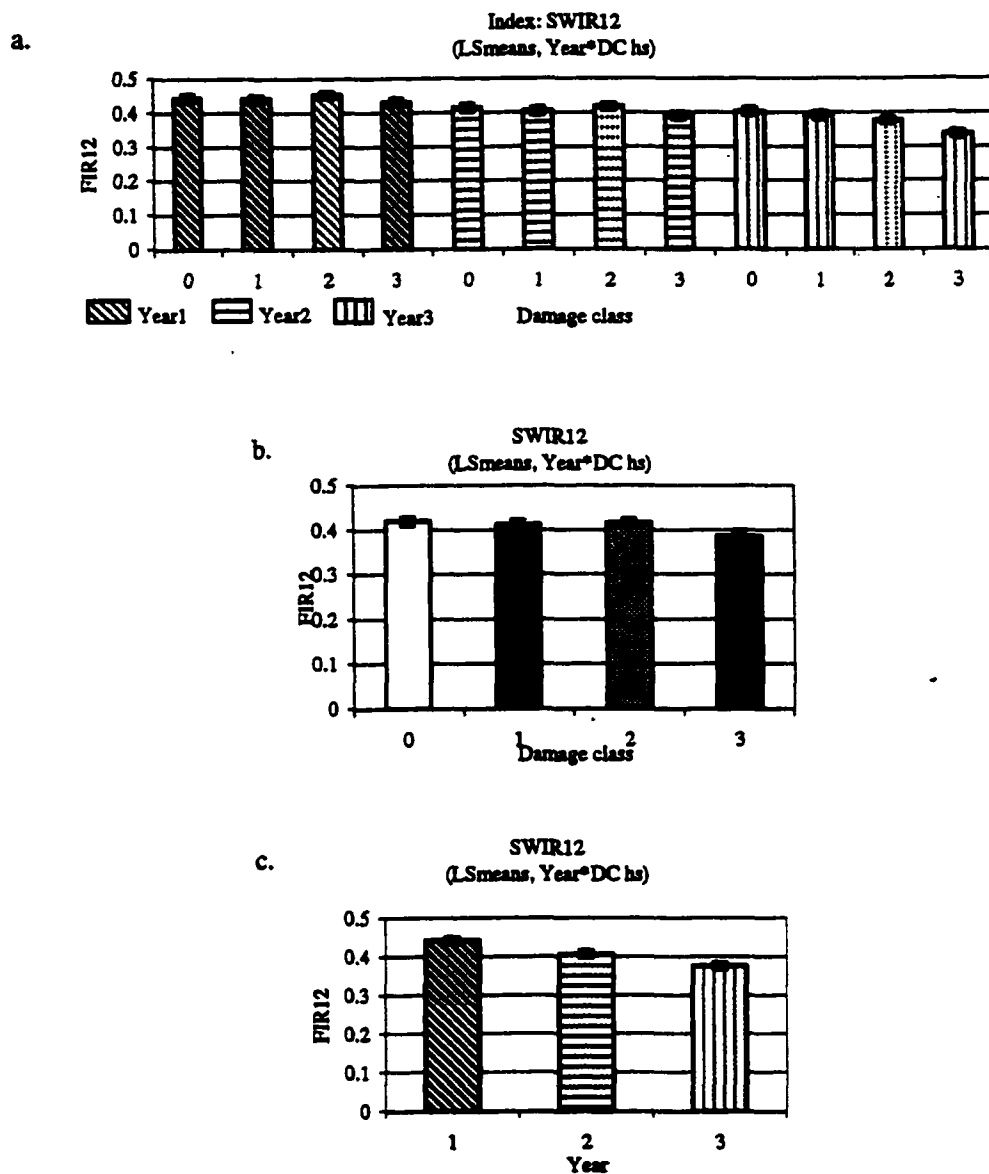


**Figure: A.6.2: SWIR indices.** SWIR12 ( $(R1365-R1456)/(R1365+R1456)$ ). Least square (LS) means and standard errors are plotted. The effects of (a) damage and age together, (b) damage and (c) age are evaluated.



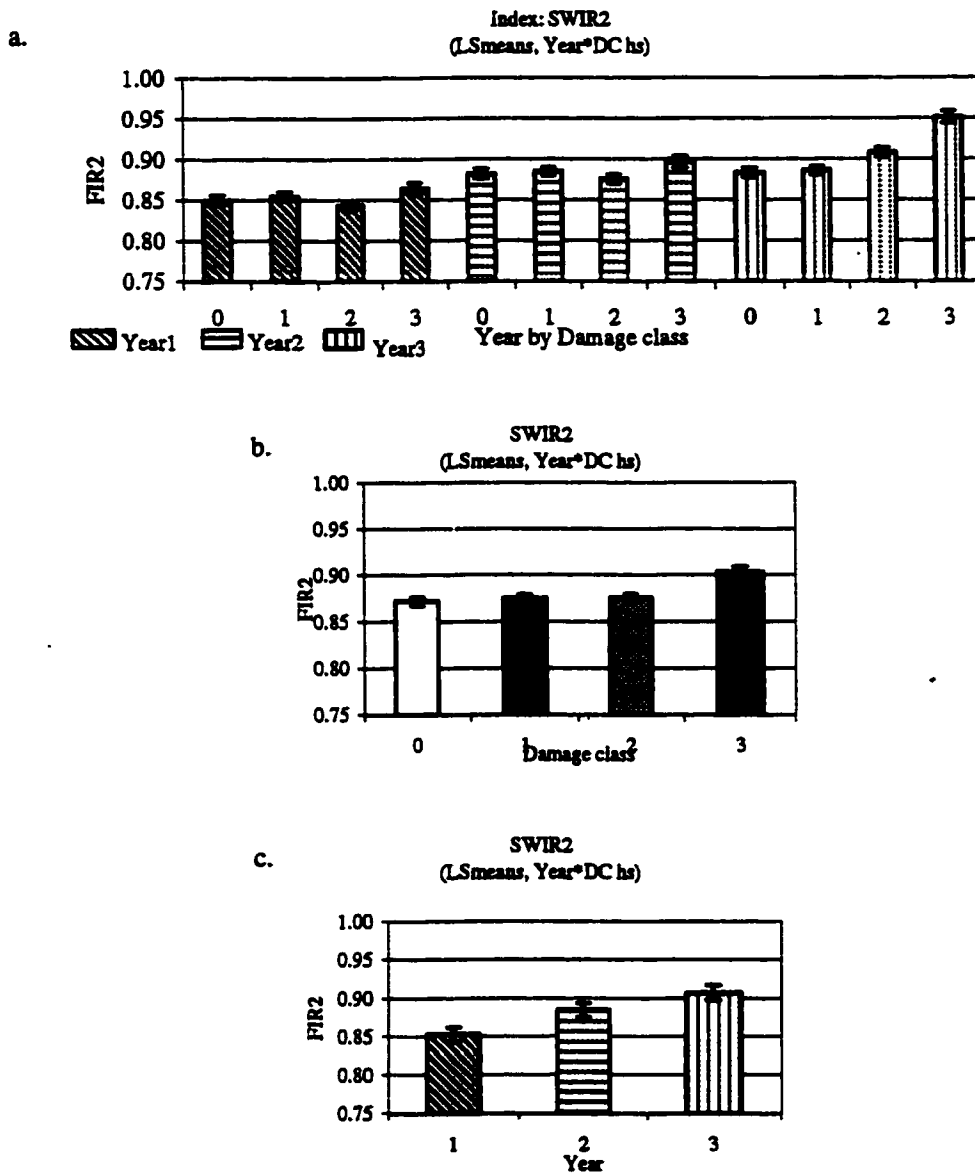
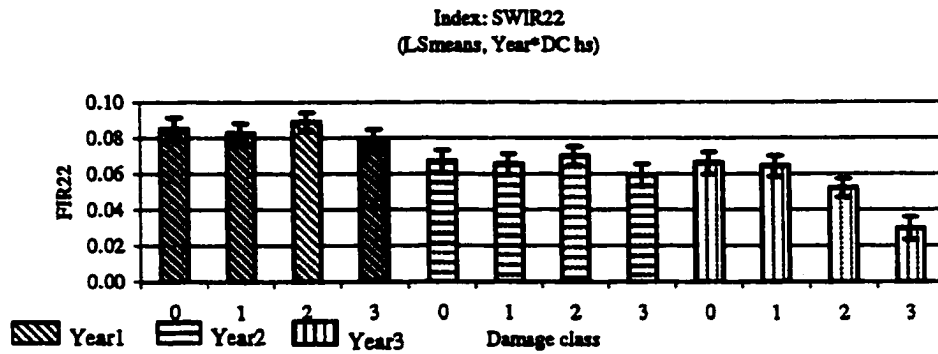
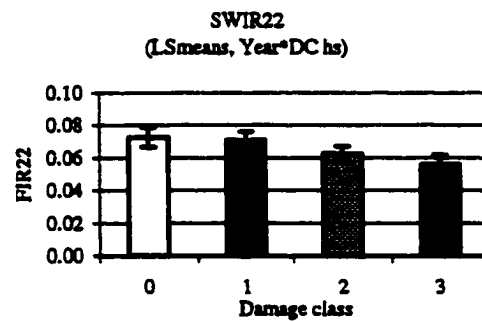


**Figure: A.6.3: SWIR indices. SWIR2 (R1890/R1950).** Least square (LS) means and standard errors are plotted. The effects of (a) damage and age together, (b) damage and (c) age are evaluated.

a.



b.



c.

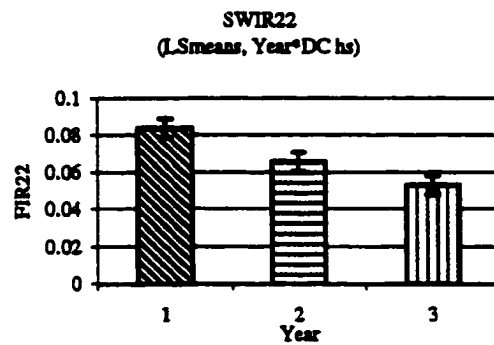


**Figure A.6.4: SWIR indices. SWIR22 ((R1890-R1951)/(R1890+R1951)). Least square (LS) means and standard errors are plotted. The effects of (a) damage and age together, (b) damage and (c) age are evaluated.**